UNIVERSITY OF CAPE TOWN

DEPARTMENT OF MECHANICAL ENGINEERING

RONDEBOSCH, CAPE TOWN, SOUTH AFRICA

Development of the Power and Communications Distribution Systems for an Underwater Remotely Operated Vehicle

Prepared by Roger de Smidt
Robotics and Agents Research Laboratory
University of Cape Town

Supervised by Stephen Marais
Robotics and Agents Research Laboratory
University of Cape Town

October 2014

Development of the Power and Communications Distribution Systems for an Underwater Remotely Operated Vehicle

University of Cape Town

Robotics and Agents Research Laboratory

Mechanical Engineering Department

Author: Roger de Smidt

Supervisor: Stephen Marais

Date: 20 October 2014

SUMMARY

Figure 1: Rendering of the new 3rd Generation ROV

This report details the research, design, development and testing of the third generation underwater remotely operated vehicle (ROV) produced by the University of Cape Town's Robotics and Agents Research Laboratory (RARL). The ROV was designed and built in response to a request from the Department of Zoology for an ROV to aid their oceanic research. The two generations that had gone before this ROV had provided the research group with good experience, but a new vehicle was required that would offer a more robust research tool for the zoologists and a more versatile platform for future development within the RARL.

ROV System

Together with project partner Thomas Knight, a new ROV design was developed that was based on the open frame designs commonly used on commercially available ROVs and is shown in Figure 1 above. The ROV was to be propelled by five individual thruster modules and carried four high-powered LED light modules to provide lighting for the ROV's forward and aft video cameras. In order to navigate the ROV a sonar unit was also incorporated on board.

In order to provide power and communications from the surface station to each of the modules on board the ROV, distribution systems for each were required. As the project progressed, it became clear that these distribution systems were critical to the reliability and versatility of the vehicle and became the focus of the author's scope.

The report starts with a description of the design process that resulted in the decision to design a new ROV and then a brief description is provided of the ROV systems incorporated in the final design. The detailed design of the power and communications distribution systems is then presented using a bottom-up design approach, starting with the distribution of power and communications on board the ROV. Brief descriptions of the major components in these systems follow below.

Electronics Pod

The Electronics Pod (E-Pod) was designed to distribute power to each module on the ROV at the required voltages and currents, and to distribute serial communications to each module over an RS-485 multi-drop network. The E-Pod incorporated two microcontrollers that were used to control the switching of power to each of the modules and were also connected on the RS-485 communications network. This RS-485 network was connected to the surface via an optical fibre link in the ROV's tether, and the two converters required to establish this link were also housed in the E-Pod. Video feeds from the on-board cameras were fed into an encoder in the E-Pod and transmitted to the surface controller also via the fibre link. The power required by the E-Pod was drawn from the Power Pod on the ROV, which is described below.

Power Pod

The Power Pod was designed to convert the 400 VDC supply from the tether into 5 V, 12 V, 15 V and 48 V, which were required by the E-Pod. A total of 1.66kW was to be supplied to the E-Pod so compact, high-power DC-DC converters were integrated into the design of custom-made printed circuit boards (PCBs) in order to provide the required power.

Currents sensors, temperature sensors and voltage level sensors were incorporated in the Power Pod circuitry. A microcontroller in the Power Pod was used to read all of the sensors and communicate the values to the surface controller via the E-Pod.

Subsea Junction Box

Because the ROV's tether contained copper cores for power transmission and optical fibres for communications transmission, a very expensive hybrid subsea connector was required if it was to plug directly into the Power Pod or E-Pod. A junction box was therefore designed in which the copper cores of tether were separated from the optical fibres. The copper cores were fed to the Power Pod and the optical fibres to the E-Pod. The junction box was filled with oil and pressure compensated to reduce the risk of water ingress.

Surface Power Supply Unit

Including power losses in the distribution system, 2kW of power was required to be supplied to the tether. A surface power supply unit (PSU) was designed with an isolated, ungrounded 400 VDC power supply, which ran off a standard 230 V, 16 A mains supply. Start and emergency-stop switches were provided on the PSU enclosure, as well as a lockable isolator.

The PSU incorporated an Ethernet network switch and fibre optic media converter to provide the link necessary between the tether and the laptop running the user interface and sonar software.

Concluding Remarks

The performance of the power and communications distribution systems was tested to benchmark them against their specifications to which they had been designed. Overall the two systems performed well and, with a couple of modifications, would provide a robust and efficient backbone of control and power for the ROV.

The primary modification recommended was for the Power Pod. During testing, the Power Pod was unable to completely dissipate the heat generated by its DC-DC converters. The lengthening of the housing and addition of a heat sink in its base was recommended, and was in production at the time of writing.

The second area noted for improvement was the speed of communications between the user interface and the ROV modules. Although it had performed within the specified limits, it was suggested that improvements could still be made in the user interface software that would speed up the communications cycle.

DECLARATION

This dissertation is submitted in complete fulfilment of a M.Sc.(Eng) (Mechanical Engineering) at the University of Cape Town.

I know the meaning of plagiarism and declare that all of the work in the thesis, save for that which is properly acknowledged, is my own. Each contribution to, and quotation in, this dissertation from the work(s) of other people has been attributed, and has been cited and referenced according to the IEEE standard.

I have not allowed, and will not allow anyone to copy my work with the intention of passing it off as their own.

_____ _____

Roger de Smidt Date

ACKNOWLEDGEMENTS

This dissertation has taken no small amount of effort and would not have been possible without the input and assistance of a number of people. I owe particular thanks to:

Stephen Marais, for his patient supervision of this project and for generously providing and entrusting us with a large budget to re-design the ROV. You have created a great research laboratory that was stimulating to work in. It has been a pleasure working with you.

ARMSCOR for their generous funding which helped cover my living expenses during the course of this project. A big thank you to Professor Jasson Gryzagoridis and Mr Dirk Findeis for allocating this funding to me. Without it, I would have been hard-pressed to complete the project within the same period.

My wife and best friend, Jacqui, for her companionship and encouragement throughout this project. "*A wife of noble character, who can find? She is worth far more than rubies.*" [Proverbs 31:10]

Thomas Knight, my project partner, for your many hours of CAD drawing and overall contribution to the project. It was a pleasure working with you and know that any engineering design team would be strengthened by your analytical and creative input.

Glenn Newins, Pierre Smith, Hubert, Gavin, Horst and the rest of the workshop team for the high quality components produced for the ROV and for the rapid procurement of last-minute parts. It has been a pleasure to work with each one of you.

Clare Bloomer for keeping the finances in order and responding so promptly to my emails.

Kevin and Barry Bey-Leveld and Egon Laaser of Marine Solutions for all your advice regarding ROVs and how to go about various aspects of their design. Thank you for opening up your facility to us and allowing us to use your pressure testing equipment, and thanks to Ismail for helping to set it up most times.

Sam Ginsberg and Chris Wozniak from the Electrical Engineering Department for your many words of advice regarding electronics and high-power electrics respectively.

Jeremy Dinklemann, partner in the Subsea Engineering and ROV Services (SERS) Group, for your technical advice regarding ROV design and insight into the ROV industry.

Michael, David, Tracy, Brad, Richard and Julian, fellow RARL residents at various stages, for the good company and for your help debugging my circuit boards and programs along the way.

Billy from False Bay Yacht Club (FBYC) for allowing us to launch and fly ROV *Robin* in the FBYC marina.

Last, but not least, my linguistically adept aunt and mother-in-law, Brenda and Christine, for proof reading and correcting large portions of this dissertation.

CONTENTS

LIST OF FIGURES

LIST OF TABLES

LIST OF ACRONYMS

AC	*Alternating Current*
ADC	*Analogue-to-Digital Converter*
BJT	*Bipolar Junction Transistor*
CAD	*Computer Aided Design*
CAN	*Controller Area Network*
Cat5e	*Category 5e*
CRC	*Cyclic Redundancy Code*
DC	*Direct Current*
DVD	*Digital Video Disc*
E-Pod	*Electronics Pod*
FEA	*Finite Element Analysis*
GFM	*Ground Fault Monitor*
HD	*High Definition*
IO	*Inputs and outputs*
MBARI	*Monterey Bay Aquarium Research Institute*
MOSFET	*Metal-Oxide-Semiconductor Field-Effect Transistor*
NI	*National Instruments*
OCROV	*Observation Class Remotely Operated Vehicle*
PCB	*Printed Circuit Board*
PSU	*Power Supply Unit*
RARL	*Robotics and Agents Research Laboratory*
ROV	*Remotely Operated Vehicle*
Sb-RIO	*Single Board Reconfigurable Inputs and Outputs*
TTL	*Transistor-Transistor Logic*
UCT	*University of Cape Town*
UI	*User Interface*

LIST OF SYMBOLS

A_P	*Plunger surface area*
D_P	*Plunger diameter*
D_S	*Spring coil mean diameter*
F_P	*Plunger force*
F_s	*Spring force*
K_s	*Stress concentration factor for static loading*
L_s	*Solid height*
L_w	*Minimum working height*
N_t	*Total number of turns*
P_{oil}	*Oil pressure*
S_Y	*Yield stress*
V_C	*Chamber volume*
d_S	*Spring wire diameter*
m_{avg}	*Average gradient*
s_P	*Plunger stroke*
δ_{max}	*Maximum deflection*
σ_{max}	*Maximum stress*
τ_s	*Stress at solid spring height*
G	*Modulus of rigidity*
h	*Height*
n	*Number of springs*
P	*Pressure*
S_u	*Ultimate tensile strength*
N	*Poisson's ratio*
C	*Spring index*
E	*Modulus of elasticity*
L	*Cylinder length*
M	*Bending moment*
N	*Number of live turns*
c	*Zero offset (Y-intercept)*
d	*Diameter*
k	*Spring rate*
t	*Thickness*

1 INTRODUCTION

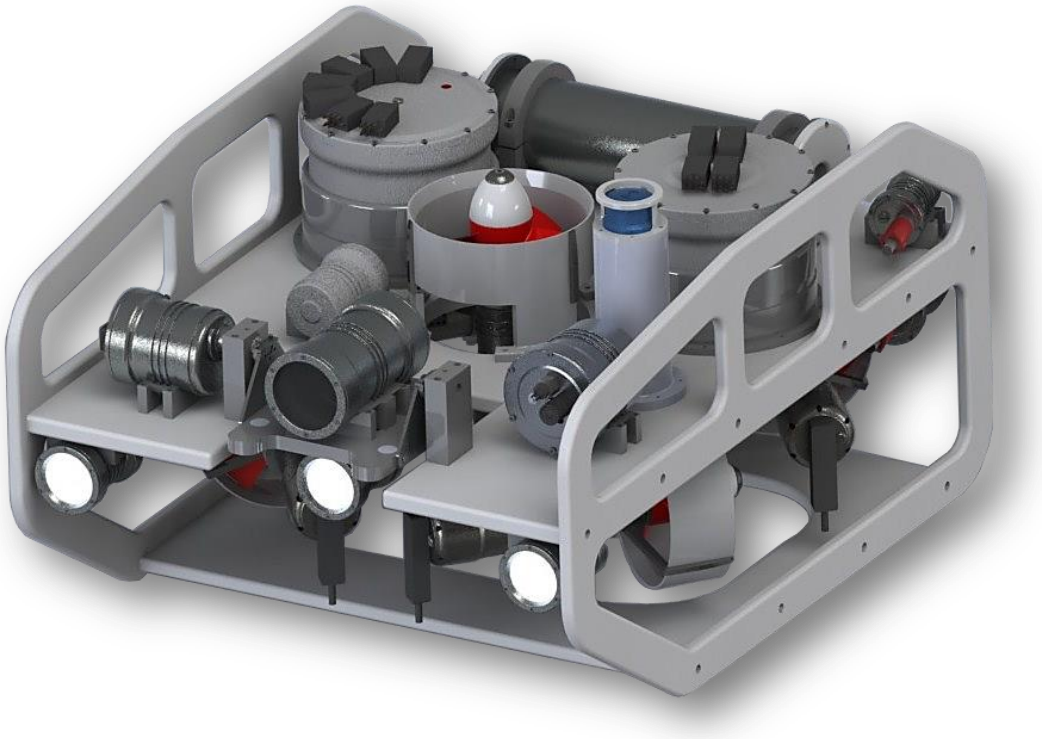

Figure 2: Rendering of the final ROV design without its cover and float block

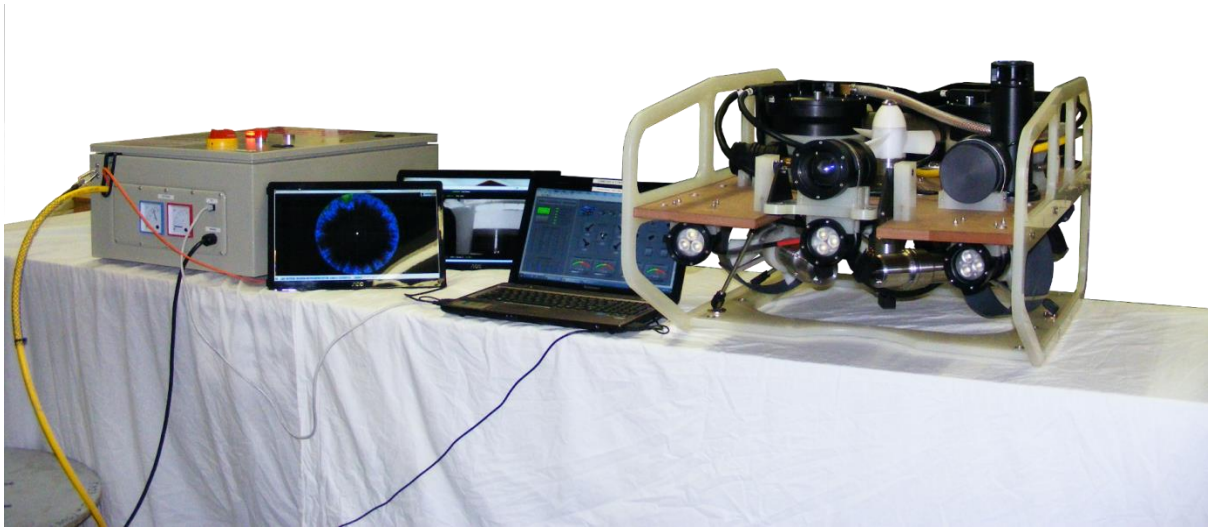

Figure 3: Photo of the ROV (without cover and float block) alongside the surface power supply and user interface

1.1 A REQUEST FROM THE DEPARTMENT OF ZOOLOGY

In 2009 the UCT Zoology Department put forward a request to UCT's Robotics and Agents Research Laboratory (RARL) to design and build an underwater remotely operated vehicle (ROV) that would be used by the Zoology Department's researchers to collect subsea environmental data and video footage.

The Zoology Department staff and students were regularly using scuba-diving equipment to go diving themselves and collect data, seawater samples and capture footage of marine life. These diving operations were easily and safely performed to depths of 30 m, but deeper than that, divers needed to start using mixed gases and the risk of injury due to decompression sickness also started to increase. The Zoology Department had also been using sensor pods that could be lowered to great depths over the side of a boat to collect data and water samples, but had no means to safely and cost-effectively search for targets deeper than 30 m, such as marine animals or shallow reefs.

The need for an unmanned, remotely operated vehicle that could deliver live video footage and environmental data to the surface was what drove Ms Andrea Plos of UCT's Zoology Department to approach the UCT RARL and request the design and manufacture of a low-cost ROV.

1.2 THE OLDER GENERATIONS THAT HAVE GONE BEFORE

After establishing a set of specifications with the Zoology Department, the RARL started on the first of its underwater ROV designs which was set as a final-year undergraduate project. *Challenger I* was the name of the ROV and it can be seen in Figure 4. The ROV was built by three students and an attempt was made to cover all systems requested by Zoology, including a manipulator arm with three degrees of freedom and a system for collecting water samples.

In addition to the basic ROV light, camera and thruster systems, the design of *Challenger I* had incorporated a gripper, active buoyancy control and a water sampling unit. However it had been built as a prototype and although rated for 60 m operating depth, it did not manage to achieve this with all its modules intact. *Challenger 1* had provided the RARL with some experience with ROV design, but it was decided to start over with a simpler and more robust design, while aiming to operate the vehicle in deeper water.

Figure 4: Photo of Challenger 1 [1]

The next year ROV *Robin* was designed and built as *Challenger 1*'s successor, also as an undergraduate final-year project. *Robin*'s body was manufactured as one complete welded assembly of stainless steel tubing, as seen below in Figure 5. The body was a lot more robust than that of its predecessor and had been rated for an operating depth of 160 m as agreed with the Zoology Department.

Figure 5: Robin, the second generation ROV from the Robotics and Agents Research Laboratory [2]

Similar to *Challenger 1*, *Robin* incorporated an electronics that housed its power supply, control electronics and camera. However, *Robin* had only three thrusters as opposed to the five thrusters used on *Challenger 1,* foregoing only the ability to thrust laterally. The gripper, water sampler and active buoyancy were done away with on *Robin* so that the design could be focused on getting the basics working well with the limited resources of time and undergraduate students available. A float block was used on *Robin* to provide its buoyancy and steel weights were added to trim the vehicle in the water.

Robin was also fed with a 230 VAC power supply, as was *Challenger 1*, and used on-board converters to supply the required DC power buses to the ROV's components. Communication between each of the ROVs and their respective user interfaces was provided by a TCP/IP protocol Ethernet link over a standard Cat5e network cable. On both of these ROVs the TCP/IP protocol was used for the video feed from the ROV's cameras. The TCP/IP protocol was converted on board the ROVs to RS-232 signals using Tibbo® DS1206 device servers to interface with the on-board control systems.

Before commencing with the design of the ROV for this project, *Robin* was thoroughly tested to assess whether it was to be developed further or whether a new ROV design was to be started, based on the experience of the first two ROVs.

Through an analytical process, it was decided to redesign the ROV using an open frame design which was commonly used on many commercially available ROVs. This style of ROV allowed for the modular design of all of its subsystems which would provide an advantage for maintenance and future modifications. A rendering and a photo of the final design is shown in Figure 2 and Figure 3.

1.3 SCOPE OF THIS PROJECT

Once the decision had been made as to what type of ROV was to be designed, the scope of the project for each of the two students working on the ROV design needed to be decided. Initially it was thought that the frame, float block, surface power supply unit and user interface would be worked on together to provide a common platform to which each student would add further components which had been developed separately. Thomas Knight was to focus on the two camera systems, the lighting system and the thruster design, while the author focused on the on-board power supply, electronics pod, navigation system and sensor payload.

However, as the project progressed, it became clear that the initial scope was too large to complete for only two students within the time allocated. It was realised that much more attention than anticipated would need to be given to the power and communications distribution system for the ROV, which would form the backbone of its operation. Some non-critical items were identified for future students to develop, while the systems critical to get the ROV up and running were re-looked at and the scope for both students was revised and the allocation to each student is shown in Figure 6.

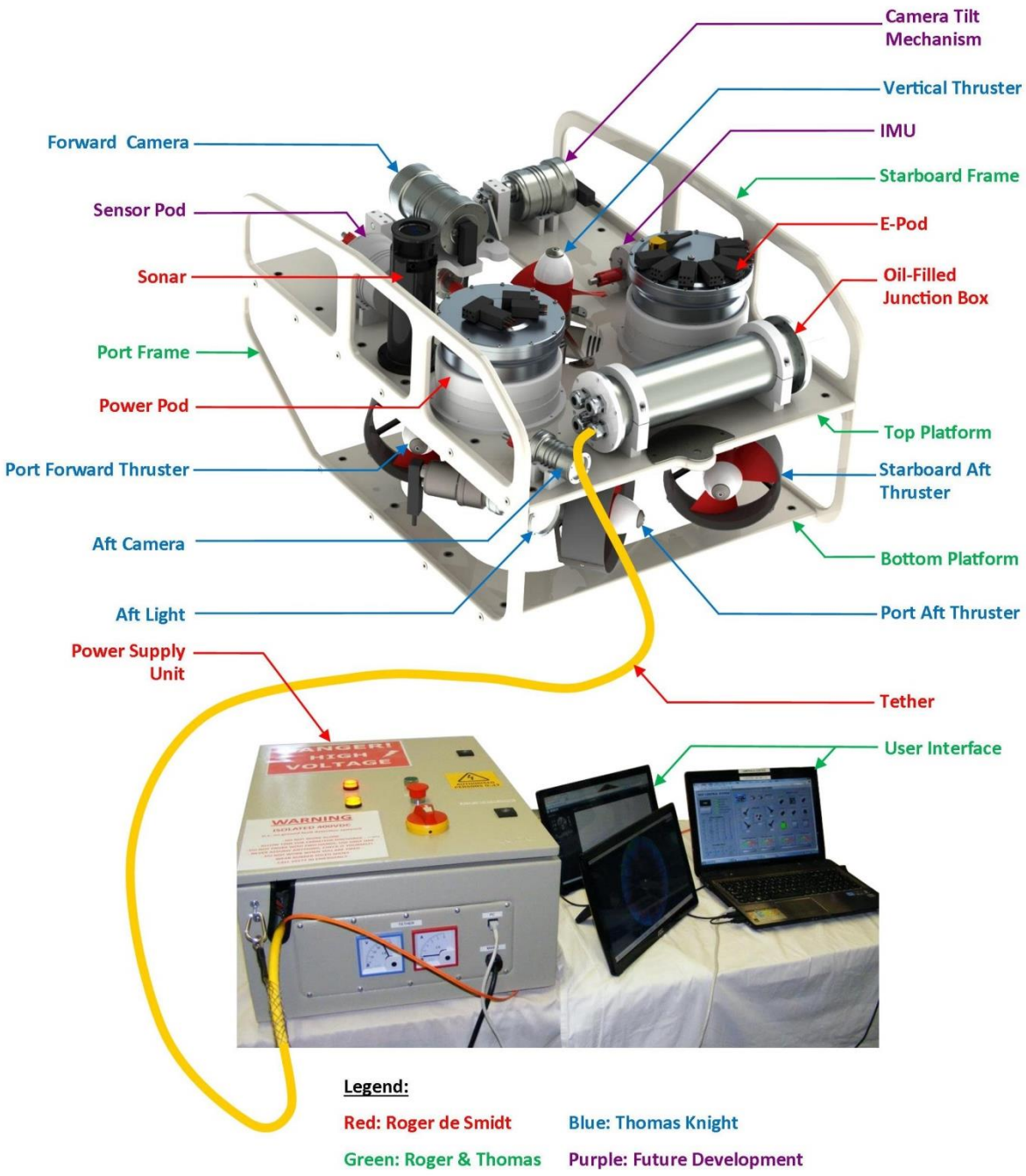

Figure 6: Diagram showing the distribution of ROV components between the project scopes for the author, Thomas Knight and future students

The scope of the project covered in this report includes primarily the power and communications distribution system, but also incorporates a brief description of the sonar unit and the design of components worked on by both students. The primary components of the power and communications distribution system are the user interface, the power supply unit, the tether, the junction box, the Power Pod and the Electronics Pod. These are indicated in Figure 6 above.

The final design of the ROV incorporated a 2kW, 400 VDC power supply (see Figure 6) that fed the ROV's on-board Power Pod via a neutrally buoyant tether and junction box. The tether included both

copper power conductors and optical fibres for communications and the junction box was used to separate them so that the power conductors could be fed to the Power Pod and the optical fibres to the Electronics Pod. Power was fed at low DC voltages from the Power Pod to the Electronics Pod and was distributed together with RS-485 serial communications to each of the ROV's modules. Freescale® MC9S08GT16A microprocessors were used as slave controllers in the Power and Electronics Pods to control the distribution of power and communications. A Labview® user interface was developed to provide control of the whole ROV system at the surface control station. Photos of the Power Pod and Electronics Pod, which together provided the electrical backbone to the ROV, can be seen below in Figure 7.

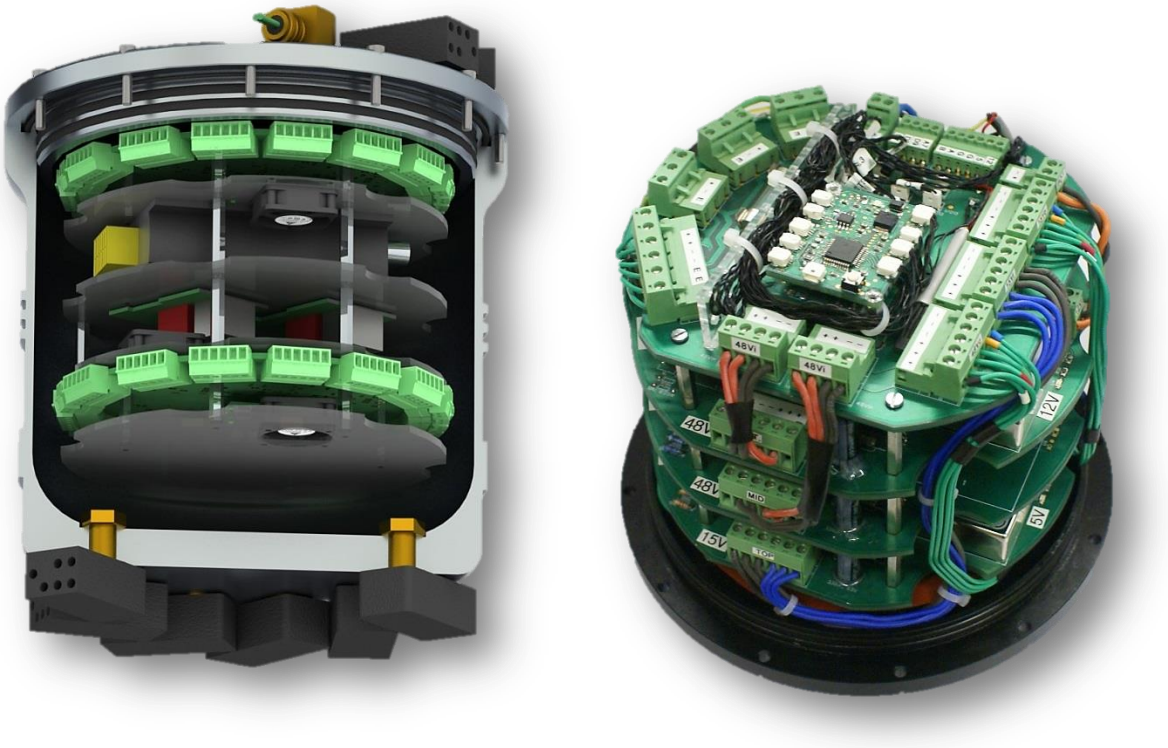

Figure 7: Rendered cut-away view of the Electronics Pod (left) and of the electronics stack assembled on the Power Pod lid (right)

The report that ensues serves to provide an account of the process and reasoning that was followed to establish the final design of the ROV's power and communications distribution systems.

The report starts by presenting some background information on ROVs and various technical aspects of the power and communications design. After this, some context for the design of these systems is provided by means of a description of the preliminary design for the overall ROV system. The report then proceeds to detail the design of the power and communications distribution system, starting with the Electronics Pod as the first subsystem in a bottom-up design hierarchy.

After the description of the design process, the procedures and results of the tests performed on the ROV systems pertinent to this project are presented in detail. Finally, conclusions are drawn, based on these results, and recommendations made for use in future development of the ROV.

2 BACKGROUND RESEARCH

2.1 UNDERWATER REMOTELY OPERATED VEHICLES

2.1.1 Introduction to ROVs

Underwater Remotely Operated Vehicles are commonly referred to as ROVs and are unmanned vessels that carry out underwater operations by remote control. The simplest ROVs carry only a camera and lights as tools and are used in shallow waters purely for observation and recording images of the environment. These simpler ROVs can be very small, some of them fitting into a briefcase-type box, making them conveniently portable [3]. On the other end of the spectrum, the most complex ROVs are designed for use in the maintenance and repair of deep-sea drilling rigs, pipe lines and cables, hundreds of meters below the ocean's surface. They are much larger and carry heavy industrial tools most often powered by hydraulics. These *work class* ROVs can weigh a few tons out of the water, and can be the size of a hatchback motorcar [4].

ROVs have great advantages over manned underwater vessels because they can be made much more compact without the cockpit space required for an operator. They are also not limited in their duration of operation because they do not depend on a limited oxygen supply. The risk associated with sending a person to great depth is also mitigated with the use of an ROV, and the comparative cost of designing to meet the required safety regulations for a manned vessel is also discounted in the use of ROVs. ROVs can also be designed to work at depths far beyond the reach of divers, and are much more efficient when only observations are required at great depths [5].

ROVs come in many different shapes and sizes and are designed with many different capabilities. Reference has already been made to the different types of underwater ROV, which have been grouped into three different classes: *Observation* Class*, Work* Class and *Special Use* Class. The work and special use class ROVs are larger vehicles with complex, application specific equipment. This report deals with the development of an observation class remotely operated vehicle (OCROV) which is a smaller and more general category of ROVs and therefore only the systems and components of ROVs of this class are discussed in this report.

2.1.2 Observation Class ROVs

Observation class ROVs come in a range of sizes, but can be grouped into two main categories. One is the "mini ROV" group, which describes ROVs designed for high portability and quick and easy deployment by one person. These ROVs can weigh just a few kilograms, but are typically less than 20kg out of the water. Examples of commercially available mini ROVs are presented in Figure 8 through Figure 10.

Figure 8: JW Fishers™ Sea Otter 2 [6]

Figure 9: SeaBotix® LBV150 [7]

Figure 10: VideoRay® Pro 4 [3]

The other group is the "general ROV" which essentially encompasses the rest of the observation class. These ROVs are bigger, more powerful and a number of these larger vehicles were designed for much deeper operations than the mini ROVs. Examples of commercially available general observation class ROVs can be seen below in Figure 11 through Figure 14. Selected specifications for each of the seven ROVs shown on this page are listed in Table 1.

Figure 11: Teledyne's new Stingray [8]

Figure 12: Outland 1000 [9]

Figure 13: SAAB Seaeye Falcon [10]

Figure 14: Seatronics Predator [11]

Table 1: Selected physical and performance specifications of some commercial observation class ROVs

Specification	Sea Otter	Seabotix LBV150	VideoRay Pro4	Teledyne Stingray	Outland 1000	Seaeye Falcon	Seatronics Predator
Max. Depth [m]	227	150	305	350	300	300	300
Length [mm]	584	530	375	1220	660	1000	900
Width [mm]	406	245	289	460	381	600	620
Height [mm]	305	254	223	460	267	500	450
Mass [kg]	19.5	11	6.1	32	17.7	55	65
Fwd Speed [kts]	3	3	4.2	>3	-	>3	>3
Fwd Thrust [kgf]	5.4	7	-	18	15	50	-
Payload [kg]	-	-	-	2.5	2.3	14	10
No. Thrusters	4	4	3	4	4	5	5
No. Lights	2	Internal array	2	2	2	2/3	6
Power Input [W]	600	1000	800	2500	1800	2800	3000

While observation class ROVs are used primarily for inspection tasks, many have been designed to carry a payload of tools that can easily be fixed to the ROV chassis. Manipulators are a common example of such a tool, and can be used for light-duty intervention tasks such as sample retrievals and cutting of ropes or small cables. Other common tools are scanning profiling sonars, imaging sonars and Doppler velocity logs [12]. Examples of these extra tools can be seen attached to the bottom skid of the *Outland 1000* and *Falcon* in Figure 12 and Figure 13 respectively.

Below is a list of some of the applications of observation class underwater ROVs at the time this report was written [5][11]:

- Oil & Gas platform inspections
- Diving support
- Leak detection on subsea oil or gas pipelines
- Deep ocean floor observation and sample collection
- Wind-farm surveys and inspections
- Ship hull and propeller visual inspections
- Police search and recovery in dams, lakes, rivers or in the ocean
- Harbour quayside inspections
- Dam inspections
- Fisheries research
- Fish-farm inspections
- Oceanographic survey
- Under-ice surveys
- Bridge inspections
- Deep-sea cable inspections

2.2 ROV COMMUNICATION SYSTEMS

Data transmission through water is limited to just less than 100 kilobytes per second which is not sufficient bandwidth to stream high quality video, sonar data and control signals between ROVs and their surface control stations [5]. A tether is therefore required to carry dedicated conductors or conduits that will provide the necessary communication bandwidth which can be tens of megabytes per second.

The communications specifications of several commercial ROVs were acquired and compiled in Table 2 below.

Table 2: Communication protocols of some commercial observation class ROVs

ROV	Operating Depth	Surface/Subsea Data Transmission	Onboard Data Transmission
Outland 1000 [9][13]	300 m	RS-485 + video differential pair	RS-485 + video
Seabotix LBV's [7][14]	150-950 m	Optical Fibre + RS-485/RS-232	Unknown
Seaeye Falcon	300 m	RS-485 (x2) + video differential pair	RS-485 + video
Seaeye Falcon DR [12]	1000 m	Optical Fibre	RS-485 + video
VideoRay [15][16]	76-300 m	RS-485/CAN Bus + video differential pair	CAN Bus + video + RS-485/RS-232/TTL

2.2.1 Serial Communication Protocols

There are a vast number of serial communication protocols that have been developed and standardised, but it is the robust industrial protocols that can operate over long distances that are of interest for communication between the surface and the ROV. On board the ROV robust, reliable protocols are again of interest, but over much shorter distances. Several of these proven industrial protocols are listed and described briefly below.

2.2.1.1 RS-232

The Recommended Standard 232 (RS-232) is a serial digital data communication protocol that was developed in the early 1960s. It was developed as a full-duplex protocol primarily for use between a computer and a peripheral device, but has been used in multi-drop networked systems with limited functionality. RS-232 was designed to be robust so that systems would generally not be damaged if the incorrect gender of connectors was used and wires were connected incorrectly. Over the years the standard has changed to incorporate faster drivers that can provide data speeds up to 1 Mbps, which is way beyond the original 20 kbps specified by the standard [17][18][19].

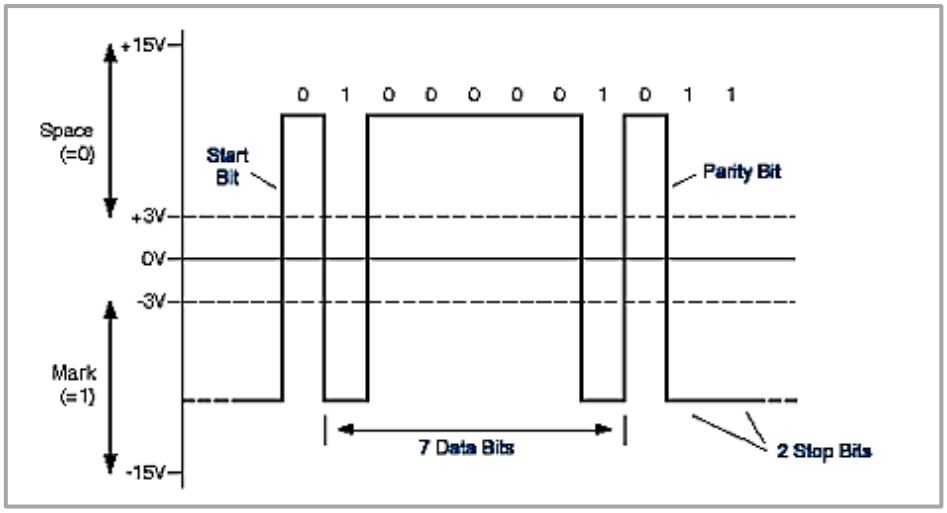

Figure 15: A typical RS-232 line signal for RS-232 data [20]

The RS-232 signal swings between a positive voltage of +5 to +15 V and a negative voltage of -5 V to -15 V. Each receiver has a threshold of ±3 V, which provides a minimum of 2 V common mode rejection. Figure 15 above shows a typical signal for one byte on an RS-232 line. RS-232 can be implemented with or without flow control, and has a minimum of 3 wires required – transmit, receive and signal ground.

The RS-232 standard specifies a maximum driver load capacitance of 2500 pF which limits the cable length between two points because of the inherent capacitance that is found in cables. A maximum cable distance of 50 m is stated in the standard, but realistically cables can be much longer provided the capacitance of the cables does not reduce the slew rate of the data signals such that it affects its reliability [19][21]. No official tables relating baud rates to maximum cable length could be found, but some estimated cable lengths and corresponding maximum data speeds can be seen in the table below.

Table 3: RS-232 maximum cable lengths for given baud rate [21]

Baud Rate [bps]	Max Distance (Shielded Cable) [m] (ft)	Max Distance (Unshielded Cable) [m] (ft)
110	1524 (5 000)	914 (3 000)
300	1524 (5 000)	914 (3 000)
1 200	914 (3 000)	914 (3 000)
2 400	305 (1 000)	152 (500)
4 800	305 (1 000)	76 (250)
9 600	76 (250)	76 (250)

Methods have been developed to enable implementation of multi-drop RS-232 networks. One commonly used method is a star configuration for the network where one controller acts as a master and multiplexes communication with several slave modules [22]. The number of slaves on a star network is limited because the minimum driver output impedance is 3 kΩ.

Another method is to daisy-chain the several slave modules. Each slave module sends the data on to the next slave unless the data address corresponds with its own. This configuration allows up to 256 nodes on the network because separate transceivers are used for receiving and sending on each slave. The signals transmitted sequentially from slave to slave, and consequently the total length of the system can be *n* cable lengths for *n* slaves. However, this system has greater risk factors because each slave is dependent on the one before it for its signals.

An alternative variation is for the hardware to be designed so that the impedance on the lines of each slave's port can be switched. This enables all the slaves to connect to one line and "listen" until addressed, at which stage they will switch into communication mode, process the data and respond if required. This configuration limits the overall distance between the master and the last slave to one cable length.

2.2.1.2 RS-485

The Recommended Standard 485 (RS-485) is a differential serial digital data communication protocol that specifies bi-directional half-duplex data transmission. It is the only Electronics Industry Association (EIA) standard that allows multiple receivers and drivers in "bus" configurations [23]. The RS-485 standard only specifies the electrical layer which affects the specifications for transceivers, and does not specify the structure of the data to be sent.

The differential signal voltage range is specified to fall between -7 V and +12 V. Driver signals range from between -1.5 V and +1.5 V to between -6 V and +6 V. Receiver sensitivity is set to acknowledge differential signals lower than -200mV and above +200mV. This means that any difference greater than 200mV between the differential pair will, depending on its polarity, produce either a high or a low signal. The differential pair is usually transmitted on a twisted pair of wires and each node on the network referenced to the same ground potential. The differential pair provides good immunity to noise and is often used on factory floors for process automation where electromagnetic noise is often high. Typical line signals on the RS-485 A and B pair are shown below in Figure 16.

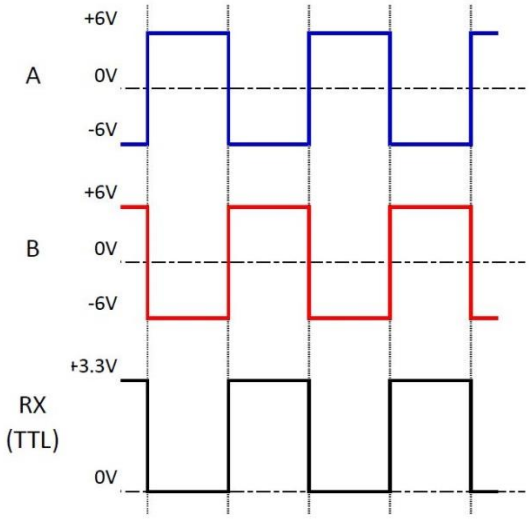

Figure 16: Typical line signals in an RS-485 system

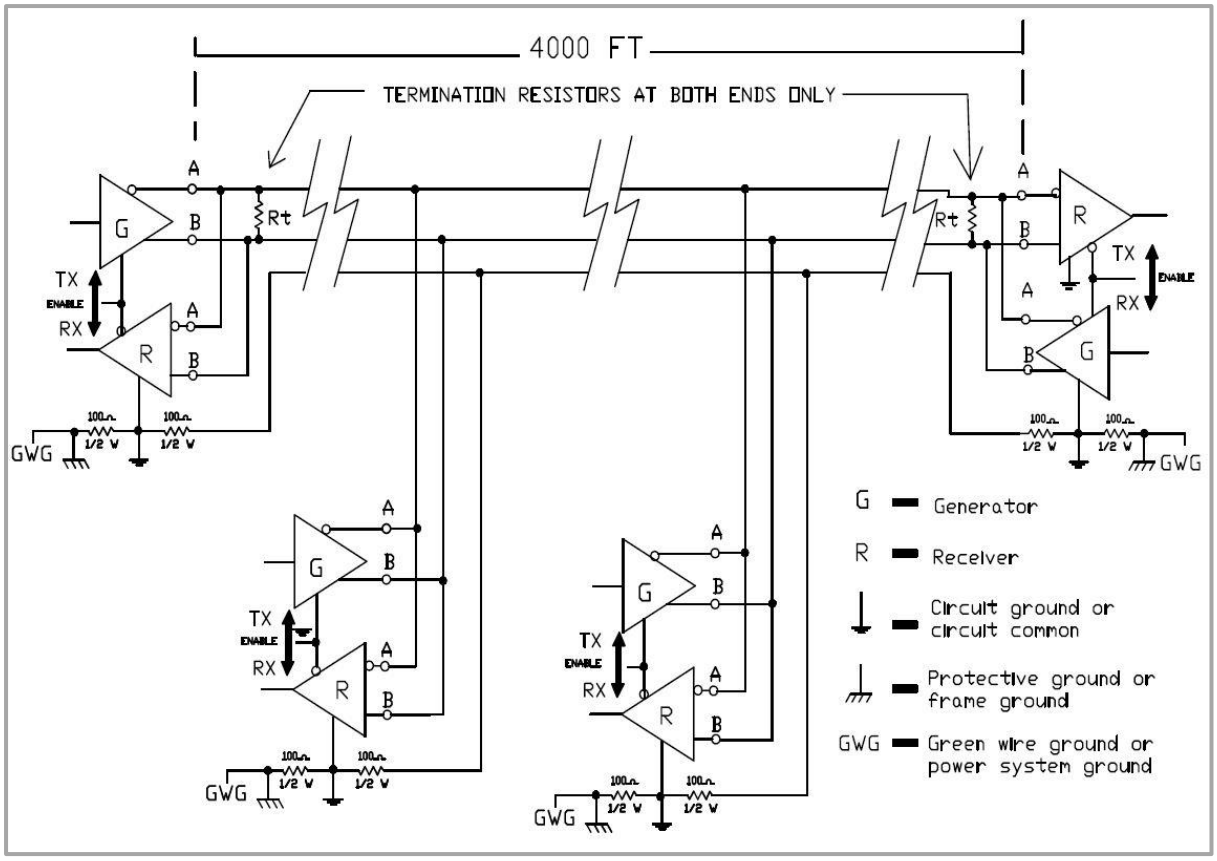

Figure 17: Typical RS-485 two wire multi-drop network [24]

Figure 17 above shows a typical wiring schematic for a RS-485 two-wire multi-drop network. The Standard allowed for a maximum of 32 nodes on one network, assuming 12 kΩ receiver impedance for all nodes. However, if higher impedance receivers are used, any number of nodes can be added, provided that any one driver does not see more than 32 unit loads (i.e. not less than 375 Ω). Communication is half-duplex so only one unit can transmit at a time, while all others "listen". The RS-485 protocol only specifies the physical layer and does not specify any structure for the communication of data. Protocols such as Modbus or CAN Bus are referred to below as options for defining a communication structure.

Figure 18 shows several different topology options for implementing a RS-485 network. The daisy-chain network was recommended as the least susceptible to signal reflections.

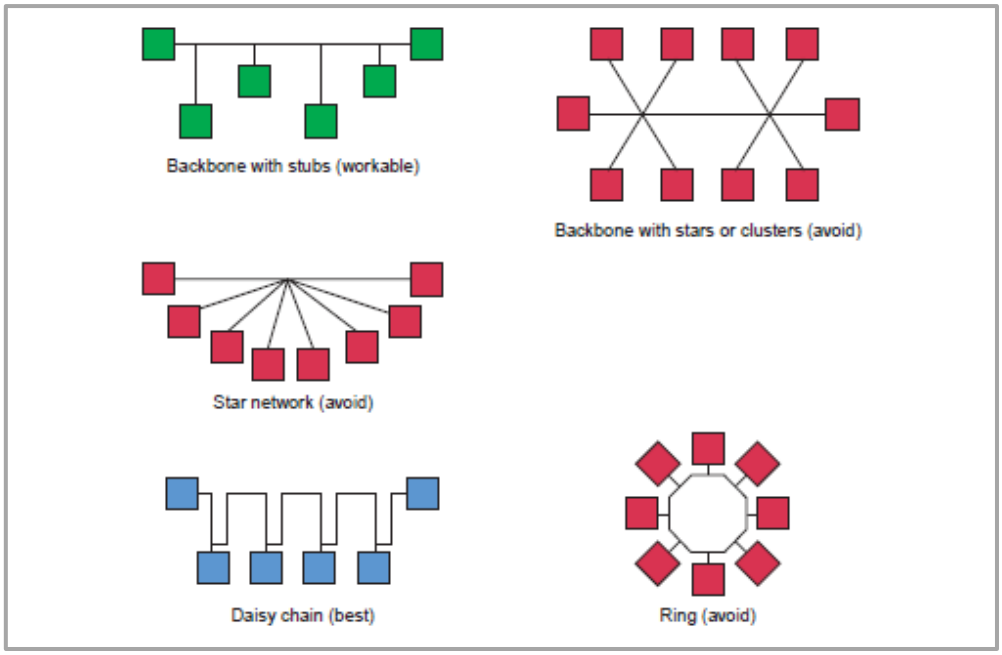

Figure 18: Common RS-485 network topologies [25]

RS-485 provides much faster data rates over much greater distances than RS-232 and approximate maximum cable lengths for given baud rates are presented in Table 4 below.

Table 4: RS-485 maximum cable lengths for given baud rates [26]

Baud Rate [kbps]	Max Distance [m] (ft)
90	1 220 (4 000)
280	305 (1000)
500	152 (500)
2 000	30 (100)
4 000	12 (40)
10 000	4.6 (15)

2.2.1.3 Controller Area Network (CAN)

The CAN protocol was developed by Robert Bosch, primarily for use in the automotive industry, and the first CAN enabled microchips were put on the market in 1987. CAN is an asynchronous multi-master data bus that uses a method of configuring the priorities of each node to determine communication access. The protocol defines the physical layer and how data links to the stack of a microcontroller running a user defined application. Most CAN devices are manufactured as on-board peripherals on microcontrollers and typically transmit data at speeds up to 500 kb/s, although speeds up to 1 Mb/s over a distance of 40m are possible. The CAN device has different registers in which the standardised protocol can be set up, making it an effective way of standardising communication [27].

The CAN protocol allows up to 32 nodes on each CAN bus and requires that the devices on its network be configured with differing levels of priority to ensure that high priority components

receive or transmit their signals before lower priority components [27]. The two possible states on the CAN bus are either the dominant “0” state, that takes precedence over the recessive “1” state. The physical layer ensures that if any device transmits a dominant low bit, the state of the bus will become dominant too. The format of a CAN message is shown below in Figure 19.

An arbitration process is performed when more than two or more nodes start to transmit simultaneously, as shown below in Figure 20. The system facilitates the arbitration process that is carried out using the 11-bit identifier (or 29-bit for the extended protocol) that precedes the control, data and error-checking fields, as shown in the structure of a CAN message in Figure 19.

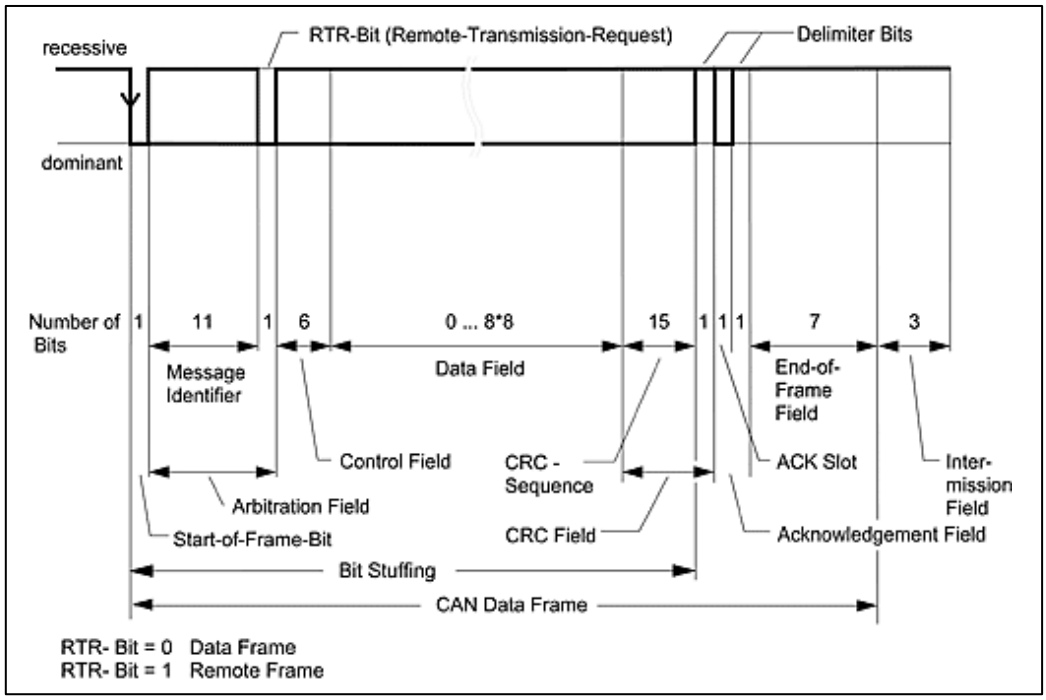

Figure 19: Format of a standard CAN message [28]

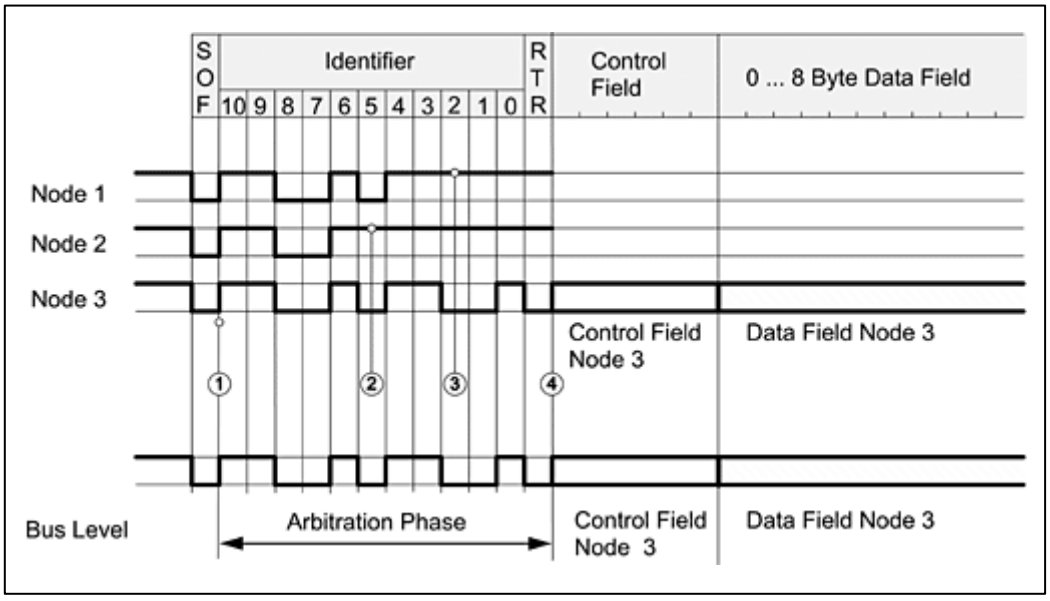

Figure 20: CAN bus bit-level arbitration [28]

Figure 20 shows the following: at point 1 nodes 1, 2 and 3 start to transmit simultaneously until at point 2 Node 2 senses that the bus has dropped to its dominant "0" state so it stops transmitting. The same occurs at point 3, where Node 1 detects a dominant state on the bus and also stops transmitting so that only Node 3 remains transmitting until it has completed sending its entire packet of data [28].

The worst case response times for messages sent on the CAN bus can be calculated in a scheduling model to ensure that critical components in the system will receive their messages in time [27].

While the CAN bus may have application to the ROV, CAN devices had not been used in the RARL at the time this project was undertaken and the primary microcontroller well-known to the RARL did not incorporate a CAN interface. It was also not apparent that CAN had been used on any commercial observation class ROV's research for this project. The CAN protocol would require a large amount of design and development to implement in the ROV. Due to time constraints it was decided not to pursue the CAN protocol for use on the ROV.

2.2.1.4 Modbus

Modbus was developed by a company called Modicon (now Schneider Electric) in 1979 as a standard protocol that specifies the structure of serial data transmission between many devices communicating over a single twisted pair wire. The structure of the Modbus protocol is independent of the type of network implemented (RS-485, TCP/IP or RS-232 for example). The protocol is a "master-slave" system where one master controls the communication with many slaves in a multi-drop configuration. Masters initiate all communication and slaves only transmit directly in response to a request for information from the master [29][30].

Due to the development time required to implement the MODBUS protocol and the fact that it had not yet been used in the RARL it was decided not to pursue this protocol for use on the ROV.

2.3 ROV Electrical Power Transmission Systems

ROV designers generally do not have the arduous task of specifying on-board battery power supplies because power is delivered together with communications via the tether. The voltage at which the power is delivered to the ROV determines the maximum current at which it will flow. Consequently, current demand determines the size of conductors needed in the tether. Also, the larger the tether the greater its drag in the water.

A survey of the transmission voltages and input power for some of the ROVs already referred to in this section was carried out, and compiled in Table 5 below.

Table 5: Input power and transmission voltages for some observation class ROVs

ROV	Power Input	Input Voltage	Depth Rating	Transmission Voltage
VideoRay Pro 4	600W	100-240 VAC	300m	74 VDC
VideoRay Scout	800W	100-240 VAC	76m	48 VDC
Teledyne Stingray	2.5kW	100-120/200-240 VAC	350m	150-300 VDC
Outland 1000	1.8kW	100-240 VAC	300m	165 VDC
Saab Seaeye Falcon	2.8kW	100-270 VAC	300m	500 VDC
Seatronics Predator	3kW	240 VAC	300m	400 VDC

From the information in Table 5 it can be seen that all the ROVs in this survey are running on a direct current power supply. DC-to-DC converters are then used on board each ROV to step the voltage down to one or more bus voltages. It can also be seen that generally as the power requirement of the ROV increases, so too does the transmission voltage.

Once voltages increase above 120 VDC, they are no longer considered Safety Extra Low Voltages [31] so protective ground fault detection (GFD) units are installed on all the ROV power supplies listed above in Table 5. These GFD units monitor the insulation resistance from the system to ground (earth) and when the resistance value falls below a pre-set value, alarm relays switch and the power supply is disconnected. Littelfuse® and Bender® are two leading suppliers of such systems and their respective GFD units are shown in Figure 21 below.

Figure 21: Littelfuse® SE-601 (left) and Bender® IRDH275 (left) ground fault detection monitors

2.4 O-RING SEALS

O-ring seals are the most common, and are claimed to be, the most effective method for sealing pressure vessels. O-ring seals are commonly used in an incredibly wide range of applications, many of which rely on the seal to protect an enclosure from water ingress and require the seal to be reusable. Providing a general seal that is resistant to liquid ingress at standard atmospheric pressures and temperatures can be accomplished with very little knowledge of O-rings. As long as the O-ring has a cosy fit in its gland (or groove), is squeezed to some degree when the vessel is closed, and does not hamper the closing of the vessel, the O-ring will generally keep liquid at the same pressure out.

However, when vessels operate at extreme pressures and at low temperatures, far more attention needs to be given to the seal design to ensure its integrity. High pressures, such as deep below the ocean's surface, will force liquid past a poorly designed or fitted seal. Low temperatures such as those experienced in the colder oceans of the world, reduce the O-ring's ability to flow into and mate with the grooves that it is sealing. If designed well, O-rings, on their own, can provide seals good for static pressures up to 103 bar (1500 psi). Above this pressure anti-extrusion back-up rings are required [32].

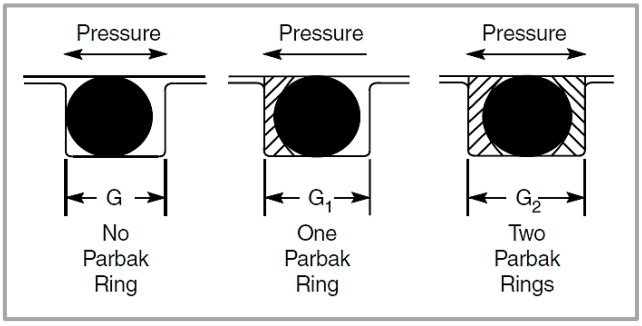

Figure 22: Static O-ring seals showing anti-extrusion back-up ring configuration options [32]

2.4.1 Static O-Ring Seal Types

Five types of static seals are shown below in Figure 23.

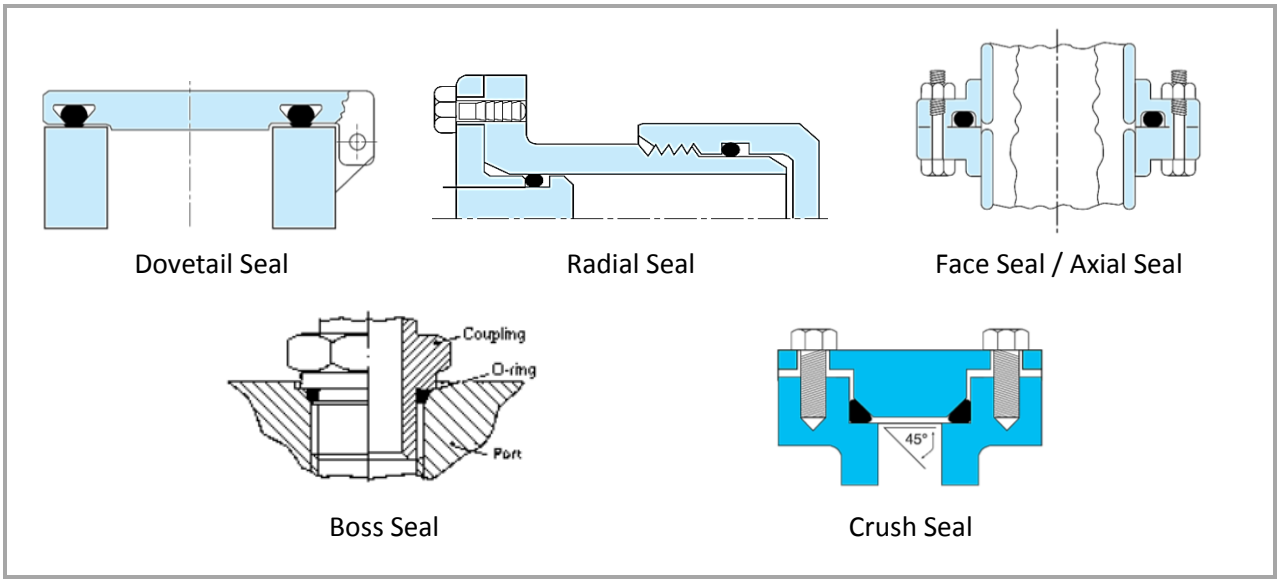

Figure 23: Different types of static O-Ring seals [33][34]

2.4.1.1 Dovetail Seals

Dovetail seals are more complicated to machine, but conveniently retain the O-ring for applications where the seal, such as a lid of a chamber, would be opened frequently.

2.4.1.2 Radial seals

For radial seal grooves the clearance between the plug (piston) and the throat (cylinder) has critical limits beyond which extrusion of the O-ring between the two surfaces will occur. The graph in Figure 24 below shows these limits for three different O-ring material hardness ratings.

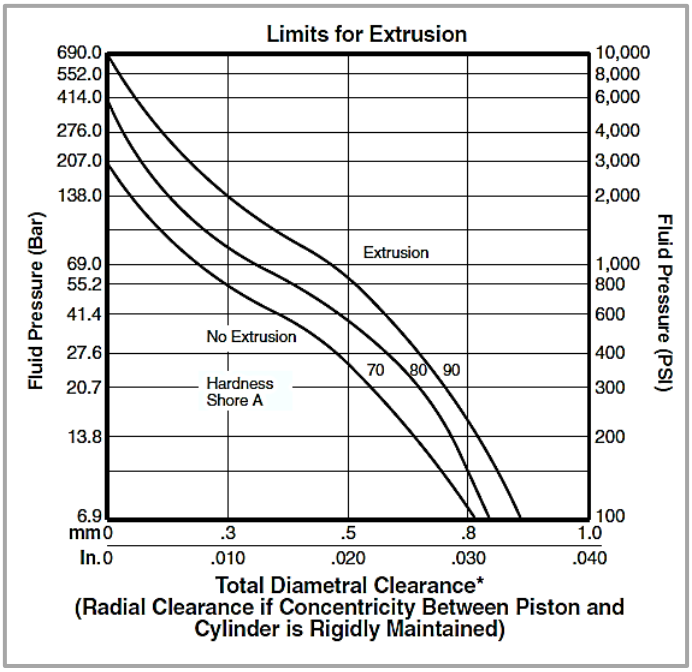

Figure 24: Diametrical clearance limits to prevent O-Ring extrusion [32]

The O-ring for a radial seal should be selected so that when fitted it will be stretched by 5% in length. Much more than this will reduce its lifespan, and much less than this will mean that it will not seat well in its groove. The images below in Figure 25 have been included to show the sealing action of the O-ring in a radial seal. The images also show how the O-ring is extruded through the clearance if the pressure difference across the seal is too great, the O-ring too soft or the clearance too large.

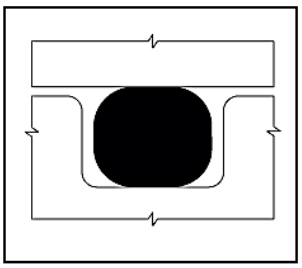

Figure 1-4: O-ring Installed

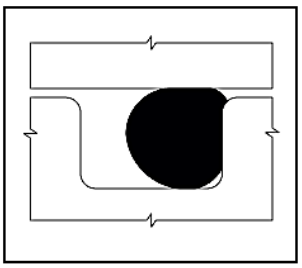

Figure 1-5: O-ring Under Pressure

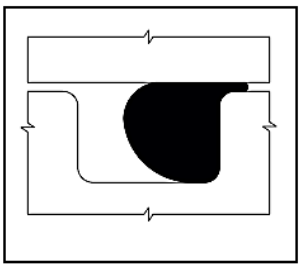

Figure 1-6: O-ring Extruding

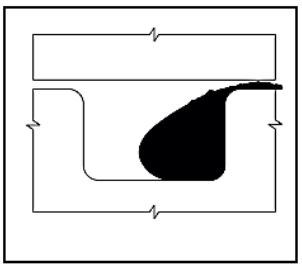

Figure 1-7: O-ring Failure

Figure 25: Excerpt from Parker's O-ring handbook showing progressive O-ring extrusion [32]

2.4.1.3 Face Seals

Face seals require a greater diameter than radial seals, but essentially perform in the same manner as radial seals. For face seals, it is recommended that, for external pressures, the O-ring inner diameter be designed to match the groove inner diameter with a tolerance of +1% of the mean inner diameter, but not more than +1.5 mm.

2.4.1.4 Boss Seals

Boss seals are used to seal straight threaded tubes that protrude as bosses, and provide more effective sealing than tapered threads used alone [33].

2.4.1.5 Crush Seals

In this seal the O-ring is crushed into a cross-section different to that of a standard gland groove. Crush seals are effective, but the O-ring is permanently deformed and is generally non-reusable [32].

2.4.2 O-Ring Materials

O-rings work so well as seals because of their material properties which allow them to deform and fill the clearances between sealing surfaces. There are a wide range of applications with differing chemical environments, temperatures and pressures which demand the correct selection of O-ring material to suit the intended application. Below in Table 7 is a list of some O-ring materials and their properties:

Table 6: O-Ring material properties [32][35]

Material	Min Temp [˚C]	Max Temp [˚C]	Resist Tear [kg/mm]	Resistance to Oil [P/F/G/E]	Relative Price [0-10]
Nitrile (NBR)	-34	121	0.45	Excellent	3
Neoprene®	-37	107	0.39	Fair/Good	4
EPDM Rubber	-57	121	0.43	-	5
Silicone	-54	232	0.20	Fair/Good	6
Viton® (flourocarbon)	-26	204	0.30	Excellent	7
Flourosilicone	-73	177	0.20	Good	8
Teflon® Encapsulated	-59	204	-	Excellent	9
Kalrez®(perflourinated)	-26	260	-	Excellent	10

2.4.3 O-Ring Glands

The O-ring gland is the space cut into the rigid material that contains and supports the O-ring [32]. The gland material, surface finish and dimensions are discussed below.

2.4.3.1 Gland Material and Surface Finish

For high pressure seals, it is recommended that the materials used in the sealing surfaces have a hardness of at least 55-60 Rockwell hardness C. The surface hardness affects the finish of the machined grooves. If the scratches in the material surface are sharp, such as after machining, the O-ring will not be able to flow into these cavities and the fluid may find its way through these miniature ducts. Turning grooves on a lathe produces scratches in the direction of the groove and is likely to provide a better seal than surface scratches incurred during milling when scratches may well run perpendicular to the groove. Surface finish in the base of the groove and on the mating surface is recommended to be between 0.4 and 0.8 µm, which should be achievable by fine finishing on a lathe or mill. Special attention should be given to softer aluminium surfaces to ensure a fine finish.

2.4.3.2 Gland Dimensions

In terms of the dimensions of the O-ring grooves, there are a few opinions on what the groove depth and height should be relative to the diameter of the O-ring. A summary of the design guidelines is presented in Figure 26 below.

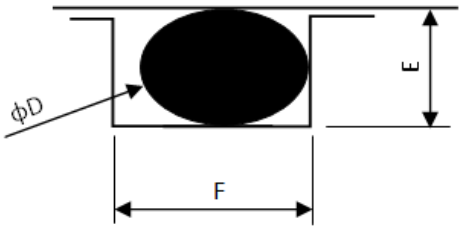

	Face Seal		Radial Seal	
D	**F**	**E**	**F**	**E**
0-2 mm	1.45D	0.75D	1.33D	0.72D
2-4 mm	1.3D		1.35D	0.8D

Figure 26: O-ring gland dimensions as per manufacturer design guidelines [32][33]

Advice was given regarding O-ring gland dimensions by an ROV specialist who had worked on ROVs for many years. Having seen what worked and what didn't, he advised that two adjacent radial seals be used and no face seals be used. His experience showed that the two radial seals were the most reliable and the face seal was redundant. A simple rule of thumb for radial gland depth and width as shown below in Figure 27 was considered to provide high reliability of the seals [36].

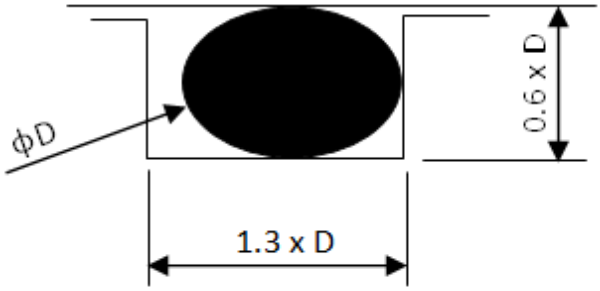

Figure 27: Radial O-ring gland dimensions as per ROV specialist's advice

2.5 ROV MARKET

The global ROV market was growing rapidly at the time this report was written. Annual expenditure on ROVs was expected to almost double from $891 million in 2010 to $1.7 billion in 2015 [37]. 50% of these sales in 2010 were to the oil and gas industry, while 25% was to defence and security and 25% to research. While the largest market drivers are in the oil and gas industry which use mainly *work* class ROVs, there was still a growing demand for *observation class* ROVs for use by organisations contracted to perform ocean rescues and port security tasks. As technology advances and sensor equipment becomes smaller, scientific researchers are expected to move towards smaller ROVs to minimise deployment and maintenance costs [38].

Table 7 below lists the budget prices of some commercially available ROV's at the time of writing. These prices were gathered to provide an indication of the price at which a new general OCROV design could be expected to sell.

Table 7: Budget prices and performance specifications of some commercial OCROVs

Specification	Depth [MSW]	Weight in Air [kg]	Surface Speed [kts]	Bollard Thrust Forward [kgf]	Power Input [W]	Budget Price
Mini ROVs						
VideoRay Scout	76	3.6	1.9	-	800	US $ 6.5k
Seabotix LBV-150-4	150	11	3	7	1 000	US$ 17k
JW Fishers SeaOtter2	152	19.5	3	5.4	600	US $ 20k
VideoRay Pro 4	305	6.1	4.2	-	-	US $ 50k
General Observation Class ROVs						
Teledyne MiniRover	300	41	>4	36.2	5 000	US$ 68k
SAAB Sea Eye Falcon	300	55	>3	50	2 800	ZAR 1.2m – 1.5m
Outland Tech 1000	300	17.7	-	15	1 725	US$ 40k

There was only one known ROV manufacturer in South Africa at the time of writing – SERS Group in Cape Town. SERS Group is a multi-national company servicing the offshore oil and gas industry. They manufacture a range of deep-sea tools, saturation diving equipment and ROV systems [39].

One of the largest ROV service providers in South Africa is Marine Solutions, also based in Cape Town. They provide support to the oil and gas industry in the Middle East and to the diamond mining industry off the Namibian coast [40]. They provide mainly technical services and also manufacture custom components for sea-floor crawlers, ROVs and divers.

2.6 CONCLUDING REMARKS

2.6.1 Observation Class ROVs

Observation class ROVs can be grouped into two categories – mini ROVs and general observation class ROVs. Mini ROVs are extremely compact and easily deployable by one person, but do not have capacity for much more than their standard set of sensors, cameras and lights. General observation class ROVs are larger, more powerful and have greater capacity to carry extra sensors or small manipulators and provide a more versatile platform for the Zoology Department's research and future development by the RARL. These general OCROVs are larger and usually require at least two people to be deployed, but underwater research teams from the Zoology Department never comprise fewer than two people due to safety requirements.

2.6.2 Communication Protocols

Most of these commercially available OCROVs used the RS-485 protocol to transmit control signals between the surface station and the ROV and separate conductor pairs for the video signals. Some ROVs, particularly the deeper 1000m depth-rated systems, were using the TCP/IP protocol over fibre optic media for communication between the surface and the ROV.

The RS-485 physical layer is the most commonly used protocol on general observation class ROVs and has been proven to provide robust communication over long distances in noisy environments. RS-485, in theory, has the potential to provide communication at 115 200 baud over a distance of almost 1 km, although ROVs working below 300 m depth tend to move toward a fibre optic link for communication with the surface control station, rather than towards RS-485. RS-485 has been around many years and there are many design examples available, making it a favourable choice for on-board communications.

2.6.3 Electrical Power Transmission

All of the commercially available OCROVs were supplied with DC power via their respective tethers. There was no clear indication why DC power was used and not AC, but the assumption is that DC-to-DC converters are generally less bulky than AC-to-DC converters and therefore take up less space in the ROV. The transmission voltages were high compared to standard mains voltage levels with several general OCROVs operating on 400-500 VDC. These higher voltages were used to provide the ROV with power at reduced currents, which allowed for smaller voltage drops and decreased I^2R losses in the tether.

2.6.4 O-Ring Seals

In order to keep all the electronic systems on the ROV dry, pressure vessels would need to be designed to contain the various systems. These vessels would need to be opened regularly for maintenance and therefore required a method of sealing that could be reused. O-rings are the primary seals used in the ROV industry and have proven to be highly effective at great depths.

There are several types of O-Ring seals, but the most widely used and recommended type was the radial O-ring seal. Two of these seals side-by-side provide the most reliable seals that are also easy to reuse.

Design guidance for the O-ring seals was available in a selection of O-ring manufacturers' handbooks and recommendations were also provided by ROV specialists.

2.6.5 ROV Market

The international ROV market was in a booming growth period at the time this report was written, with the oil and gas industry being the dominant driving force. However, there was very little manufacturing of ROVs happening in South Africa and it seemed that there was opportunity for growth in this industry in the South African economy. Manufacturing costs for the project would be limited to the available resources of the RARL and Zoology Department. To be competitive with commercially available ROVs the final design of a general OCROV should not sell for more than US$64k, which was the average of available ROV pricing presented in Table 7.

The conclusions drawn above were used to draw up specifications and begin the design of a new general observation class ROV. These specifications and the overall system design are presented in the next chapter.

3 ROV SYSTEM DESIGN

This section provides an overview of the entire system design and covers some of the preliminary design work and decision making processes that were required before the components of the power and communications systems could be developed in detail.

A list of the specifications drawn up for the ROV is presented and is followed by a description of the decision making process for which style of ROV was to be used. The various subsystems of the ROV are then described to complete the system overview.

3.1 SPECIFICATIONS

Table 8: ROV Specifications

Number	Description of Requirement	Target Values
	Functional Specifications	
3.1.1	ROV class	Gen. Observation
3.1.2	Number of pilots and assistants	1 pilot + 1 assistant
3.1.3	Maximum number of people required to deploy ROV	2
	Physical Specifications	
3.1.4	Maximum operating depth	160m
3.1.5	Mass	65kg
3.1.6	Forward speed	2kts
	Electrical Specifications	
3.1.7	Input voltage	230 VAC
3.1.8	Maximum input current	15A
	Communication Specifications	
3.1.9	Communication media between surface and ROV	Fibre optic 100BASE-FX
3.1.10	Data speed over tether	30Mbps
3.1.11	Max. period for one communication cycle with all modules	0.5s
3.1.12	Min. number of video channels available	2
	Tether Specifications	
3.1.13	Buoyancy	Neutral
3.1.14	Max length	350m
3.1.15	Quantity and type of optical fibres in tether	2 x Multimode
3.1.16	Number of copper power conductors	3
3.1.17	Rated working load	70kg
	Camera Specifications	
3.1.18	Forward-facing video tilt range	-90° to +90°
3.1.19	Aft-facing video camera	Yes
	Sensor Specifications	
3.1.20	Sensors	
	Depth gauge	Yes
	Sonar	Yes

	Sonar arc of operation	360°
	Sonar range	50m
Safety Specifications		
3.1.21	Isolated power supply	Yes
3.1.22	Ground fault detection on power supply output	Yes

3.1.1 ROV Class

The ROV was being built for a research environment and could be required in the future to have capability to carry additional sensor payloads and tool skids. It was therefore decided to design a general observation class type ROV and not the smaller, more limited “Mini ROV”. The larger general observation class ROV also lends itself more easily to modular design of all the on-board subsystems.

3.1.2 Number of Pilots and Assistants

The ROV was not to be cumbersome in operational overheads. Most general OCROVs are operated by one pilot and often assisted by one person to co-navigate and/or handle the tether.

3.1.3 Maximum Number of People Required to Deploy ROV

The pilot and his/her assistant should be able to deploy the ROV together, without assistance from any other personnel.

3.1.4 Maximum Operating Depth

As shown in Figure 28, there is a large shelf to the south and to the west of the South African coastline that does not exceed 200m in depth. The west coast contains numerous undocumented reefs that researchers from the Zoology Department wanted to explore using the ROV. A 300m depth rating for the ROV would comfortably provide for operations along the South African coast.

Should any commercial opportunities transpire from the project, a 300m depth rating would also be competitive with currently available ROVs such as the Seaeye Falcon, Predator and Outland 1000.

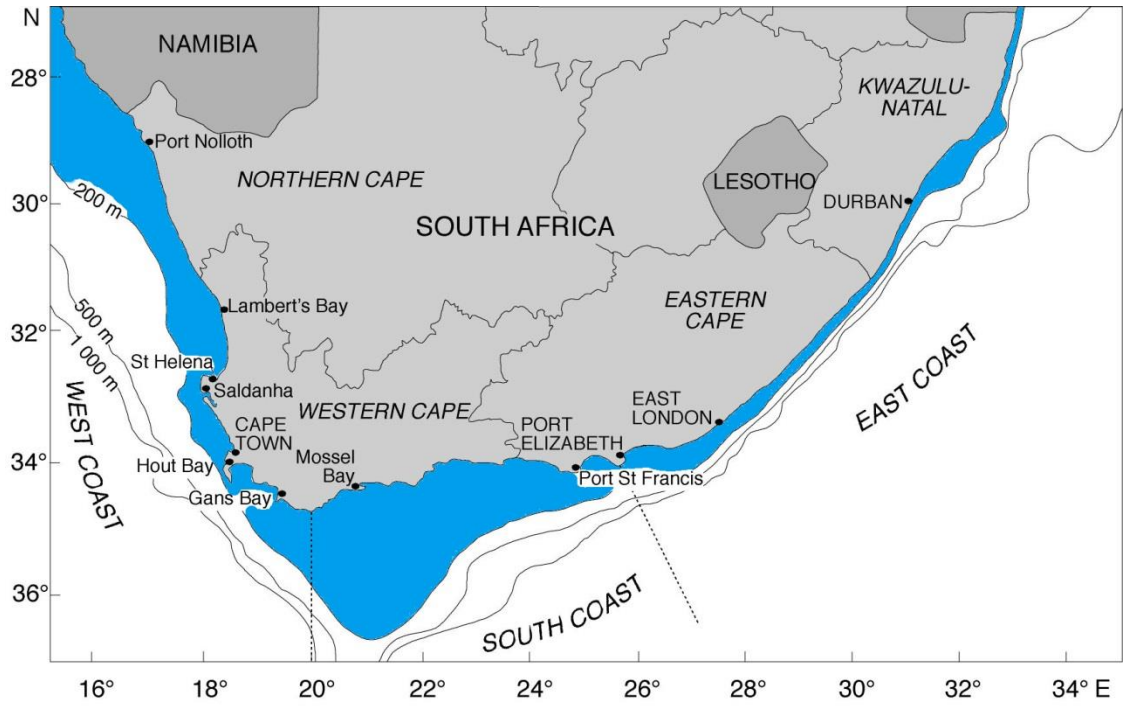

Figure 28: Chart of the South African coast with waters from the shore to 200m depth highlighted [41]

3.1.5 Mass

The ROV mass was not to exceed that which would be reasonably easy for two people to deploy and recover when operating over the side of a boat. The commercially available ROVs with a similar depth rating range in mass from 25kg to 65kg.

3.1.6 Forward Speed

The ROV was to be able to hold its position when motoring forward into a 2 knot current at the surface [42].

3.1.7 Input Voltage

230 VAC is the standard single-phase mains supply voltage in South Africa

3.1.8 Maximum Input Current

Most mains sockets in South Africa are rated for 16A.

3.1.9 Communication Media between Surface and ROV

The RS-485 communication protocol transmitted over a twisted pair in the tether was found to be the most common method of communicating control information between the surface control station and the ROV. This required at least one extra pair of conductors to transmit the video signals through the tether, and RS-485 is limited to roughly 200kbps over a distance of 300m. Because this ROV would be a platform for researchers, both Zoologists and engineers, it was decided to provide a large bandwidth connection between the surface and the ROV. This would provide capacity for additional equipment, such as High Definition (HD) cameras or an on-board computer, in the future.

A D-Link® media converter had already been acquired by the author's research group which provided 100BASE-FX data transmission over multimode optical fibre up to 2 km in length.

3.1.10 Data Speed Over Tether

The required bandwidth for communication over the length of the tether was determined by adding the data requirements as shown in Table 9 below.

Table 9: Tether bandwidth requirement

Communication	Bandwidth [Mbps]
Control (RS-485)	0.2
Sonar (RS-232)	0.1
4 x Video @ 6 Mbps each	24.0
Headroom/Spare	5.7
Total	**30.0**

3.1.11 Maximum Period for One Communications Cycle with all Modules

The operator should not perceive a noticeable lag in the response of the ROV control system. 0.5 seconds was therefore determined to be the maximum allowable period for one communication cycle between the operator controls and all modules on the ROV. All efforts were to be made to reduce this period so that the vehicle would be as responsive as possible.

3.1.12 Minimum Number of Video Channels Available

The main forward-facing camera would be one of the primary instruments on the ROV and at least one more channel was required for redundancy or for a second view.

3.1.13 Tether Buoyancy

A tether that was either negatively or positively buoyant would require constant upward or downward thrusting by the ROV and would make controlling the ROV unnecessarily complicated for the pilot. The tether was therefore to be neutrally buoyant and should certain applications require a positively or negatively buoyant tether, floats or weights could be attached along its length.

3.1.14 Maximum Tether Length

350m of tether would allow a vertical descent of 300m and an operational area with a radius of about 50m around the deploying vessel. In reality this radius would be a lot larger because the tether would follow the vehicle and not necessarily hang vertically down. Excessive length was not desirable because of the expense of the tether and the power loss in the tether which increases with distance.

3.1.15 Quantity and Type of Optical Fibres in Tether

A minimum of 2 multimode fibres were required for communication via the D-Link® media converter. These 2 lines would be the transmit (Tx) and receive (Rx) pair.

3.1.16 Number of Copper Power Conductors in Tether

Three power conductors were required: one for earth and two for positive and negative DC power.

3.1.17 Rated Working Load of Tether

The minimum working load for the tether was determined by adding 5kg for an optional payload to the 65kg mass specification for the ROV.

3.1.18 Forward-Facing Video Camera Tilt Range

The ROV would not be designed with any ability to pitch. In order to be able to see above and below without adding extra camera modules, the main camera would be designed to tilt through a full 180° arc, from vertically up to vertically down.

3.1.19 Aft-Facing Video Camera

An aft-facing camera was required so that the pilot could monitor the tether at the rear of the vehicle. This was anticipated to avoid fouling it when moving astern and to manage the number of turns in the tether.

3.1.20 Sensors

Depth gauge

Knowing the depth of the vehicle would be critical locating the vehicle, navigating it to its targets and protecting it from descending below its maximum rated depth.

Sonar

Visibility below the water's surface is often limited to a metre or less. A sonar would be required to navigate the ROV to its target once the ROV was out of sight of the operator. A full 360° sensing angle and a 50m range was required to provide sufficient information to orientate the pilot.

3.1.21 Isolated Power Supply

An isolated power supply would provide a higher level of protection for operators of the ROV. The output of the power supply could then be ungrounded and therefore not referenced to Earth. This would leave both positive and negative buses of the output floating. If a person were to make contact with one of these buses accidentally, that bus would be brought to the same potential as the person and the other bus would shift accordingly.

3.1.22 Ground Fault Detection on Power Supply Output

Because the power supply output would not be grounded, a special ground fault detection device would be required to monitor the isolation between each output bus and Earth potential, and trip the output switchgear if there was a fault.

3.2 INITIAL ROV DESIGN DEVELOPMENT

3.2.1 ROV Robin

Robin was the 2nd generation ROV built by undergraduate students in UCT's RARL in 2010 as the successor to *Challenger 1* and can be seen in Figure 5 and below in Figure 29. *Robin* was the starting point for the design of the 3rd generation ROV, which is the subject of this report. *Robin* was to be fully tested and, if possible, re-used so that only specific systems would be developed further, as required.

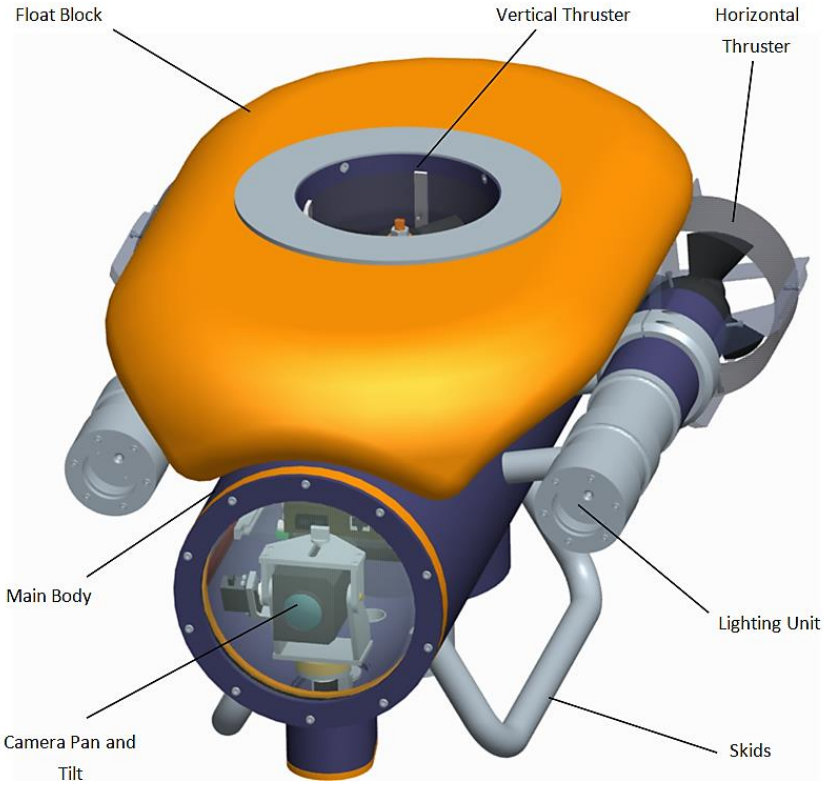

Figure 29: Rendered image of the 2nd generation ROV, Robin [2]

Robin was propelled by two longitudinal thrusters, which also provided steerage when driven at differential speeds, and a vertical thruster positioned at the centre of gravity of the vehicle.

The power and control electronics were housed together inside the body and incorporated the main forward-looking camera, a downward-looking camera and downward-looking light. As seen above, the forward-facing lights were integrated into the front of the port and starboard thruster housings.

The rendered image in Figure 30 shows the bare structure of the main body which was made from stainless steel piping for the main electronics housing, the vertical thruster pipe and the skids, and mild steel for the rest of the body. All these components were welded together to provide the strength and sealing required. The ROV was designed to operate at a depth of 160m and

penetrations through the body for wiring were avoided, apart from that for the tether, so that the risk of water leaking into the ROV was minimised.

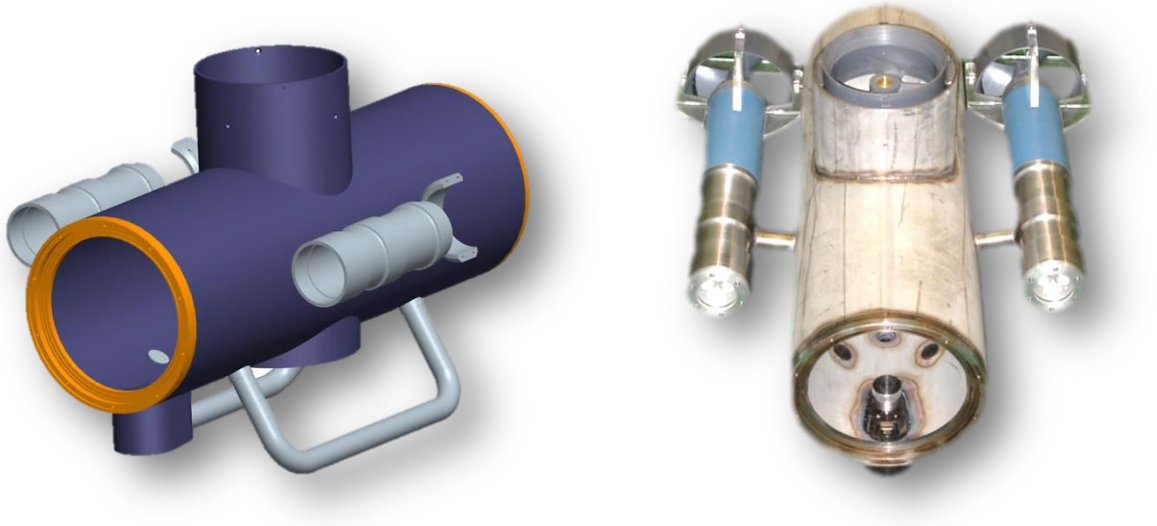

Figure 30: Rendered image of Robin's main body (left) and photo of main body with thrusters and lights installed [2]

Robin's tether carried power at 200 VAC through two conductors and Ethernet communications via an integrated Cat5e network cable. On-board the ROV, power was converted to 36 VDC for the thrusters, 12 VDC for the cameras and lights and 5 VDC for the control circuitry and network switch.

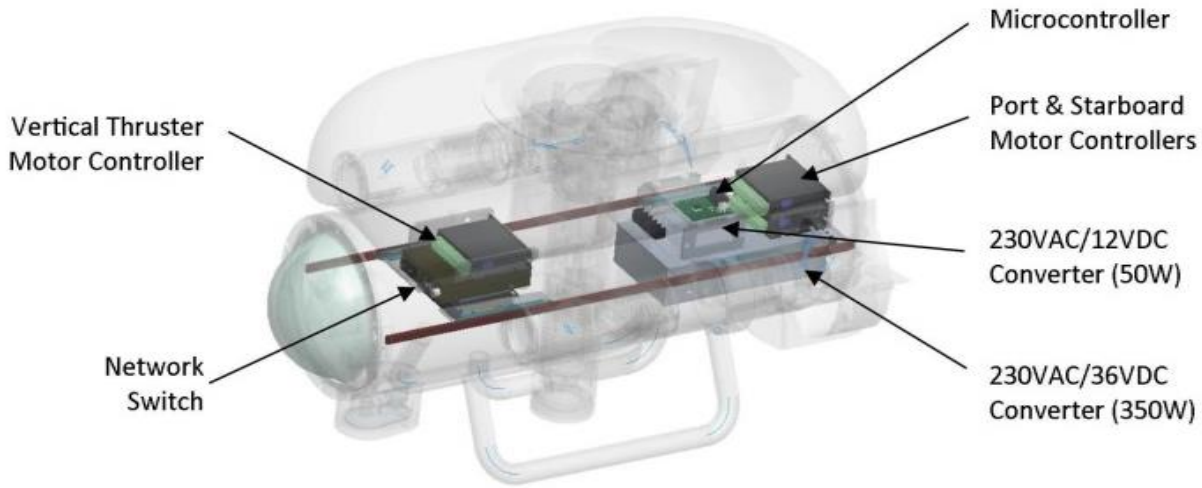

Figure 31: Rendered image showing position of electrical power and control components inside **Robin**

Although Robin was fit for pool tests when first commissioned, several systems have needed repair and re-wiring since then. These repairs and a few minor modifications were carried out so that a full assessment of the vehicle could be performed in an operational test. Robin went through a few pool test iterations and then was finally tested in a yacht club marina. Throughout these repairs and tests the ROV was assessed and Table 10, was drawn up. It lists the advantages and disadvantages of the

system. A full report on the tests and repairs performed on Robin can be found on the accompanying DVD.

Table 10: Advantages and disadvantages of reusing ROV Robin

Disadvantages	Advantages
Future modifications constrained to existing body dimensions	Bulk of ROV designed and built, only modifications and additions required
Mild steel components in body highly susceptible to rusting and would also provide magnetic anomalies for any compass added to the ROV in future	Some experience flying and repairing *Robin* already gained
Awkward to carry, even with two people	Good acceleration and response to controller input
Some welds leaked and needed re-welding – difficult to test the sealing integrity of welds, particularly before taking to full rated depth	Good surface speed of 2 knots (forward) and efficient hydrodynamic shape compared to many other ROVs
Vertical thruster very difficult to access for maintenance or repair	Good quality video image with very little distortion
Not tested to rated depth of 160m	ROV provided plenty lighting for video image
No navigational aids	

The Robin ROV had the basic systems to get the ROV moving and to provide a video feed to the pilot, but it would need sonar, a compass and a depth gauge to be added before it would be fit for use by researchers at depths of 160m. At a depth of 160m almost all natural light has been attenuated and the pilot would be flying the ROV blindly without these additional navigational aids.

3.2.2 Open Frame ROVs

The general observation class ROVs discussed in Section 2.1 are representative of the commercially available range of ROVs with similar performance. One of the key features in the construction of these ROVs was the open frame used as the chassis, onto which all functional modules were fitted (see Figure 32). This type of design lent itself to a very modular set of subsystems that could be relatively easily modified and changed with less of an impact on the rest of the vehicle. Also, if the equipment is all housed inside one pod, then one leak could damage it all. With an open frame design, the larger number of modules spreads the risk of damage due to leaks across the different modules, thereby reducing the probability of all the equipment being damaged at once in this way.

From a maintenance perspective, each component could also be easily isolated and swapped out just by unplugging the faulty component and plugging in a spare one – an advantage on time-critical missions or when operating from a small and uncomfortable vessel where repairs could sometimes be a stomach-turning reality.

Figure 32: Photos showing the open Frame designs of the old Teledyne Stingray (top), Falcon (left) and Predator (right) [8][10][11]

From a research and development perspective, an open frame type design would mean greater flexibility for future design changes and sensor payload options, but it would come at a large design and financial cost. All systems would have to be redesigned, assembled and tested by a design team of only two students. Furthermore the financial cost and machining hours required for a completely new system would require a huge portion of the research group's funds and would demand many hours from the Department's workshop. Table 11 below lists a complete set of advantages and disadvantages of designing a new open frame type ROV.

Table 11: Advantages and disadvantages of designing a new open frame type ROV

Disadvantages	Advantages
Restart design with small, two-man team	Modular design will allow greater flexibility for future modifications and interchangeability of components
Many more modules would need to be machined by a small workshop team	Greater depth possible which would be more competitive with similar commercially available ROVs
More external wiring and special subsea connectors required which would be a great expense, greater potential for water leaks and greater maintenance load	Options for different thruster configurations possible that could provide greater manoeuvrability
Large budget required to build new ROV	Simpler to integrate additional sensor payloads and tools
Generally a less efficient hydrodynamic shape than the existing *Robin* ROV	Modular system reduces risk of damage to entire system if one seal fails – any seal failures are confined to that one unit
Complete new set of test and modification iterations to be performed	Modular designs could provide scope for standardization and increase manufacturing efficiency
	Modular components could potentially be marketed and sold as replacement units for other commercially available ROVs

3.2.3 Preliminary Concept Design

Looking beyond the option of reusing *Robin*, one of the initial concepts for the new ROV was an open-frame design that combined features of *Robin* and of the older version of Teledyne Benthos' Stingray ROV (Figure 32). The concept incorporated an open frame constructed from welded stainless steel tubing onto which the various components would be fixed, as seen in Figure 33 below.

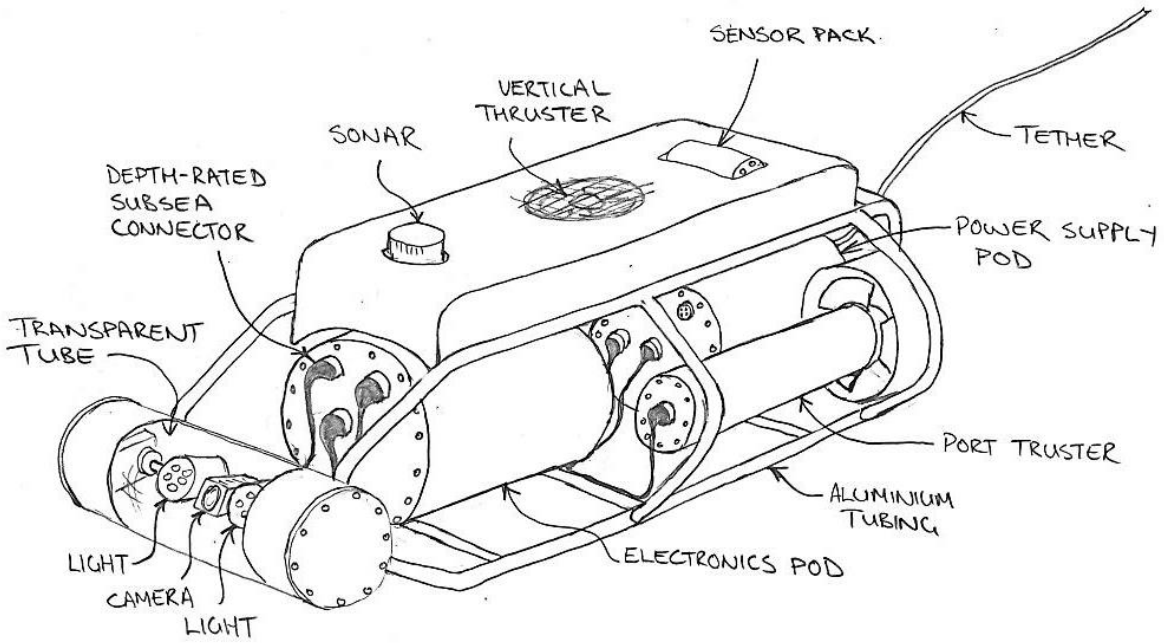

Figure 33: Concept sketches for an open frame ROV

The thrusting configuration was kept the same as *Robin's* proven 3-thruster setup and the electronics would again be housed in round cylindrical pods running fore and aft. However, these electronics pods would be split up with the power electronics in a pod aft of the vertical thruster and the control and communication circuitry sitting forward of it, allowing for easier access to each set of electronics. The forward camera and two lights would be fitted in their own pod at the front of the ROV. A tilt system would be integrated into the camera and light pod so that the lights would follow the camera through a full 180° arc from vertically down to vertically up. The sensor payload and sonar would be integrated into the float block.

With this design two disadvantages still remained. Firstly, the ROV still would not have the ability to thrust laterally, which would have provided for better manual position control and possibly autonomous position control in the future. Secondly, the welded frame was once again a monolithic structure that could not easily be modified without cutting and welding and was seen as a limitation for the flexibility of future modifications.

Realising these constraints and seeing that there was not much that could be salvaged from *Robin*, even in the concept above, a design based on the Seaeye Falcon and Seatronics Predator was pursued. An overview of this final design for the ROV is described in the next section.

3.2.4 The 3rd Generation ROV

ROV *Robin* had provided the design team with some good experience in ROV design and maintenance issues, but the scope of design going forward with *Robin* was limited. A budget of approximately R 335 000 was available to the team and it was decided that a new open frame type ROV would be designed to meet similar specifications to commercially available ROVs in its class. There would be a great deal of work to get through before focusing on the development of specific subsystems and some of the systems would be left to future students and researchers to complete. The open frame ROV would provide a much more flexible platform for future modifications and upgrades. The final design can be seen in Figure 34 below.

Figure 34: Rendering of the new 3rd Generation ROV

The four horizontal thrusters were set in a vectored thrust configuration that would provide greater manoeuvrability in close-quarters situations than the two aft thrusters on *Robin.* The thrusters were angled at 40° from the longitudinal midline of the vehicle. This provided the ROV with the ability to thrust in any horizontal direction by adjusting the speed and direction of each thruster according to a predetermined algorithm [5].

The electronics pod cylinders had been separated from the forward camera and were seated in a vertical orientation in the upper platform of the ROV, as seen in Figure 35 and Figure 36. An aft camera and light had been included to help manage the tether and navigate when thrusting astern. All the ROV components were fastened to the topside or underside of this upper deck and were covered by the float block, which is shown in red in Figure 34 above. Structural stability was provided by adjustable cross-bracing struts fitted between the upper and lower platforms. The major dimensions of the ROV can be seen in Figure 37 on the following page.

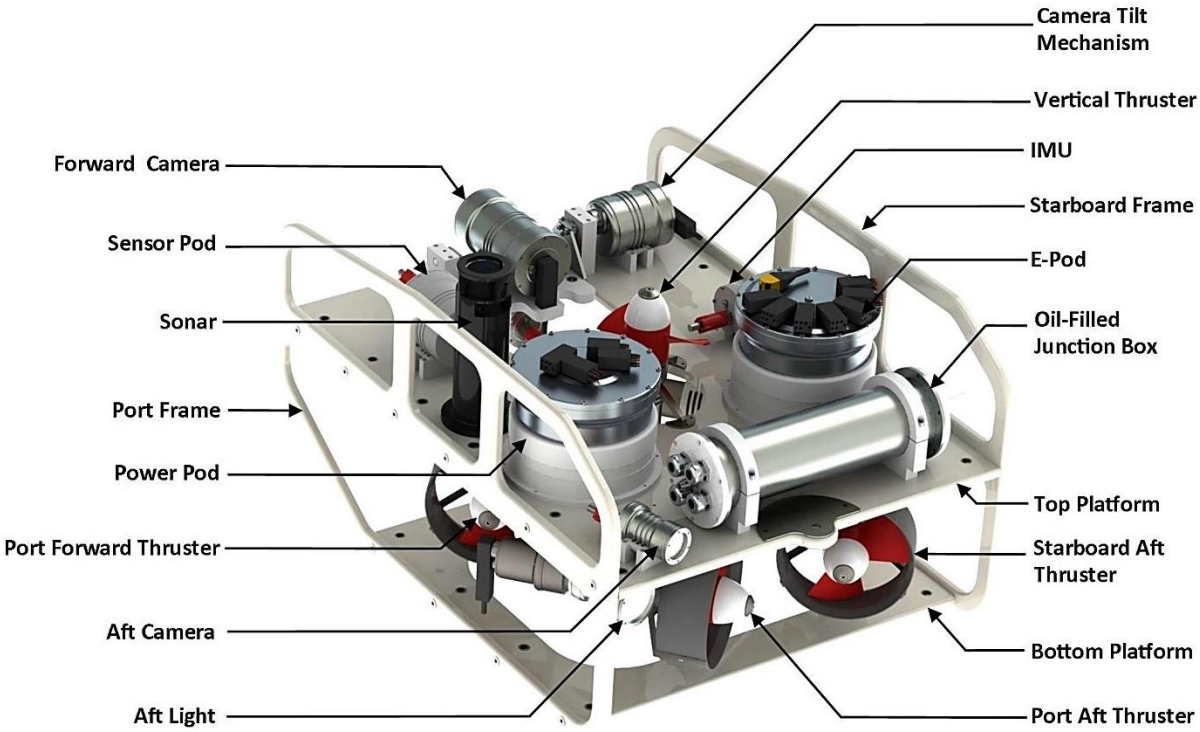

Figure 35: Rendering of final open frame design for the 3rd Generation ROV

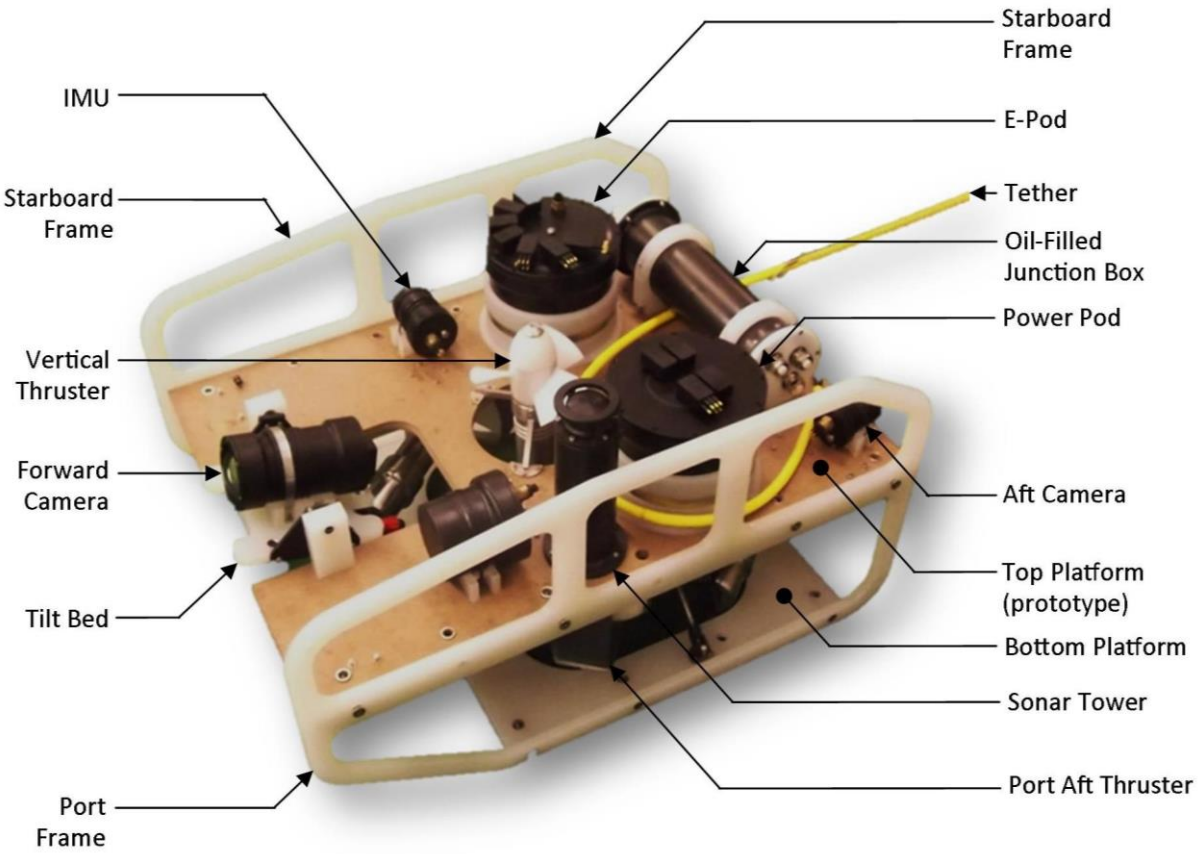

Figure 36: Photo of the 3rd generation ROV without its float block

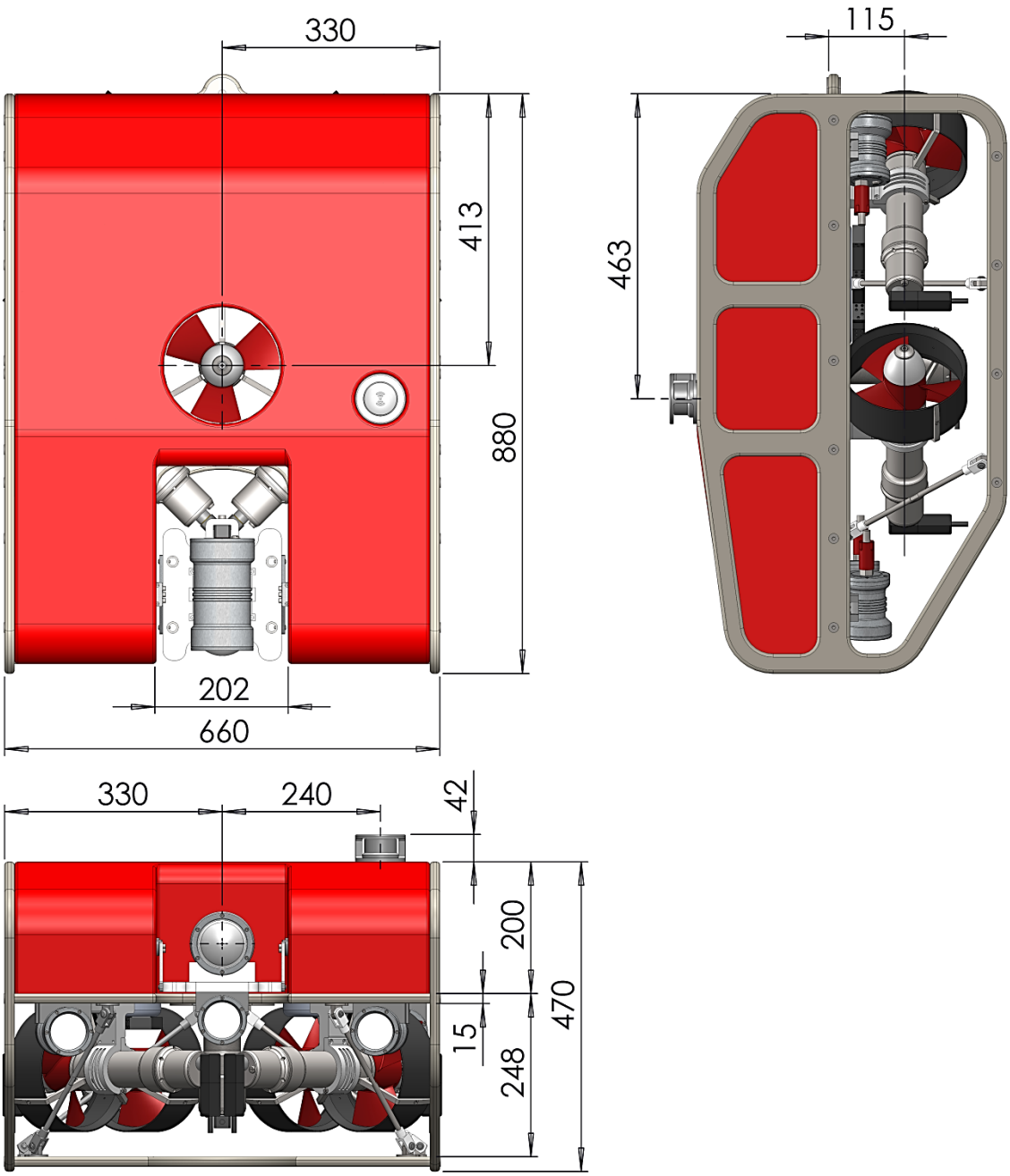

Figure 37: Dimensioned Renderings of the fully assembled ROV

This section has provided a brief overview of the final ROV design. The remaining sections in this chapter provide short descriptions of the design of the ROV modules that were not central to the focus of this report, but provide context for the design of the power and communications distribution system.

3.3 ROV FRAME DESIGN

The ROV frame was manufactured from plastic sheets and assembled with stainless steel fasteners. Polypropylene was chosen for the frame because it has very low water absorption and creep properties. Water absorption in the frame would cause it to swell, spoiling all fit dimensions and would potentially cause fasteners to pull through the plastic. Low creep properties meant that screws and nuts could be used to fasten components to the frames because the material would retain its shape when compressed by the tightened screws. Polypropylene is also a relatively flexible polymer and would absorb the impact from knocks and bumps that the ROV was bound to encounter.

Figure 38: Rendering of the ROV frame assembly

The method used to join the frames together was based on that used by the Falcon ROV. Tapped inserts of a stronger material were inserted into holes in the frame and used to fasten the stainless steel screws. This fastening system, using seamless stainless steel pipe for the inserts, can be seen in Figure 39 below.

Figure 39: Fastener system used to join the ROV frames

The photo in Figure 36 shows a wooden upper deck which was used for prototyping, at a lower cost than the polypropylene, because changes in layout were almost guaranteed during float, thrust and drag tests.

3.4 WATERTIGHT HOUSINGS

The effective protection of the electronic systems on board the ROV from water ingress was critical to the success of the ROV. There are two main options when it comes to the design of electronics housings for use underwater. The first is to design a housing that is strong enough to enclose the dry electronic components at atmospheric pressure and that will not collapse or deform significantly while operating at the rated depth. This approach would mean that housings would need to become stronger as the working depth increased, thus generally making the housings heavier and bulkier or much more expensive. The second option is to design a housing that will enclose the electronics in oil, which can be considered incompressible compared to air. The external pressure on the housing when operating at depth would be transferred directly into the oil bath which would not compress and therefore an almost zero pressure difference would be experienced across the walls of the housing. This would allow for the design of a much lighter housing that did not need to withstand much pressure at all. However, the drawbacks with this option are that the electronics would have to be rated for at least the same pressure and the oil-bathed components would be very messy to work with when performing maintenance and repairs.

The MBARI ROV *Tiburon* incorporated "data concentrators" as shown in Figure 40 below. Several of these "data concentrators" were part of a decentralised control network on the ROV. The housing was designed to be a combination of the two approaches mentioned above, with the electronics being housed in the dry titanium housing and all the wiring connections housed in an adjoining oil-filled junction box [43].

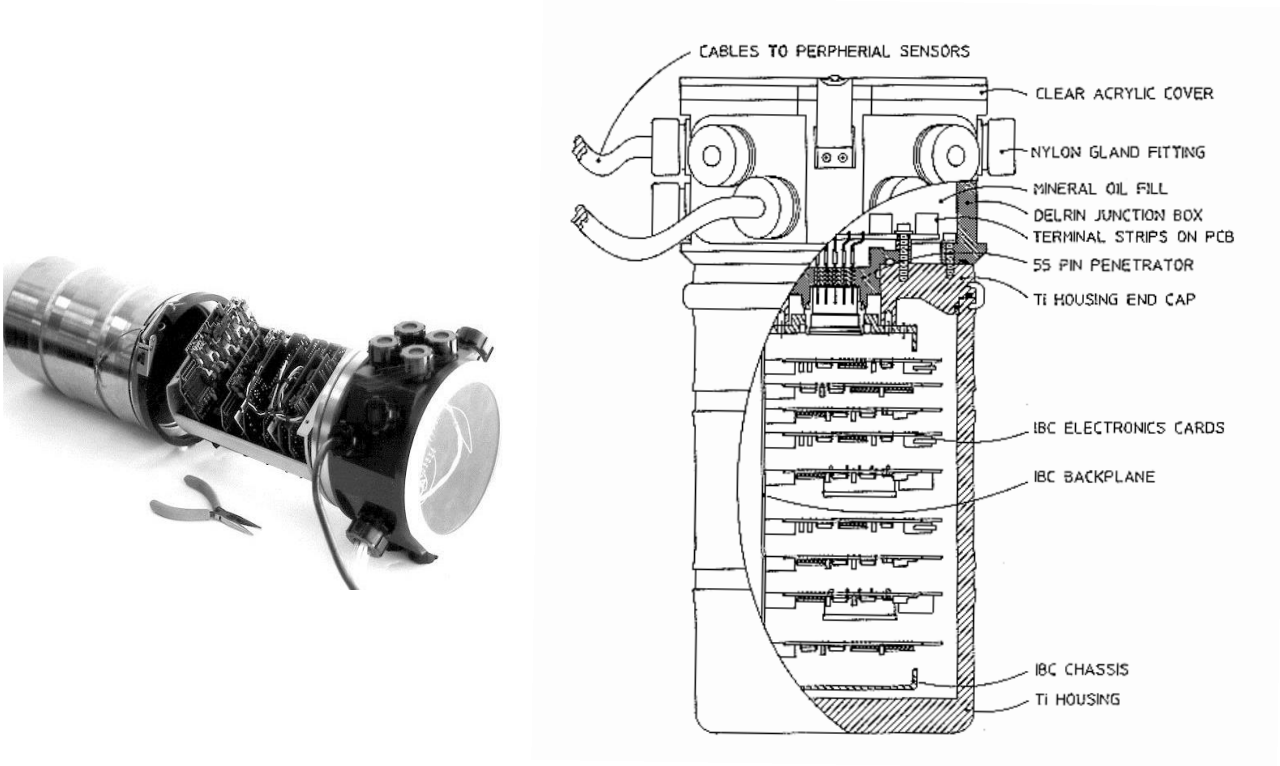

Figure 40: Photo of MBARI's ROV "data concentrator" (left) and its cutaway view (right) [43]

MBARI's *Tiburon* was a 4000m depth rated working class ROV so its electronics housings needed to be particularly strong. For most ROVs rated to 300m though, electronics housings were not oil-filled and it was decided to first pursue such a design so as to avoid the hassle the oil bath would be each time the pod was opened.

Anodised aluminium was the primary material of choice because of its strength to weight ratio and the fact that it was resistant to corrosion in salt water if well maintained. Stainless steel was used for the thruster modules where a lower conductivity in the housing was needed to reduce eddy currents in the magnetic coupling assemblies [42]. A full description of the pressure vessel design that was applied to all of the ROV housings has been included in Appendix C. Figure 41 below shows a photo of the Power Pod before anodizing.

Figure 41: Photo of the Power Pod's aluminium housing

All aluminium parts that would be exposed to sea water were hard-anodised. This process is similar to standard anodising, but is performed at a lower temperature and a thicker oxidised layer is formed. The standard thickness for the plant that anodised this ROV's components was 40 µm.

3.5 SUBSEA ELECTRICAL CONNECTORS

3.5.1 Copper Connectors

To provide a reliable and standardised connection method for the ROV modules it was decided to purchase industrial quality subsea connectors. Given the available project budget and the scarcity of time available for the project, it was not worth designing and producing connectors in-house. Birns® connection technologies were found to be the most cost-effective commercially available connector

and were supplied by their local agent, Marine Solutions. At an average price of R835 per connector the connection system was the single largest cost on the ROV.

The Birns® 6-pin Low Profile and Mini Connector inline and bulkhead connectors were purchased and can be seen in Figure 42 and Figure 43 below.

Figure 42: Birns® Low Profile Bulkhead connector fitted with acetyl spacer

Figure 43: Birns® Low Profile and Mini Connector inline connector joined together

3.5.2 Fibre Optic Penetrator

One of the challenges faced with the fibre optic link design was providing a water-tight connection for the optical fibres through the E-Pod housing. Commercially available hybrid subsea connectors, that would provide a watertight connection of fibre optics and copper cores, were priced at over £6 000 each from manufacturer Seacon® at the end of 2011. Although it would be very useful to be able to disconnect the fibre link from the E-Pod, it was too expensive to purchase these connectors and there was not sufficient time to design one from scratch. The alternative was to design some sort of penetrator that would provide a fibre link with a glanded seal through the E-Pod housing.

The penetrator was designed with dimensions similar to those of the Birns® low profile bulkhead connectors used throughout the ROV and manufactured using brass. A standard multimode fibre optic patch cord had its connectors removed from the one end and was fed through the penetrator and trimmed to the required length. Polyurethane potting compound was then used to fill the remaining spaces inside the penetrator and provide the necessary water-block. A photo of this process is shown in Figure 44. As seen in Figure 44 the penetrator was fitted with an O-ring face seal to prevent water leaking in between it and the penetration in the E-Pod lid.

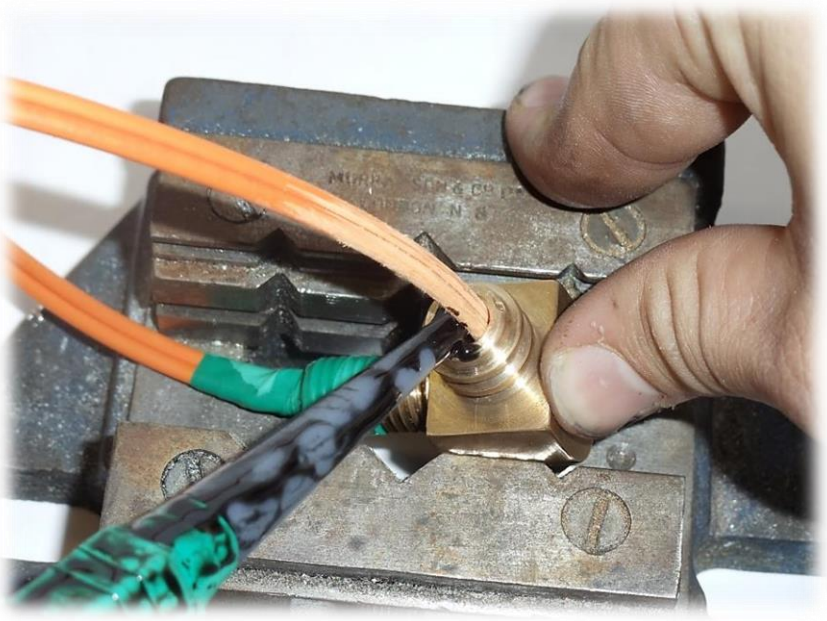

Figure 44: Photo of the penetrator being filled with polyurethane potting compound

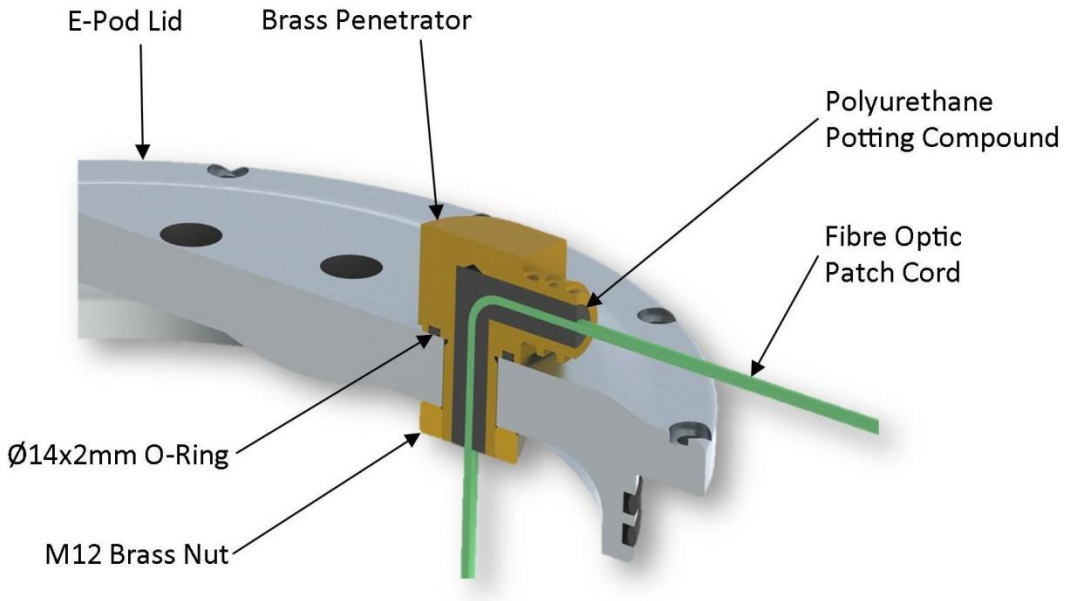

Figure 45: Rendering of the fibre optic penetrator fitted in the E-Pod lid

3.6 THRUSTERS, CAMERAS & LIGHTS

The thrusters, cameras and lights were the primary active components of the ROV, the design of which would determine the level of power required by the ROV.

These components were designed and built by Thomas Knight, as shown in Figure 6 in Section 1.3. The specific voltage and current specifications of each module are listed in Section 5, which details the Power Pod design. Further details on the design of the thrusters, cameras and lights can be found in Thomas Knight's dissertation [42] which has been included on the accompanying DVD.

3.7 SONAR

A Tritech Micron was bought by the research group early on in the project, before designs had been finalised. The Micron was one of the most compact and robust imaging sonars on the market at the time. The RS-232 version was purchased before the primary ROV communication protocol was changed to RS-485. Whether RS-485 or RS-232, a separate and dedicated channel would be required for the sonar so the hardware requirement would have been similar for either protocol. Initial tests found the unit to be working as shown by the sonar image of a swimming pool in Figure 46 below.

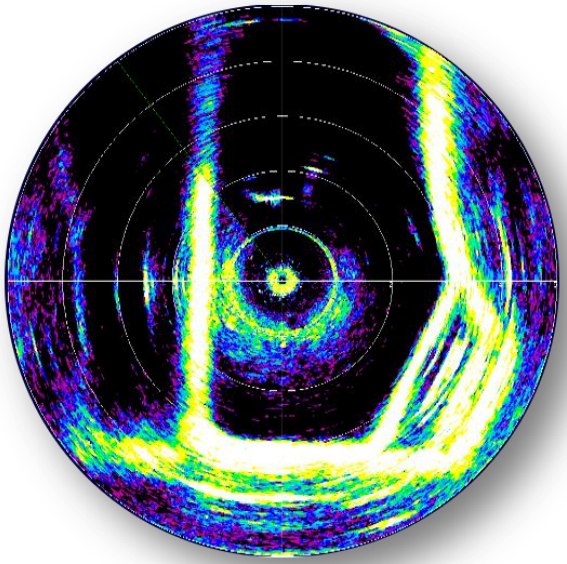

Figure 46: Sonar test image of swimming pool

Figure 47: Rendered exploded view of the Tritech Micron sonar, its tower-like base and its cap

The sonar tower was designed to house the sonar transponder such that it sat just proud of the body and had a protective covering, as shown in the rendering above.

3.8 SENSOR PAYLOAD

Two modules were designed to house the sensors required on the ROV. The first module was designed to house the pressure transducer, the microcontroller used to communicate with the rest of the ROV and a set of sensors requested by the Zoology Department to measure conductivity, oxygen concentration and pH levels. The second module was to house an inertial measurement unit (IMU) that also incorporated a gyro compass and a microcontroller for communication with the rest of the ROV.

Housings were manufactured for each of these modules, the IMU and pressure transducer were purchased, and provision was made in the control and power circuitry for them. However, these items fell beyond the scope of the current project and would be integrated fully in the future. The sensors requested by the Zoology Department required their funding and would be added in future as they became available. Renderings of the two units can be seen below in Figure 48 and Figure 49.

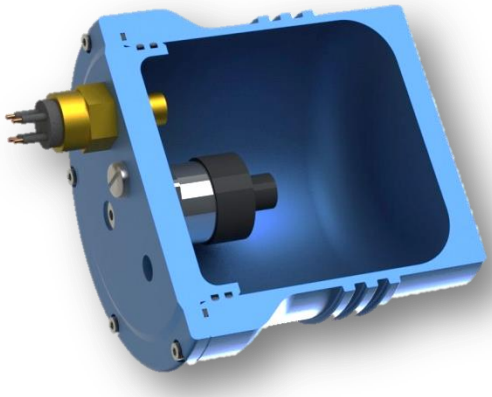

Figure 48: Rendered cross-sections of sensor pod with only pressure sensor installed

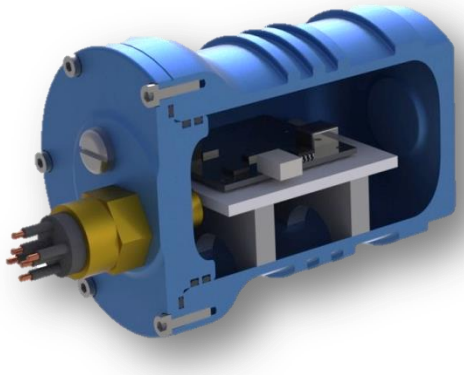

Figure 49: Rendered cross-section of IMU pod

3.9 GRIPPER

ROV *Challenger 1* had a manipulator as seen in Figure 4, but it was not strong enough or robust enough for use on the new 3rd generation ROV. During the development of this new ROV a gripper had been developed by an undergrad student. This gripper was a lot more powerful than the original manipulator, but proved to be too bulky and extremely over-powered for the uses of the Zoology Department. At the time that this report was written, a third generation gripper was being developed for future attachment to the ROV. Provision was made in the power and control system for the gripper.

3.10 ELECTRICAL POWER DISTRIBUTION

A bottom-up design approach was followed with the power distribution system on the ROV. The components to be incorporated in the ROV were first established and then the power system was designed around it, with one or two iterative processes to help optimise the system.

First, all the ROV modules were identified and power requirements for each one established. The voltages and current drawn by each module were then totalled to determine the power supply requirements as shown in Table 12.

Table 12: ROV Power Requirements

Description of Requirement	Current [A]	Power [W]
48 VDC		
Port Forward Thruster	4.5	216
Starboard Forward Thruster	4.5	216
Port Aft Thruster	4.5	216
Starboard Aft Thruster	4.5	216
Vertical Thruster	4.5	216
Gripper (provisional)	4.5	216
Sonar	0.1	5
Sensors (provisional)	0.3	15
Sub-Total	**27.4**	**1316**
15 VDC		
Port Light	1.7	26
Centre Light	1.7	26
Starboard Light	1.7	26
Aft Light	1.7	26
Sensors (provisional)	0.5	8
Camera Tilt (provisional)	1.5	23
Sub-Total	**8.8**	**135**
12 VDC		
Forward Camera @ 12 VDC	0.5	6.0
Aft Camera @ 12 VDC	0.3	3.6
Sub-Total	**0.8**	**10.0**
5 VDC		
IMU (provisional)	0.5	2.5
Sensors (provisional)	0.5	2.5
Sub-Total	**1.0**	**5**
Total Power Consumed by ROV Modules [W]		**1466**

The E-Pod would therefore have to supply power at four different voltage levels and at the currents as listed above.

When designing the power supplies on board the ROV, there were three main factors to consider:

1. Size and weight of power converters – AC-DC converters much bulkier than DC-DC converters
2. Size of conductor available in tether – the higher the current transmitted, the larger the conductor required
3. Noise of power supply in tether – AC power supply in tether could produce noise in communication lines, or shielding of AC power conductors could weigh tether down [5]. However, the noise of an AC supply in the tether could be disregarded because optical fibre, which is immune to electrical noise, was used to transmit the communications.

As seen in Table 12, it was calculated that 1.5kW would be drawn by the active modules on the ROV and due to the limited space available it was decided to use DC-DC converters on-board. DC power transmitted through the tether would automatically negate the need to consider noise produced by the power conductors in the tether, and even more so if fibre optics were to be used for the communications.

Next, the voltage of the current to be transmitted in the tether had to be decided. Because the research group had specified a fibre optic link between the surface controller and the ROV, the selection of tethers through local suppliers was limited. A good relationship had been established with Marine Solutions in Cape Town and it was decided to purchase the tether which they supplied for use with the 1000m rated Seaeye Falcon DR. At R25 000 for 120m it was deemed wise to buy from a supplier who could provide good technical support and customer service rather than to source the tether abroad. The tether incorporated four 1.6mm^2 copper power conductors, each rated at 18 Ω/km.

Through an iterative process of trying to limit the current in the tether, and therefore the voltage drop over the specified 350m tether, and sourcing DC-DC converters to suit a high-voltage input range, it was decided to supply the ROV with power at 400 VDC. This was the same voltage as that used by the Predator ROV and was less than that used by the Falcon ROVs, which were used as a reference for what was commercially acceptable.

Due to the inefficiencies of the DC-DC converters (typically 85.3-88.5%) and the power losses in the tether, close to 2kW of power would be required from the surface power supply unit, and therefore would be supplied by the 400 VDC supply at a nominal 5A. Complete tables of these power supply characteristics can be seen in Section 5 for the Power Pod and in Section 7 for the surface Power Supply Unit.

A schematic of the power distribution system described above can be seen in Figure 50.

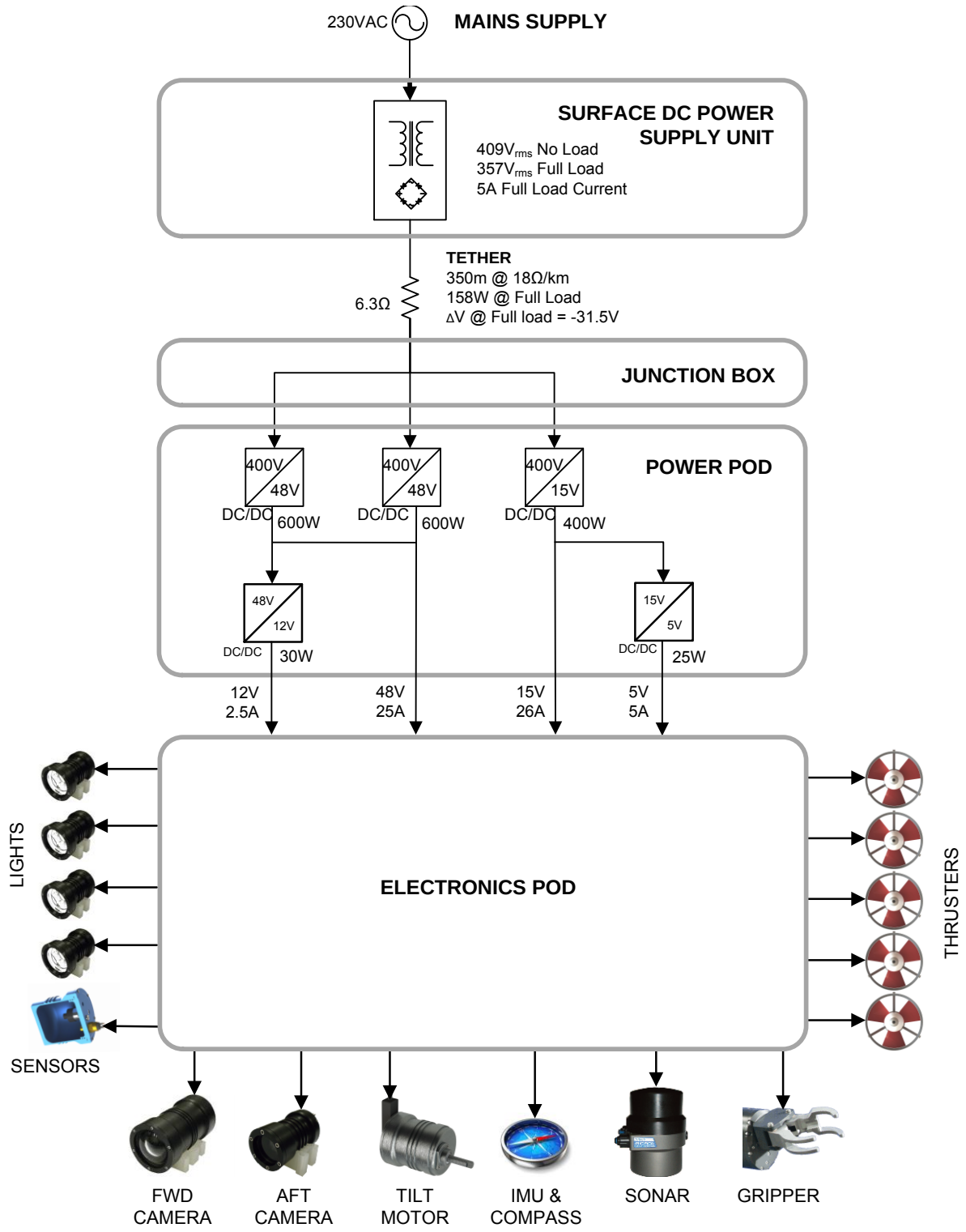

Figure 50: Schematic of the ROV's power distribution system

3.11 COMMUNICATION

As specified in Section 3.1, fibre optics were to carry data transmissions between the surface control station and the ROV. The standard TCP/IP protocol was used over the fibre link, using media converters at each end to convert the light signals in the fibre to electrical signals in the Cat5e network cables. At the surface station the network cable was plugged directly into a laptop and on the ROV a converter would be required to convert from TCP/IP to the on-board serial protocol that was still to be determined.

The RS-232 serial communications protocol had been widely used in the RARL for point-to-point communication systems, but it was not well suited for use within a multi-drop network that required high data rates.

During the ROV design process, another RARL team had started to use the RS-485 serial communications protocol on a search and rescue robot and were already developing hardware and software for it. With a larger team to work on developing the RS-485 network, it became a more feasible option to use on the ROV than other untried protocols, such as the CAN protocol. The implementation of a CAN protocol would require extensive development that was unrealistic for the scope of this project.

The half-duplex RS-485 protocol required only 2 wires for transmission and up to 32 nodes could be daisy-chained on the same bus using standard RS-485 transceivers. RS-485 uses a Master and Slave configuration, where one or more nodes control the communications on the bus populated with other slave nodes that respond to messages received from the Master node(s). While being a half-duplex protocol with only 2 wires, the data speeds of up to 1Mbps with RS-485 outweighed that of RS-232. For the ROV communications on-board, the RS-485 protocol would be an advantage because a minimum of only one channel would be required for all nodes, as opposed to the 18 channels that would be provided by the National Instruments Sb-RIO® (Single board reconfigurable inputs and outputs), therefore saving valuable space. The schematic of the final communications network design is shown in Figure 51.

As seen in Figure 51, an RS-232 channel was still required for the sonar. The sonar had been purchased early on in the project while RS-232 was still the specified communications protocol on-board the ROV. As a result, two serial converters would be required – one for RS-485 to TCP/IP and one for RS-232 to TCP/IP. In view of the available options, it was clear that these two converters would still be far less cumbersome than the Sb-RIO.

After it was established that RS-485 would govern the characteristics of the physical layer, a communication structure was needed to manage the messages sent back and forth between Masters and Slaves on the bus. A similar structure to that developed by the RARL Search and Rescue Robot team was employed on the ROV.

The messages would be controlled by the one master node which would be the host controller PC, via the RS-485 serial converter. A sequential structure was used and in it, each ROV module, or slave, was addressed by the master in turn. The master would send a packet of bytes to each slave, wait for a return message from the slave, and then move on to addressing the next slave after receipt of the message or after a predefined timeout.

Because all nodes on the bus would "hear" every message sent over the bus, an addressing system was needed. Each node was given its own unique 2-byte address. A one-byte address could easily be mistaken for the same value found amongst a set of data so a unique pair was used for each address to significantly reduce the chance of data bytes being mistaken for address bytes.

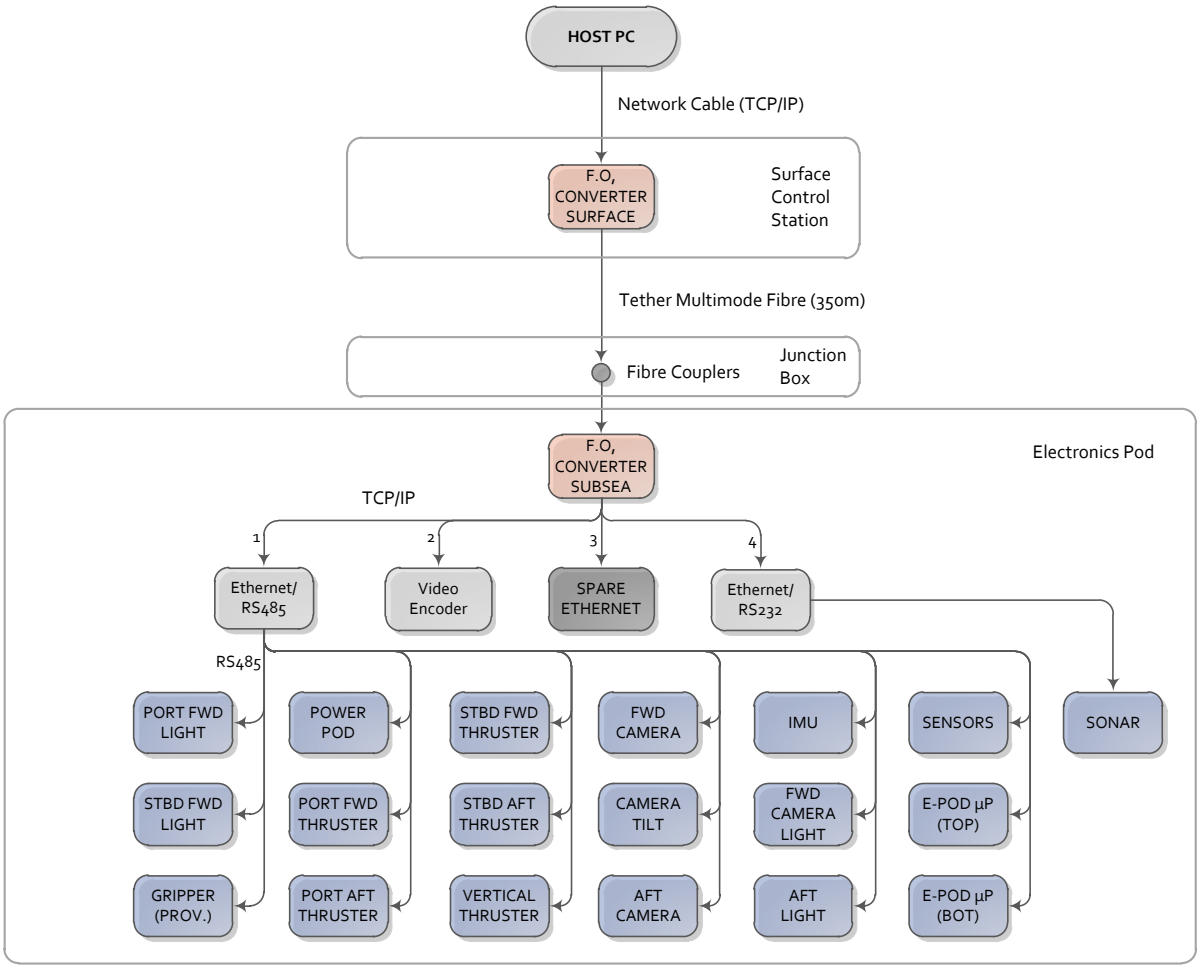

Figure 51: Schematic of final communication network design

To minimise the complexity of the system, particularly in the earlier stages of development, it was decided that a standard length packet of bytes be used for each message rather than a variable length packet. The thrusters were identified as the highest priority modules on the ROV in terms of frequency of communication because this would directly affect the response rate of the vehicle to the pilot's commands. It was determined that 8 data bytes would provide sufficient information for all the required information to be sent to each thruster in one packet. Each packet, together with its initial address bytes, would then be 10 bytes long, as shown in Table 13.

Table 13: Serial communications packet structure

Serial Communications Packet									
Address 1	Address 2	Data 1	Data 2	Data 3	Data 4	Data 5	Data 6	Data 7	Data 8

On the ROV, there were two modules which required the sending and receiving of more information than what could fit into one packet. The Power Pod, which had the most information to send, needed to transmit 22 bytes back to the host controller. It was decided to split this information up into separate packets and make the *Data 1* byte a packet identifier, which left 7 bytes in each packet available for data. Messages for specific nodes only would be split up into these separate packets and the packet identifier incremented on each cycle of communications from the Master. This would slow down the communication frequency with these modules, but their information was not time critical and a cycle period for a full set of information four to five times slower than the nodes was considered quite acceptable. Figure 52 below describes the communication sequence followed by the Master and Slave controllers on the ROV.

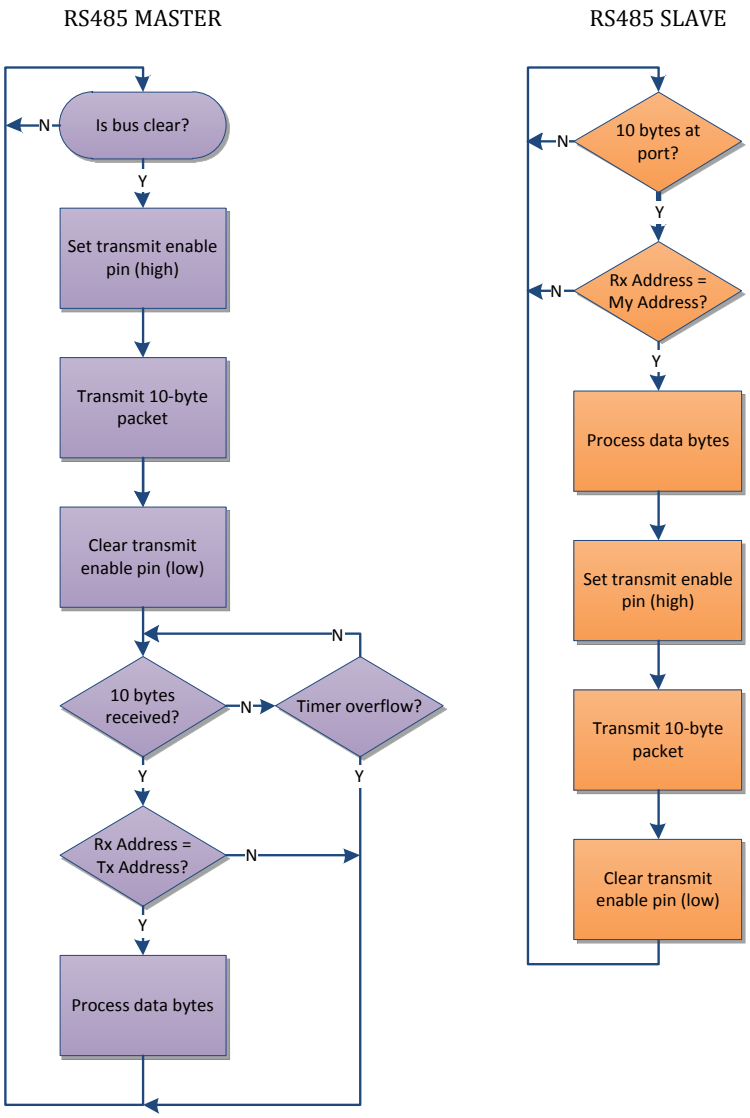

Figure 52: Flow chart describing communication between RS-485 master and slave

Once the higher level power distribution and communications systems had been designed, it was possible to proceed with the more detailed design of the Electronics Pod (E-Pod), Power Pod, Junction Box and Surface Power Supply. These components of the ROV system became the core focus of this project and are described in detail, each in their own section, below.

3.12 SUMMARY

The ROV was designed to meet all of the specifications laid out at the beginning of this chapter. Descriptions of the systems developed as part of this project and within the scope of the author were provided to give some context to the power and communications system, which had become the focus of this report. A detailed report on the design of the systems falling outside of the authors scope were referenced and can be found on the accompanying DVD.

The chapter that follows details the design of the E-Pod which was the first subsystem in the power and communications distribution design hierarchy. The chapter starts with an overview of the system and then proceeds with design specifications and the detailed design of its constituent components.

4 ELECTRONICS POD DESIGN

The E-Pod was designed to manage the distribution of power and communications to each module on the ROV. Once all the modules on the ROV that would depend on the E-Pod for power had been identified and preliminary designs decided upon, a list of specifications for the E-Pod was drawn up and is presented in Section 4.1. The complete E-Pod assembly is shown below in Figure 53, Figure 54 and Figure 55.

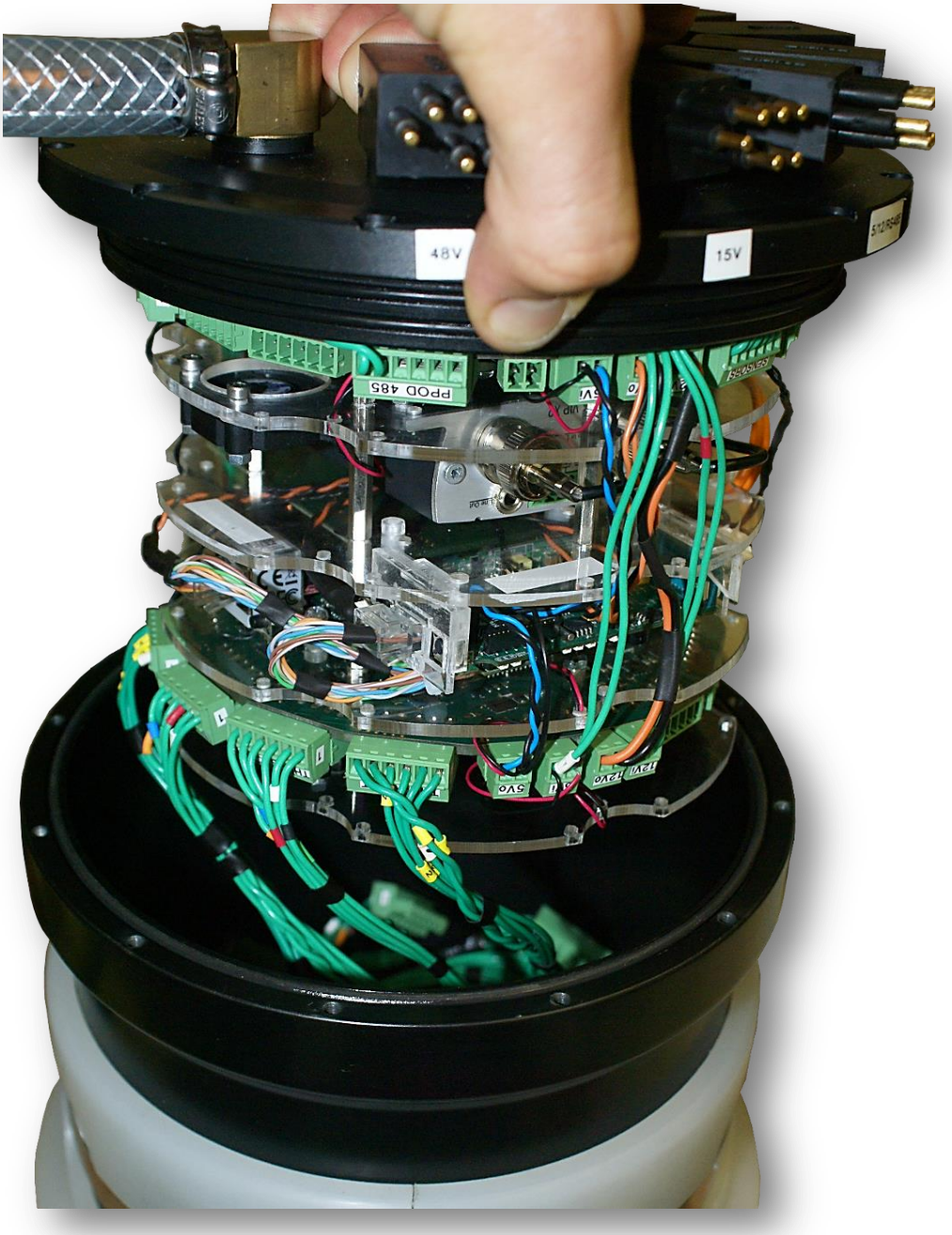

Figure 53: E-Pod electronics being inserted into housing

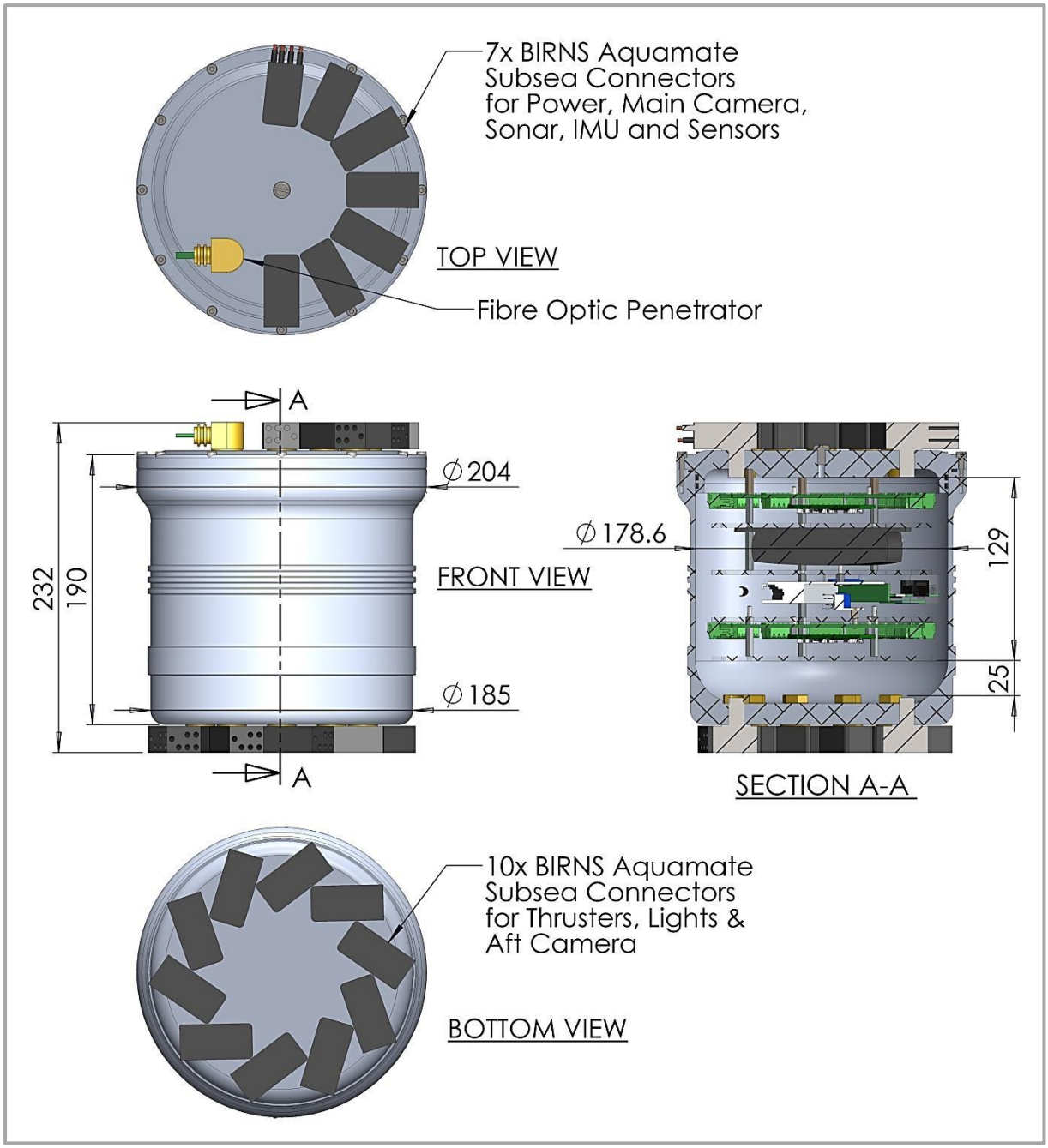

Figure 54: Dimensioned renderings of the Electronics Pod

1. Top distribution PCB

2. First shelf with video encoder & 1st fan

3. Second shelf with fibre optic switch & RS-485 Tibbo®

4. Third shelf with RS-232 Tibbo® & 2nd fan

5. Bottom distribution PCB

6. Bottom cover with 3rd fan

Figure 55: Progressive assembly of the electronics stack on the E-Pod lid

4.1 SPECIFICATIONS

Table 14: E-Pod Specifications

Number	Description of Requirement	Target Values
	Mechanical Specifications	
4.1.1	Operating depth below surface	300m
4.1.2	Standardised electrical connection system	Yes
	Electrical Specifications	
4.1.3	Output voltages	5/12/15/48 VDC
4.1.4	**Supply Currents to ROV Modules**	
	48 V	
	Port Forward Thruster	4.5A
	Starboard Forward Thruster	4.5A
	Port Aft Thruster	4.5A
	Starboard Aft Thruster	4.5A
	Vertical Thruster	4.5A
	Gripper (provisional)	4.5A
	Sonar	0.1A
	Sensors (provisional)	0.3A
	48 V Sub Total	***27.4A***
	15 V	
	Port Light	1.9A
	Centre Light	1.9A
	Starboard Light	1.9A
	Aft Light	1.9A
	Camera Tilt (provisional)	1.5A
	Sensors (provisional)	0.5A
	15 V Sub Total	***9.6A***
	12 V	
	Forward Camera	0.5A
	Aft Camera	0.3A
	12 V Sub Total	***0.8A***
	5 V	
	IMU (provisional)	0.5A
	Sensors (provisional)	0.5A
	5 V Sub Total	***1.0A***
4.1.5	Power to each module to be switched inside E-Pod	Yes
4.1.6	Current monitoring accuracy for thruster power lines	±10%
	Communication Specifications	
4.1.7	TCP/IP over optical fibre connection to surface	Yes
4.1.8	Serial communication protocol between ROV modules	RS-485
4.1.9	Minimum frequency of sending commands to each thruster	2Hz
4.1.10	Minimum number of video channels available	2
	Thermal Specifications	
4.1.11	Ambient temperature monitoring accuracy	±2 °C

4.1.1 Operating Depth Below Surface

As specified in Section 3, the ROV was to operate at a depth of 300 m.

4.1.2 Standardised Electrical Connection System

The design of the ROV was based on having all ROV components housed in separate modules and electrically connected to the central E-Pod. To facilitate the intended modularity and ease of swapping out the different modules, standard connections would be required on each module. It would be more cost effective to purchase or manufacture the specialised connectors in larger quantities of the same type than in ones and twos of different configurations.

4.1.3 Output Voltages

The thrusters were specified for 48 VDC, which was higher than the 36 VDC used on *Robin*. This would help to reduce the current that would need to be supplied and therefore the size of associated connectors and conductors.

The lights were to be driven from a 15 VDC bus which would provide some overhead that would allow the *BUCPUC®* LED drivers to deliver their maximum power.

The video cameras already in the possession of the research group all ran off 12 VDC and most commercially available video cameras would run off 12 VDC – a standard in the surveillance industry.

5 VDC is a common level used to power microcontrollers and their associated inputs, outputs (I/O) and communication circuitry.

So DC voltages of 48 V, 15 V, 12 V and 5 V would be provided as system buses. Any voltages in between could be made available locally on components that required it.

4.1.4 Supply Currents to ROV Modules

Each current rating listed in the table was taken from data sheets for each of the components specified for the different modules.

4.1.5 Power to Each module to be Switched Inside the E-Pod

It should be possible to enable or disable power to each individual module on the ROV without toggling power to the entire ROV. This would be useful during dry tests and maintenance work at the surface, and would provide a means by which the power could be cycled to a module to reset it in the event of a malfunction.

4.1.6 Current Monitoring Provided for Thruster Power Lines

The thruster housings were very limited for space and as a result current sensing components would not fit onto the thruster PCBs. Current monitoring would provide important feedback for the thruster control system so it was decided to incorporate current sensors on each thruster's 48 V line inside the E-Pod. A tolerance of ±10% of the actual current value would be sufficient for the

purposes of controlling the ROV as it would be used mainly for over current limiting and visual feedback to the operator, rather than for position or torque control, which would require a much greater degree of accuracy.

4.1.7 TCP/IP Over Optical Fibre Connection to Surface

A fibre optic link had been specified as the medium for communication between the ROV and the surface controller and would be terminated in the E-Pod.

4.1.8 Serial Communication Protocol Between ROV modules

As described in Section 3.11, RS-485 had been chosen as the communication protocol on board the ROV.

4.1.9 Minimum Frequency of Sending Commands to Each Thruster

The frequency at which each thruster received its commands from the host PC at the surface would determine the response rate of the ROV to the pilot's inputs. It was determined that delays up to a maximum of 500 milliseconds would be permissible before a lag would become sufficiently noticeable to the operator. This would require that the full communications cycle with all modules operate at a minimum of 2Hz.

4.1.10 Minimum Number of Video Channels Available

The main camera and aft camera would each require an independent channel. Any more than 2 channels would be a bonus.

4.1.11 Ambient Temperature Monitoring Accuracy

Temperature sensors were to be incorporated inside the E-Pod to help prevent its components from exceeding their maximum ratings. The control system was set with temperature limits for the Power Pod and Electronics Pod that were 5 °C lower than the maximum ratings for their respective components. It was therefore deemed reasonable to have a ±2 °C tolerance specified for the sensors.

4.2 DESIGN DEVELOPMENT

4.2.1 Housing

During a site visit to an ROV course given by Marine Solutions, one of their associates, an experienced ROV engineer, suggested that an old dive cylinder be used as a cost-effective and simple housing for an ROV electronics pod. While the budget for this project was not extremely limited, the idea stuck and a search was made for condemned aluminium cylinders. The largest aluminium dive cylinders found had an internal diameter of approximately 175 mm, a wall thickness of about 15 mm and a base thickness of up to 30 mm. Cylinders with these dimensions could be used to provide housings similar in dimension to those found on the Falcon and Predator ROVs. Because they were condemned cylinders, they would cost considerably less than a full billet of aluminium and drastically reduce the machining hours required to turn out a hollow cylinder. The condemned cylinders had hairline cracks at the neck of each bottle, just below the threaded valve hole. Failures in these dive cylinders had occurred due to the incorrect aluminium grade specified for their 200 bar working pressure.

Initial design and calculations were performed to determine whether the dive cylinders would work. Once it was established that they would be sufficiently strong and that the electronics selected to use on the vehicle would fit into the housing, the detailed design was completed using the same approach as detailed in Appendix C.

4.2.2 Electronics Stack

Some of the electronics required inside the E-Pod were already in the research group's possession and it was decided to use a shelving system to mount the components inside the pod. The stack of "shelves" for the E-Pod electronics was mounted on the lid of the E-Pod and can be seen below in Figure 56.

Figure 56: Rendering of the E-Pod "shelving" system mounted on the underside of the housing lid

The mounting boards were laser-cut from Perspex® and fastened with nickel-plated brass stand-offs. Cutouts on the perimeter of each mounting board allowed space for wiring to be routed vertically between boards. The stack would allow access to all sides of any level, but if access to the top or bottom of any components was required, the stack could be easily dismantled, provided that pluggable connectors were used for all electrical connections.

4.2.3 Electrical Components

The components to populate the E-Pod shelves would provide communication between the ROV modules and the surface control station, video channels to selected modules and a means to control power to each module. The E-Pod components are listed in Table 15 below with their rated currents and voltages.

Table 15: E-Pod internal power consumption

	Current [A]			
E-Pod Component	**5 V**	**12 V**	**15 V**	**48 V**
Top Distribution PCB	0.34	0.10	0.10	0.10
Bottom Distribution PCB	0.48	0.10	0.10	0.10
Bosch Box	-	-	0.83	-
Tibbo RS-485	-	0.50	-	-
Tibbo RS-232	-	0.50	-	-
Stride Fiber Link	-	-	0.20	-
Total	**0.82**	**1.2**	**1.23**	**0.2**

In order to distribute the communication signals, video signals and power to each module, unique circuit boards were designed. The detail of the design of these circuit boards follows after a description of the communications and video equipment.

4.3 COMMUNICATIONS EQUIPMENT

4.3.1 Fibre Optic Media Conversion

As seen in Figure 51, the optical fibre link needed to be split into a minimum of 3 Ethernet ports. This was achieved by using a 5-port unmanaged Ethernet switch that included one fibre port. The SE-SW5U-ST unit from Stride® seen below in Figure 57 was one of the most compact units of its type on the market at the time. Four RJ45 ports were available, therefore provided one spare port for future expansion.

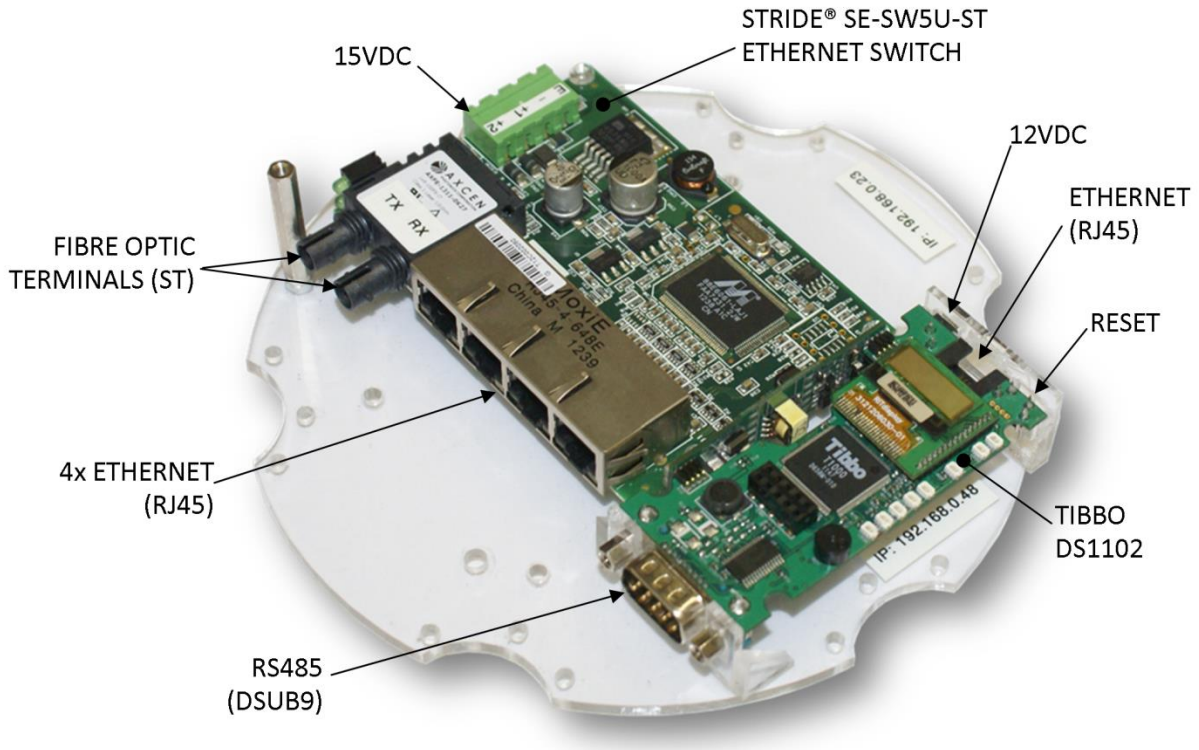

Figure 57: Photo of the E-Pod's communication shelf and components

The Ethernet switch had an allowable input voltage range of 10-30 VDC so was powered off the 15 V rail which had much greater headroom than the 12 V supply. ST connectors were chosen because of their positive and secure locking mechanism that would ensure that no bumps or vibrations on the vehicle would shake them loose.

4.3.2 Ethernet to Serial Conversion

As seen above in Figure 57 an Ethernet-to-RS-485 Tibbo® DS1102 unit was mounted alongside the Stride switch. The DS1102 was an Ethernet to Serial converter that was connected to the host PC via the fibre link. It was configured using proprietary Tibbo® software as a Device Server and setup on the PC as a virtual COM port. This was done so that the DS1102 device would enable the PC to act remotely as the RS-485 Master on board the ROV. The DS1206, seen in Figure 58 and mounted directly above the communications shelf, was configured in a very similar way as another virtual

COM port on the PC that would operate as the RS-232 Device Server. This device was required for dedicated communications with the Tritech Micron imaging sonar.

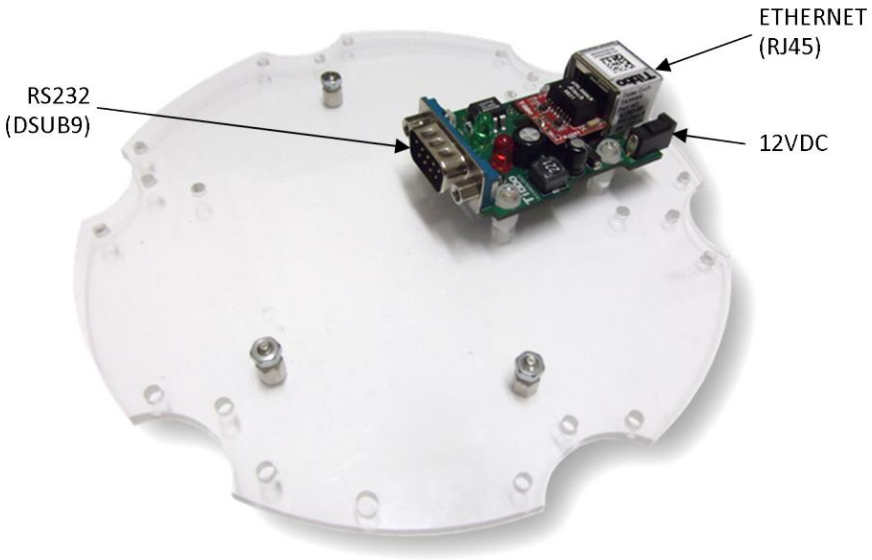

Figure 58: Tibbo DS1206 Ethernet to RS-232 converter mounted on underside of third shelf

The pin assignments for each of the Device Servers described in this section are listed in Table 16 below.

Table 16: Pin assignments for Tibbo serial Device Servers

Pin	RS-485 (DS1102)	RS-232 (DS1206)
1	-	-
2	RX- (B)	RX
3	TX+ (A)	TX
4	TX- (B)	-
5	GND	GND
6	RX+ (A)	-
7	-	-
8	-	-
9	-	-

4.4 VIDEO FEED

The video cameras used on-board the ROV produced PAL video signals that would need to be encoded for transmission in the TCP/IP protocol over the fibre link to the host PC. The RARL already had in stock a Bosch® VIP X2 video encoder that had two independent video inputs and would stream the video signals in MPEG-4 format at up to 30 frames per second out of its Ethernet port. The VIP X2 was a very compact design and fitted neatly within the dimensions of the E-Pod. A photo of the unit mounted on its shelf, ready for installation, can be seen in Figure 59. Power was supplied at 15 VDC via spring cage terminals on the one end and the video signals were delivered via the two BNC connectors at the opposite end. A schematic of the video system is shown in

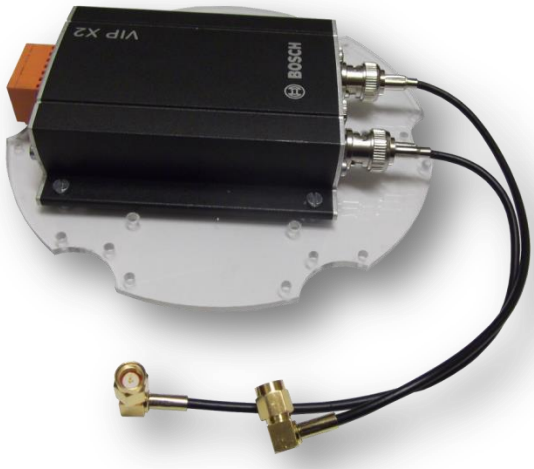

Figure 59: Photo of the Bosch VIP X2 video encoder mounted on its Perspex® shelf

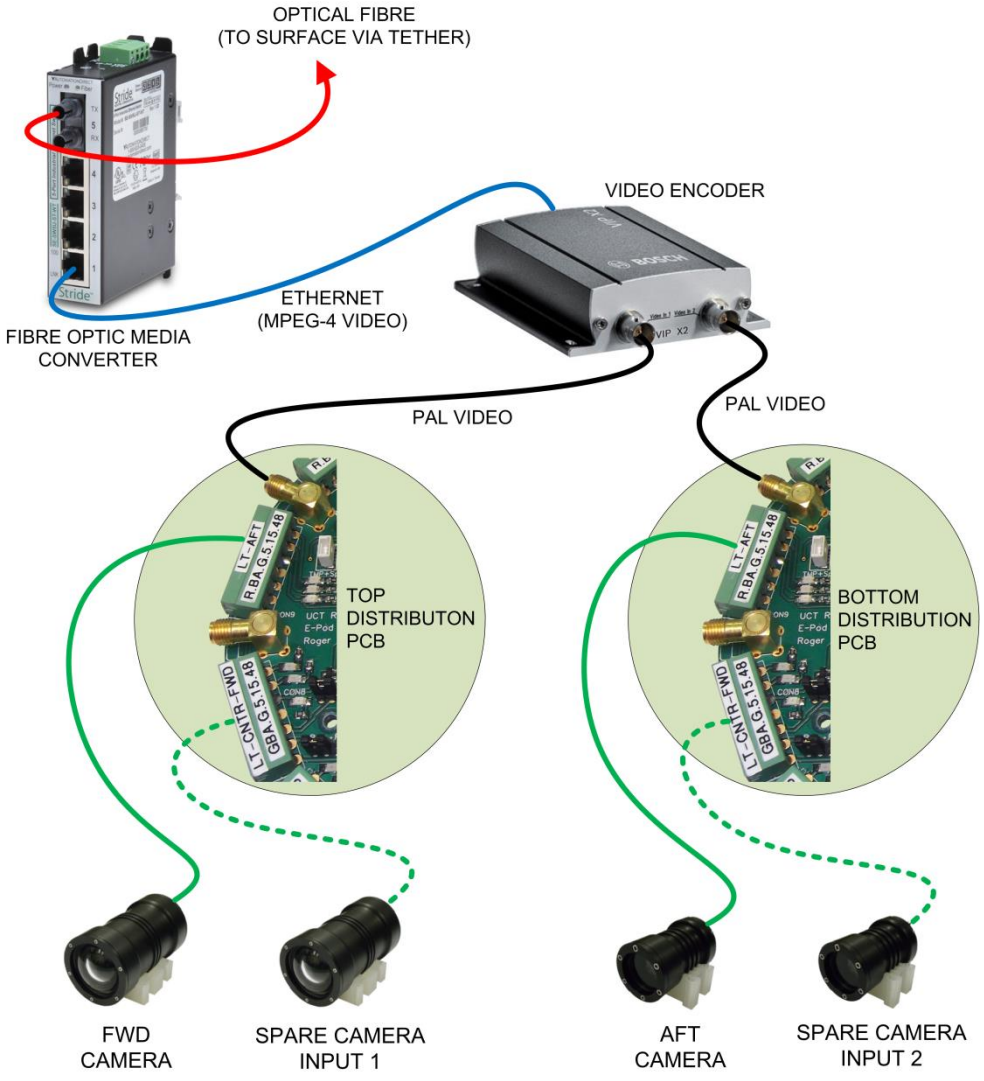

Figure 60: Schematic of video system

4.5 POWER AND COMMUNICATIONS DISTRIBUTION TO ROV

The communications and video equipment that would enable all signals to be funnelled through the fibre optic link had been specified and integrated into the E-Pod design. These signals, along with the power supplies, needed to be distributed as required to each module. The final design of these distribution circuit boards is shown below in Figure 61. Specifications and a detailed description of the design follow in the sections below.

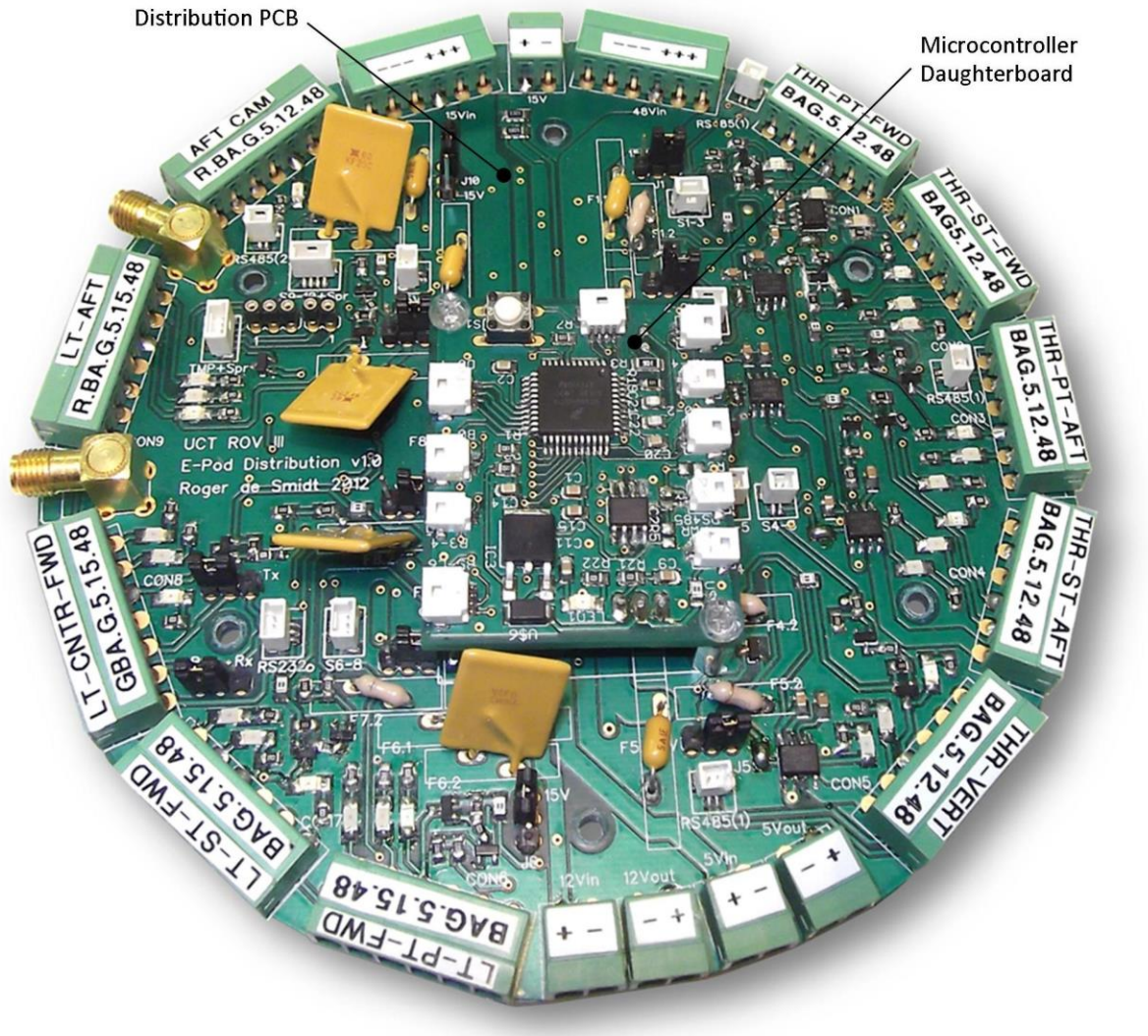

Figure 61: Photo of the E-Pod distribution PCB

4.5.1 Specifications

Table 17: E-Pod distribution PCB specifications

Number	Description of Requirement	Target Values
Physical Specifications		
4.5.1.1	Total number of modules to service	20
4.5.1.2	Maximum dimensions available	Ø168x60 mm
Electrical Specifications		
4.5.1.3	Input Currents	
	48 V input current	27.4A
	15 V input current	12.6A
	12 V input current	2.5A
	5 V input current	5.0A
4.5.1.4	Temperature measurement range	0-100 °C
4.5.1.5	Maximum copper track temperature	150 °C
Communication Specifications		
4.5.1.6	Number of RS-485 network channels	2
4.5.1.7	Number of RS-232 output channels	1
4.5.1.8	Number of video channels available	4

4.5.1.1 Total Number of Modules to Service

As listed in Table 14 above, 16 modules were listed for connection to the E-Pod. It was decided to provide 4 spare outputs for future expansion, bringing the total to 20.

4.5.1.2 Maximum Dimensions Available

The inside of the E-Pod chamber was set at Ø178 mm. A 5 mm gap between the housing and the circuit boards was required for routing wiring inside the E-Pod. This left a remaining Ø168 mm available for the circuitry. In terms of height available, Ø165 mm was the total depth of the E-Pod and after the communication and video equipment had been added, 60 mm was the remaining height available for the distribution electronics. This would also allow space for bulkhead connectors in the bottom of the E-Pod.

4.5.1.3 Input Currents

The input current specifications were adjusted from those in Table 14 to accommodate extra headroom on some of the supplies. 3A headroom was added for the 15 V supply so that distribution PCBs could supply the power required by the Bosch® video encoder and Stride® switch inside the E-Pod. The current capacities of the 12 V and 5 V buses on the PCB were increased to match the rated current output of their respective power supplies.

The current capacity of the 48 V bus remained unchanged because no extra demand was expected.

4.5.1.4 Temperature Measurement Range

The ROV was not expected to operate in temperatures lower than 10 °C if it was going to be confined to missions on the South African coast. However, 0 °C would provide a safe lower limit should the vehicle be used further afield in icy sea waters. The upper limit of 100 °C was chosen so

that it would incorporate the maximum operating limit of most electronics, even though operating limits were to be set much lower.

4.5.1.5 Maximum Copper Track Temperature

150 °C was the glass transition temperature of the FR4 laminates supplied by Trax, a vendor regularly used by the RARL [44].

4.5.1.6 Number of RS-485 Network Channels

Although only one channel would be used on the ROV in its current design, provision for a second channel would increase the fault tolerance of the system. This could be done if the distribution of communication to the ROV modules was split between two networks in future upgrades. A minimum of two RS-485 channels was therefore required.

4.5.1.7 Number of RS-232 Output Channels

A Tibbo DS1206 that was regularly used in the RARL would be used to provide this channel. The DS1206 had three full duplex channels and one transmit-only channel. Only one RS-232 channel was required for the Tritech Micron sonar unit and therefore the DS1206 provided two and a half spare RS-232 channels on board the ROV.

4.5.1.8 Number of Video Channels Available

Two working video channels were required on the ROV as specified in Table 14, but it was decided to provide two extra channels for future expansion should they be required.

4.5.2 Distribution PCB Design

Some simple preliminary layouts of connectors required for all the ROV's modules showed that one PCB would not be large enough to accommodate the 16 modules that were to be serviced with communications and power. The distribution was therefore to be split between two PCBs that would operate in parallel. The PCBs were identical so as to reduce direct manufacturing costs and promote standardisation and flexibility within the design. Each PCB was designed to service 10 modules, which would provide 4 spare outputs for future development or that could be used as backups in the event of PCB component failures. The complete assembly of one of these PCBs can be seen below in Figure 62.

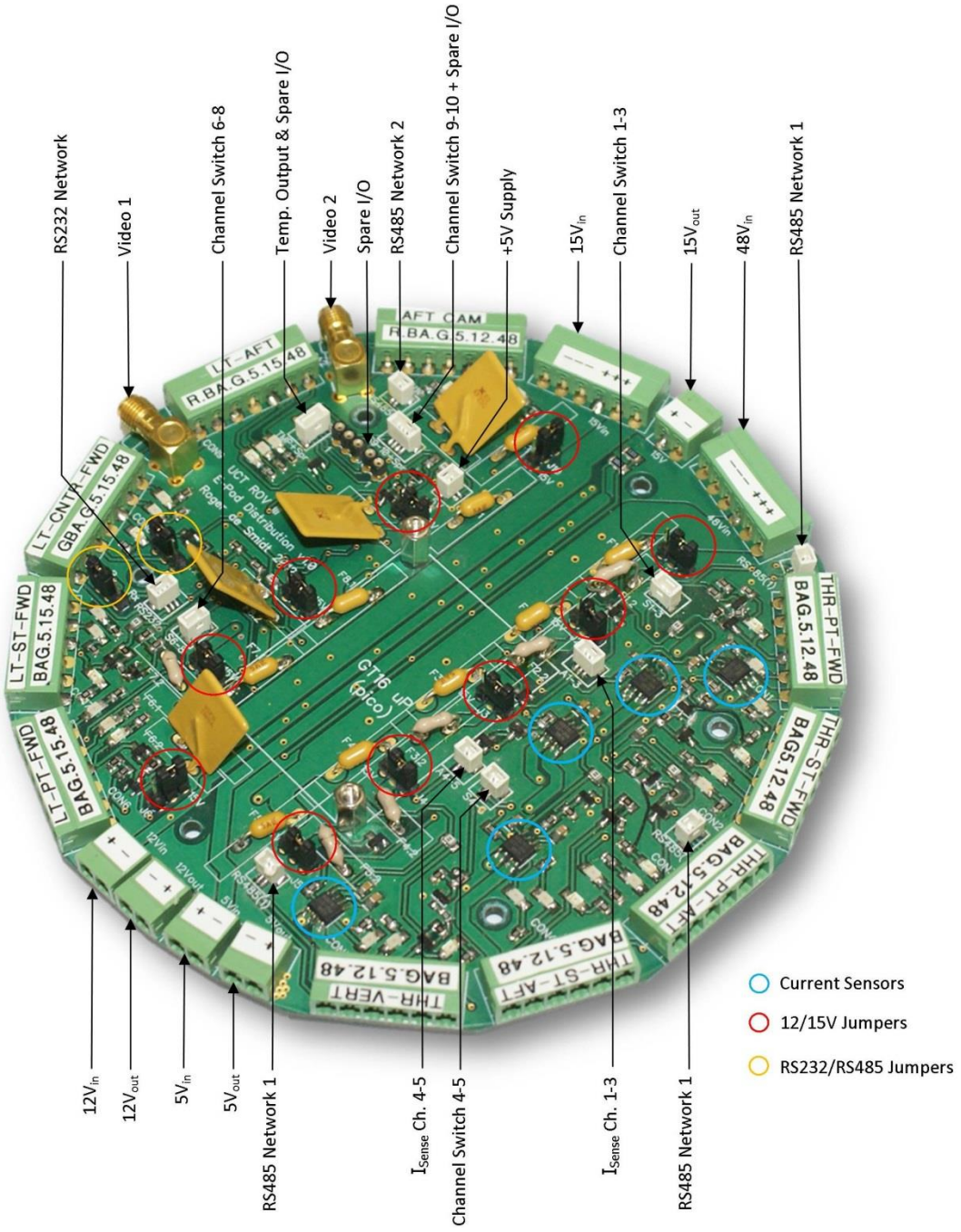

Figure 62: E-Pod distribution PCB inboard component identification

The design of the distribution PCBs was complex due to the space required and it demanded a large degree of modularity for each of the output channels. The design of the PCB is discussed below with particular focus on the following areas:

- Circuit design
- Connectors
- PCB Dimensions
- Copper Track Current Capacities

4.5.2.1 Circuit Design

In this section specific aspects of the PCB circuits are detailed and discussed. For a full set of schematics for the distribution PCB circuitry, see those for the E-Pod Distribution PCB included on the accompanying DVD.

4.5.2.1.1 Circuit Protection

Over-current protection was built into each power supply line on every output channel to protect the copper tracks and connectors of the PCBs. Fuses were integrated between the input power buses on the PCB and the switching components of each line.

A compromise between fusing speed and certainty and the cost of time spent in replacing blown fuses was to be considered. Because the primary function of the fuses on the E-Pod PCBs was to protect the copper tracks and connectors from overheating and most of the on-board componentry was relatively robust, it was decided to use resettable fuses. Resettable fuses operate much slower than non-resettable fuses in most cases, but would save a lot of time, particularly during prototype testing. A list of the resettable fuses used on each line can be seen in Table 18 below.

Table 18: List of fuse ratings

Line Voltage	Line Current	Cu Track Rating	Connector Rating	Fuse Trip Current
5 V	0.5A	2.5A	8A	0.5A
12/15 V	1.9A	7.5A	8A	2.5A
48 V	4.5A	7.5A	8A	5.0A

4.5.2.1.2 Power Switches

Each channel on the PCBs required a digitally operated switch for each power bus. Due to the limited space on the PCBs for components, two of the power buses, namely the 12 V and 15 V buses, were designed to share a line on each output. It was established that none of the ROV modules were designed to receive 12 V and 15 V together; it would always be one or the other. This meant that a jumper could be used to select whether 12 V or 15 V was to be supplied to each of the modules, as indicated in Figure 62.

Each of the 20 output channels required three power switches for each of the 5 V, 12/15 V and 48 V buses, amounting to a total of 30 switches required on each of the PCBs. Relays were considered as options for these switches because if correctly selected they would be easily replaceable in the

event of switch failure. However, relays would require far too much surface area on the PCB and their contacts would wear over time if inductive loads, such as the thruster motors, were switched often. Transistors were therefore chosen as the main power switching components. Bipolar Junction Transistors (BJT's) were used for the light current, low voltage requirements of the 5 V lines, and MOSFETs were selected for the higher powered 15 V and 48 V lines. The circuits for each of these switches are discussed in the two sections that follow.

4.5.2.1.3 5 V Switch Circuit

The 5 V switch was designed to provide a maximum of 500mA on its output and would be controlled by a logic signal. A high signal at 3.3 V from the system's microcontroller would turn the output ON and a 0 V low signal would turn it OFF. As seen in the circuit diagram for the 5 V switch below, the digital control signal would cause an NPN transistor to turn on a PNP transistor, which in turn would control the 5 V power output. The selected 2STR2230 PNP transistor was rated for a maximum continuous current of 1.5A which provided 1A of headroom and therefore cooler operation at the rated 500mA.

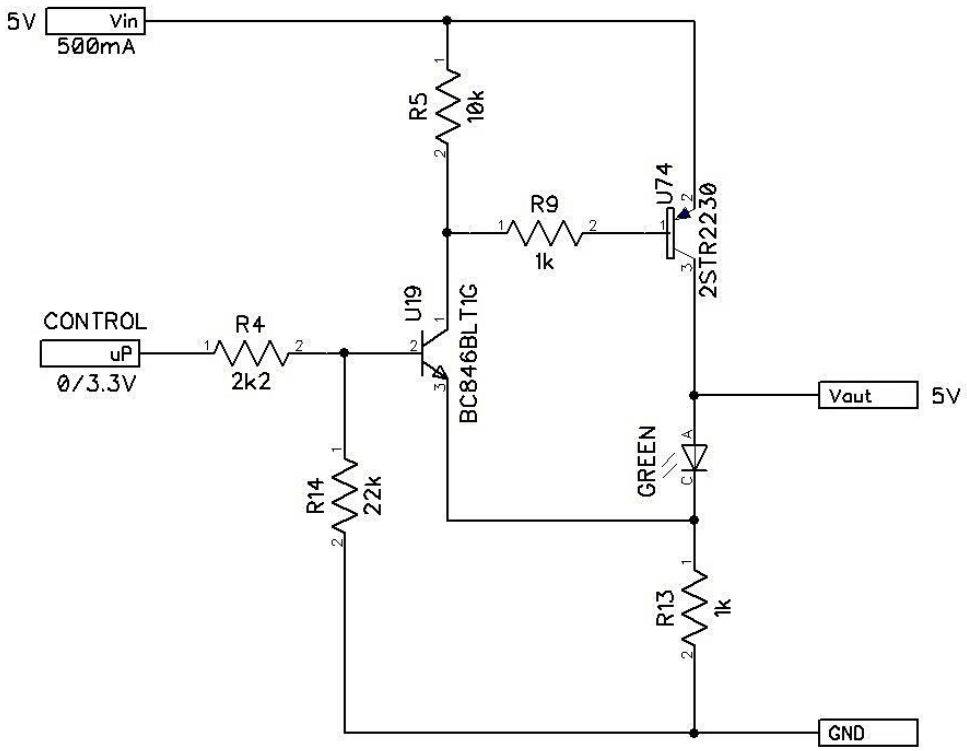

Figure 63: Power switch circuit for 5 V lines

4.5.2.1.4 12/15 V & 48 V Switch Circuit

A similar circuit was designed to switch power on the 12/15 V and 48 V lines and its schematic is shown in Figure 64. Because of the higher current and voltage to be switched, a P-Channel Power MOSFET was used instead of the PNP bipolar transistor. The MOSFET afforded a lower on-state resistance which would result in less heat generation. Size was also a significant constraint because 20 of these circuits would need to fit onto the PCB. The Si7461DP from Vishay® in its PowerPAK® SO-

8 surface mount package was one of the smallest MOSFETs available at the time that had the required electrical characteristics.

In principle, this higher voltage switching circuit was very similar to the circuit used for the 5 V lines in the Figure 63, although some extra provision was required for operation of the P-Channel MOSFET. Because a MOSFET requires a voltage drop of approximately 10 V from its source to its gate before it will turn on fully, a zener diode was added to provide at least the minimum drop when the microcontroller signal was set high and transistor U67 turned on. When the microcontroller signal was returned low, the gate voltage would be pulled up to the 12/15 V rail again and the MOSFET turned off.

Values for resistors R1 and R2 were chosen to minimize leakage current through R1 and to minimize R2's resistance while not exceeding its power rating or that of the zener diode. Because the same 12/15 V circuit would switch either 12 V or 15 V, its components needed to be selected to operate with either supply voltage. Optimisation of the component values was performed in an iterative process, using an Excel® spreadsheet and component supplier specifications. All component values are shown in Figure 64 below for both the 12/15 V circuit and the 48 V circuit. The first value for each component corresponds to the circuits that receive 12 V or 15 V (manually selected using jumper) and the second value corresponds to the circuits receiving 48 V.

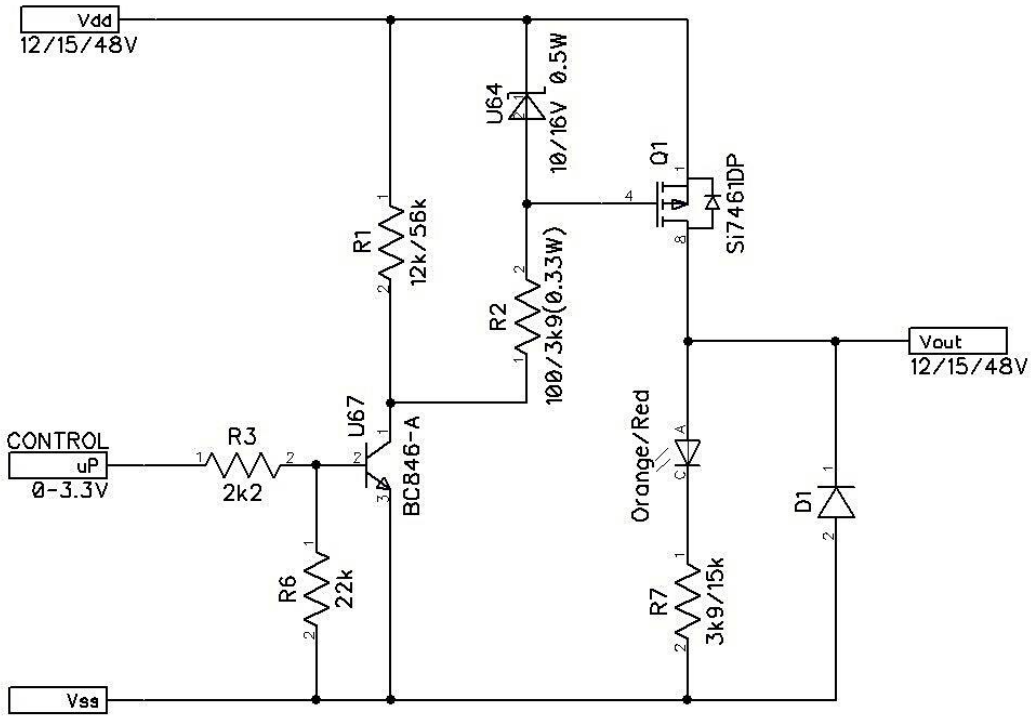

Figure 64: Power switching circuit for 12/15 V and 48 V lines

Diode D1 shown in the circuit diagram was incorporated as an optional suppression diode that could be soldered into place if the loads on the output line were heavily inductive. Alternatively, the same

surface mount pads intended for the diodes could be used to add capacitance across the load, if required.

4.5.2.1.5 Current Sensing

The current in the 48 V lines of five of the output channels on each PCB was to be monitored. The RARL had already started using Hall-effect current sensors produced by Allegro®. The sensors were compact and produced a linear output voltage that could be fed into an analogue-to-digital converter (ADC) port of a microcontroller. A search was performed for alternative components, but the ACS715 IC from Allegro® provided one of the smallest packages available and having had its circuitry already tested and successfully implemented within the RARL research group it was chosen as the sensor to use on the E-Pod PCBs and is incorporated in the circuit schematic below.

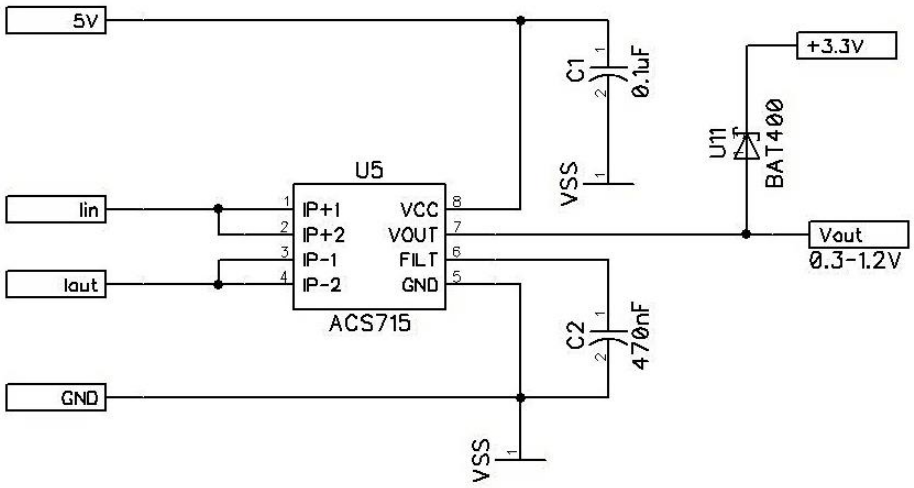

Figure 65: Schematic of the current sensing circuit on the E-Pod distribution PCB

The ACS715 IC was used and would measure currents from 0A to 20A and provide an output voltage with a zero offset of $0.1xV_{CC}$ that increased at a rate of 185mV/A. It was therefore decided that with a 10-bit ADC converter on the system's microcontroller referenced to 3.3 V, no amplification on the output was required to provide the required precision of 0.1A. The calculation of the expected resolution is presented in the equations below.

$$ADC\ Resolution = \frac{3.3}{1023} = 3.2mV$$

$$Total\ Resolution = \frac{3.2mV}{185mV.A^{-1}} = 0.02mA$$

The schematic for this current sensing part of the circuit is shown above in Figure 65, including power supply bypass capacitor and output filter capacitor as recommended by the manufacturer. A Shottky diode was added between the output line and a 3.3 V reference to protect the microcontroller ADC input from an overvoltage condition.

The minimum output voltage was expected to be 0.33 V and the maximum, at 4.5A current, 1.16 V. A set of results for the calibration of these sensors on the bottom distribution PCB is included in Appendix D.

4.5.2.1.6 Communications

Two separate RS-485 networks were to be made available on each of the PCBs. The intention was to provide a dedicated communication link with the thruster modules so it was decided to split the network on each PCB so that the thrusters could be controlled independently if need be. This would be fine for the one PCB with all the thrusters connected to it, but the other PCB would not require the same splitting of communications. A link was therefore provided so that all the modules could be linked together onto the same network. The structure of this connection logic is shown below in Figure 66.

The initial production of the ROV would be completed using one network until the system and communications had been developed to a point where the complexity of a second network could be considered. The Tibbo® DS1102 Ethernet-to-Serial converter would also have to be replaced with a unit that could provide two RS-485 channels.

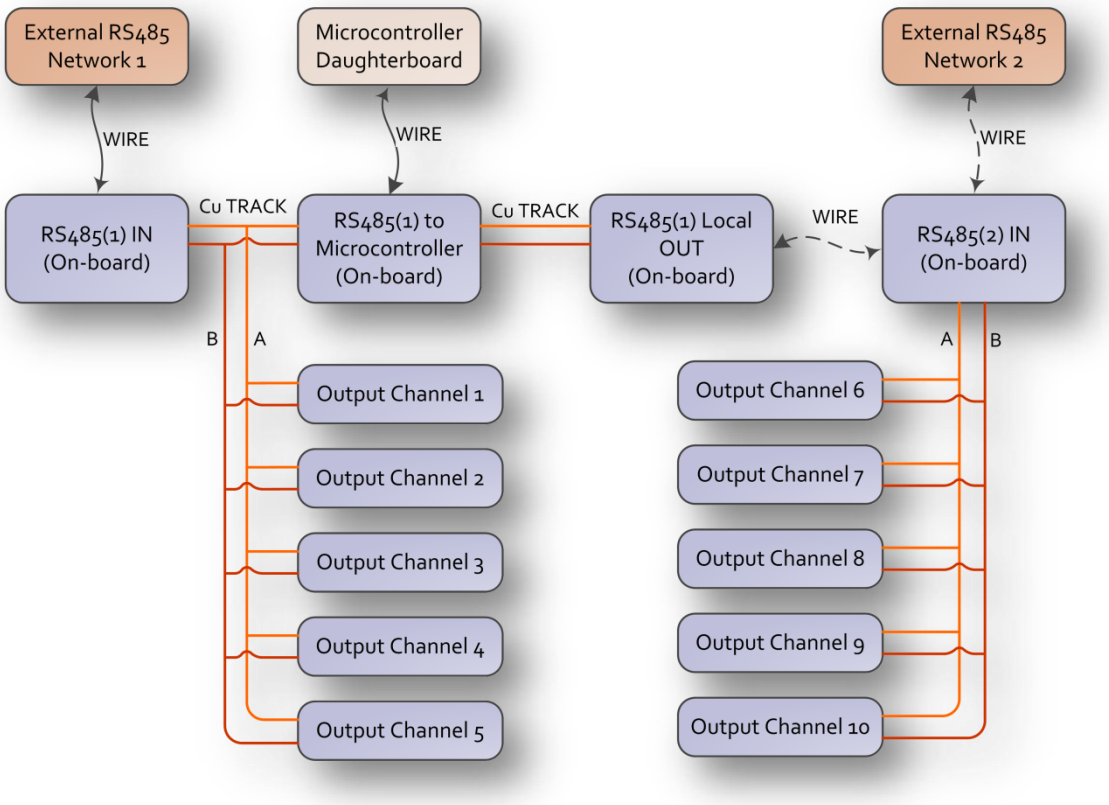

Figure 66: RS-485 network connection structure on the E-Pod distribution PCB

4.5.2.1.7 Video

The distribution PCB would only act as a junction point between the ROV modules with a video output and the video encoder in the E-Pod. Video signals were to be received via the ROV module

Phoenix® connectors and then directly connected with a short copper track on the PCB to the output SMA co-axial connectors which fed the signals to the video encoder unit.

4.5.2.2 PCB Dimensions

After the circuit diagrams had been completed and connector quantities were established, the circuit board was laid out so that all connectors were just about touching around the perimeter of the board. This way a PCB diameter of 145 mm was achieved.

The FR-4 substrate from which the PCB would be constructed was selected to be 2.4 mm thick to minimise flex in the board and weakening of solder joints while plugging and unplugging the array of connectors.

4.5.2.3 Copper Track Current Capacities

Because the E-Pod PCBs were designed to distribute power to each of the ROV modules, its copper tracks would require sufficient capacity to deliver the specified currents without overheating. The current ratings for each of the modules and the total current demand on each power supply bus can be seen in Table 14 and Table 17.

The current capacity of copper tracks in PCBs was researched and the values for track dimensions shown below in Table 19 were selected from PCB manufacturer, Beta Layouts, as representative of the range of data available. Track dimensions not available for exact track width required were attained by interpolation using graphical methods in Excel® because the relationship between track widths and current capacity was not linear. The ratings in this table are for a 45 °C temperature rise above ambient, which in the case of the ROV would always be below the approximate 150 °C glass transition temperature of the FR-4 PCB substrate material.

Table 19: PCB Track widths and current capacities for 45°C rise [45]

Track Width [mm]	Current Capacity [A] (35 µm Copper)	Current Capacity [A] (70 µm Copper)
0.5	2.5	4.0
1.0	4.2	6.8
2.0	7.5	12.0
2.5	8.5	14.0
5.6	15.4	24.8
7.0	18.0	28.4

The design of the PCBs was initially based on the use of copper tracks that were to be 70 µm in thickness which allowed for track widths of 7 mm for the 48 V input, 5.6 mm for the 15 V input and 2 mm for each of the 48 V and 15 V outputs. The 12 V and 5 V input lines were designed to be 2 mm and 2.5 mm respectively. Layouts of the PCB topside and underside showing these tracks can be seen in Figure 67.

The tracks were specified for a thickness of 70 µm because space on the PCBs was limited and the thicker the tracks, the narrower they could be for the same cross-sectional area. However, pricing on

the final design for 70 µm tracks was significantly more expensive than the 35 µm option. The design had been extensive and the layout of the PCBs had taken weeks of work so changing the track widths would have cost not only in available space on the PCBs but also many more days of design time. Although there would be a theoretical 37-40% loss in capacity, the tracks were relatively short and because the PCBs were also prototypes, it was decided to proceed with manufacture of the cheaper 35 µm option. If the tracks proved to be insufficiently sized and overheat, 70 µm tracks could be ordered for the next iteration.

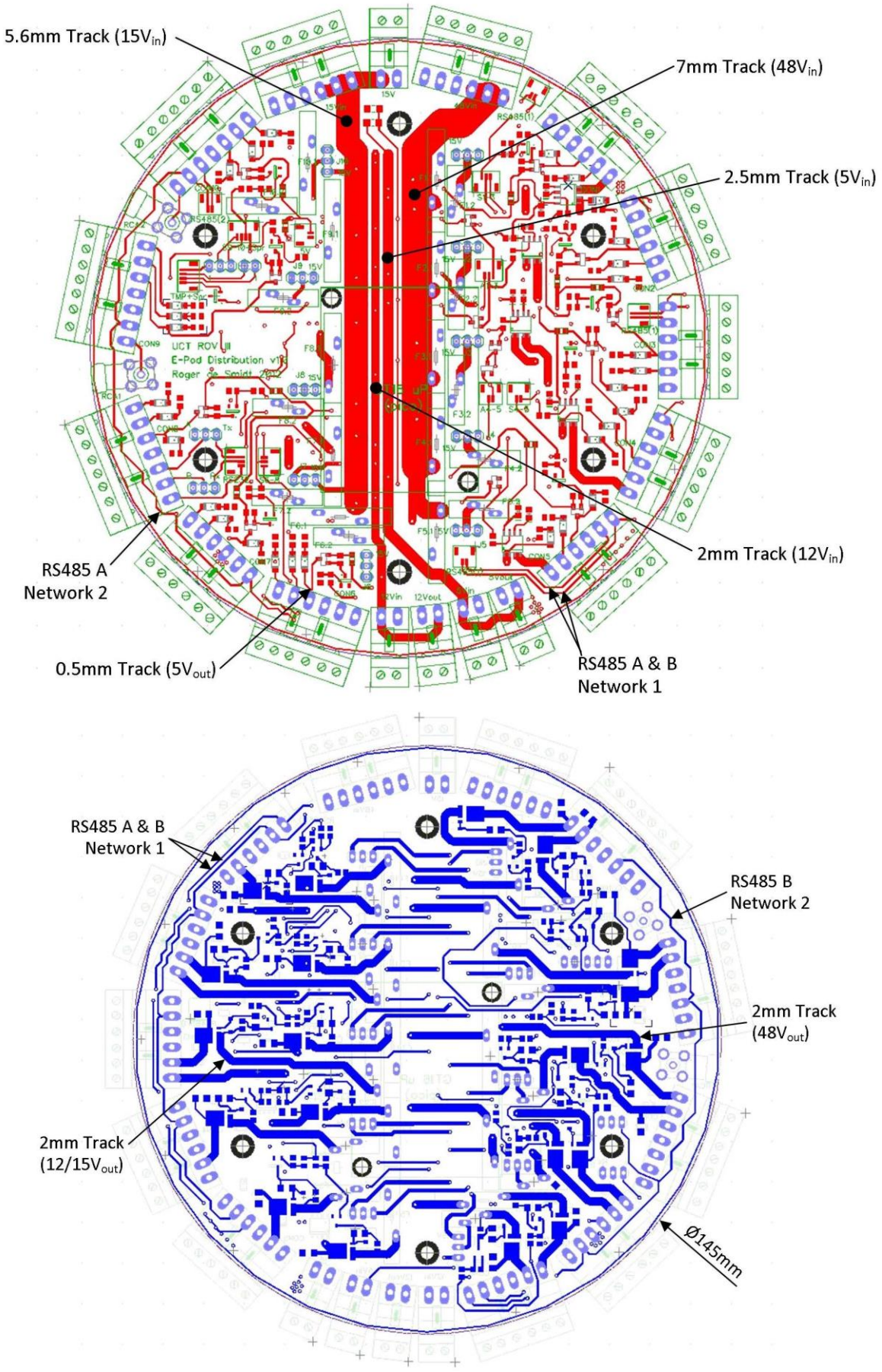

Figure 67: E-Pod distribution PCB upper side (top) and underside (bottom) layout (ground plane not shown)

4.5.2.4 Connectors

The connectors used on the PCBs needed to have reliable positive connections that were rated for a minimum of 1000 cycles. Screw terminals were preferred over crimped terminals because crimp terminals could not be easily repaired. Phoenix® Combicon® MC connectors were rated for 8A per pin and had performed well for the RARL in the past so were selected for use on these distribution PCBs.

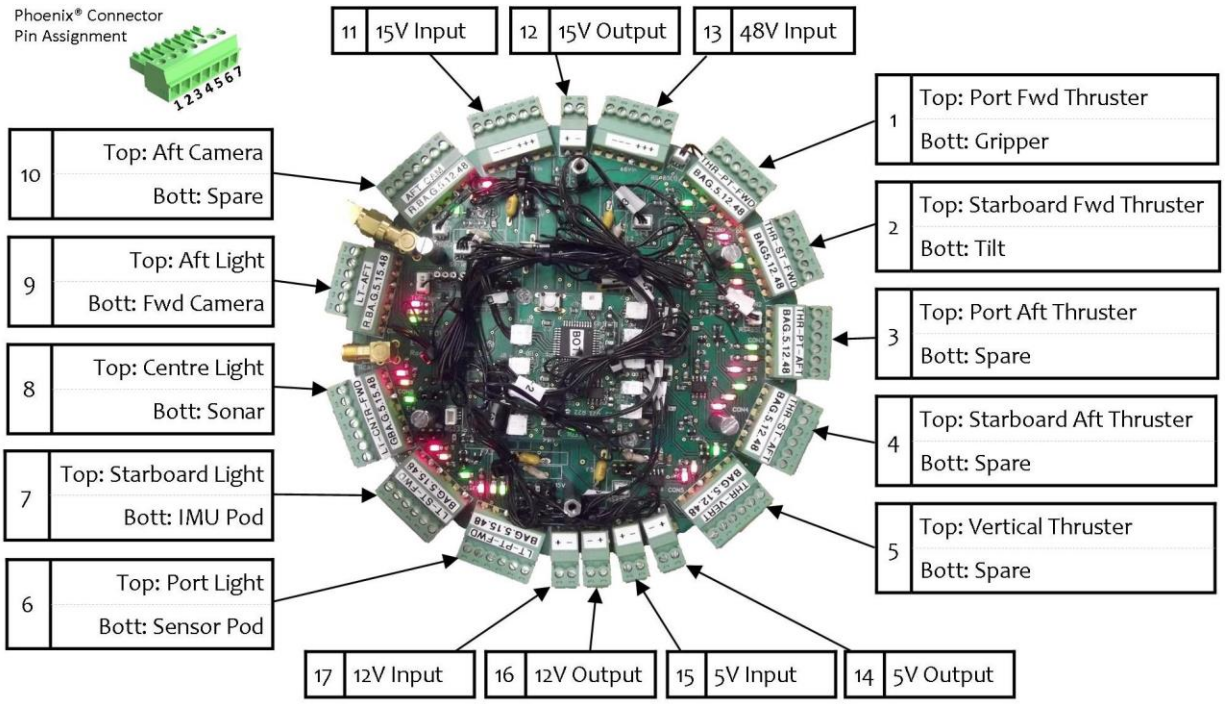

Figure 68: E-Pod top and bottom distribution PCB connector assignment

Table 20: Phoenix® connector pin assignments for distribution PCBs

Phoenix Connectors (see Figure 68)																	
	Top PCB																
Pin	1	2	3	4	5	6	7	8	9	10	11	12	13	14	15	16	17
1	48 V	48 V	-	-	-	48 V	48 V	48 V	48 V	-	15 V	15 V	48 V	GND	5 V	GND	12 V
2	12 V	12 V	-	-	-	15 V	15 V	15 V	12 V	-	15 V	GND	48 V	5 V	GND	12 V	GND
3	5 V	5 V	-	-	-	5 V	5 V	5 V	5 V	-	15 V	-	48 V	-	-	-	-
4	GND	GND	-	-	-	GND	GND	GND	GND	-	GND	-	GND	-	-	-	-
5	A	A	-	-	-	A	A	TX	A	-	GND	-	GND	-	-	-	-
6	B	B	-	-	-	B	B	RX	B	-	GND	-	GND	-	-	-	-
7	-	-	-	-	-	-	-	GND	RCA	-	-	-	-	-	-	-	-
	Bottom PCB																
Pin	1	2	3	4	5	6	7	8	9	10	11	12	13	14	15	16	17
1	48 V	48 V	48 V	48 V	48 V	48 V	48 V	48 V	48 V	48 V	15 V	15 V	48 V	GND	5 V	GND	12 V
2	12 V	12 V	12 V	12 V	12 V	15 V	15 V	15 V	15 V	12 V	15 V	GND	48 V	5 V	GND	12 V	GND
3	5 V	5 V	5 V	5 V	5 V	5 V	5 V	5 V	5 V	5 V	15 V	-	48 V	-	-	-	-
4	GND	GND	GND	GND	GND	GND	GND	GND	GND	GND	GND	-	GND	-	-	-	-
5	A	A	A	A	A	A	A	A	A	A	GND	-	GND	-	-	-	-
6	B	B	B	B	B	B	B	B	B	B	GND	-	GND	-	-	-	-
7	-	-	-	-	-	-	-	GND	RCA	RCA	-	-	-	-	-	-	-

The two distribution PCBs were to be mounted at the top and bottom ends of the E-Pod where the two groups of bulkhead connectors were installed. The assignment of the output channels to the ROV modules was therefore based on which modules were connected through the top of the E-Pod and which were connected through the bottom. Figure 68 shows the assignment of connectors on each PCB and Table 20 lists the assignment of each pin on these connectors.

For on-board low current signals much more compact connectors were required. The RARL had already had much success with the Molex® Pico-Clasp™ range of connectors that provided a secure positive connection, a very small footprint and was rated for currents up to 2A on each pin. The assignment of each of these Pico-Clasp™ connectors on the PCBs and their corresponding pin assignments are shown below in Figure 69 and listed in Table 21.

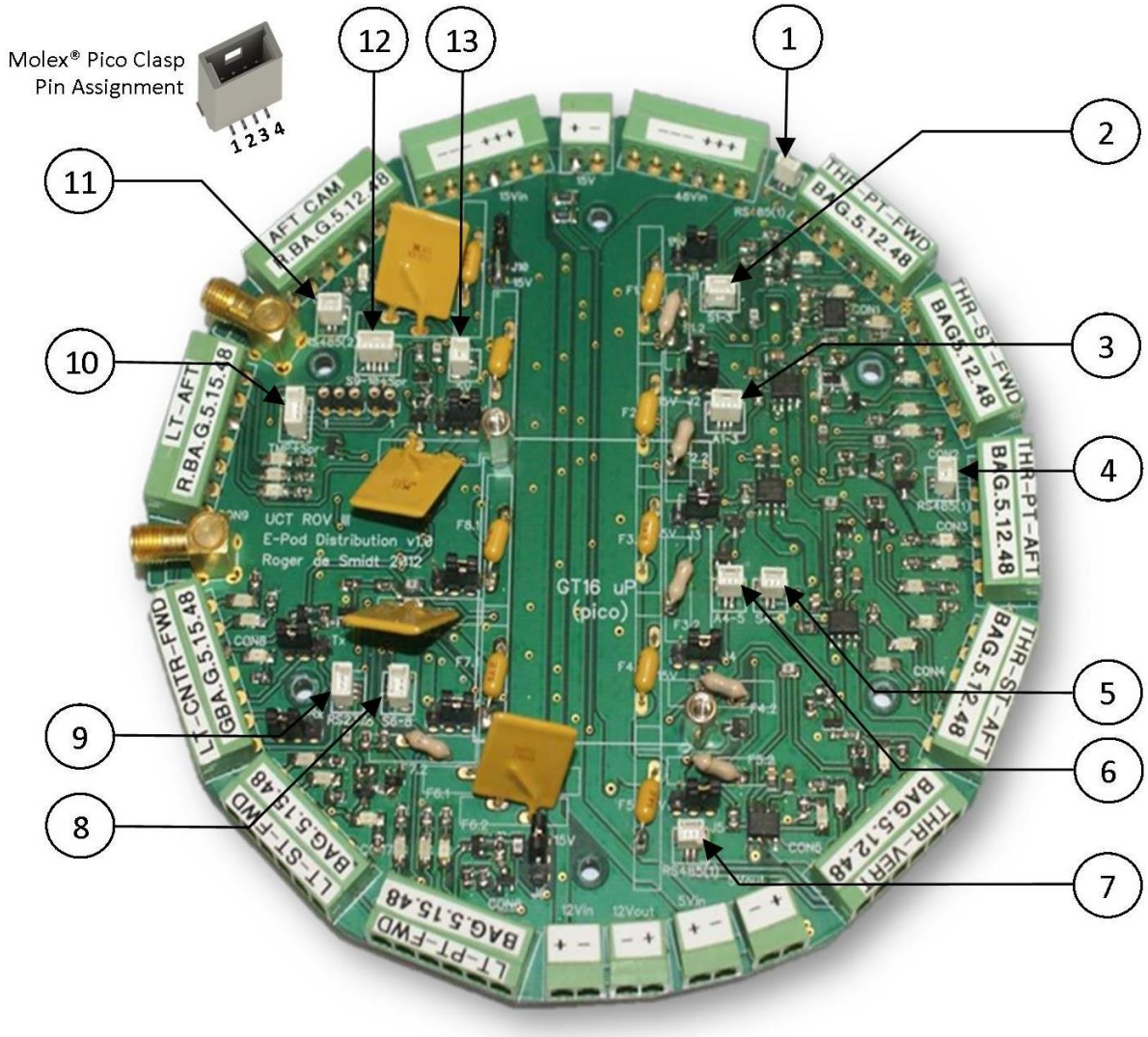

Figure 69: Distribution PCB Pico-Clasp™ connector numbering for Table 21

Table 21: Molex® Pico-Clasp™ connector pin assignments for distribution PCBs

Pico-Clasp™ Connectors (see Figure 69)							
Pin	**1**	**2**	**3**	**4**	**5**	**6**	**7**
	RS-485(1)	**S1-3**	**A1-3**	**RS-485(1)**	**S4-5**	**A4-5**	**RS-485(1)**
1	A	Switch 1	I_{SENSE} 1	A	Switch 4	I_{SENSE} 4	A
2	B	Switch 2	I_{SENSE} 2	B	Switch 5	I_{SENSE} 5	B
3	-	Switch 3	I_{SENSE} 3	-	-	-	-
4	-	-	-	-	-	-	-
	8	**9**	**10**	**11**	**12**	**13**	
Pin	**S6-8**	**RS-232**	**Temp & Spr**	**RS-485(2)**	**S9-10 & Spr**	**5 V**	
1	Switch 6	TX	Temperature	A	S9	+5 V	
2	Switch 7	RX	Spare I/O	B	S10	GND	
3	Switch 8	GND	Spare I/O	-	Spare I/O	-	
4	-	-	Spare I/O	-	Spare I/O	-	

4.5.3 Microcontroller Daughterboard

4.5.3.1 PCB Design

A microcontroller was required on each of the E-Pod's distribution PCBs to provide control of each output channel's power, read sensor outputs and communicate with the RS-485 Master unit. The Freescale® MC9S08GT16A microcontroller was chosen because it had been well used by the RARL for similar tasks. Furthermore, circuit schematics and software had already been developed and well tested using RS-232 communication interfaces. The RS-485 interface would be a relatively small change to the circuitry and new compact PCBs would need to be developed in any case to meet the requirements of the ROV. A full circuit schematic is included in Appendix B.

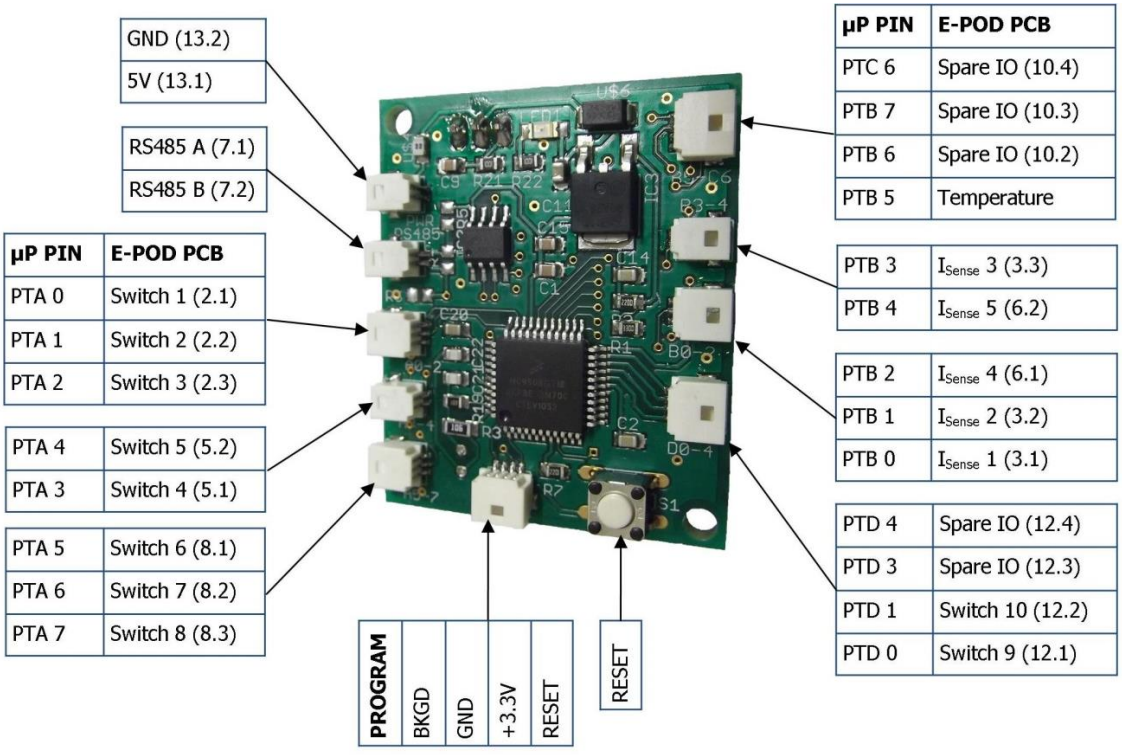

Figure 70: Pin assignment for the E-Pod microcontroller daughter board referenced to Figure 69 and Table 21

The two E-Pod distribution PCBs and a different distribution PCB designed for the Power Pod required a microcontroller so it was decided that its design be standardised as a daughterboard that could be mounted on each of these distribution PCBs. Header pins would have been a first choice for connecting the daughterboard to its host PCBs, but the layout of the E-Pod distribution PCBs would not accommodate such connectors easily. Molex® Pico-Clasp™ connectors and wiring were therefore used as the means of connection, and stand-offs were used for mounting the daughter boards. The microcontroller daughterboard and its pin assignments can be seen in Figure 70. The number in brackets next to each of the pin names refers to its corresponding pin on the E-Pod PCB.

Programming and debugging of the microcontroller was done using a P&E Micro® Background Debug Mode (BDM) Multilink unit and a connector for this purpose was provided at the bottom end of the PCB, as seen in Figure 70.

4.5.3.2 Software Design

The software written for each of the microcontrollers was very similar in structure, only varying on number of outputs to control and number of analogue signals to read. The programming structure applied to each controller is shown in the flowchart below.

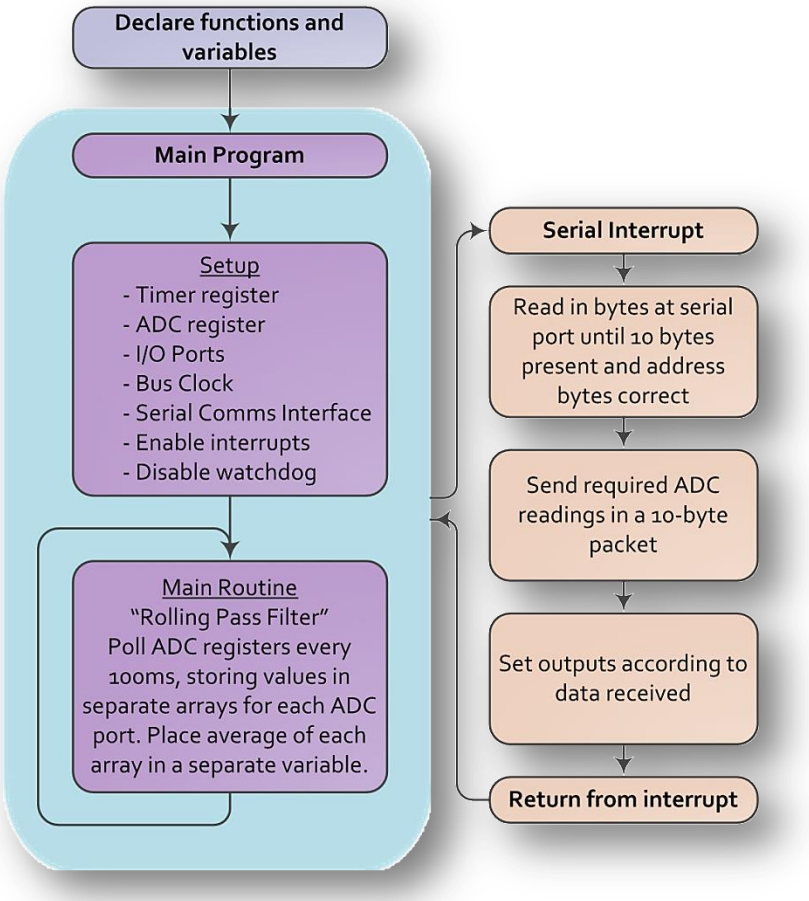

Figure 71: Flow chart of the programming structure for the MC9S08GT16A microcontrollers

4.5.3.3 Data Assignment in Communications Packets

The structure of the packets of data to be transmitted over the RS-485 network were the same as that described in Section 3.11. The top E-Pod PCB's controller was programmed to receive and send one packet of data only. Because of the greater number of channels to control and sensors to read on the bottom PCB, 2 packets of data were required for both receiving commands and returning sensor data. The assignment of data in the communications packets is shown in Table E1 and Table E2 in Appendix E.

4.6 SUMMARY

The E-Pod was designed to meet all of the specifications laid out at the beginning of this chapter. The E-Pod incorporated two microcontrollers and two custom-designed circuit boards that would manage the distribution of power and communications to each ROV module. Thruster current and E-Pod temperature monitoring were incorporated in the circuitry to provide feedback to the surface control station. A video encoder and communications modules were also incorporated to provide the necessary interface between the distribution circuitry and the fibre-optic link to the surface control station.

Detailed testing of the E-Pod's performance is presented in Chapter 8 and the calibration results for each of its sensors is provided in Appendix D.

The chapter that follows details the design of the Power Pod which was the next component in the power and communications distribution design hierarchy. The chapter starts with an overview of the system and then proceeds with design specifications and the detailed design of its constituent circuit boards.

5 POWER POD DESIGN

The Power Pod was to be the link in the power distribution system between the E-Pod and the tether's junction box on board the ROV. It would need to convert the 400 VDC power delivered via the tether to the voltage levels required by the modules on-board the ROV.

The rendered 3D model of the Power Pod design below in Figure 72 shows its stack of PCBs mounted on the housing lid, similar in concept to the method used to assemble the E-Pod electronics.

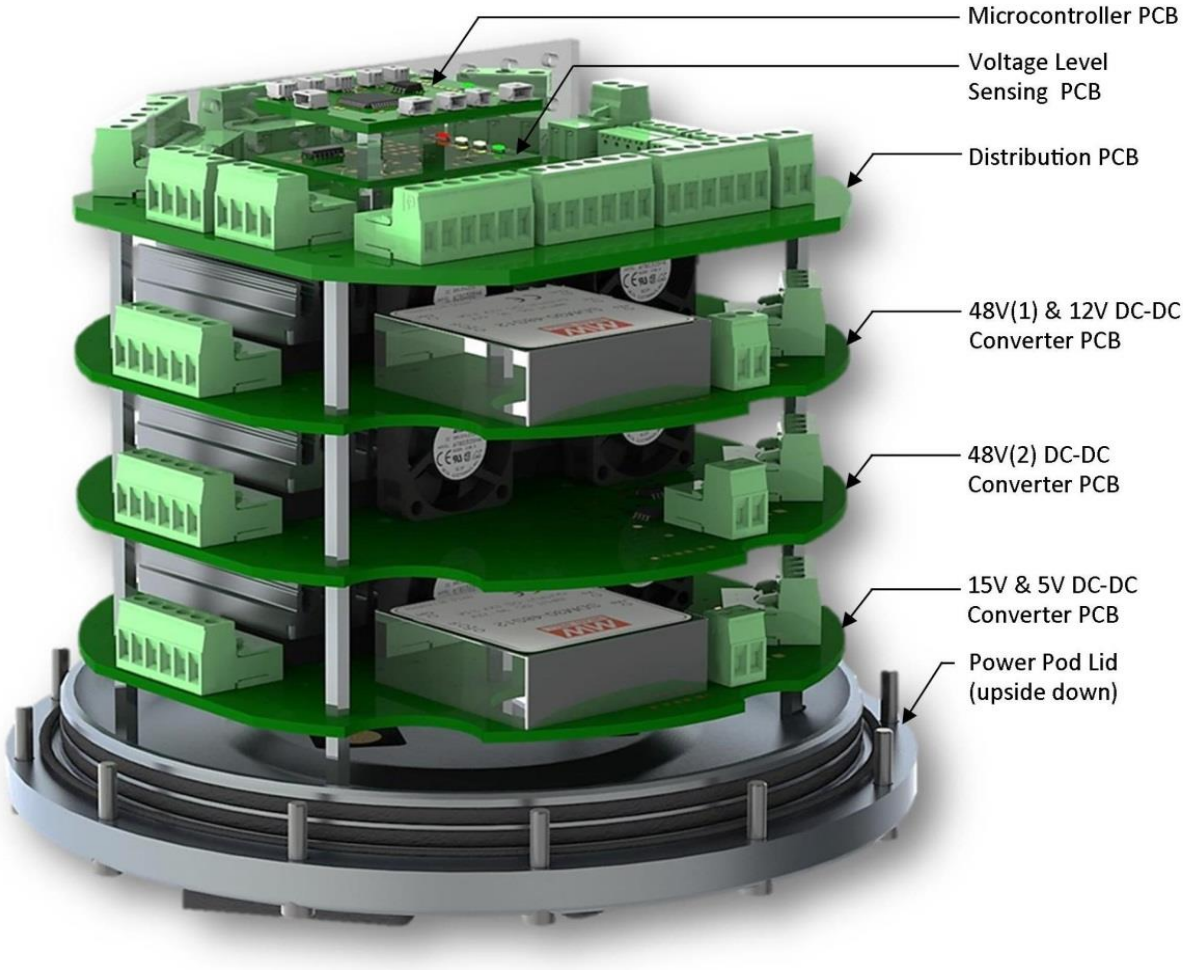

Figure 72: Rendering of the final design for the stack of PCBs in the Power Pod

After designing the housing for the E-Pod that would be reused for the Power Pod, specifying the ROV's tether transmission voltage to be 400 VDC, and establishing the supply voltages to each ROV module the primary constraints were already set for the design of the Power Pod. The challenge then was to design the DC voltage conversion circuits, the current sensing circuits and the power distribution circuit so that they would fit into the housing and provide the required performance.

Dimensioned views of the Power Pod are presented below in Figure 73 after which a progressive assembly of Power Pod circuit boards that embodied the final design is presented in Figure 74.

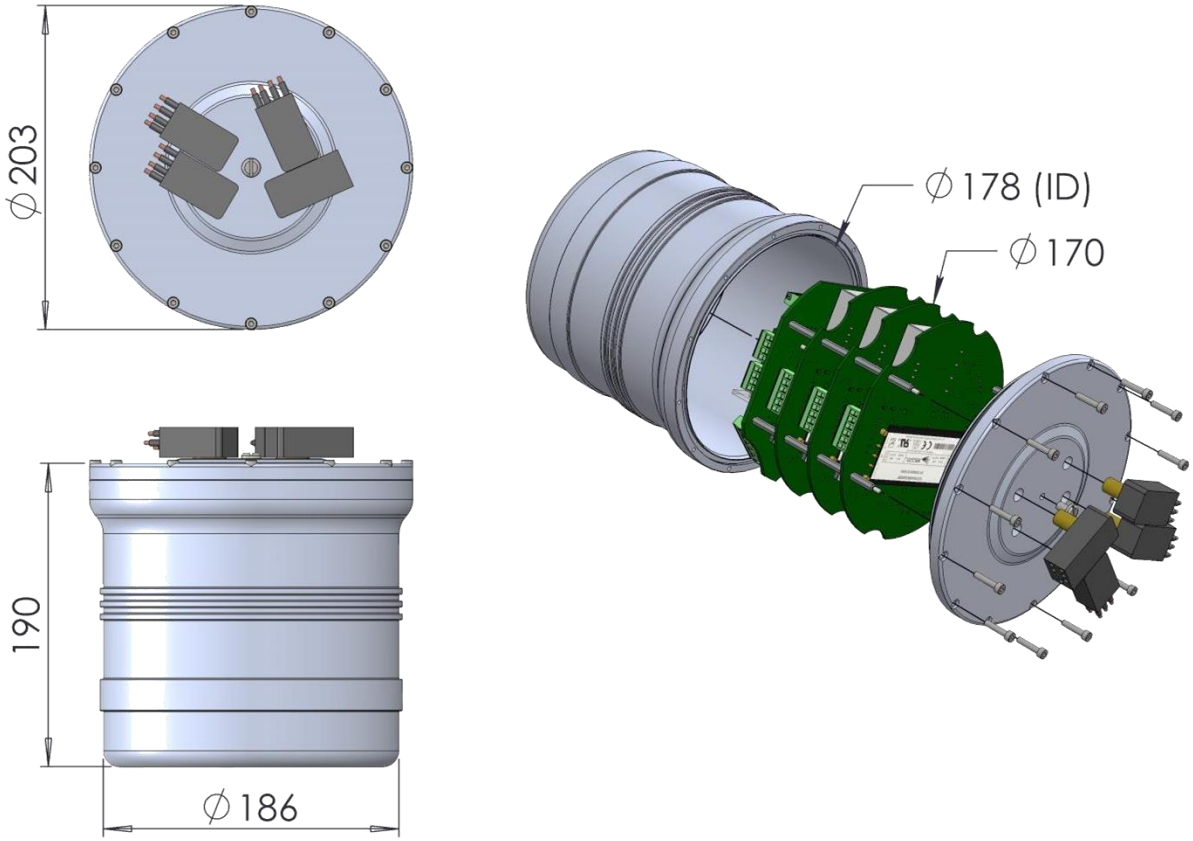

Figure 73: Dimensioned views of the Power Pod assembly

1. 15 V and 5 V DC-DC Converter PCB

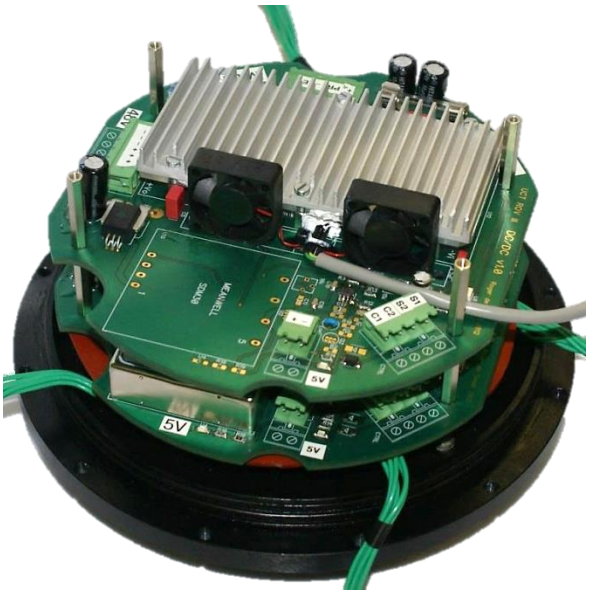

2. 48 V(2) DC-DC Converter PCB

3. 48 V and 12 V DC-DC Converter PCB

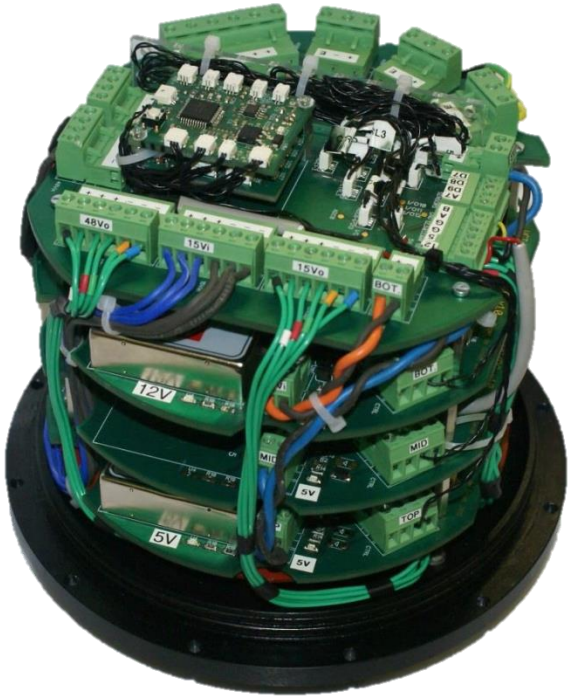

4. Distribution and control PCBs + wiring

Figure 74: Progressive assembly of electronics stack on the Power Pod lid

This chapter details the design of the different Power Pod circuit boards and their integration into the housing and with the rest of the ROV system. First, a list of the specifications and corresponding explanations for the design are presented below.

5.1 SPECIFICATIONS

Table 22: Power Pod specifications

Number	Description of Requirement	Target Values
Mechanical Specifications		
5.1.1	Internal dimensions	Ø178x165 mm
Electrical Specifications		
5.1.2	Output voltages	5, 12, 15 & 48 VDC
5.1.3	Output currents	
	48 VDC supply current to E-Pod	25A
	15 VDC supply current to E-Pod	14A
	12 VDC supply current to E-Pod	2.4A
	5 VDC supply current to E-Pod	2.2A
5.1.4	Input voltage	368-400 VDC
5.1.5	Ungrounded input voltage	Yes
5.1.6	Current monitoring accuracy on all outputs	±10%
Communication Specifications		
5.1.7	Serial communication protocol with E-Pod	RS-485
Thermal Specifications		
5.1.8	Ambient temperature monitoring accuracy	±2 °C

5.1.1 Internal Dimensions

The same pressure vessel design for the E-Pod electronics housing was to be used for the Power Pod. This would help minimise design time and provide the potential for standardisation on components such as brackets and fasteners. The detailed design of the housings is included in Appendix C at the end of this document.

5.1.2 Output Voltages

The output voltages were those required by the E-Pod. See Section 4.1.

5.1.3 Output Currents

The Power Pod was to supply the E-Pod with the power it required and therefore its output currents were based on those specified in Table 14 of Section 4.1 and Table 15 of Section 4.2.3. The 48 V supply would need to provide 1.08kW if all five thrusters were operating at full load. Because this was already a large demand for the power pod and because it was unlikely that the gripper module would draw its full load at the same time as all five thrusters, the power rating for the 48 V supply was set at 1.2kW. This would equate to a current demand of 25A.

For the other power supplies 20% extra headroom was specified to allow for future changes and additions to the lower power components in the system.

5.1.4 Input Voltage

In Section 3.10 the ROV power distribution system was discussed and 400 VDC was the voltage specified for power transmission to the ROV via the tether. As seen in Figure 50, a drop of 32 V was expected across the tether when operating at full load in which case only 368 V would be seen by the Power Pod. The expected input range to the Power Pod was therefore 368-400 VDC.

5.1.5 Ungrounded Input Voltage

Ungrounded power supply systems are considered safer than grounded systems where one rail of the supply, usually the negative rail, is referenced to earth potential. In a grounded system, if a person touches the earthed rail there will be no effect, while touching the other rail will induce an electric shock if the voltage is high enough. In the ungrounded system the rails are unreferenced and "floating". If a person is connected to earth and touches one of the floating supply rails, the other rail should shift relative to earth and the person will not be shocked, unless both rails are touched at the same time. The ungrounded system is widely used on commercially available ROVs and was specified for the Power Pod.

5.1.6 Current Monitoring on All Outputs

Feedback of the system electrical load was required as part of the system information to be displayed for the ROV pilot in the user interface. Current sensing would be performed for each major power consuming module of the ROV, but current sensing was also required to determine the total load on each power supply. The feedback could also be used to program load limiting functions into the control software of the host computer, if required. A tolerance of ±10% of the actual current value would be sufficient for the purposes of controlling the ROV as it would be used mainly for over current limiting and visual feedback to the operator, rather than for position or torque control, which would require a much greater degree of accuracy.

5.1.7 Serial Communication Protocol with E-Pod

To be easily integrated with the rest of the ROV modules, the Power Pod was to communicate over the RS-485 network.

5.1.8 Ambient Temperature Monitoring Accuracy

Temperature sensors were to be incorporated inside the Power Pod to help prevent its components from exceeding their maximum ratings. The control system was set with temperature limits for the Power Pod and Electronics Pod that were 5 °C lower than the maximum ratings for their respective components. It was therefore deemed reasonable to have a ±2 °C tolerance specified for the sensors.

5.2 DC-TO-DC CONVERTER CIRCUIT BOARDS

The DC-DC converter circuit boards were to be the primary components of the Power Pod, providing the four different power supply buses to the E-Pod. These circuit boards incorporated the DC-DC converter equipment, current sensing circuitry, ON/OFF control circuitry and cooling fans. A complete assembly of one of these boards is shown in Figure 75 below.

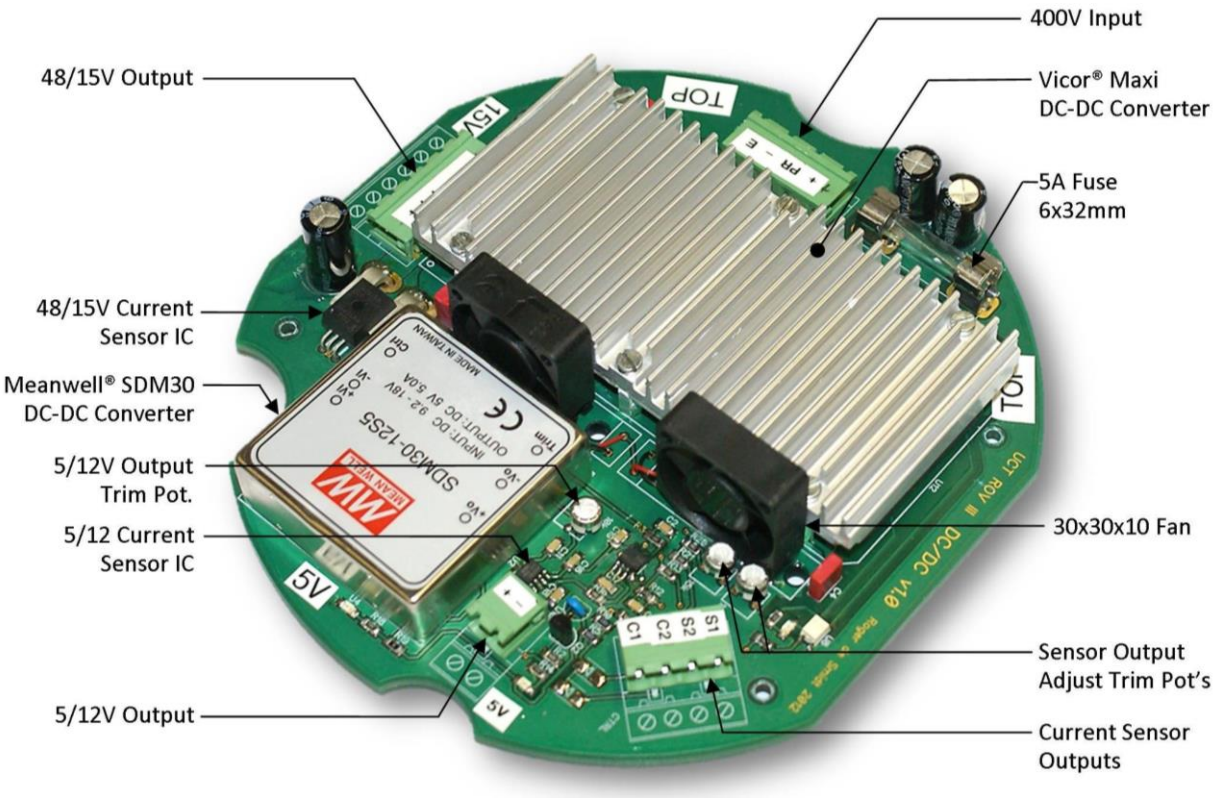

Figure 75: Power Pod DC-DC converter PCB assembled

The sections that follow below detail the design of these circuit boards with particular focus on the following main areas:

- selection of DC-DC converters
- DC-DC converter circuitry
- current sensing circuitry
- design of the PCB

5.2.1 DC-DC Converter Selection

There were four different voltage levels that were required on-board the ROV, each at a different current rating as listed in Table 22. The 48 V and 15 V supply buses required power outputs of 1344W and 210W respectively, and the 12 V and 5 V supplies required outputs of 29W and 11W respectively. There were therefore two large supplies and two small supplies to design.

High Power Converters

An extensive search was performed for compact DC-DC converters that would provide the required voltage and power levels. The commercially available complete DC-DC converter assembled units found on the market were too bulky to fit into the Power Pod. However, during the search for these units, DC-DC converter "bricks" from two different manufacturers were found. These "bricks", seen below in Figure 76, were extremely compact for their power throughput, but were produced for mounting on customer designed PCBs.

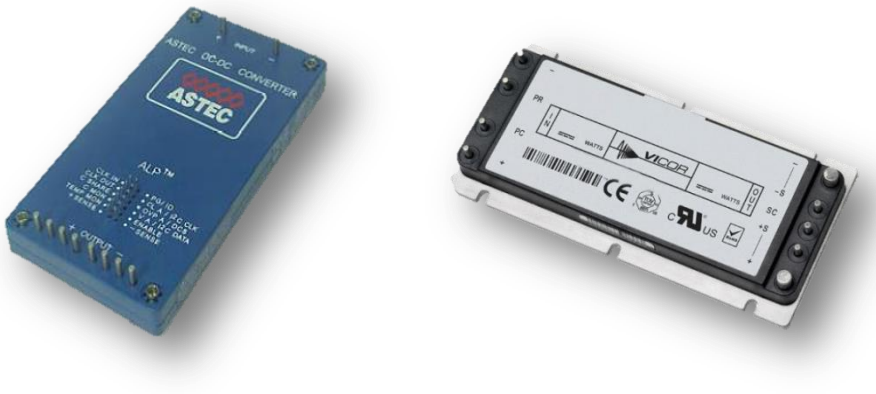

Figure 76: DC-DC Converter bricks from Astec® and Vicor®

The brick type DC-DC converters were the most compact and affordable voltage conversion modules that could be found on the market and no voltage converters with the required current sensing circuitry were available in a complete, stand-alone sealed unit that fitted into the Power Pod. The brick type converter was therefore selected for integration into a customised PCB that would meet the requirements of the Power Pod.

Both the Astec® AIF12W300 and the Vicor® Maxi converters could supply up to 600W, provide the voltage level conversions required on the ROV, and could be paralleled to increase power capacity on a given supply. However, the Vicor® module was available at about half the price of the Astec® unit so was selected for use in the Power Pod.

Two Vicor® Maxi 375 V input modules with output power ratings of 600W each were selected for the 48 V supply bus and a 375 V input, 400W output module was selected for the 15 V bus. The 375 V input was the nominal voltage of an allowable input 250-420 V range. The 1200W 48 V supply would comfortably provide the 1080W required by the full thruster compliment on the ROV and still have a little to spare. The 15 V bus was well over-specified at 400W, but had the smaller power

capacity of the two options available and, being the same size as the 600W 48 V unit would provide opportunity to standardise the PCB layout. The 400W unit would also provide capacity for potential added demand in the future.

The 48 V and 15 V Maxi converters operated at efficiencies of 88.5% and 85.3% respectively. This meant that the 48 V converter would need to dissipate up to 78 W of heat energy and the 15 V converter up to 69 W. To help facilitate this, aluminium heat sinks supplied by Vicor® were bolted to the baseplate of each converter using silicone heat transfer compound on the mating surfaces to ensure low thermal resistance between them. The heat sinks effectively increased the baseplate surface area which was to be force-cooled using fans mounted on the PCB.

Low Power DC-DC Converters

For the lower power DC-DC converters required for the 12 V and 5 V buses, Meanwell® SDM units were used. The RARL had used these units and other Meanwell® voltage converters in the past with great success. These units were also the type that would need to be mounted on a custom-designed PCB.

For the 12 V supply bus the 30 W, 2.5 A module was selected and for the 5 V bus the 5 A module was selected. The 5 V, 5 A module had more than double the capacity required, but this would provide for potential added future requirements and also came in the same package as the 12 V unit which would allow for standardisation of PCB layouts.

The details of the control circuitry design for the DC-DC converters follow in the next section.

5.2.2 DC-DC Converter Circuitry

The circuit design for each of the DC-DC converters was based upon the recommended circuits by the respective manufacturers. These circuits are described below, each in their own section. Table 23 below lists the maximum ratings for each of the DC-DC converters.

Table 23: Maximum ratings for the Power Pod DC-DC converters

DC-DC Converter	Voltage In [VDC]	Voltage Out [VDC]	Current Out [A]	Max. Working Temp. [°C]	Overload/ Over-voltage
Vicor® Maxi 375/48 V	250-425	43.2-52.8	12.5	100	16.3A/17.8 V
Vicor® Maxi 375/15 V	250-425	13.5-16.5	26.7	100	30.7A/55.2 V
Meanwell® 48/12 V	36-72	10.8-13.2	12.5	85	31.5W
Meanwell® 12/5 V	9.2-18	4.5-5.5	2.5	85	26.25W

5.2.2.1 Vicor® Maxi Converter Circuit

The high power DC-DC converter circuit was designed for a nominal input of 400 VDC and an output of either 48 VDC or 15 VDC, depending on exactly which Vicor® Maxi module was used. The final circuit diagram for these modules is presented in Figure 77 after which its key components are described.

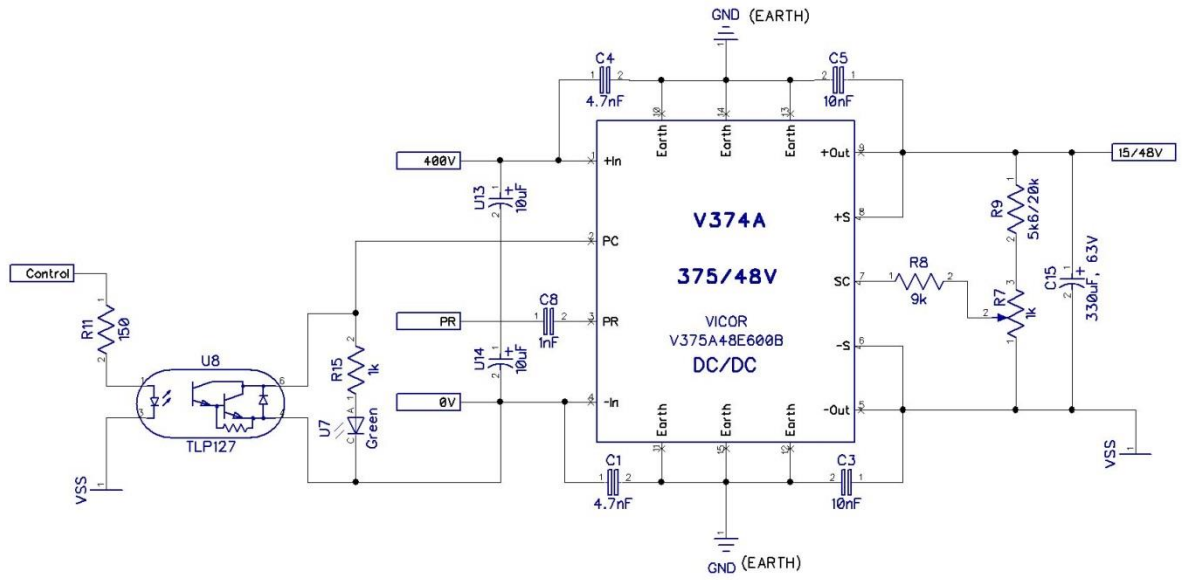

Figure 77: Circuit schematic for high power DC-DC converters

5.2.2.1.1 Capacitors

Although the 400 V input was an ungrounded supply, decoupling capacitors were still required between positive and earth and between negative and earth on both input and output terminals. The capacitance values were selected according to Vicor's recommendations [46] and are shown in the schematic above. Y-rated capacitors were required for this application to ensure that if they were to fail, they would fail in an open-circuit state. This would help ensure that none of the power supply lines would connect to earth and thereby create a shock hazard, and was particularly important on the 400 V input side. Wima® MKP 2 Capacitors were sourced for this application.

The bypass capacitors between the input rails and between the output rails were specified for the greatest capacitance possible to remove transient spikes and as much noise as possible. The limiting factor with these capacitors was the physical dimensions of each capacitor, and they were chosen to suit the dimensions available on the PCB. Due to the 400 V potential difference across the input, two 250 V electrolytic capacitors were used in series so as to reduce the size of the capacitors required. With a standard ±20% tolerance on these 250 V capacitors, they would provide a minimum voltage rating of 400 V across their terminals, as required.

5.2.2.1.2 Output Voltage Adjustment

The Vicor® Maxi converters were supplied with sensing terminals that could be configured to adjust the output voltage between 10% and 110% of the nominal value. As seen in Figure 77 above, an adjustable resistor divider provided feedback to the sensing input. The **SC** pin of the module when not connected sits at 1.23 V above the **-Out** pin. Applying a voltage relative to the 1.23 V to the **SC** pin will produce a change on the **+Out** pin of the same proportion. So, for example, if 13.5 V is required from the 15 V module output, a voltage of 1.107 V should be applied to the **SC** pin (-10%) [46]. An online Vicor® calculator was then used to establish the required resistor and potentiometer

values for ±10% trim on each module's output [47]. This was the only method provided by the manufacturer and unfortunately no formulae were provided for calculation from first principles.

5.2.2.1.3 ON/OFF Control

The DC-DC converters as designed for this application would not have their outputs controlled remotely because any shutdown of the outputs would shut down the control circuitry, thereby committing a form of ROV suicide. However, this functionality was built into the design should the power supply be restructured in the future and a power supply reset function desirable.

In order to disable the output of any Maxi module the **PC** pin which normally sits at 5.75 V above **-In** needed to be pulled below 2.3 V relative to **-In**. To maintain isolation between the input and output side of the converters, a Toshiba® TLP127 opto-coupler was used like a transistor to pull the PC voltage down if a logic high signal was provided by the microcontroller (see Figure 77).

5.2.2.2 Meanwell® SDM30 Converter Circuit

The low power DC-DC converter circuit was designed for a nominal input of 48 V or 15 V and an output of either 12 V or 5 V respectively, depending on exactly which Meanwell® SDM30 module was used. The final circuit diagram for these modules is presented below in Figure 78.

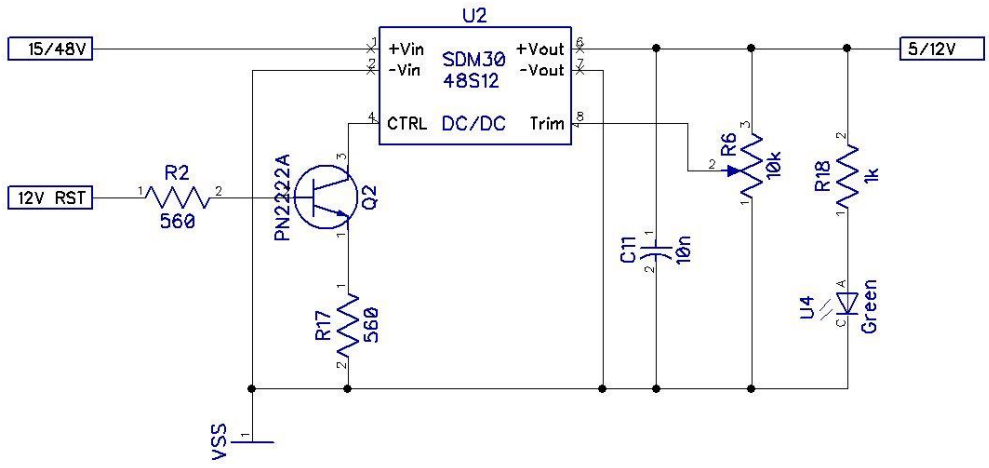

Figure 78: Circuit schematic for low power DC-DC converters

Although the SDM30 modules required less circuitry than the Maxi modules, its structure was very similar to that of the Maxi modules and each of the key components is described below.

5.2.2.2.1 Capacitance

With no isolation required between input and output, no decoupling capacitance was required in the circuit. Bypass capacitance was also excluded from the input because it would be connected close to the output of the Maxi module, which was fitted with a 330 µF bypass capacitor. However, a small bypass capacitor was connected across the output to smooth out potential noise.

5.2.2.2.2 Output Voltage Adjustment

The output of both SDM30 modules could be trimmed over a ±10% range. To do this, a trim-pot was connected between the output pins and the **Trim** pin as shown in Figure 78 and as per recommendation in the SDM30 datasheet which can be found on the accompanying DVD.

5.2.2.2.3 ON/OFF Control

The circuit was configured so that a logic high signal from the microcontroller would disable the output of the converter. A transistor was used to do this switching, as shown in Figure 78. The remote reset function that this part of the circuit provided, similar to the Maxi module's circuit, was as an option for future modifications and was not incorporated in the current operation of the system.

In order to monitor the currents drawn from each of the supplies described above, additional circuitry would be required. The sections that follow describe the design of these current-sensing circuits.

5.2.3 Current-Sensing Circuitry

Similar to the current sensing circuitry implemented on the E-Pod distribution PCBs, Allegro® ACS sensors were used to measure the Power Pod output currents. The same ACS715 IC was used to measure the outputs of the 5 V and 12 V supplies, while a heavier duty ACS758 was used for the 15 V and 48 V supplies.

The ACS758 IC had a current sensing range of 0-50 A. This would be excessive for the rated 12.5 A from each of the 48 V converters, but was needed to accommodate the 26.7 A from the 15 V converter. While an ACS715 could have been used for the 48 V current sensing, using the ACS758, which was a different package to the ACS715, would allow for standardisation on the design of the PCBs.

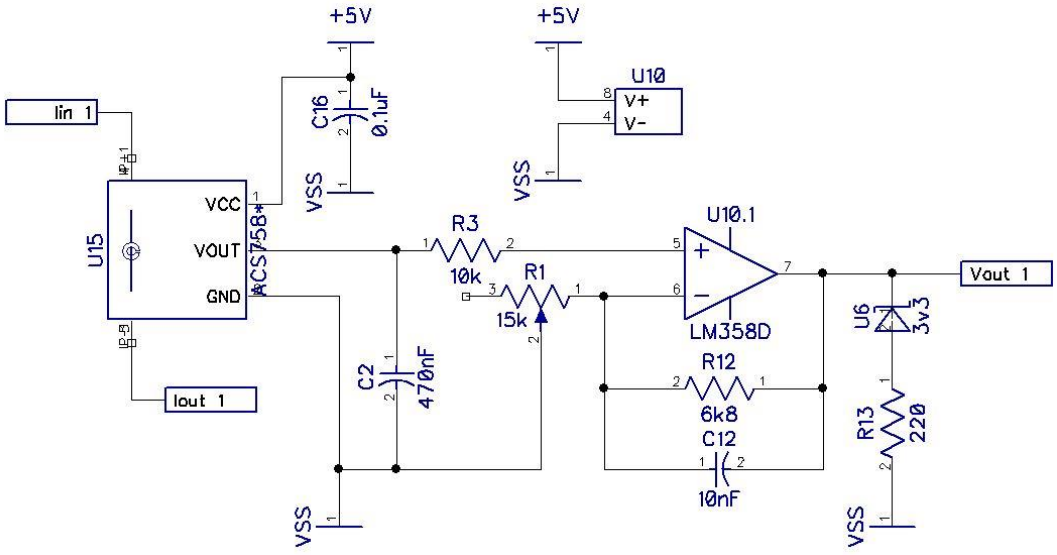

Figure 79: Schematic of the current sensing circuit for the 15 V & 48 V output

The schematic in Figure 79 shows the current sensing part of the circuit for the 15 V and 48 V outputs. The circuitry for the 5 V and 12 V outputs is very similar, schematics of which can be found on the accompanying DVD. The schematic shows the amplification circuit on the output of the ACS758. An LM358 operational amplifier was used to implement a variable amplifier that could be adjusted to amplify the output voltage to its ideal value during testing. Once potentiometer R1 had been adjusted, polyurethane paint or epoxy resin could be used to secure its position. The output voltage could not exceed 3.3 V without risking damage to the microcontroller ADC input that would be reading this signal so adjustments would have to take into account what output voltage the maximum current would induce. To help protect the microcontroller input from over-voltage conditions, a 3.3 V zener diode was connected between the output signal and ground.

5.2.4 PCB Design

Standardisation of the PCBs for the DC-DC converter circuits was one of the key goals during the design process. Standardised PCBs would reduce manufacturing costs, increase the ability to interchange components and potentially decrease initial design time.

DC-DC Converter Configuration

Although two Vicor® Maxi converters could fit side by side on one PCB, the build-up of heat expected from the two adjacent Vicor® modules would create a challenge to provide sufficient cooling. Two Maxi modules placed side-by-side would also allow little remaining space on the PCB for sensing and control circuitry and would require two different types of PCBs to be manufactured: one for the Maxi modules and one for the SDM30 modules. These three factors led to the standardised design seen in Figure 75. The final PCB assembly incorporated one Vicor® module and one Meanwell® module per PCB as well as standardised sensing and control circuits as described in the preceding sections. The final design of the PCB can be seen in the layout and schematic in Figure 80 and Figure 81 respectively.

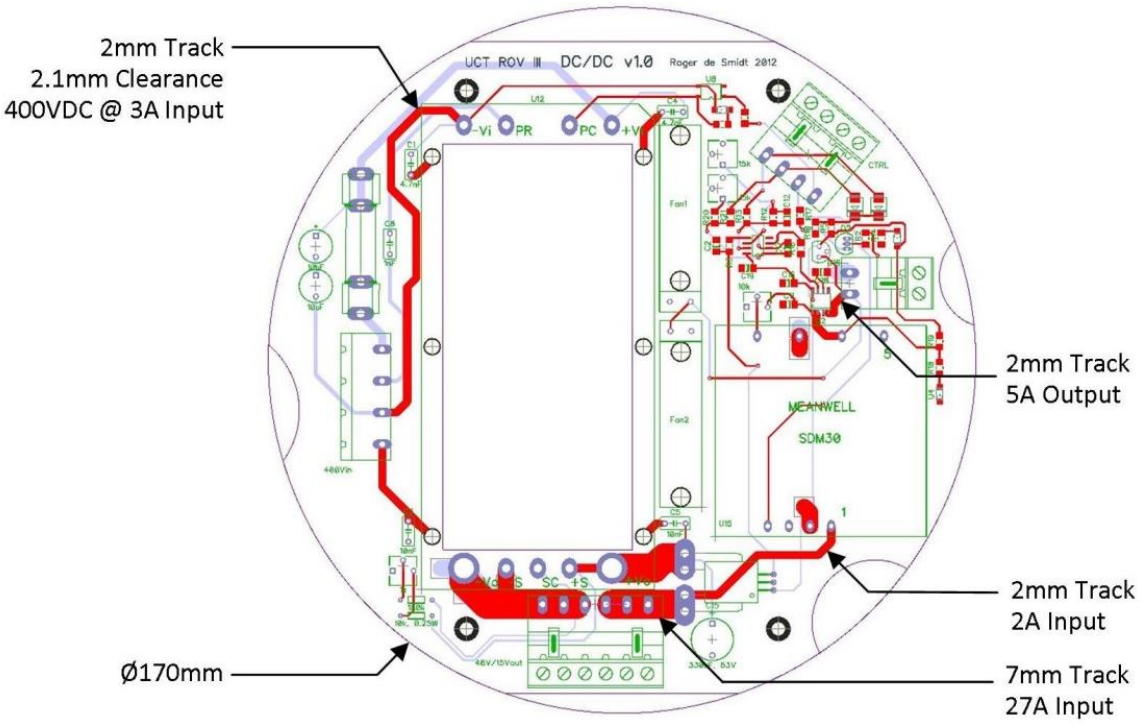

Figure 80: Power Pod DC-DC converter PCB layout

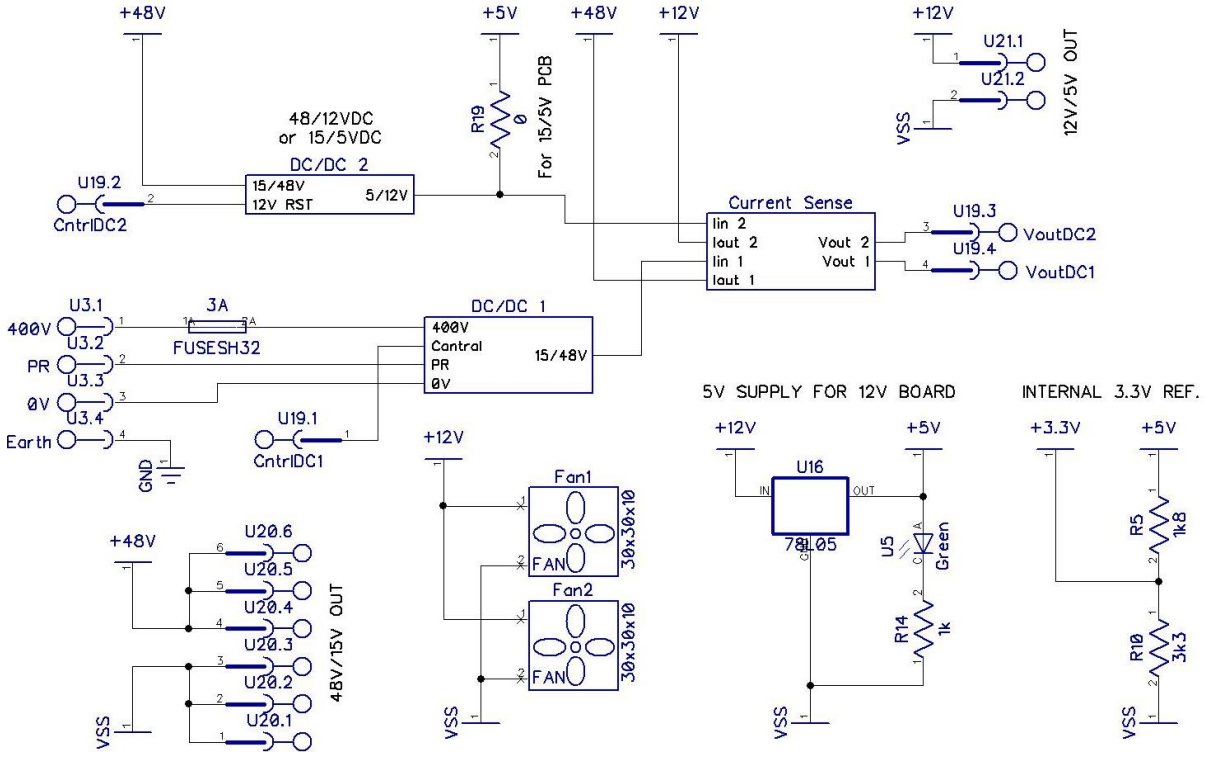

Figure 81: Main circuit schematic for DC-DC converter PCBs

The circuit schematic above incorporates function blocks for each of the circuits described in the relevant preceding sections. For a full set of circuit schematics, refer to the accompanying DVD.

Copper Track Sizing

As shown in the PCB layout in Figure 80, the copper tracks were sized according to the rated current that they would carry. The same design principles were used as described for the E-Pod distribution PCBs in Section 4.5.2.3. The only difference in design rules used for the Power Pod PCB layout was a significant increase in clearance required around the tracks and pads carrying the 400 VDC supply. A clearance of 0.005 mm per volt was specified by the IPC-2221 printed circuit design standard for external conductors on a bare board at less than 3050 m above sea-level [48]. This was considered to be an extreme case the ROV was not likely to encounter. Allowing for a design voltage of 420 V which was the maximum allowable input for the Maxi module, a total minimum clearance of 2.1 mm was calculated. The PCB would be coated with a solder mask that would provide increased insulation for the copper tracks so in most cases on the PCB the allowable voltage rating would be much higher.

Connectors

A 7.62 mm pitch Phoenix® Combicon GMSTBA connector, rated for 600 V and 16A per pin was used for the 400 VDC supply input. 5.08 mm MSTBA connectors were used for the output connectors and were rated for 10 A per pin at 300 V.

Cooling

As mentioned in 5.2.1, cooling fans were required to transfer heat away from the Vicor® module heat sink. Due to the limited height available for the Power Pod electronics stack the height of components on the PCB needed to be minimized. Two small PCB axial fans with dimensions of 30x30x10 mm were therefore placed alongside each other to blow air across the transverse fins of the heat sinks, as seen in Figure 75.

5.2.5 Temperature Sensing

In order to monitor the temperature of the DC-DC converters to help reduce the risk of damage to system components, a Texas Instruments® LM60 temperature transducer was placed against the side of the 48 V Maxi module on the mid-level PCB. Silicone heat transfer compound was applied to the transducer to ensure a good thermal connection to the side of the module. It was connected electrically to the Power Pod distribution board using screened cable to reduce the electro-magnetic interference (EMI) noise on its output. Figure 82 below shows the LM60 secured against the side of the Maxi module.

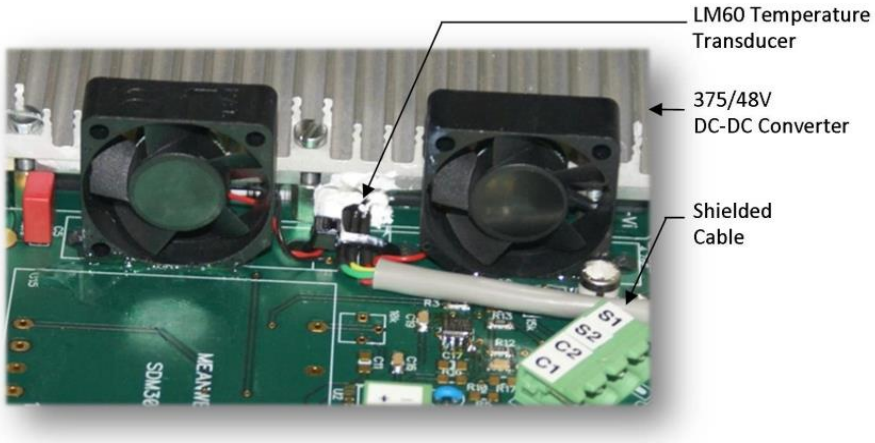

Figure 82: Temperature Transducer position on 48 V DC-DC converter PCB

5.3 POWER DISTRIBUTION CIRCUIT BOARD

A centralised connection point was needed inside the Power Pod as a junction between all the DC-DC converter outputs and the wiring to the bulkhead connectors that would feed the E-Pod. A centralised connection point was also required for the microcontroller that would be receiving information and potentially providing control to each of the PCBs.

The distribution PCB was designed to provide this centralised connection point for the power supply buses and the microcontroller connections. The final design is shown below in Figure 83.

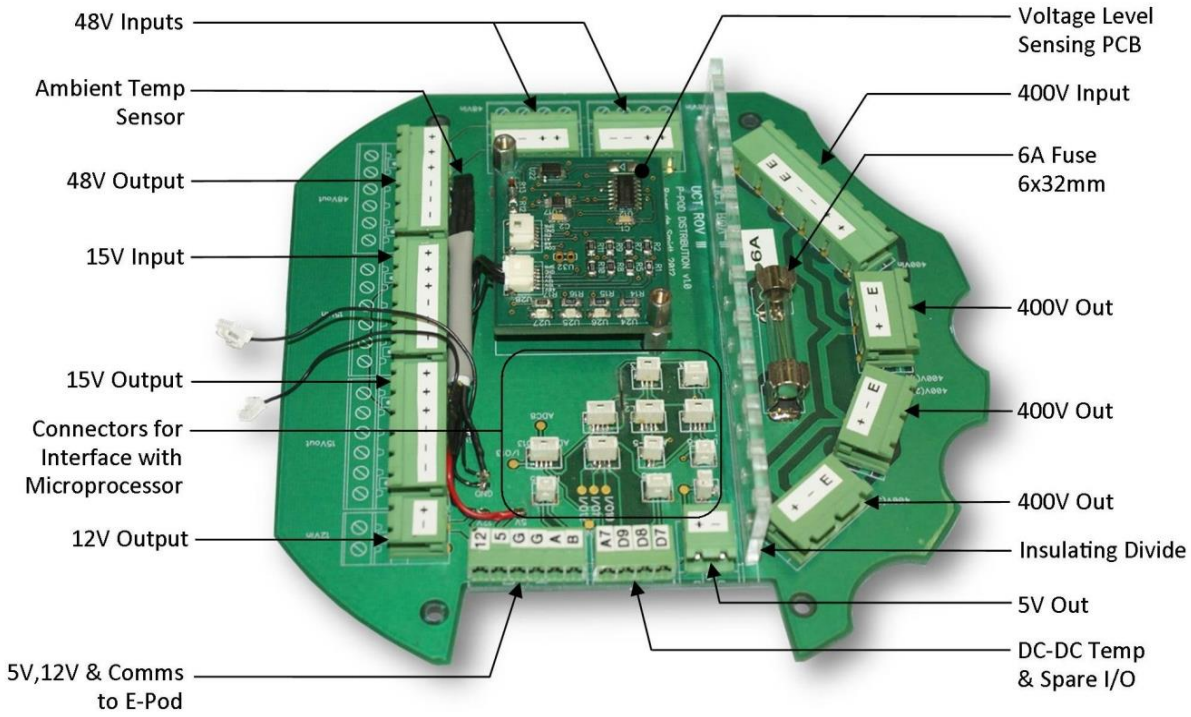

Figure 83: Photo of the Power Pod's distribution PCB

5.3.1.1 High Voltage Connections

On the right side of the image above the high voltage connections are shown. These were to provide the link between the incoming 400 VDC power supply from the tether and each of the three DC-DC converter PCBs. The connectors used were the Phoenix® Combicon GMSTBA type with a 7.62 mm pitch, and were rated for 600 V and 16A per pin. A fuse was incorporated to provide protection for the main incoming connection. Due to the high voltages used, it was necessary to install a 6.3x32 mm cartridge fuse that would provide the isolation required in the event of it fusing.

5.3.1.2 Low Voltage Connections

The low voltage connections that provided the link between the DC-DC converter PCBs and the bulkhead output connectors to the E-Pod are shown on the left side of the PCB in the image above. The GMSTBA type connectors were also used for these connections because of their high current rating. Up to 8.5A was expected to flow through some of these pins so the greater the current capacity, the less chance there was for them to heat up when connected poorly.

The low power 12 V and 5 V supplies were connected to a bulkhead output via the smaller 6-pin Phoenix® MC connector which was rated for 8 A per pin.

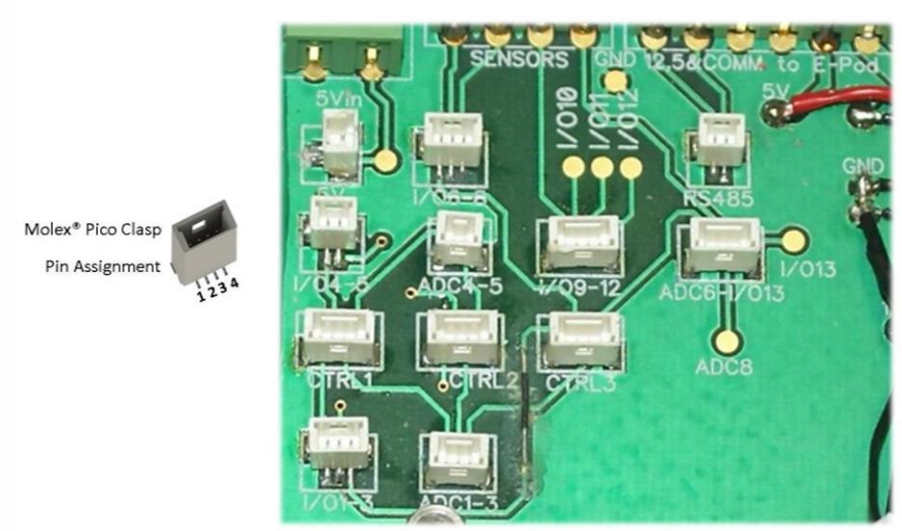

Pico-Clasp™ Connectors (see Figure 83)						
Pin	**I/O 1-3**	**I/O 4-5**	**I/O 6-8**	**I/O 9-12**	**ADC 1-3**	**ADC 4-5**
1	PTA7	PTA3	PTA2	PTD0	PTB3	PTB0
2	PTA6	PTA4	PTA1	PTC6	PTB4	NC
3	PTA5	-	PTA0	NC	PTB5	-
4	-	-	-	NC	-	-
Pin	**ADC 6 – I/O 13**	**CTRL 1**	**CTRL 2**	**CTRL 3**	**5 Vin**	**RS-485**
1	PTB2	NC	NC	NC	+5 V	A
2	PTB6	NC	NC	NC	GND	B
3	NC	48 V(1) I_{Sense} (S1)	48 V(2) I_{Sense} (S1)	15 V I_{Sense} (S1)	-	-
4	NC	12 V I_{Sense} (S2)	NC	5 V I_{Sense} (S2)	-	-

Figure 84: Zoomed-In view and pin assignment of the distribution PCB Pico-Clasp™ connectors

5.3.1.3 Microcontroller and Temperature Sensing

The microcontroller daughterboard detailed in Section 4.5.3 was incorporated into the design of the distribution PCB. It would be mounted on stand-offs above the voltage level sensing (VLS) daughterboard shown in Figure 83 and connect to the distribution board via Molex® Pico-Clasp™ connectors and wires. These Pico-Clasp™ connectors and their pin assignments are presented above in Figure 84.

Temperature sensing was setup in two locations inside the Power Pod, one to monitor the ambient temperature and the other to monitor the temperature of one of the 48 V DC-DC converters. The ambient temperature sensor is shown in Figure 83 and is connected directly to a microcontroller ADC input. The 48 V converter temperature sensor location is shown in Figure 82 in Section 5.2.5 and is connected to the microcontroller via pin A7 on the 4-pin Phoenix® MC connector (*DC-DC Temp & Spare I/O*) on the distribution PCB.

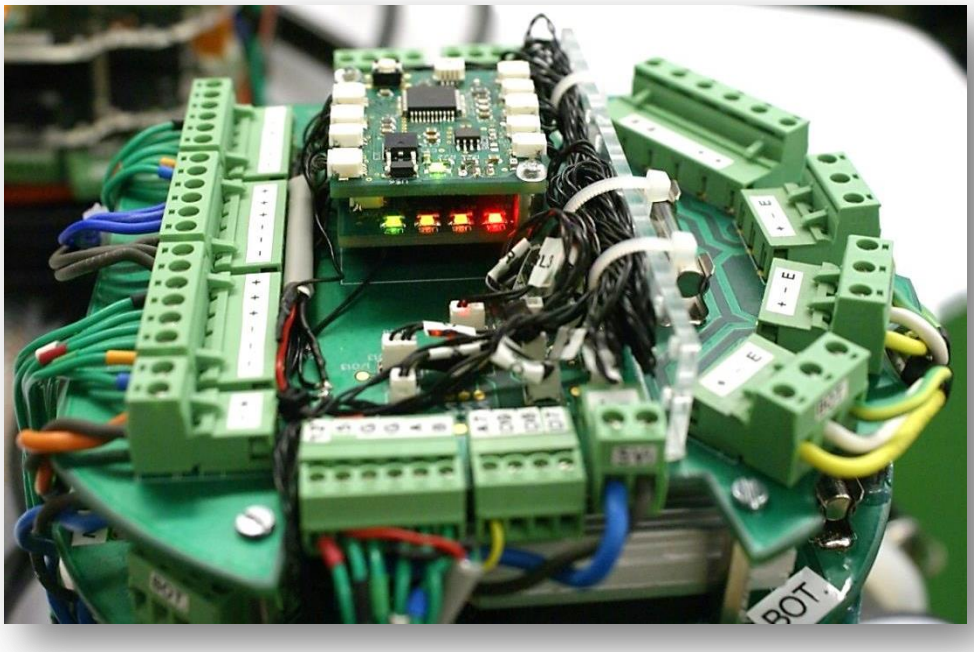

Figure 85: Photo of the Power Pod distribution PCB in operation

5.4 VOLTAGE LEVEL SENSING CIRCUIT BOARD

The voltage level sensing (VLS) circuit was designed to facilitate monitoring of the power supply bus voltages and is shown mounted on the distribution PCB in Figure 83. A photo of the board with pin assignments overlaid is shown below in Figure 86.

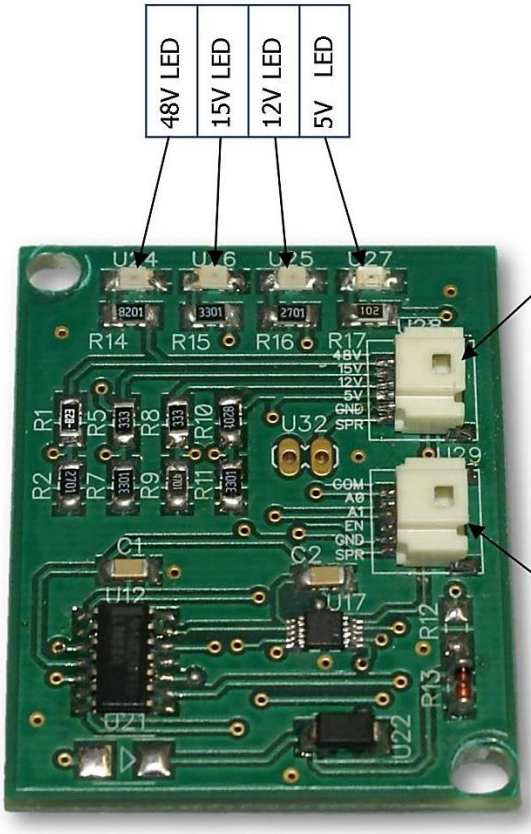

PIN	Distribution PCB
48V	48V
15V	15V
12V	12V
5V	5V
GND	0V
SPR	Spare

PIN	GT16 µP PCB
COM (ADC)	PTB7
A0 (MUX)	PTD3
A1 (MUX)	PTD4
EN (MUX)	PTD1
GND	GND
SPR	Spare

Figure 86: Photo of the voltage level sensing PCB and pin assignments overlaid

The microcontroller ADC inputs could only read voltage levels up to its positive supply rail voltage of 3.3 V. The voltage level of each power supply was therefore passed through a voltage divider and then buffered before being fed through a multiplexer to the micro controller ADC input. Because only one ADC input was available for the VLS signals and because the signals could be acquired at low speed, it was decided that an analogue multiplexer was to be used to feed the four signals sequentially to the microcontroller. Three digital outputs were required from the microcontroller to control the multiplexer and its pin configuration is shown below in Table 24. A full circuit schematic can be found on the accompanying DVD and calibration results of the measured levels are presented in Appendix D.

Table 24: Multiplexer pin configuration for voltage level sensing circuit

A1 (PTD4)	A0 (PDT3)	EN (PTD1)	Power Supply
X	X	0	-
0	0	1	**48 V**
0	1	1	**15 V**
1	0	1	**12 V**
1	1	1	**5 V**

5.5 MICROCONTROLLER DAUGHTERBOARD

5.5.1 Pin Assignment

The microcontroller PCB designed for use in the Power Pod and E-Pod is described in Section 4.5.3. It was standardised to suit the applications of both pods. The description of the design is not repeated here, but the assignment of its connector pins configured for the Power Pod is presented below in Figure 87.

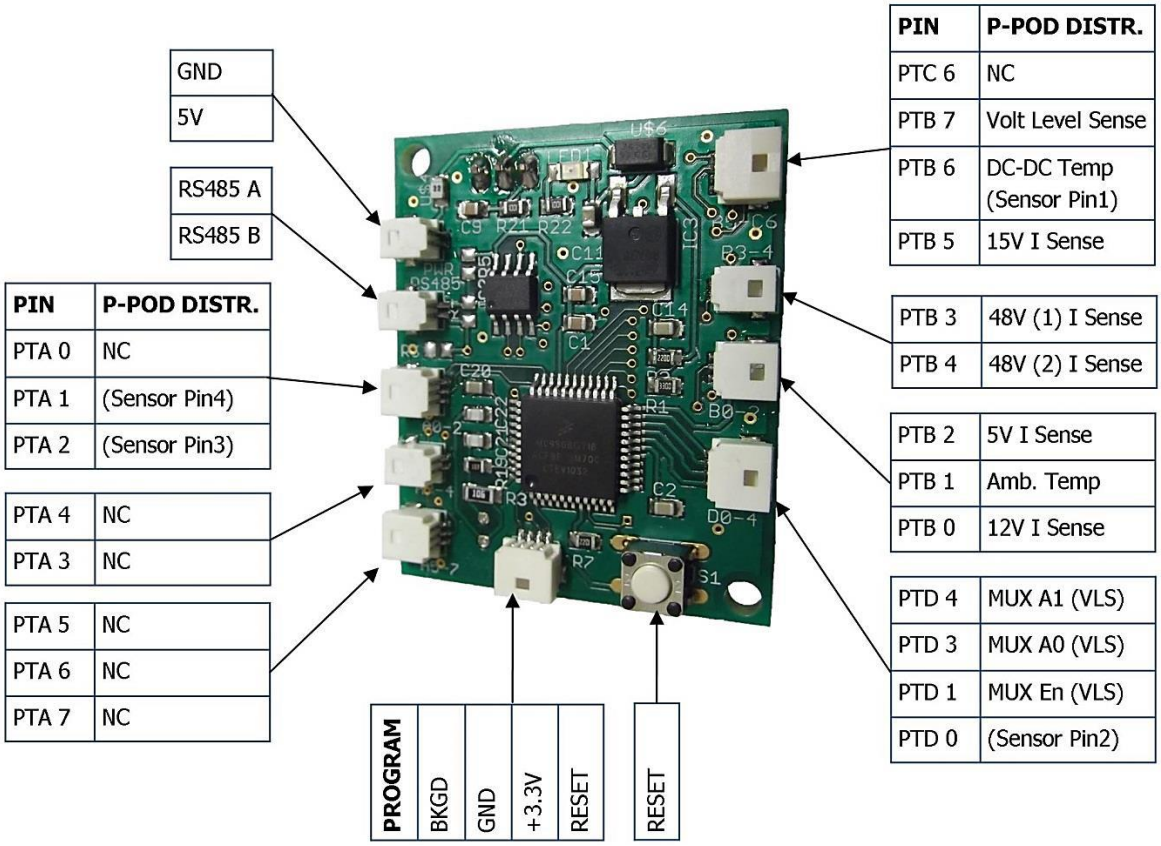

Figure 87: Power Pod microcontroller daughter board pin assignment

5.5.2 Data assignment in Communication Packets

There were no components in the Power Pod that required control, but there were enough sensors that needed reading to use up all of the available ADC pins on the microcontroller. Because the ADC was set to read analogue signals with 10-bit resolution two bytes were required to communicate each ADC value to the host computer. The net result of all the sensor readings at 10-bit resolution was that 22 bytes of sensor data needed to be sent from the Power Pod microcontroller to the host computer. As seen in Table 25 three bytes were taken up with addressing and packet identification, so a total of 4 different packets were needed to contain the data. This table shows the assignment of each of these bytes within the different packets for the Power Pod. The set of packets would be cycled through repeatedly using the same communication structure described in Section 4.5.3.

Table 25: E-Pod bottom microcontroller serial communications data assignment

RECEIVE	**Addr. 1**	**Addr. 2**	**Data 1**	**Data 2**	**Data 3**	**Data 4**	**Data 5**	**Data 6**	**Data 7**	**Data 8**
	1st Address	2nd Address	Packet ID	-	-	-	-	-	-	-
	240	120	**1/2/3/4**	0	0	0	0	0	0	0
SEND	**Addr. 1**	**Addr. 2**	**Data 1**	**Data 2**	**Data 3**	**Data 4**	**Data 5**	**Data 6**	**Data 7**	**Data 8**
	1st Address	2nd Address	Packet ID	12 V I_{sense} (hi)	12 V I_{sense} (lo)	5 V I_{sense} (hi)	5 V I_{sense} (lo)	48 V(1) I_{sense} (hi)	48 V(1) I_{sense} (lo)	-
	240	120	**1**	0-3	0-255	0-3	0-255	0-3	0-255	0
	Addr. 1	**Addr. 2**	**Data 1**	**Data 2**	**Data 3**	**Data 4**	**Data 5**	**Data 6**	**Data 7**	**Data 8**
	1st Address	2nd Address	Packet ID	48 V(1) I_{sense} (hi)	48 V(1) I_{sense} (lo)	15 V I_{sense} (hi)	15 V I_{sense} (lo)	48 V DC-DC Temp (hi)	48 V DC-DC Temp (lo)	-
	240	120	**2**	0-3	0-255	0-3	0-255	0-3	0-255	0
	Addr. 1	**Addr. 2**	**Data 1**	**Data 2**	**Data 3**	**Data 4**	**Data 5**	**Data 6**	**Data 7**	**Data 8**
	1st Address	2nd Address	Packet ID	48 V Level (hi)	48 V Level (lo)	15 V Level (hi)	15 V Level (lo)	12 V Level (hi)	12 V Level (lo)	-
	240	120	**3**	0-3	0-255	0-3	0-255	0-3	0-255	0
	Addr. 1	**Addr. 2**	**Data 1**	**Data 2**	**Data 3**	**Data 4**	**Data 5**	**Data 6**	**Data 7**	**Data 8**
	1st Address	2nd Address	Packet ID	5 V Level (hi)	5 V Level (lo)	Ambient Temp (hi)	Ambient Temp (lo)	-	-	-
	240	120	**4**	0-3	0-255	0-3	0-255	0	0	0

5.6 SUMMARY

The Power Pod was designed to meet all of the specifications laid out at the beginning of this chapter. The Power Pod incorporated three Vicor® Maxi DC-DC converters and two Meanwell® SDM30 DC-DC converters that could supply a total of 1655 W to the ROV. Current, voltage and temperature monitoring were incorporated in the circuitry to provide feedback to the surface control station.

Detailed testing of the Power Pod's performance is presented in Chapter 8 and the calibration results for each of its sensors is provided in Appendix D.

The chapter that follows details the design of the Subsea Junction Box which was the next component in the power and communications distribution design hierarchy. The chapter starts with an overview of the system and then proceeds with design specifications and the detailed design of its constituent components.

6 SUBSEA JUNCTION BOX DESIGN

The subsea junction box was designed to provide two main functions for the ROV. The first was to provide a connection point for the tether where it could be connected and disconnected for each mission. Its second function was to provide a water-tight junction where the copper conductors and optical fibres could be separated from each other and routed through separate cables to the Power Pod and E-Pod. Hybrid underwater connectors that included copper and optical fibre connections were extremely costly and not affordable with this project's budget. It was therefore necessary to come up with a cost-effective method for terminating the tether. The final design of the ROV's junction box is shown below in Figure 88.

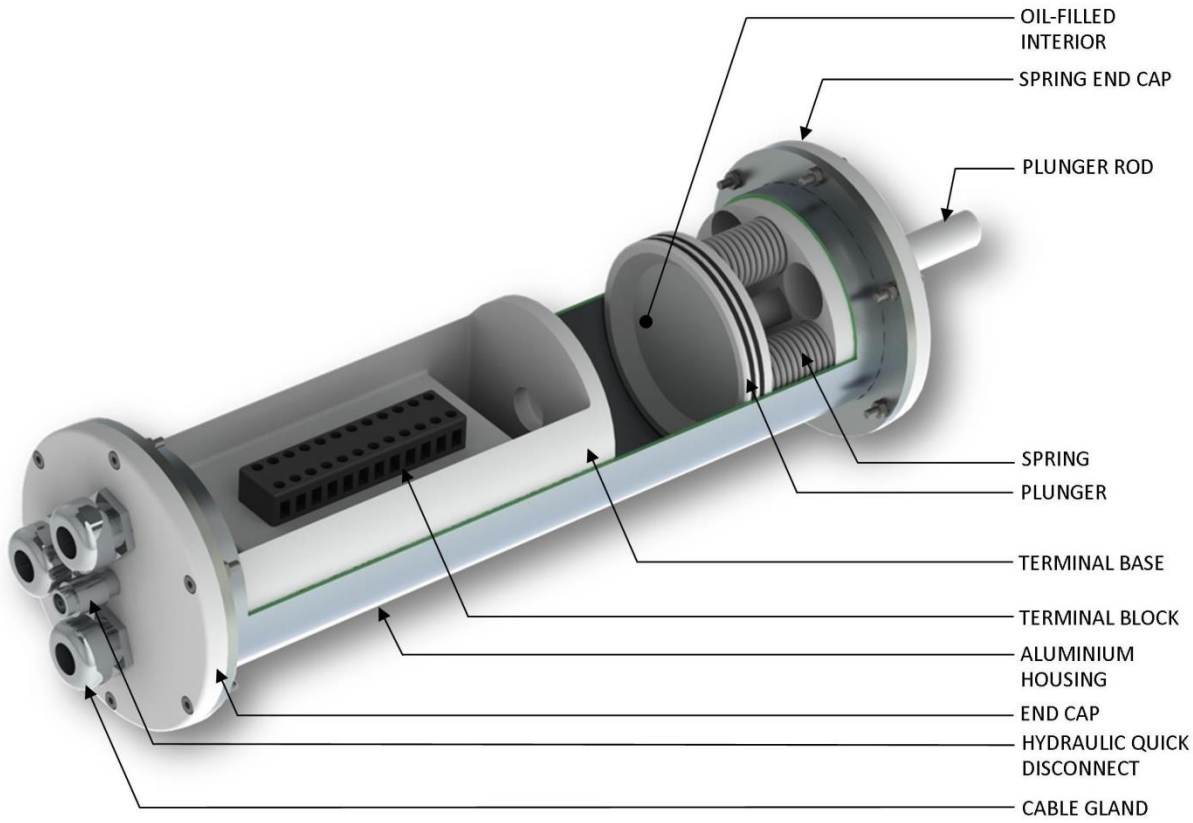

Figure 88: Final design of the ROV's junction box for the tether

The junction box incorporates a terminal block and a fibre optic coupler pair mounted on either side of an acetyl baseboard that slides into the oil-filled aluminium housing. The oil is pressurized to 0.7-1.0 bar above the ambient, external pressure on the housing. This pressure is produced by pumping the oil into the housing through the hydraulic quick-disconnect fitting so that the plunger moves out and compresses the springs behind it, as seen in Figure 88 above. A bleed screw was fitted in line with the tube used to pump oil into the housing so that air bubbles could be removed from the junction box. A large hole in the spring end cap would allow seawater to fill the space behind the plunger. This would result in the housing's internal pressure always being 0.7-1.0 bar greater than the pressure outside the housing. Figure 89 shows a dimensioned view of the junction box and

Figure 90 below shows the junction box fixed in its position at the rear of the ROV, connected to the tether, Power Pod and E-Pod.

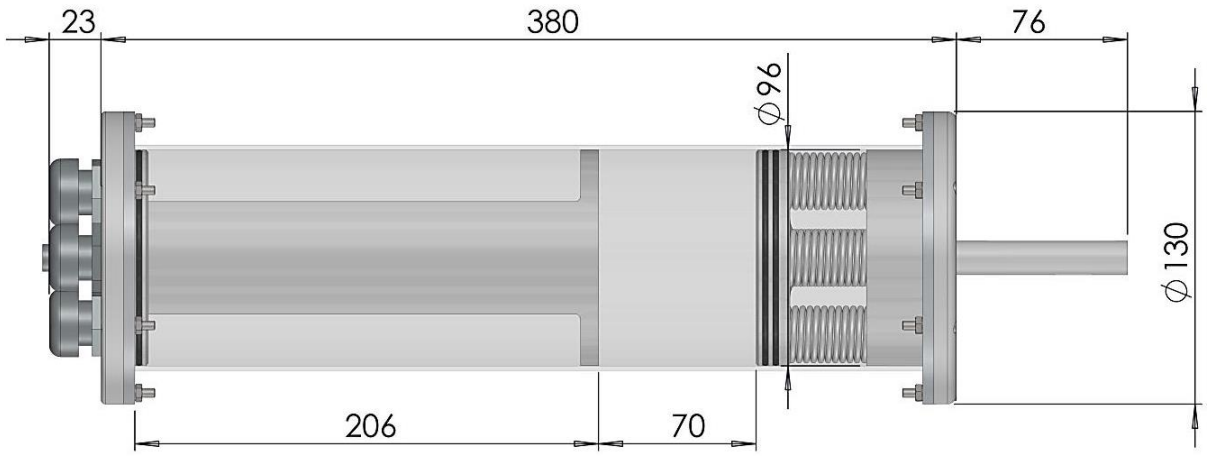

Figure 89: Dimensioned view of the junction box (housing rendered translucent)

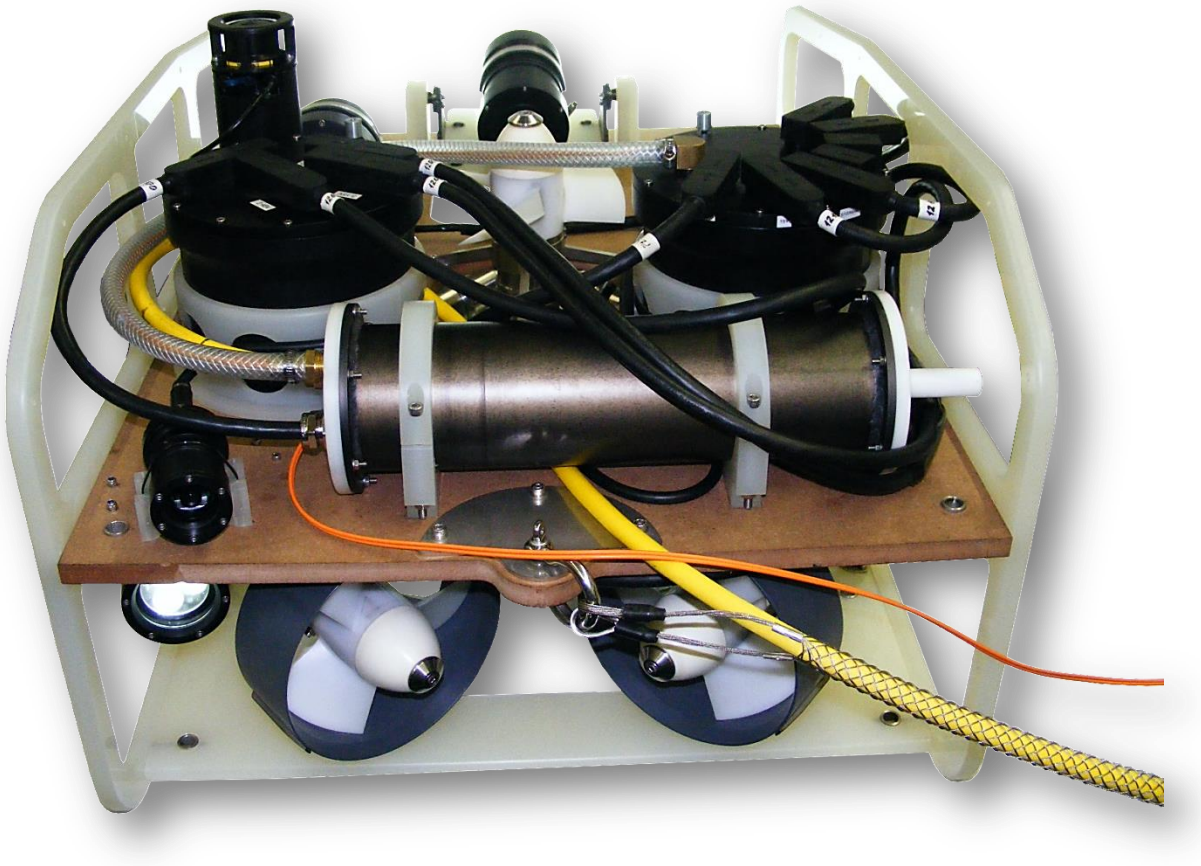

Figure 90: Photo of junction box at rear of ROV, connected to the tether, Power Pod and E-Pod

6.1 SPECIFICATIONS

Table 26: Power Pod specifications

Number	Description of Requirement	Target Values
Functional Specifications		
6.1.1	Number of copper junction terminals	6
6.1.2	Number of optical fibre couplings	2
6.1.3	Frequency of connection and disconnection	Each deployment
Mechanical Specifications		
6.1.4	Oil filled and pressure compensated	Yes
6.1.5	Oil compensation pressure	0.7-1.0 bar
Electrical Specifications		
6.1.6	Voltage Rating	470 VDC

6.1.1 Number of Copper Connections

The tether contained four copper power conductors and one twisted pair of copper wires. It was therefore necessary to have a total of 6 copper junction terminals.

6.1.2 Number of Optical Fibre Connections

Two multimode fibres were required for communication with the ROV therefore only two couplings were required. The tether did not have any spare multimode fibres so additional couplings for auxiliary or spare connections were not necessary.

6.1.3 Frequency of Connection and Disconnection

The ROV and tether were too large and heavy to be handled together in between deployments. The tether would therefore need to be disconnected from the ROV each time it was to be transported or moved away from its current deployment site.

6.1.4 Oil Filled and Pressure Compensated

The junction box would be opened and closed regularly in order to perform the connections and disconnections of the tether. The more regularly the seals would be opened and closed, the greater the risk of them leaking. Filling the junction box housing and an incorporated reservoir with insulating oil would create an incompressible interior. In addition, pressurising the oil relative to the ambient pressure would ensure that any leaking seals would result in oil escaping from the housing rather than water leaking in and shorting out the electrical connections.

6.1.5 Oil Compensation Pressure

It was established through conversations with ROV engineers that 0.7-1.0 bar relative pressure was the best pressure to use in oil filled, pressure compensated systems on ROVs. This value was based on experience in the ROV industry primarily in the oil and gas fields.

6.1.6 Voltage Rating

The ROV's maximum input voltage limit was 425 VDC. A 10% additional allowance was provided for transient voltage spikes on the power supply line, and was rounded up to 470 VDC.

6.2 DESIGN DEVELOPMENT

VOFT Concept

Very little information was available or could be accessed through published media regarding the design of junction boxes on board ROVs. It was through discussion with ROV specialists at Marine Solutions that information was acquired regarding common systems used on-board observation class ROVs to terminate and split hybrid tethers. The "VOFT" was a device that had been used by the Marine Solutions team, a sketch of which is shown below in Figure 91.

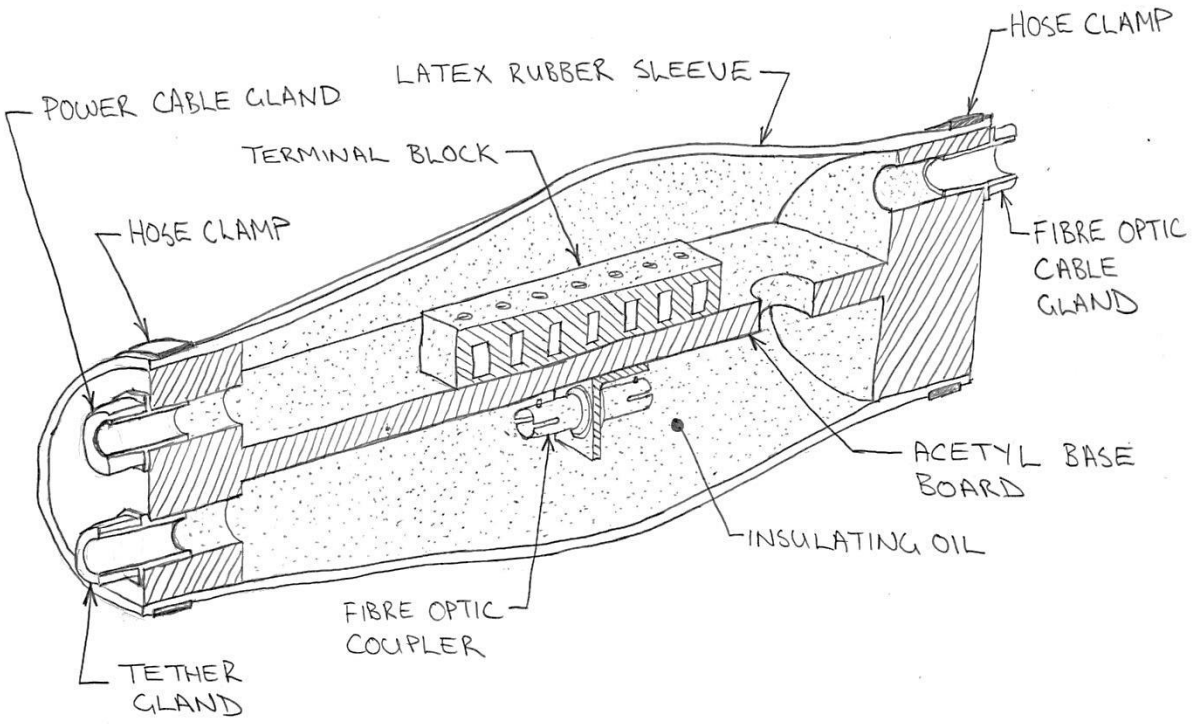

Figure 91: Concept Sketch for a "VOFT" junction box

The VOFT base board was machined from a plastic, such as acetyl, and provided the chassis for the device. It would be the platform for the terminals and couplers to be mounted on and at its ends it would provide threaded holes for the cable glands to screw into. Once all copper and fibre optic connections were fastened, a rubber sleeve with an internal diameter to match that of the base board ends would be slipped over it and secured with a hose clamp at one end. The tube would then be filled with insulating oil and the other end of the tube secured with a second hose clamp. More oil would then be pumped into the VOFT chamber through a hydraulic fitting so that the rubber membrane would be stretched and thereby create an internal pressure greater than the ambient pressure.

The flexible rubber tube would provide the compensation required. If any glands were to leak, the oil which would be at a higher pressure than the water outside the VOFT, would leak out rather than water leaking in.

A cylindrical cover, split longitudinally into two halves, would be used to protect the VOFT and would provide a rigid body to mount on the ROV.

The VOFT had been successfully used in industry, but was expected to be awkward to use because of the number of parts that would need to be disassembled in order to disconnect the tether.

Perspex® Concept

A new concept for the junction box was developed using the same principles as the VOFT, but rather providing a rigid chamber that could remain filled with oil while the terminal board was removed and connections fastened or loosened. The housing was to be machined from clear Perspex® which would allow operators to see into the housing and a similar base board would be machined for the connection terminals and couplers. A flange containing cable glands and a hydraulic fitting for filling and emptying the chamber of oil would seal the chamber at one end. At the other end a spring-loaded plunger would provide the seal, as shown in Figure 92 below.

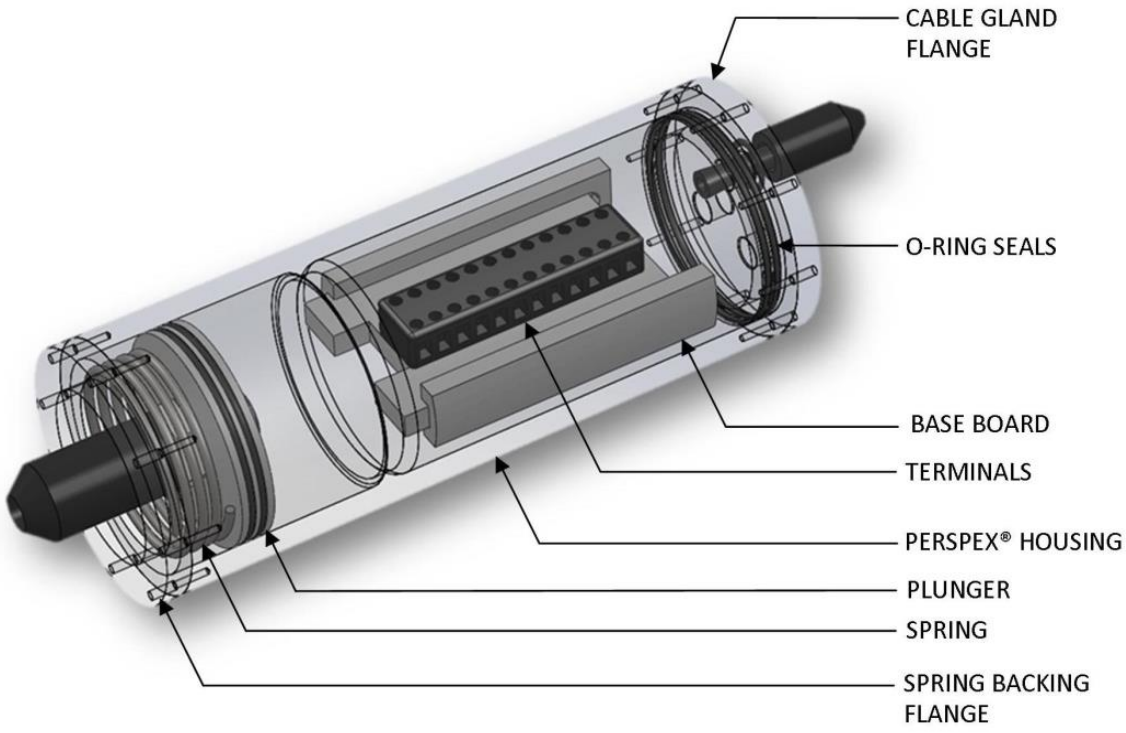

Figure 92: Rendering of Perspex® concept for the junction box

The oil would be pressurised by pumping oil into the housing through the hydraulic fitting in the cable gland flange so that the plunger was displaced and the spring compressed. The rigid housing would provide the protection the junction box needed, without an extra cover as the VOFT would. In order to disconnect the terminals, only the additional oil used to displace the plunger would need to

be drained before the cable gland flange and the terminal board could be removed from the housing, provided it was held upright to keep the oil in.

6.3 FINAL DESIGN

It had been established in industry that a VOFT style junction box worked reliably and would perform the required task, but concerns had been raised about how awkward it would be to use. The new concept that incorporated a rigid housing and a simpler process for connecting and disconnecting the tether was selected to take forward into the detailed design phase.

The final design of the junction box is shown in Figure 88 through Figure 90 at the start of this chapter and an exploded assembly drawing is available in Appendix A. This section details the design of the key components of the junction box listed below.

- Housing
- Plunger springs
- Plunger
- Cable gland flange and base board

6.3.1.1 Housing

The Perspex® housing initially proposed was replaced with an aluminium housing. Not much strength was required to contain the 0.7-1.0 bar relative internal pressure, but the Perspex® would have been too brittle to withstand the impact expected from the rough handling often associated with transporting and operating ROVs. The clear Perspex® housing would have provided a view into the junction box, but because there were no moving parts inside, it was not critical that the housing be transparent. The aluminium housing which was almost four times longer than its diameter would also be easier to grip in a lathe than most polymers.

A standard four inch aluminium tube was machined to an inside diameter of 96 mm and a wall thickness of 2 mm. Flanges that would be used to secure the end caps of the junction box were welded to each end.

6.3.1.2 Plunger Springs

Calculations were carried out to determine the properties required for the compression spring that would provide the 0.7-1.0 bar of relative pressure inside the junction box. Initial calculations showed that, due to the limited length of the housing, several smaller springs working in parallel would be required rather than one large spring. The specifications that were used to calculate the spring properties are listed in initial calculations that provided the basis for the spring design in Table 27.

Table 27: Specifications used to calculate junction box spring properties

Specification	Value
Maximum relative oil pressure, P_{oil} [bar]	1.0
Compensation volume, V_C [ℓ]	0.5
Plunger diameter, D_P [mm]	96
Maximum free length, L_f [mm]	135

An iterative process was followed using an Excel® spread sheet to calculate the properties of the springs. The formulae used and results of the calculations are presented in Table 28 below.

Table 28: List of symbols and formulae used in spring calculations [49]

Property	Symbol/Formulae	Value
Plunger surface area [mm^2]	$A_P = \frac{\pi {D_P}^2}{4}$	7200
Plunger stroke [mm]	$s_P = \frac{V_C}{A_P}$	65
Plunger force [N]	$F_P = A_P \times P_{oil}$	749
Number of springs	n	6
Spring force [N]	$F_s = \frac{F_P}{n}$	125
Spring rate [N.mm^{-1}]	$k = \frac{F_s}{s_P}$	1.86
Spring wire diameter [mm]	$\boldsymbol{d_s}$	**2.5**
Spring coil mean diameter [mm]	$\boldsymbol{D_s}$	**22.5**
Spring index	$C = \frac{D_S}{d_S}$	9.0
Stress concentration factor for static loading	$K_s = 1 + \frac{0.5}{C}$	1.06
Spring end condition	-	Squared & ground
Number of live turns	$\boldsymbol{N = \frac{d^4 G}{8D^3 k}}$	**18.6**
Total number of turns	$N_t \approx N + 2$	20.6
Solid height [mm]	$L_s = (N_t - 0.5)(1.01 d_S)$	45
Minimum working height	$L_w = \frac{L_s}{0.9}$	50
Modulus of rigidity for Stainless 302 Spring Steel [GPa]	G	68.9
Ultimate tensile strength [MPa]	S_u	1633
Stress at minimum working height [MPa]	$\boldsymbol{\tau_s = \frac{8F_s}{\pi d^2} C K_s}$	**467**
Maximum allowable shear stress at solid height [MPa]	$\tau_s \leq 0.35 S_u$	572

6.3.1.3 Plunger

The plunger was machined from acetyl and an indicator rod was added to the back of it so that the oil volume inside the housing could be monitored by checking how far it protruded from the housing. Its two end positions are shown below in Figure 93.

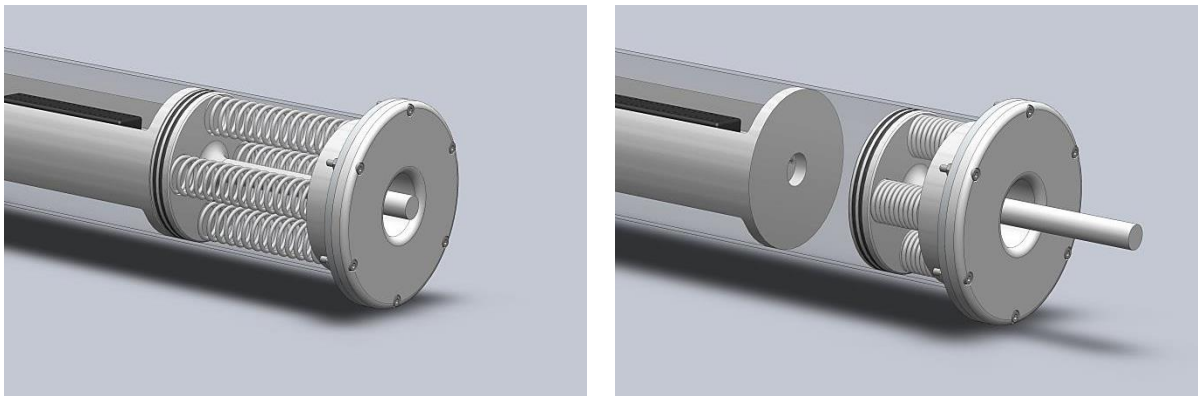

Figure 93: Extended and compressed positions of the junction box plunger(housing rendered translucent)

The plunger incorporated two radial O-ring seals to contain the insulating oil. Viton® O-rings that would withstand the chemical exposure to insulating oil better than standard Nitrile O-rings were specified for the junction box. Six pockets were machined in the back of the plunger to seat each of the compression springs.

6.3.1.4 Cable Gland Flange & Base Board

The cable gland flange and the base board were also manufactured from acetyl because of its low water absorption and low creep properties. Acetyl is also a relatively easy material to machine. The base board was designed to fit snugly in the housing and to allow opening for the routing of wires and for the flow of oil. A terminal block was fitted to the upper side and an optical fibre coupler pair fitted to the underside as shown in the photos of Figure 94 below. The high voltage connections on the terminal block were separated so that there was at least 2.1 mm gap between the positive and negative terminals of the 400 VDC supply (see section 5.2.4).

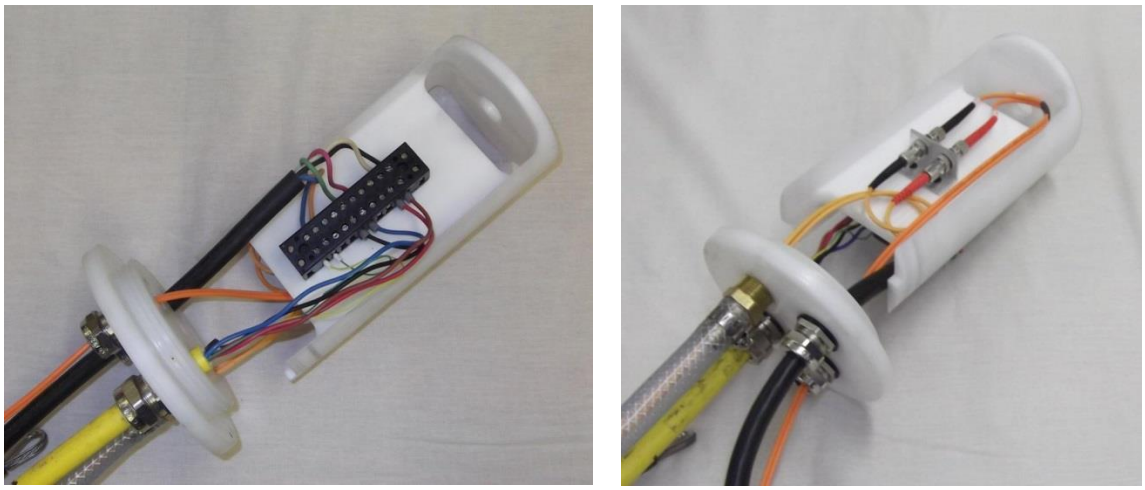

Figure 94: Photos of the cable gland flange and baseboard

6.4 SUMMARY

The subsea junction box was designed to meet all of the specifications laid out at the beginning of this chapter. The junction box design incorporated an oil-filled and compensated housing with connections for both the copper and fibre cores of the tether to the Power Pod and E-Pod respectively.

Testing of the junction box internal relative pressure is presented in Section 8.7.

The chapter that follows details the design of the surface control station. The surface control station incorporates the power supply unit, which was the final component in the power and communications distribution design hierarchy. The chapter starts with an overview of the system and then proceeds with design specifications and the detailed design of its circuitry and user interface.

7 SURFACE CONTROL STATION DESIGN

The surface control station was comprised of the power supply unit (PSU) and the user interface (UI) which were primarily designed for testing the ROV system. The PSU was designed to supply 400 VDC at 5A to the ROV, via the tether, and to provide the connection point for the tether's optical fibres. The UI was designed to control and communicate with the ROV modules that were ready and working at the time of testing. The modules ready and working were the E-Pod, the Power Pod, the sonar and the four light modules. A photo of the PSU set up alongside the user interface laptop and auxiliary screens is shown in Figure 95 below.

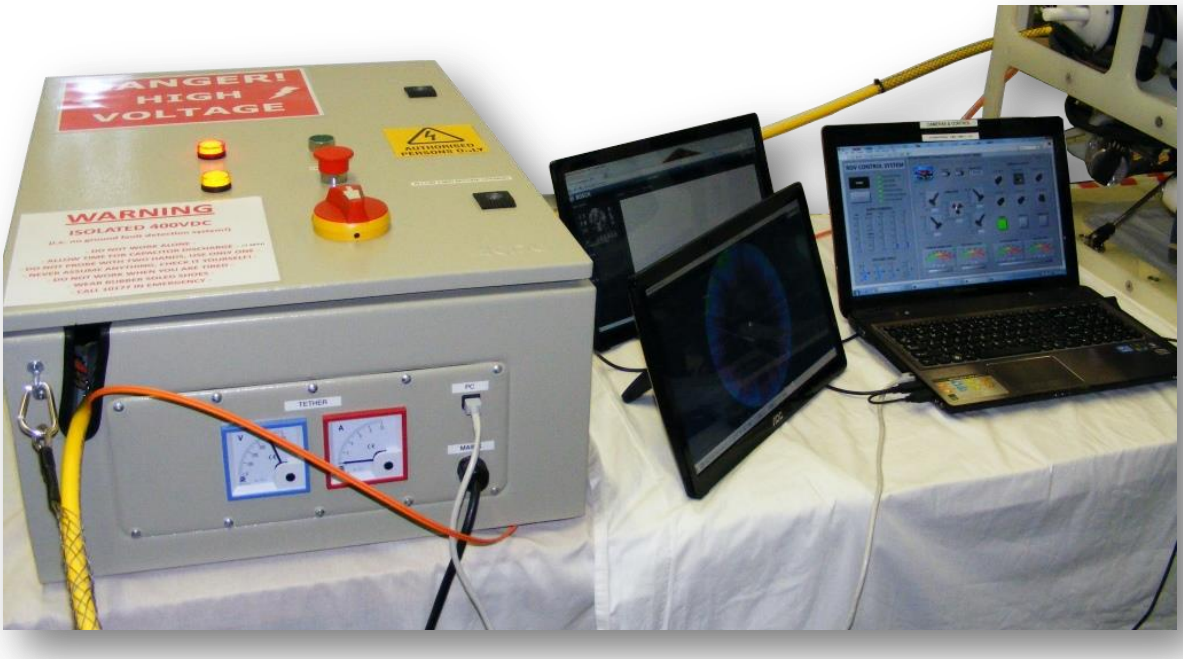

Figure 95: Photo of the surface control station with the PSU enclosure (left) and laptop with auxiliary screens displaying the user interface (right)

This chapter proceeds with a list of specifications for the surface control station and is followed by a description of the power supply unit design and then the design of the user interface.

7.1 SPECIFICATIONS

Table 29: Specifications for surface power supply and user interface

Number	Description of Requirement	Target Values
Functional Specifications		
7.1.1	Simple connection and disconnection of power and communications	Yes
Electrical Specifications		
7.1.2	Input voltage	230 VAC
7.1.3	Output voltage	400 VDC
7.1.4	Output current	5A
Safety Specifications		
7.1.5	Redundant contactors for switching output	Yes
7.1.6	Ground isolated output	Yes
7.1.7	Ground fault detection on 400 VDC output	Yes
7.1.8	Emergency-Stop pushbutton	Yes
7.1.9	Lockable isolator switch	Yes
Communication Specifications		
7.1.10	TCP/IP Copper to Fibre converter	Yes

7.1.1 Simple Connection and Disconnection of Power and Communications

The ROV, the tether and the power supply unit would always be transported separately from each other to aid their portability. A means of connecting the ROV's tether quickly and effectively to the power supply was therefore required to reduce the setup and pack up times for each deployment.

7.1.2 Input Voltage

The input voltage was to be a nominal 230 VAC, as per the standard single-phase mains voltage in South Africa.

7.1.3 Output Voltage

As specified in Section 3.10 the nominal ROV supply voltage was to be 400 VDC.

7.1.4 Output Current

According to Table 12 the ROV would only need a little less than 4 A to power the ROV at 400 VDC. However, 5 A was specified for the power supply because it would provide headroom for future expansion.

7.1.5 Redundant Contactors for Switching Output

Due to the risks associated with the 400 VDC output, it was considered prudent to incorporate a second contactor with its set of contact wired in series with the first. In the event of an emergency pushbutton being pressed, the redundant contactor would reduce the probability of the output power not cutting out due to the contacts of one contactor welding closed.

7.1.6 Ground Isolated Output

Both positive and negative terminals of the power supply unit output were to be isolated from ground potential to reduce the risk of shock from the system. If a person connected to ground were to touch either of the terminals, that terminal would be pulled to ground potential and the other terminal would remain either 400 V above or below ground potential.

7.1.7 Ground Fault Detection on 400 VDC Output

Ground fault detection was an industry norm on ROVs. The ground fault detection (GFD) unit would be required to isolate the tether and ROV from its power supply in the event of a shock or insulation breakdown between one of the conductors and ground (earth) potential. It would detect if a person, connected to ground, touched either the 400 V or 0 V conductor. The GFD unit, though, could not protect against the shock hazard between the positive and negative high voltage conductors.

7.1.8 Emergency Stop Pushbutton

It should be possible to cut power to the tether and ROV fast and effectively by the user. To provide this feature, an emergency stop pushbutton was to be installed on the power supply unit, located in an easily accessible position and clearly marked.

7.1.9 Lockable Isolator Switch

In order to protect users from switching the power to the surface station ON during maintenance or repair periods, a standard lockable isolator switch was to be used. The isolator could then be locked in its OFF position during these periods.

7.2 POWER SUPPLY UNIT

The design of the PSU was based on the power and communications requirements of the E-Pod, Power Pod and tether, which had been built up in an iterative process. The primary constraints with regards to the power system that affected the PSU had been the space available for DC to DC power conversion on board the ROV and the voltage drop across the tether. The result was, as mentioned in 7.1.3 and 7.1.4, that the PSU was required to supply power to the tether at 400 VDC and 5 A.

The tether was to be connected to the PSU so it was also necessary to provide a connection point for the tether's optical fibres. The PSU enclosure was therefore used to house the D-LINK® DMC300-SC fibre optic media converter and a 5-port network switch that would provide a hub into which the UI laptop could be connected. A photo showing the layout of the PSU enclosure is shown below in Figure 96.

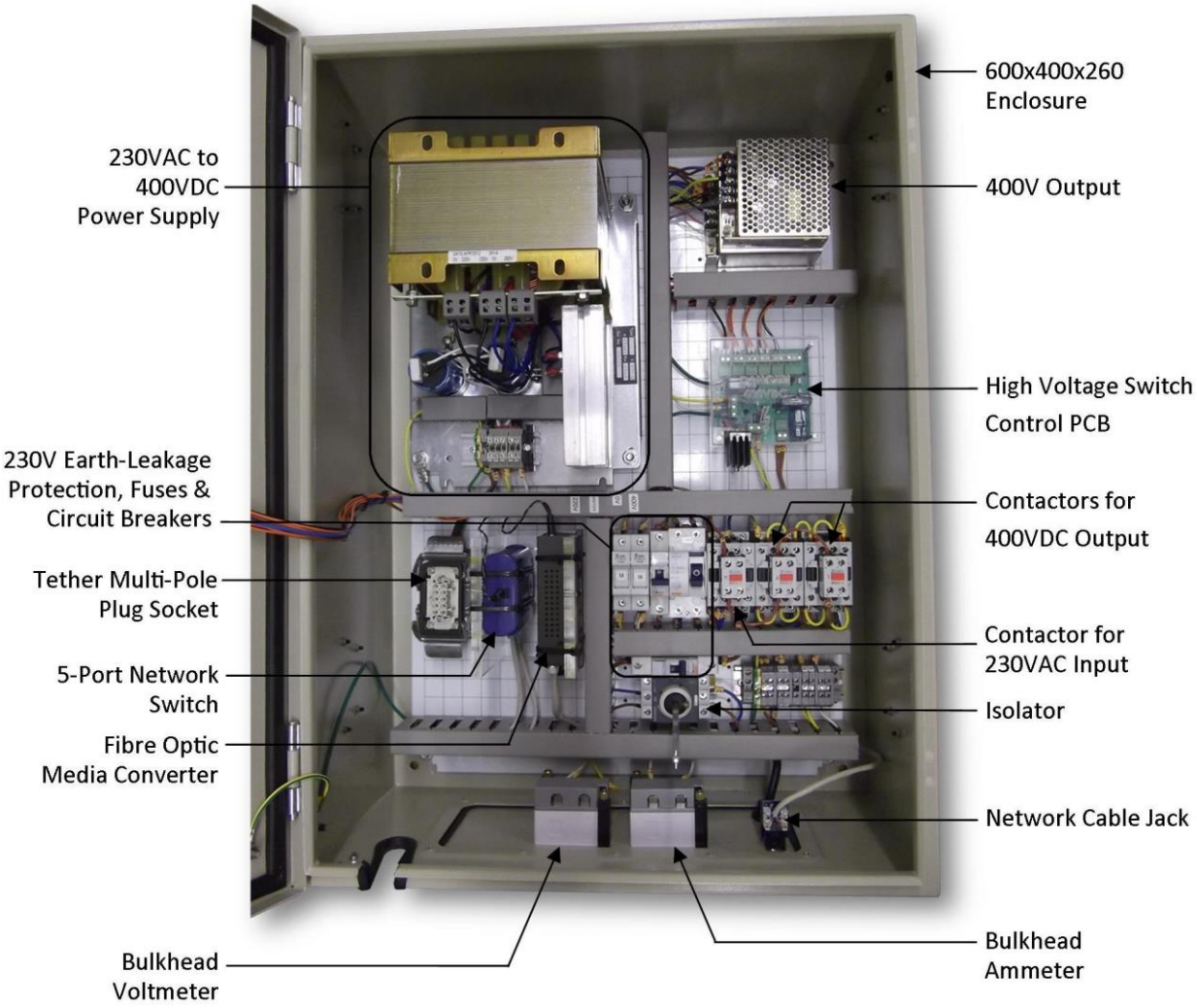

Figure 96: Layout of components inside the PSU enclosure

7.2.1 400 VDC Supply

The primary function of the PSU was to convert 230 VAC mains into 400 VDC and supply it at a rate of 5A to the ROV. One of the requirements for the ROV was to provide an isolated or ungrounded DC supply to the ROV. One of the safest and most reliable ways to do this was to use a toroidal transformer with double windings to step up the mains supply voltage before rectifying it. The toroidal transformer would provide complete isolation between the inputs and outputs, unlike some switch-mode supplies, and the double windings would provide greater reliability than single-wound auto-transformers.

The transformer was fed through a bridge rectifier and smoothing capacitors to provide the nominal 400 VDC output as shown in Figure 97 below.

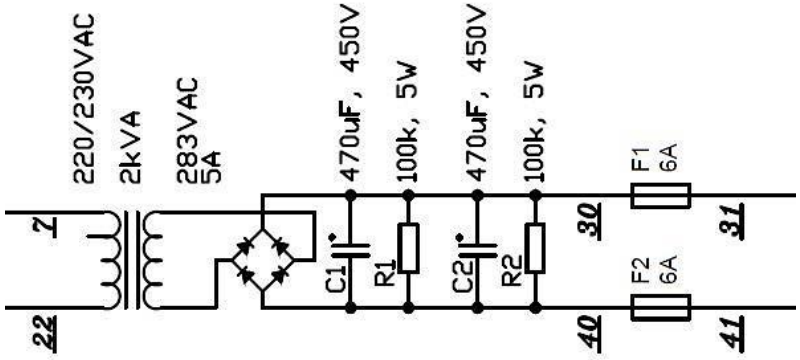

Figure 97: Circuit schematic for the 400 VDC power supply

This power supply was ordered from a local manufacturer in order to save time spent on design, procurement and assembly.

7.2.2 Power Switch

The design of the switch that would open and close the 400 VDC circuit was critical to the safety of the system. The switch was required to reliably break a current of 5 A with a potential difference across its contacts of 400 VDC. At such a voltage, arcing was expected to occur between the contacts of conventional relays and contactors rated for standard power supplies of 250 VAC or 380 VAC. This arcing had the potential to weld the switch contacts closed, therefore rendering any emergency stop features of the system useless.

In order to avoid mechanical contacts welding closed, two options were available. The first was to use a contactor rated for 400 VDC and at least 5 A. This method would provide a switch with negligible on-resistance, but arcing would still occur during switching and eventually wear out the contacts. The second option was to use a solid-state switch, such as a MOSFET, that would replace the mechanical contacts. No arcing would occur in the solid-state switch and it would not have contacts that would wear out over time. Solid-state switches are compact in size compared to contactors and can be controlled with a digital signal, if required. However, two disadvantages of solid-state switches, MOSFETs in particular, are their susceptibility to electrostatic discharge, and

their inherent resistance when conducting. This on-resistance results in power losses and the build-up of heat in the semiconductor.

The initial design incorporated a solid-state switch so that the high-voltage switch did not have contacts that would wear out over time and require replacement. A P-Channel MOSFET was selected as the switching component and it was driven by an IC that was designed specifically to drive high-voltage MOSFETs. The Supertex® HT0440 MOSFET driver provided isolated digital switching of two MOSFETs. A schematic of the MOSFET control circuit is shown in Figure 98 and a full set of the schematics for the high-voltage switch control PCB is included on the accompanying DVD.

The switch control PCB was designed to provide safety monitoring features for the power supply. The circuit incorporated the following safety controls:

- Emergency-stop switch monitoring (230 VAC & 12 VDC)
- Option to monitor safety signal from a microcontroller output (3.3 VDC)
- Relay switches to cut power to contactors if safety circuits not healthy (230 VAC)

A photo of the switch control PCB can be seen in Figure 99 below.

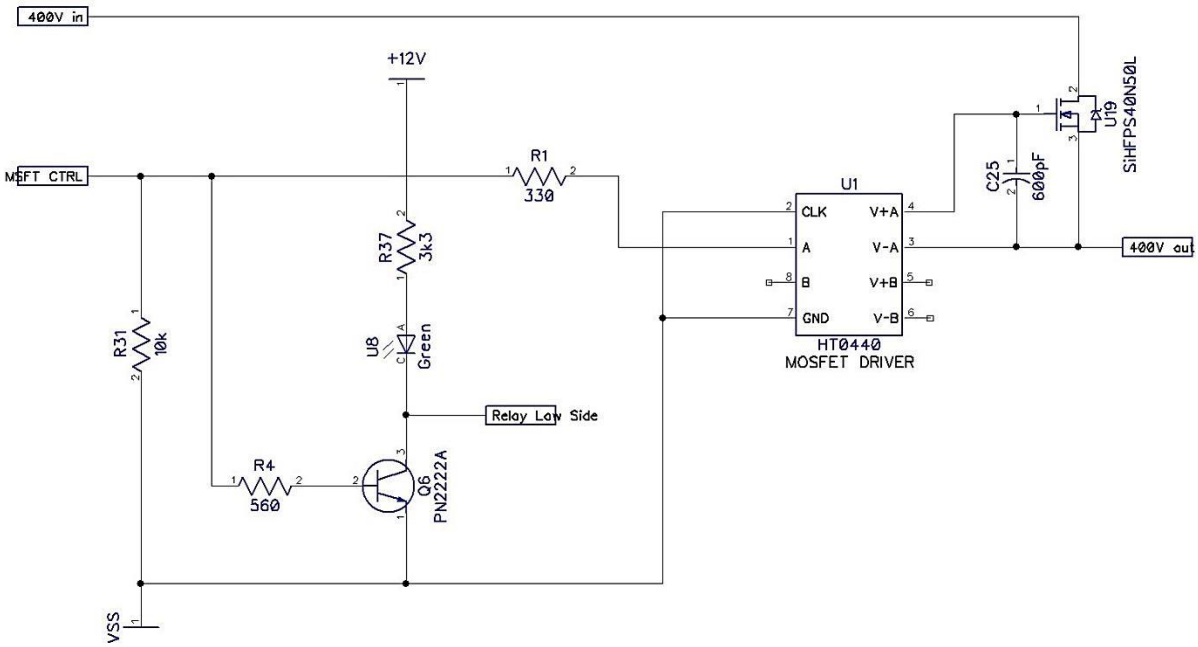

Figure 98: Circuit schematic for the 400 VDC high side switch

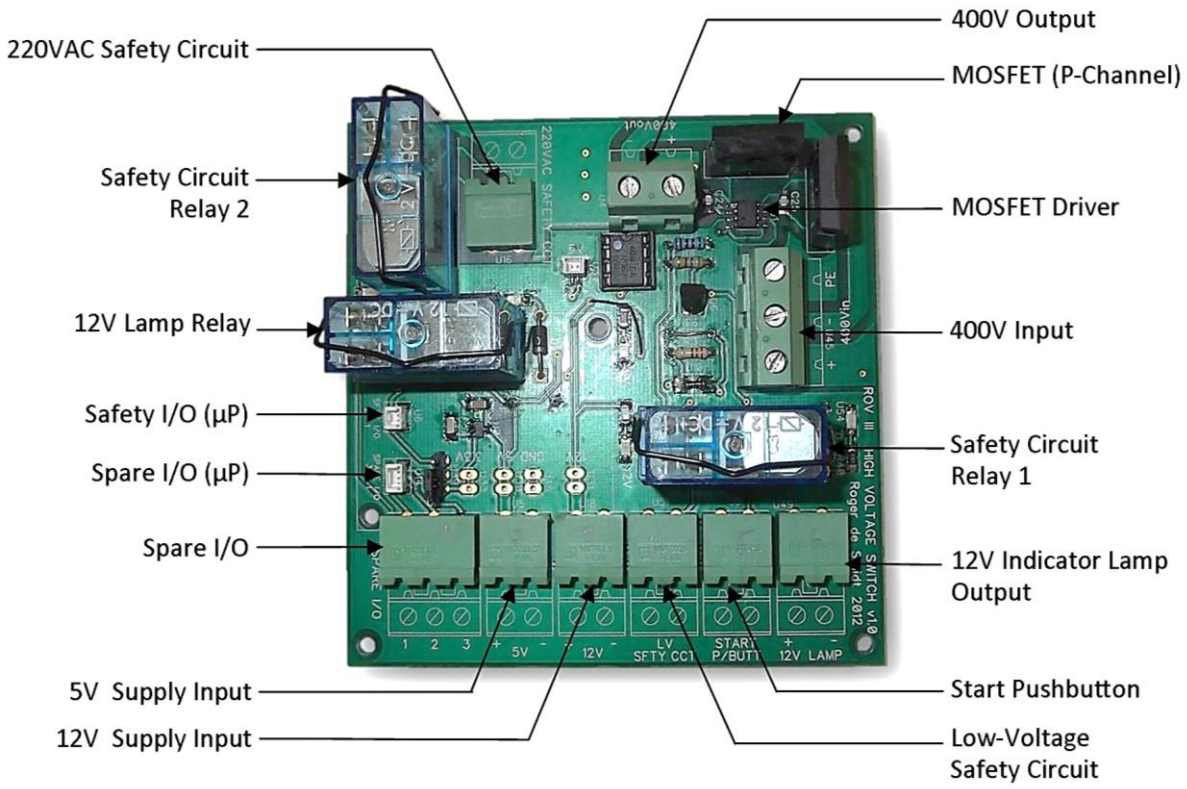

Figure 99: Photo of the high-voltage switch control PCB

When testing the ROV it was found that the P-Channel MOSFET overheated and failed in a closed state, rendering the switch useless. One failure of this nature was sufficient reason to overhaul the design and replace the MOSFET switch with contactors rated for switching DC current. If the MOSFETs failed to a closed state, they were not safe to use as the ROV power switch.

The switch control PCB was retained and only the 400 VDC input and output were re-routed through two contactors as shown in the schematic below.

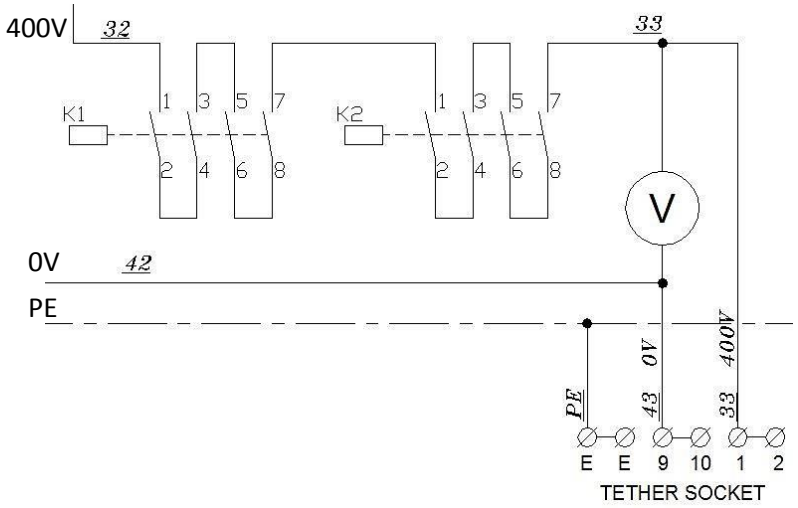

Figure 100: Excerpt from wiring diagram to show wiring of contactors

The contactors were each rated for 300 VDC when wired with each contact in series with the next as shown above. Two of these contactors were wired in series to increase the voltage rating to 600 VDC. Two contactors operating in parallel and wired in series also provide increased fault tolerance because the circuit will have a good chance of opening even if one contactor fails to release.

7.2.3 Ground Fault protection

As discussed in Section 2.3, ground fault monitors (GFMs) were commonly used in ungrounded ROV power systems to detect ground faults, thereby providing protection from certain shock hazards. However, the GFMs were expensive, costing R36 260 for a Bender® GFM unit at the time of writing. It was therefore the intention of the author to design and build a GFM for the ROV at a significantly reduced cost.

A GFM was designed, but due to time constraints on the project it could not be completed. By this stage the project budget had been allocated and almost completely spent so a commercial GFM unit could not be afforded. A commercial GFM would require very little modification to the existing circuit design. All that would be required is for its sensing terminals to be connected to the positive and negative terminals of the 400 VDC output, and its output relay would need to be wired in series with the control circuit for the power switch contactors.

7.3 HOST CONTROLLER AND USER INTERFACE

The host controller for the ROV was to be a laptop that was running the Microsoft® Windows 7 operating system and was to incorporate a working Ethernet network port. The laptop supplied by the RARL for use with the ROV was a Lenovo® Y570, comprising an i7 processor and a dedicated 1GB graphics card. The laptop was required to have installed on it a minimum of the latest version of National Instruments Labview® Run-Time Engine (if not a complete installation of Labview® 2012) and the Tritech® Micron Sonar software.

The user interface (UI) was developed primarily for testing the E-Pod and Power Pod, but was designed so that it could be expanded upon to incorporate control of the entire ROV in the future. National Instruments' Labview® graphical programming software was used to create the UI because it had many built-in functions that drastically reduced development time, particularly with regards to the design of graphical user interfaces (GUIs).

Various parts of software developed by Cameron Sharp, Thomas Knight, Bradley Springer and Michael Rieger, all former students at the RARL, were used as a base for the UI developed in this project. The home screen of the final UI is shown below in Figure 101.

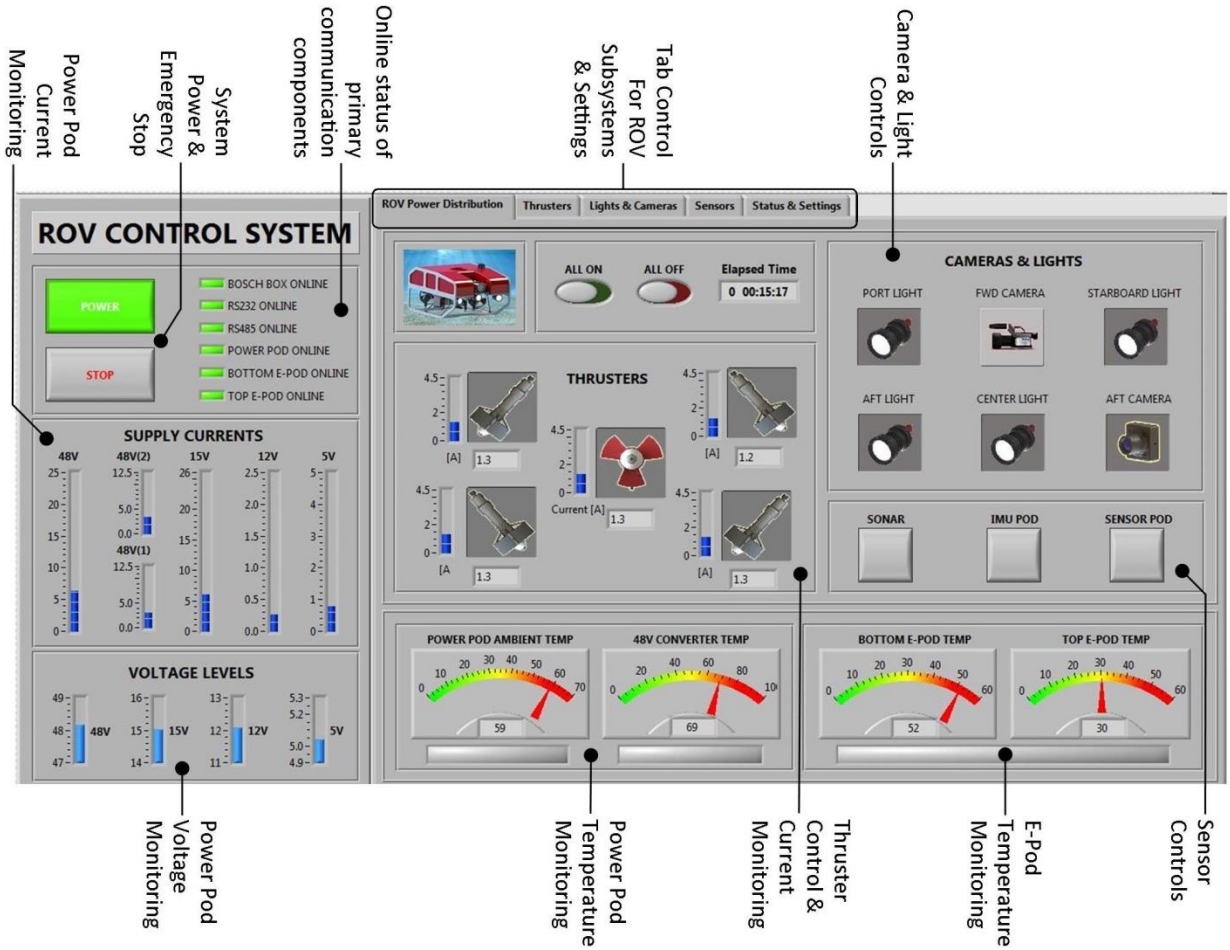

Figure 101: User interface home screen

The UI was linked to the ROV via a local TCP/IP network over the tether fibre optic link and used the Tibbo® DS1102 device server as a virtual COM port to communicate with the various ROV microcontrollers. The UI was therefore programmed to function as the RS-485 master and initiate all communication transactions.

As described in Section 3.11, the RS-485 master, or UI in this case, would cycle through communication with each ROV module in a pre-determined order. The screen capture of the section of Labview® graphical code that shows this order of communication is shown below in Figure 102 .

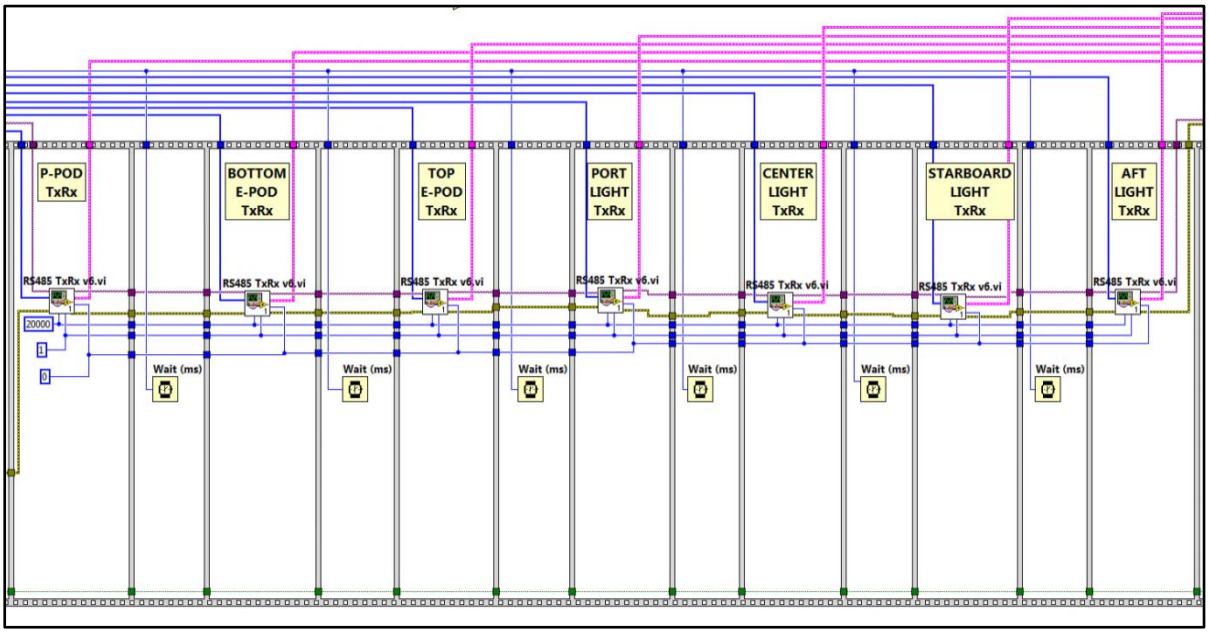

Figure 102: Labview block diagram showing the order of RS-485 communications between the UI and selected ROV modules

7.3.1 User Interface Features

Apart from the direct display of data received from the ROV modules or direct control commands sent to the modules, the UI incorporated a few extra features to enhance control of the ROV. These features are described briefly below.

All On/Off

Two controls were provided to simplify the task of turning on or turning off all of the individual ROV module controls at once.

Line Status Monitoring

Indicators were incorporated in the UI to show when each of the Tibbo® device servers and the Bosch® video encoder were online. The status of these components was determined by a “ping test” that was repeated periodically to determine the status of connection to each of these three devices. The status of connection with each of the three primary microcontrollers on board the ROV was also monitored and shown on indicators on the UI home screen. As long as 10-byte packets of data were

being returned with the correct address from the two E-Pod microcontrollers and the Power Pod microcontroller, their status was shown as online.

Thermal Overload Limiting

The E-Pod and Power Pod both incorporated temperature monitoring and their maximum allowable ambient temperatures were 60 °C and 65 °C respectively.

Module Disabling

In the *Status & Settings* tab, seen below in Figure 103, a list of all the ROV modules was provided as well as the option to enable or disable each module. This function was incorporated to protect selected modules from being accidentally turned on by the user on the home screen.

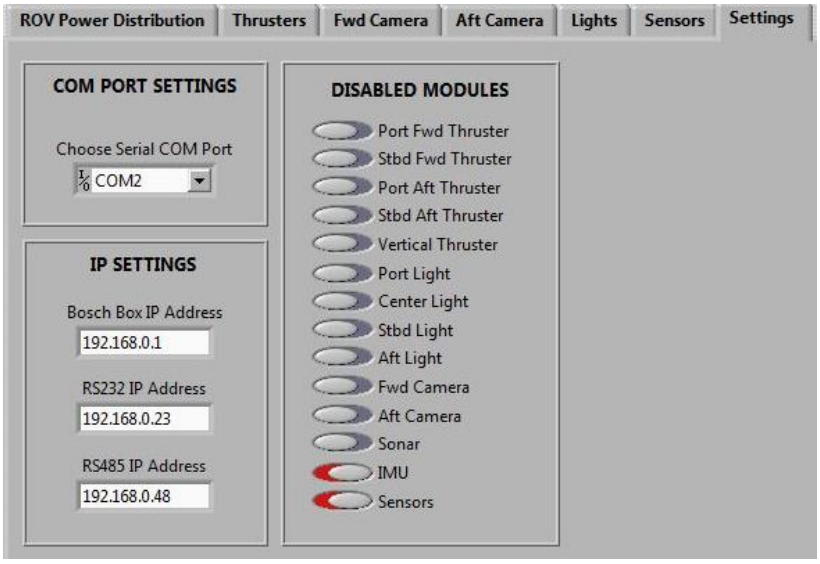

Figure 103: Screen shot of the UI Settings tab

7.3.2 Sonar

The image from the Tritech® sonar was to be viewed and controlled using the proprietary Micron® software with which it was supplied. An auxiliary screen that was connected to the laptop's USB ports was dedicated to the sonar image display (see Section 3.7).

7.4 SUMMARY

The PSU was the final subsystem to be designed in the power and communications distribution design hierarchy. It was designed to meet all of the specifications laid out at the beginning of this chapter. Installation of the ground fault monitoring device was still pending, and could easily be integrated into the circuit at a later stage when funds were available. A user interface was programmed in Labview® and provided control and monitoring for all modules encompassed in the scope of this project.

Detailed testing of the performance of the PSU is presented in Section 8.6.

The chapter that follows details the testing procedures and results for the ROV power and communications distribution systems. The chapter starts with an overview of the testing procedures used and then continues with the detailed testing of each subsystem in a logical order of dependence.

8 TESTS & RESULTS

8.1 TESTING PROCEDURES

In Chapters 3 through 7 specifications were laid out for each of the systems covered in this project to provide criteria against which the final product could be measured. This section describes the methods used to test each of these systems and components against their specifications, and provides the information necessary to reproduce the same tests at a later date.

There were a large number of systems that formed part of the Remotely Operated Underwater Vehicle (ROV) and each component and system was to be thoroughly tested before final assembly of the ROV. The ROV also needed to be thoroughly tested as a complete system before being put into service for the client. However, the complete assembly and testing of all components is beyond the scope of this project and this section of testing procedures deals with those components and systems covered by the scope of this dissertation only.

The tests were performed systematically on components, working upward in increasing level of dependence, from the seals on the pressure vessels, to the controlling computer and user interface that forms part of the surface control station. These tests and their respective results are described and discussed in the sections that follow.

8.2 PRESSURE VESSELS

8.2.1 O-Ring Seal Tests

8.2.1.1 Purpose and Scope of the Test

The ROV was designed to operate at a depth of 300 m below the water's surface and each subsea module was designed to house dry electronics (as opposed to oil-bathed) at atmospheric pressure. Because these electronic components were highly sensitive to water ingress and were expensive to replace, the effective sealing of each pressure vessel was of paramount importance.

In the commercial servicing and maintenance of ROVs a test depth of twice the rated operational depth is the accepted norm. The test chamber available at Marine Solutions at the time of testing, however, was only able to reach a pressure of 45 bar (450 m), which was only one and a half times the pressure that the ROV would operate at. It was considered sufficient pressure for testing purposes though, because this ROV would be unlikely to work in waters much deeper than 200 m, and even so, 150 m extra depth beyond the rated 300 m would give plenty allowance for operator error.

The two ROV housings to be tested were pressurised to the equivalent of 150% of their rated depths and held there for a set period. The modules were empty when tested to reduce the risk of damage to their contents should there be any seal failures. Testing of the modules with their electronics and other hardware fitted inside was deemed unnecessary until the whole ROV was ready for underwater operation.

If the seals on any of the ROV modules are opened, these pressure tests should be performed before the module is used again in an underwater operation.

This set of tests and corresponding results are described below and are followed by concluding remarks and a recommendation for future tests.

8.2.1.2 Test Equipment

- Marine Solutions pressure test rig including the following main items of equipment:
  - Pressure vessel with lid, O-ring seal and all flange bolts
  - Chain block and tackle to raise and lower lid
  - Hydraulic pump and valve system to pressurise the chamber
  - 5 m nylon string and float for retrieving ROV components from the chamber
  - Integrated pressure transducer and digital read-out
  - Compressed air supply
- ROV Electronics Pod
- ROV Power Pod
- 2 kg steel weight

Figure 104: Marine Solutions pressure testing rig

8.2.1.3 Preparation of Equipment

The pressure tests of the ROV housing seals were performed at the Marine Solutions workshop in Paarden Eiland, Cape Town. The test chamber diameter was approximately 250 mm which was a large enough opening to accept both the Electronics and Power pods.

The pressure testing rig at Marine Solutions was in regular use by the company's technicians at the time of testing and very little preparation was required. The electronic pressure gauge was maintained by Marine Solutions so no calibrations were carried out.

The Electronics Pod and Power Pod were cleaned and carefully sealed using the correct type of O-Rings and lubricants. Instructions on how to seal these pressure vessels can be found on the accompanying DVD.

8.2.1.4 Test Procedure

One end of the nylon string was tied to the ROV modules and steel weight, and the other end tied to the foam float so that it would be easy to retrieve after the test. The modules were lowered gently into the test chamber which was already half-full of water so that filling time would be reduced. The chamber lid was lowered using the chain-block and tackle, ensuring that its O-ring was correctly seated in its groove, and its entire set of flange bolts inserted and fastened.

Once the chamber lid was fastened the vent cap in the lid was released and the tank filled with water through its valve system situated below the tank. Once the water spurted out of the vent cap it was quickly fastened, the filling was stopped, and the filling valves closed off.

The pressure gauge was checked for a zero reading before the valves were changed over to receive pressure from the hydraulic pump. The test tank pressure was then increased by slowly pumping the hydraulic pump handle.

At every 5 bar increase in pressure, a pause of 5-10 seconds was given to check that the pressure was indeed holding at that level and not decreasing rapidly, which would indicate a leak in the system. A record was kept of the time of each test and of each 5 bar increase achieved in the test.

Once the pressure reached the rated operating pressure of the ROV (30 bar), a one minute pause was made to check for leaks. After this pause, pumping was resumed with the short pauses every 5 bar increase. Once 45 bar was reached, the chamber valve was closed and a reading of the pressure recorded.

The test chamber was monitored for an hour and any significant changes in pressure and the respective times were recorded. Significant decreases in pressure that occurred gradually were corrected by adding more pressure with the hand pump and the new pressure recorded.

After the final reading was taken, the pressure was slowly released from the chamber by opening the bleed tap below the chamber. Once the chamber was at zero pressure again, the vent cap was released, the chamber emptied of some water, the lid removed and the ROV modules retrieved.

The ROV modules were dried with paper towels, blown off with compressed air, and then wiped again with paper towels. Once the modules were completely dry on the outside, all screws were removed and the lids opened using compressed air carefully pumped through the vent plug hole. Caution was taken not to drop the lids as they popped open. The ROV modules were then inspected for any signs of water leakage into their chambers.

8.2.1.5 Test Results and Analysis

A record of the chamber pressure versus time is shown below in Figure 105.

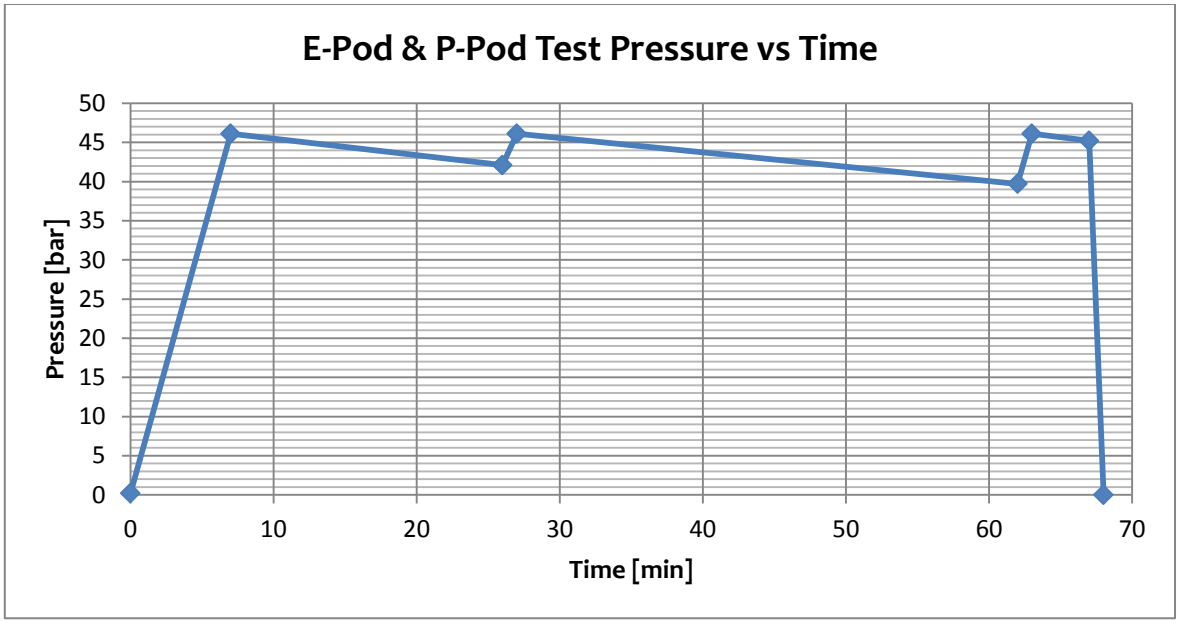

Figure 105: Graph of E-Pod & P-Pod Test Pressure vs Time

Figure 105 above shows a gradual drop in pressure after the maximum test pressure of 46.1 bar was reached at the 7 minute mark. Because the pressure had dropped gradually and not suddenly, it was assumed that the ROV module seals had not failed, but rather that there was a leak in the test rig valves. After the pressure had dropped to 42.1 bar it was increased again to 46.1 bar with the pump. Again the pressure decreased gradually and was restored again to its maximum at 62 minutes, shortly before the test ended.

The E-Pod and P-Pod were retrieved and found to have no signs of water ingress into their chambers. The ROV modules also showed no signs of permanent deformation as a result of the induced external pressures.

8.3 COMMUNICATIONS TESTS

8.3.1 Optical Fibre Bandwidth

8.3.1.1 Purpose and Scope of the Test

The primary communications link between the user interface and ROV was the optical fibre in the tether. To make use of this fibre link, two conversions between fibre and copper media were required as well as three optical connections. It was therefore necessary to ensure that the losses in efficiency incurred at each of these points did not negatively impact the performance of the ROV.

The actual attenuation of light through the fibre link could only be measured using specialised and expensive equipment, so instead the data transfer speed was compared between a direct copper cable connection and the fibre link.

8.3.1.2 Test Equipment

- Two laptops (laptop A & laptop B)
- D-Link 100BASE-TX to 100BASE-FX Multimode SC Media Converter[50] with power supply
- Stride® Ethernet Unmanaged Switch, 5-Port 10/100, 1-Port Multi-Mode ST Fibre [51] with power supply
- Fibre optic patch-cord, 2 x 50 µm multimode fibres with ST connectors one end and SC connector on the other
- Two standard Cat5e Ethernet network cables, 2 m long
- Timer

8.3.1.3 Test Procedure

The network ports of the two laptops were first connected to each other using only the one network cable. Once connected, a large file, over 1 GB in size was transferred from the laptop A to laptop B, while the transfer period was timed on a stop watch type timer. The transfer was performed and timed three times in the same direction and the average transfer rate was calculated.

Next, the two laptops were connected via the fibre link, as shown in Figure 106. The patch cord was used to simulate the tether connection because the fibre connectors on either end of the tether were not yet prepared at the time of testing. The file was again transferred three times from laptop A to laptop B, the times recorded and the average transfer rate calculated.

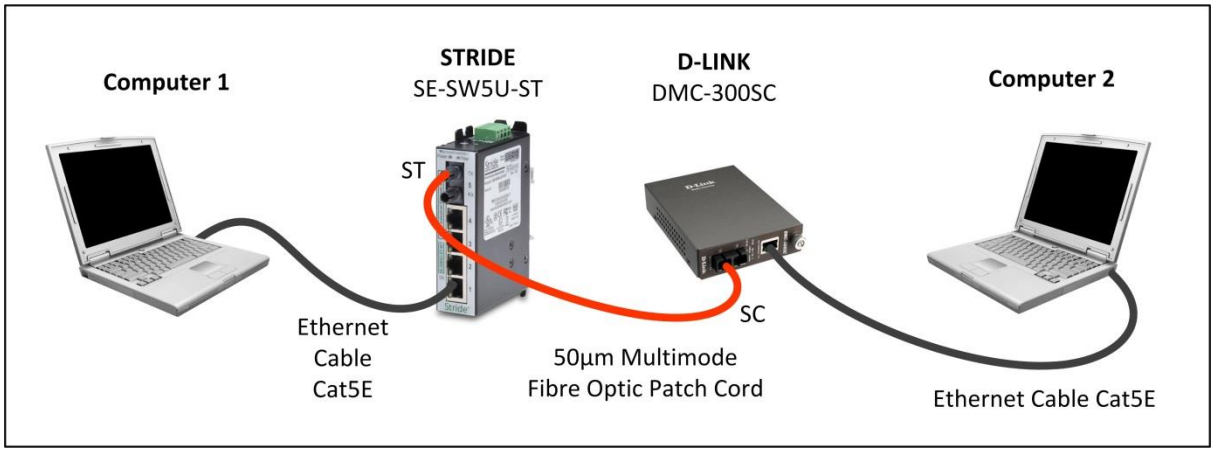

Figure 106: Schematic showing connections for fibre optic bandwidth test

8.3.1.4 Test Results and Analysis

The times taken to transfer the file in each test using the direct network connection and using the fibre link are presented in Table 30 below. The transfer rates presented were calculated by dividing the file size by the period taken to transfer it, and a corresponding rate in Mbps was also calculated.

Table 30: Comparison of file transfer rates over Cat5e cable and over fibre link

Test #	File Size [MB]	Transfer Period [s]	Transfer Rate [MB/s]	Transfer Rate [Mbps]
Connection with Cat5e cable only				
1	1 927	17.3	111.7	893.7
2		17.1	112.5	900.0
3		17.3	111.4	891.1
Avg		**17.2**	**111.9**	**894.9**
Connection with Fibre link				
4	1 927	166.0	11.6	92.9
5		165.8	11.6	93.0
6		165.8	11.6	93.0
Avg		**165.8**	**11.6**	**93.0**

8.3.2 Serial Network Speed Test

8.3.2.1 Purpose and Scope of the Test

On board the ROV, a virtual COM port was established via the fibre link with the host computer and a local RS-485 Master was set up to communicate with each ROV module. The speed of this RS-485 network on board the ROV was one of the critical factors that would determine how fast the overall control system would respond.

As laid out in the specifications for the ROV in Section 3.1, it should take no longer than 0.5 seconds to complete one cycle of commands to all modules on the ROV so that no significant lag is noticeable to the operator. These tests were carried out to determine the overall performance of the serial network and whether this goal had been achieved.

The procedures for performing these tests are described below and are followed by the corresponding results and concluding remarks.

8.3.2.2 Test Equipment

- Agilent DSO1004 60MHz Oscilloscope, complete with 3 probes
- ROV surface power supply unit (PSU) connected to mains power supply
- Power Pod connected to the ROV's PSU
- E-Pod, open and connected the Power Pod with its underwater connecting cables and to the PSU using a 2m fibre optic patch cord
- Laptop connected via a network cable to the PSU
- Simplified version of the user interface control software

8.3.2.3 Preparation of Equipment

Setup of COM Port on Laptop

To establish communication between the Labview® UI and the ROV serial network, the Tibbo® DS1102 Ethernet-to-serial converter (or serial device server) which resides in the E-Pod, needed to be configured as a Virtual Serial Port (VSP) on the laptop. The laptop's IP address was set at 192.168.0.127 and the Subnet mask at 255.255.255.0 to allow communication between the laptop and Tibbo® unit. The Tibbo® Connection Wizard application was then used to configure the VSP and device server settings. All microcontroller baud rates were set at 115 200 baud, so the device server and VSP were configured to match this rate.

Oscilloscope Setup

Before powering up the ROV, a ground wire was connected to a spare ground terminal on the bottom control board of the E-Pod and the ground reference clip of the three oscilloscope probes attached to it.

8.3.2.4 Test Procedure

The ROV system was then powered up by turning on the PSU's power switch and pressing the Start button. The user interface program was loaded on the laptop and switched into RUN mode, which initiated the start of communications on the RS-485 network.

The most useful serial communication signals to read were the Transmit (TX), Receive (RX) and Transmit Enable signals passing between the microcontroller and MAX3485 chip on each of the microcontroller daughter boards. The microcontroller daughter board mounted on the bottom control board of the E-Pod was used for this because it was the most easily accessible of the assembled circuit boards. Scope probes were placed on the Receive pin (RO), the Transmit pin (DI) and the Transmit-Enable pins (RE/DE) of the MAX3485 integrated circuit (IC) which is shown below in Figure 107.

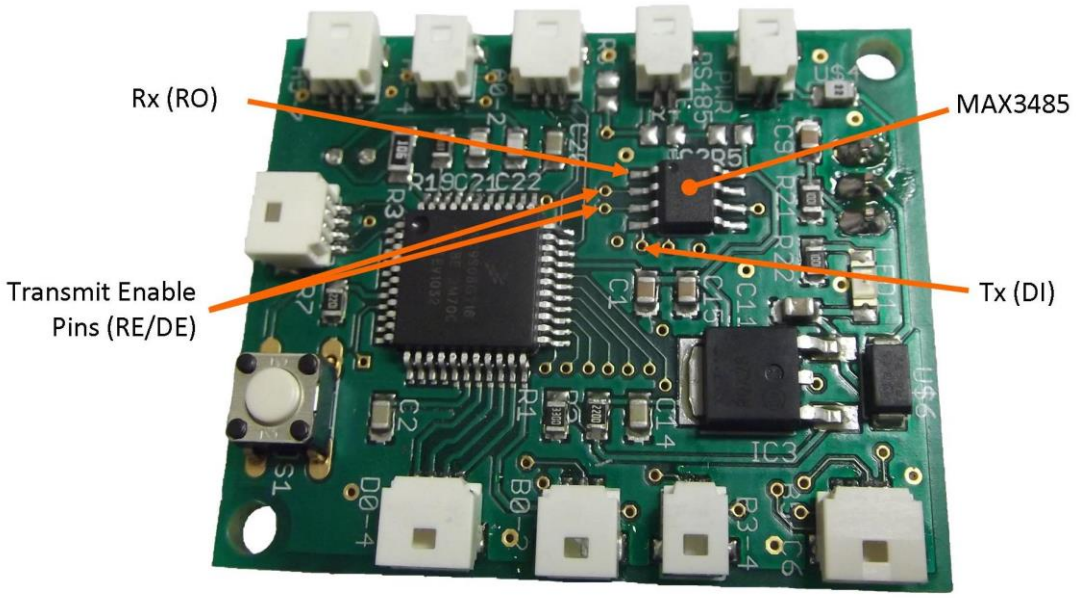

Figure 107: Photo showing serial communications probe points on microcontroller PCB

8.3.2.4.1 Tests Using the Standard ROV User Interface

The first three sets of measurements were taken when using the standard ROV user interface, as developed for use by the operator. The first set of measurements was taken to determine the characteristics and performance of data transmission within each byte. The second set of measurements was taken to determine the performance and characteristics of the data transmission during the receiving and sending of data packets, and the third set of measurements was taken to determine the overall serial network performance.

8.3.2.4.2 Tests Using the Standard ROV User Interface

As the tests were done, it became evident that there were delays on the serial network when the more complicated ROV user interface was used. This interface had been developed as the main interface for the end user. To determine whether some of the delays experienced could be

attributed to the user interface program, the third set of tests described above were repeated using a simpler version of the user interface. This version had been used earlier in the development of the system and was re-implemented to run these tests. The simpler version repeatedly sent packets of data over the serial network, but only communicated with one RS-485 slave at a time. This reduced the processing required in the user interface program and was expected to speed up the communications cycle frequency. A screen shot of this user interface can be seen below in Figure 108.

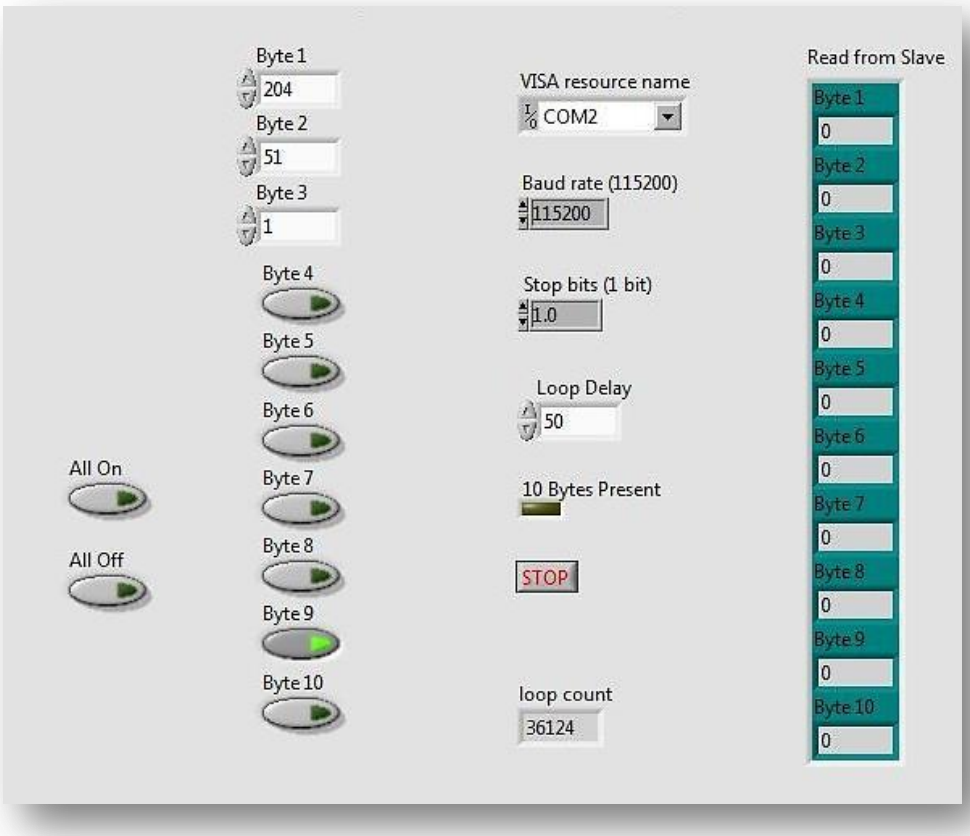

Figure 108: Screen capture of simple Labview® user interface for basic communication with RS-485 slaves on ROV serial network

8.3.2.5 Test Results and Analysis

8.3.2.5.1 Bit-Level Readings

The serial communications were set to operate at a baud rate of 115 200, which corresponds to a calculated period of 8.68 µs per bit. Figure 109 below shows 4 bits transmitted in approximately 35 µs, which confirms that data was sent at the set rate. All signal levels were found to be stable and switch fully across their full amplitude with negligible slew. There was also very little noise or overshoot on the rise or fall of the signals.

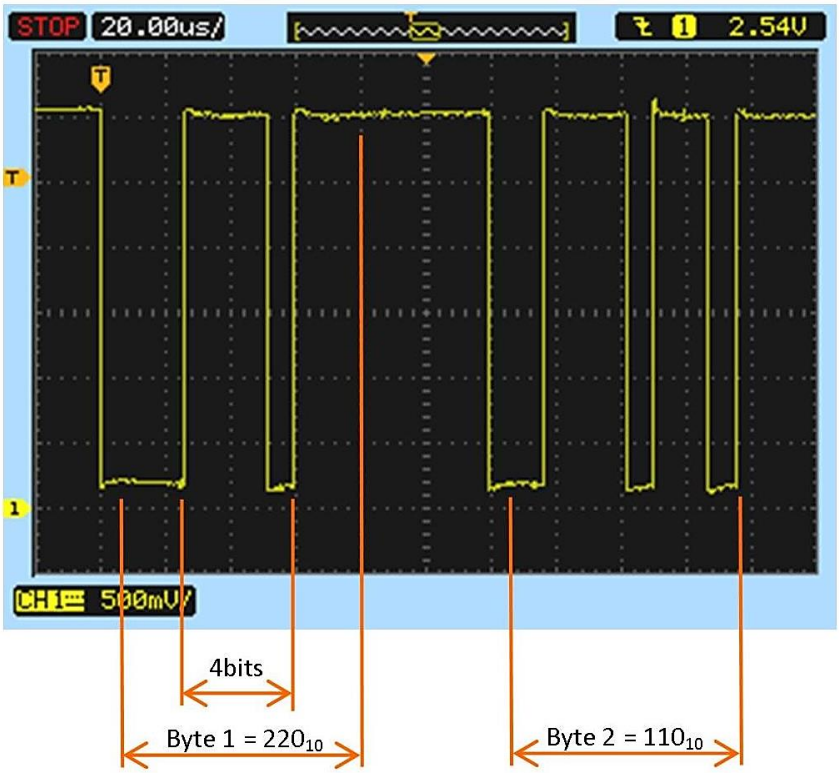

Figure 109: Oscilloscope screen capture of the Tx signal showing the data bits of the two address bytes at the start of the transmit packet from the bottom E-Pod controller

8.3.2.5.2 Byte-Level Readings

Once the data had been analysed within each byte to ensure that the correct data was being transmitted, the data inside each packet was analysed to determine whether all the data bytes were being transmitted correctly and at what efficiency.

In the 10-byte packets of data, each byte contained 8 data bits plus one start bit and one stop bit, and therefore each packet contained a total of 100 bits. Without any processing delays, to receive and send a 100-bit packet of data at 115200 baud would take 1736 µs. However, oscilloscope readings showed that to receive and send the two packets actually took approximately 2.20 ms. The efficiency of data transmission from when the first receive bit started until the final transmit bit ended could be calculated using the formula below, where η_{packet} is the efficiency.

$$\eta_{packet} = \frac{Ideal\ data\ transmission\ period}{Actual\ data\ transmission\ period} \times 100\%$$

$$\eta_{packet} = \frac{1.74ms}{2.20ms} \times 100\%$$

$$\boldsymbol{\eta_{packet}} = \mathbf{79}\%$$

The 21% loss of efficiency was due to time delays between bytes and delays between receiving and transmitting each packet. These were attributed to the processing delays on the microcontroller. In the development of the system, it was found that there were certain minimum delays necessary for the serial port on the MC9S08GT16A microprocessor and the MAX3485 chip to work well together. The largest delays were those between the Transmit Enable signal's rise and the start of transmitting data, and between the end of transmitting data and the Transmit Enable signal's fall. The measured delays were about 125 µs and 30 µs respectively.

8.3.2.5.3 Network-Level Readings

Once it was determined that the data in each packet was being transmitted correctly and as efficiently as possible, measurements were taken of the frequency at which packets of data were being transmitted. Figure 110 shows that communication with each module – where a packet of data was sent and received – occurred approximately every 20 ms. Tests were not carried out with the full set of modules connected and powered up on the ROV because half of them were still in production at the time of testing. If the full complement of sixteen modules had been connected on the RS-485 network, a period of about **320 ms** per cycle would have been expected at a rate of 20ms per module.

A further test was performed to determine whether a simplified version of the Labview® user interface would speed up the communication cycle. This was indeed the case and a screenshot showing the frequency of packets transmitted can be seen in Figure 111. The period between packets was measured at approximately 10 ms, which was half of the period needed in the more complex, standard user interface.

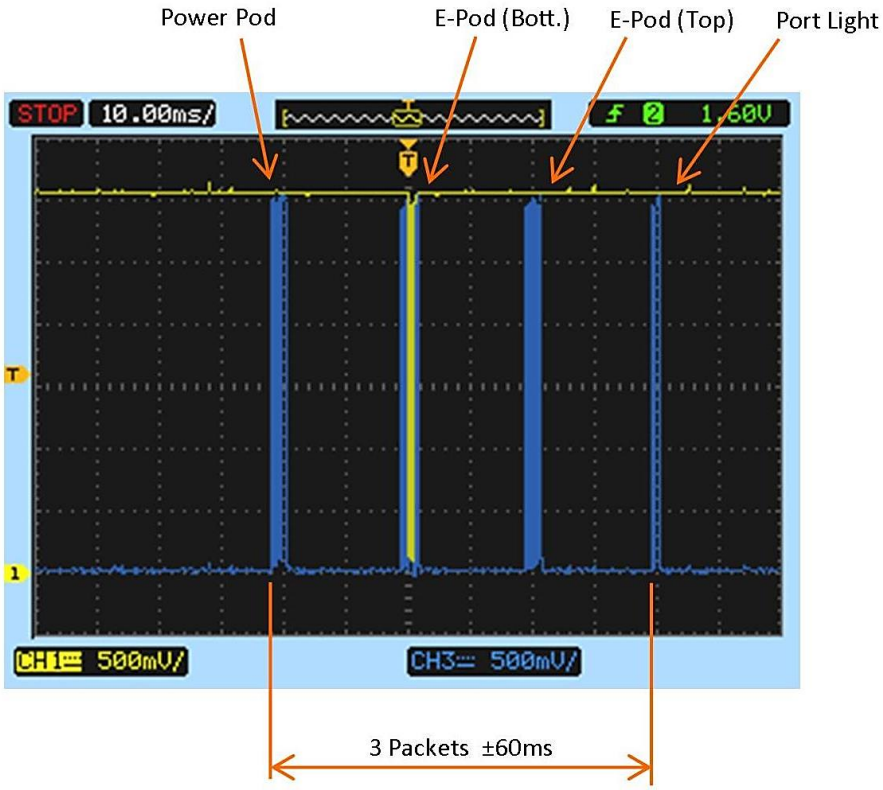

Figure 110: Oscilloscope screen capture showing the frequency of serial data packets (blue) and the frequency of each transmitted packet from the bottom E-Pod controller (yellow) when using the standard ROV user interface

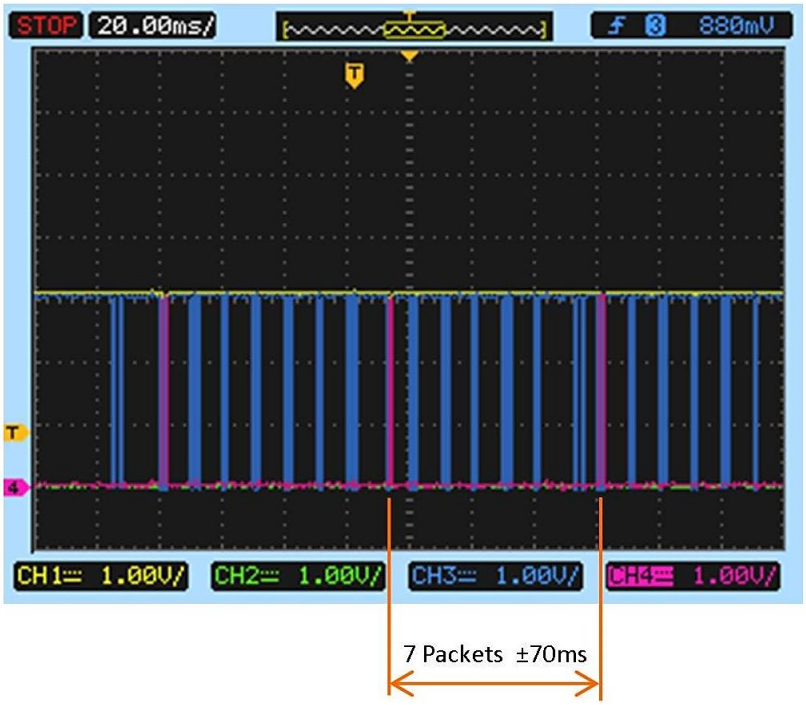

Figure 111: Oscilloscope screen capture showing the frequency of serial data packets (blue) and the frequency of each transmitted byte from the bottom E-Pod controller (magenta) when using the simplified user interface

8.4 PRELIMINARY THERMAL TESTS

8.4.1 Preliminary E-Pod Thermal Tests - Rise in Temperature of PCB Tracks and Components as Current Increases

8.4.1.1 Purpose and Scope of the Test

This set of preliminary tests was performed to establish that the current sensors could be safely calibrated without any of the related PCB components or copper tracks overheating at the rated currents. Because the top and bottom PCBs were identical, only one was tested thoroughly and the results considered applicable to the other.

The voltage and maximum current requirements of each module that would be connected to the bottom control PCB are displayed in Figure 112 below.

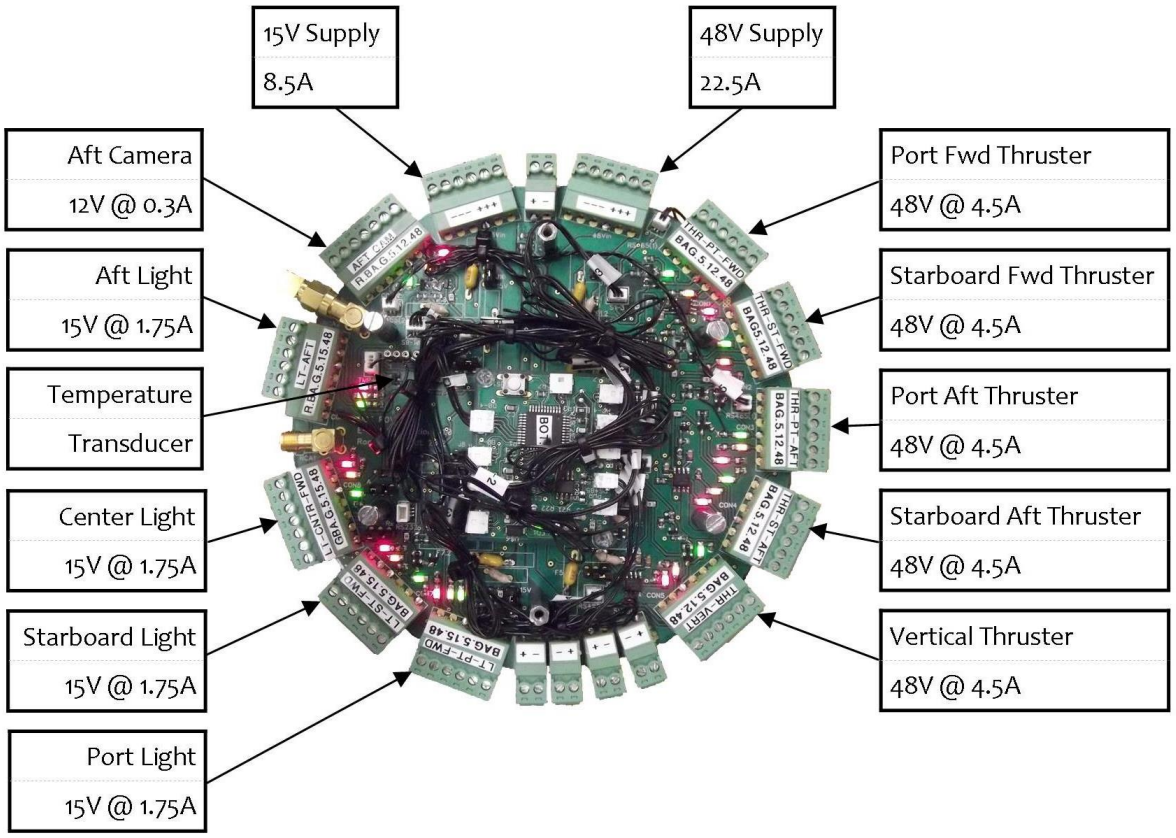

Figure 112: Voltage and current ratings for E-Pod bottom control PCB

Only the 48 V and 12/15 V lines on each channel were tested because of the heavier current requirements on these lines. The 5 V line of each channel was not load tested due to the low 500 mA load requirement on each one and the low overall current draw on the 5 V supply.

This set of tests was performed on the bottom control PCB in isolation from the rest of the E-Pod circuitry and outside of the E-pod chamber so that thermal imaging could be used to characterise its thermal performance. Later thermal tests of the assembled and sealed E-Pod would determine the overall thermal performance of the system.

8.4.1.2 Test Equipment

- Bottom E- Pod control distribution circuit board connected to stack of E-Pod control electronics
- PC running a simplified version of the ROV user interface
- Manson® HCS-3302 Power supply set at 5 V with a current limit of 0.7 A
- Topward 6303D Power supply set at 12 V with a current limit of 0.7 A
- Topward 6303D Power supply set at 15 V with a current limit of 8.7 A
- Topward 6303D Power supply set at 48 V with a current limit of 4.7 A
- Variable resistor network to provide 10-25 Ω with a current rating no less than 4.5 A
- Variable resistor to provide 1.5-10 Ω with a minimum current rating of 8.5 A
- FLIR® Thermovision A320 thermal camera, tripod and laptop with FLIR® software
- Agilent® U1242B Multimeter

8.4.1.3 Preparation of Equipment

8.4.1.3.1 PCB

The supply voltage to each connector's Pin 2 was determined by using the on-board jumper provided to select either the 12 V or 15 V supply. Because the temperature rise is related only to the current drawn through the conductors the line was tested using only the supply rated for the greater current, which was the 15 V supply (see Table 12 in Section 3.10 for the complete list of power requirements on the ROV).

8.4.1.3.2 Thermal Camera

The FLIR Thermovision camera was set up on its tripod to look down on each of the circuit boards. The temperature range was fixed from 5 °C to 55 °C in the IR Monitor® software.

8.4.1.3.3 Connection to Load Resistors

For testing the power supply buses on the PCB, one large variable resistor was used and all connectors connected in parallel. This was far more cost effective and convenient than sourcing ten different resistors. Each connector was fitted with a diode to stop voltages being fed back onto other power-switching components of the PCB. A 6A rated general purpose diode was soldered in line with the main output line on each thruster's connector and a 3 A rated diode soldered in line with the remaining five connector outputs to provide the protection. A strip of terminals mounted on a 35 mm DIN rail was used to simplify the wiring and connections to the resistor. A schematic of this arrangement and the in-line connection to the ammeter is shown in Figure 113.

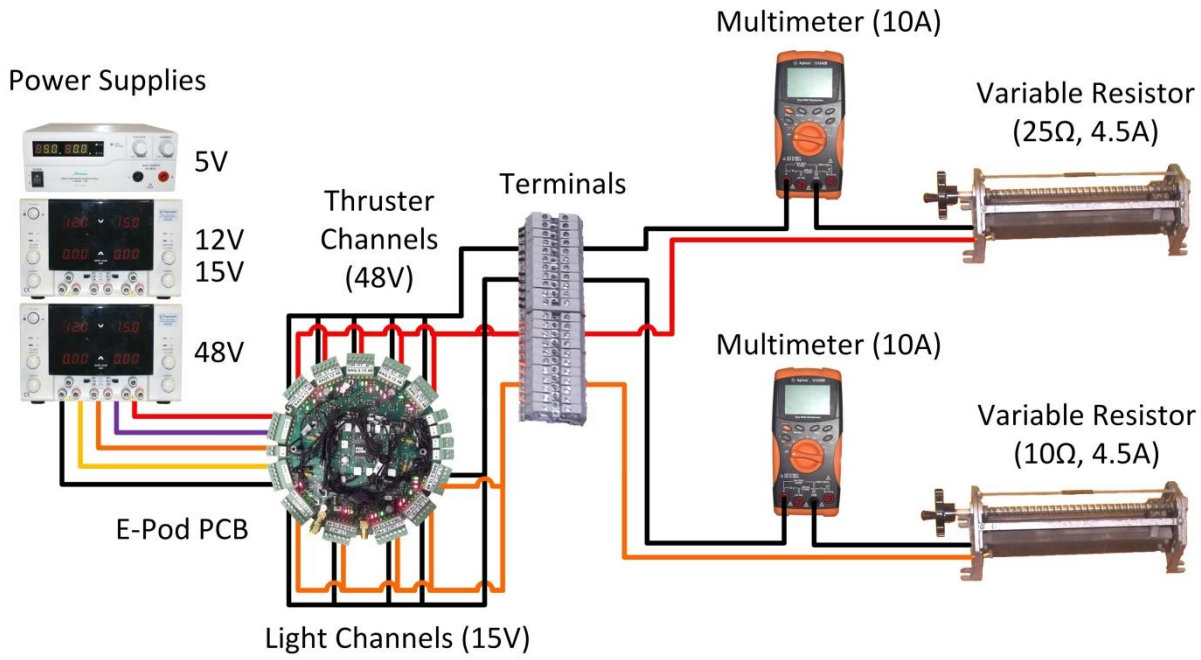

Figure 113: Wiring schematic for E-Pod PCB thermal tests and current sensor calibrations

8.4.1.4 Test Procedure

The critical tracks and components supplying each connector were tested by completing two rounds of load tests on each output channel. In the first round only the 48 V line of each channel was tested and in the second round only the 12/15 V line of each channel was tested. The variable resistors were adjusted to produce specified currents at set time intervals, as listed in Table 31, while the switching on or off of the channel power was controlled remotely via the PC. The thermal camera was set up above the PCB (see Figure 114 below) to record the temperatures of the PCB tracks and components as the current was increased.

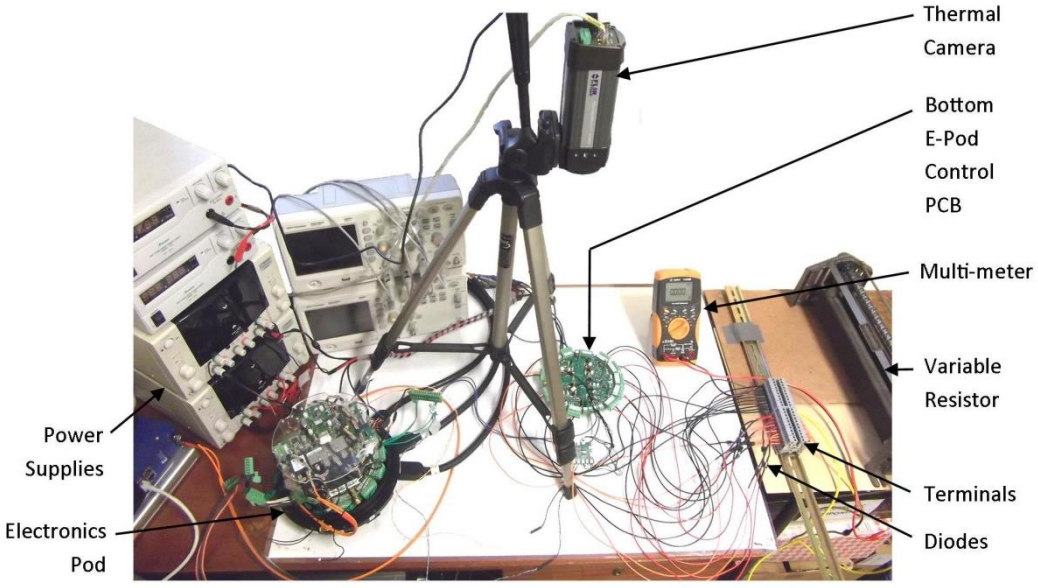

Figure 114: Photo of thermal test setup for E-Pod distribution PCB

Using the user interface (UI) on the PC, the selected output channel under test was turned on and the time recorded. After each time interval the temperature image was captured and current adjusted according to Table 31. Once hotspots were identified on the thermal image, spot markers were added in the IR Monitor® software to measure the temperature of these tracks or components more accurately.

Table 31: Current settings for thermal testing of E-Pod PCB output channel circuits

	Current [A]											
Time [min]	**0**	**1**	**2**	**3**	**4**	**5**	**6**	**7**	**8**	**9**	**10**	**40**
15 V Line	0.5	0.75	1.0	1.25	1.5	1.6	1.7	1.7	1.7	1.7	1.7	-
48 V Line	2.0	2.25	2.5	2.75	3.0	3.25	3.5	3.75	4.0	4.25	4.5	4.5

If tracks and components reached their maximum rated current without overheating, they were initially held at the rated current for 30 minutes [52], and temperature readings taken every minute. To speed up the testing process, the extra 30 minutes was skipped for circuits that showed similar thermal characteristics in the first 10 minutes.

If any components reached 60 °C the current was to be reduced by adjusting the current limit knob on the power supply. If this did occur, the maximum current that would not push the component temperatures above 60 °C over a period of 30 minutes was to be determined.

The PCB tested was mounted on 30 mm long standoffs on both topside and underside, and was cooled by natural convection only.

8.4.1.5 Test Results and Analysis

8.4.1.5.1 48 V Lines

The hottest components measured on the 48 V lines of the E-Pod control PCBs were the MOSFETs on the underside and the resettable fuses on the topside (see Figure 115 and Figure 116).

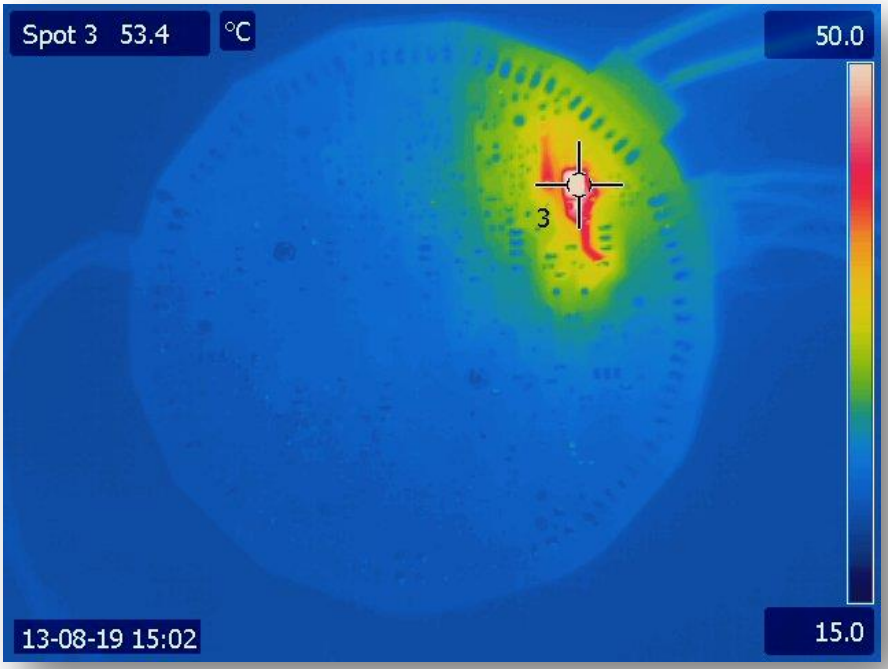

Figure 115: Thermal image of E-Pod PCB underside after 39min at 4.5A on Channel 1's 48 V line

Figure 116 shows two hotspots on the topside of the PCB. The hot region below Spot 3 was the resettable fuse and the hot region below Spot 4 was a copper track connected through the PCB to the MOSFET on the underside. It appeared, by the fact that the temperature rise in this region was localised, that the high temperature at this point was predominantly from heat conducted away from the MOSFET. If it had been generated by resistive heating in the copper track, the full length of track between the resettable fuse and the output connector would have been expected to heat up to a similar temperature. The same reasoning was applied to understand the rise in temperature of the hot copper track pictured below the MOSFET in Figure 115. It was virtually impossible to determine how heating affected the copper tracks solely due to resistance. However, using the scale on the right of these thermal images, it could be seen that the 48 V copper tracks, close to where they met the output connectors, did not rise above 40 °C. It was determined therefore, that the temperature rise due to resistance in the 48 V copper tracks was less than 30 °C.

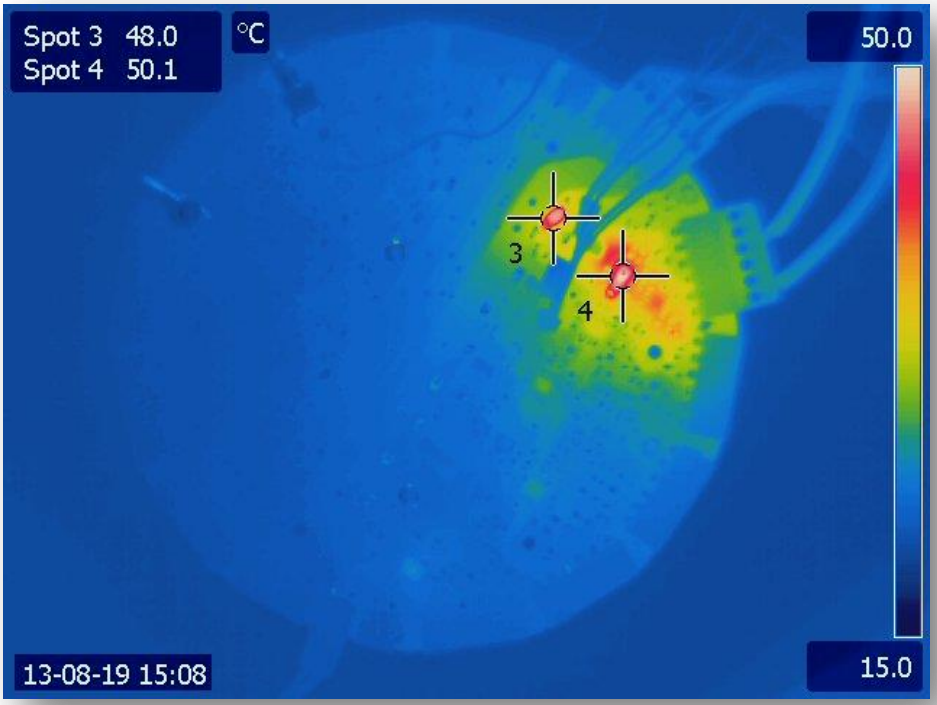

Figure 116: Thermal image of E-Pod PCB topside after 45min at 4.5A on Channel 1's 48 V line

The graph in Figure 117 below shows a graph of the temperatures recorded at each time interval for each channel's 48 V line. All readings followed a similar trend in the first 15-20 minutes so it was possible to shorten the test period after establishing a trend for the first channel in a full 40 minute test.

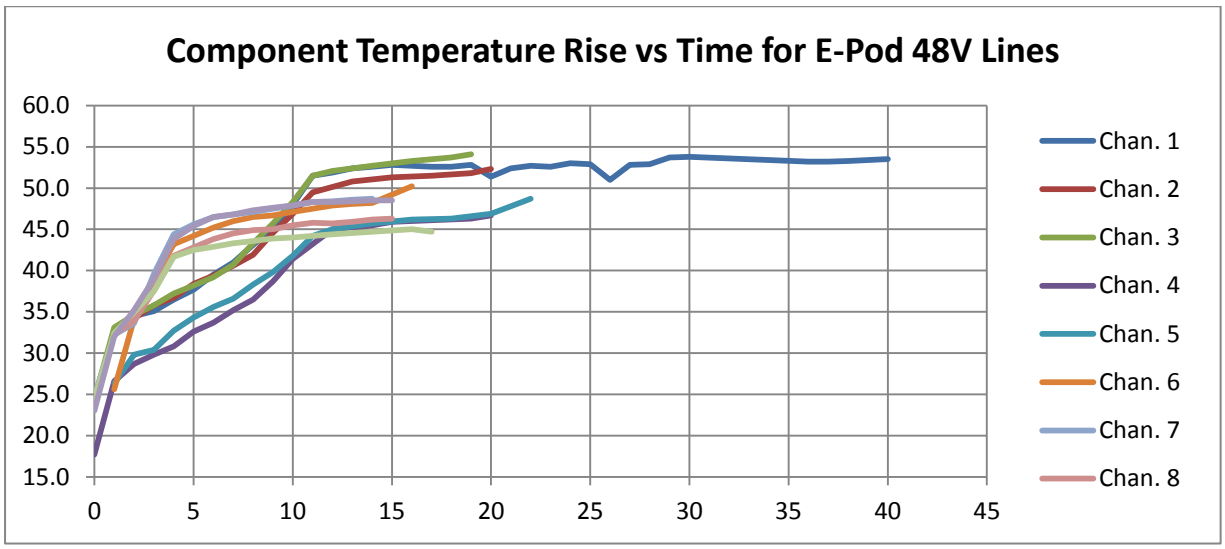

Figure 117: Graph of E-Pod PCB component temperatures over time for current flow in the 48 V line of each channel

The ambient temperature at the time of testing ranged from 18 °C to 21 °C and the maximum component temperature recorded was 54.1 °C. Rounding up, this was a 37 °C temperature rise above ambient.

8.4.1.5.2 15 V Lines

The thermal readings of component temperature rise on the 15 V lines of each channel were much lower than the measurements on the 48 V lines. Despite the fact that five channels were tested simultaneously, the combined heating effects were negligible and at currents of only 1.7A in each channel, component temperatures did not rise above 40 °C. Thermal images showing the final readings of the second five channels can be seen below in Figure 118. The hottest component recorded was a resettable fuse at 35.1 °C on channel 10 after 10 minutes at 1.7A (Spot 2).

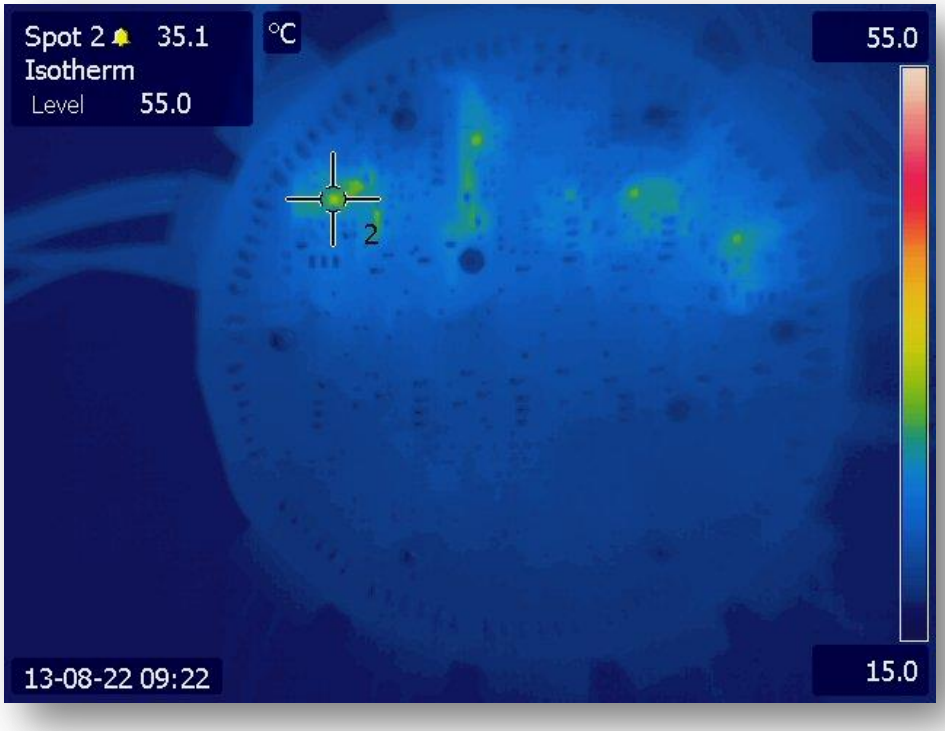

Figure 118: Thermal image of E-Pod PCB underside after 10min at 1.7A on each of Channels 6-10's 15 V line

The copper tracks used for the 15 V line were the same width as those used for the 48 V lines and showed a negligible rise in temperature due to resistive heating.

The ambient temperature for these tests started at 16 °C and the maximum temperature recorded was 39 °C, which indicated a 23 °C rise above ambient.

8.4.2 Preliminary Power Pod Thermal Tests - Rise in Temperature of PCB Tracks and Components as Current Increases

8.4.2.1 Purpose and Scope of the Test

Similar to the preliminary E-Pod tests described above, this set of tests was performed to establish that the current sensors integrated into the Power Pod's PCBs could be safely calibrated without any of the related PCB components or copper tracks overheating at their rated currents. These tests were also used to characterise the thermal performance of the PCBs in open air before enclosing the circuits in the Power Pod. This was done so that a temperature sensor could be strategically placed to provide over-temperature monitoring of one of the 48 V DC-DC converters.

The voltage and maximum current requirements for each of the power supply PCBs can be seen in Figure 119 below.

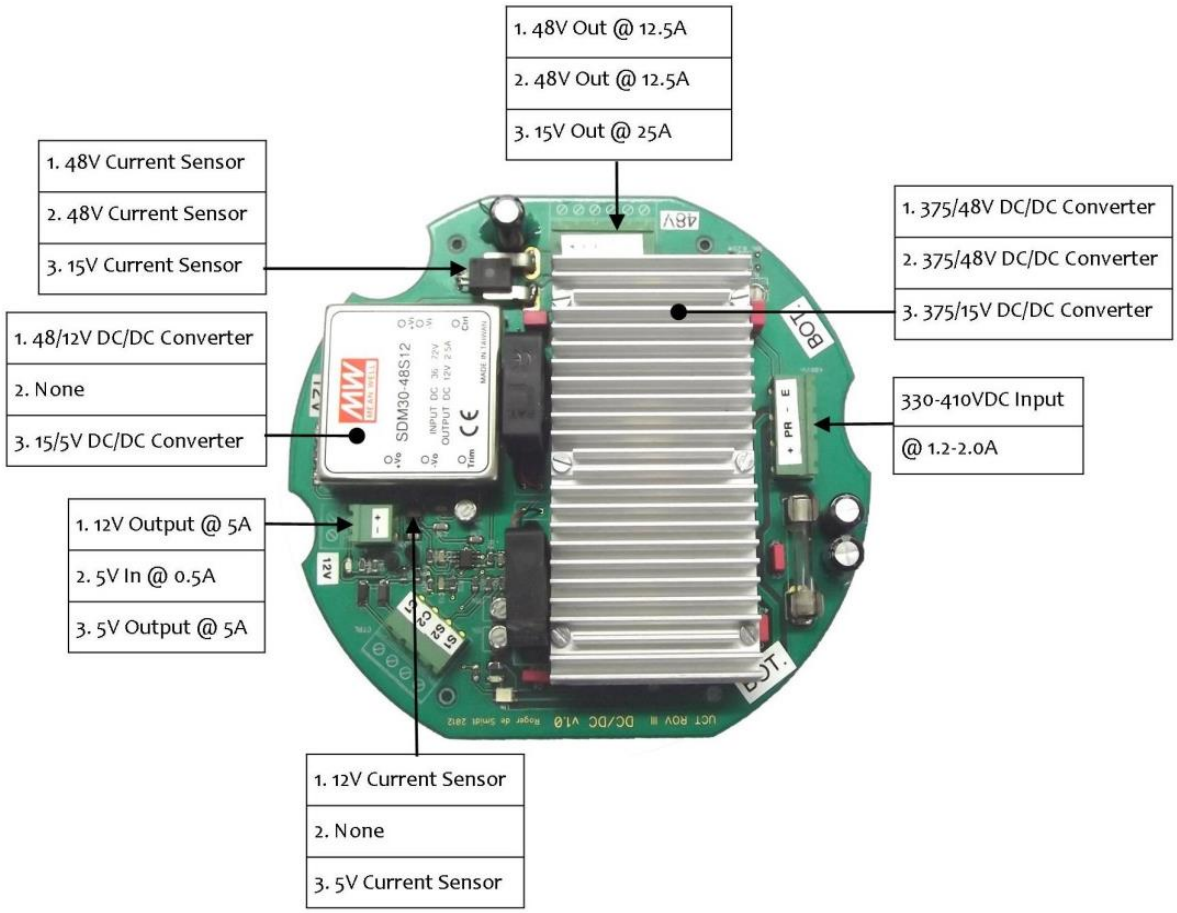

Figure 119: Voltage and current ratings for the Power Pod 48 VDC and 12 VDC Power Supply PCB

After these preliminary tests were completed, thermal tests of the assembled and sealed Power Pod would be performed to determine the overall thermal performance of this subsystem.

8.4.2.1.1 Precautions Taken with High-Voltage Equipment

The tests on the Power Pod supply circuits were the first official tests that employed the use of the 400 VDC ROV Power Supply Unit (PSU). The PSU and all the high voltage connections were treated with extreme caution because a shock at such high voltage and power could easily have been lethal.

It was necessary, therefore, to cordon off the test area with hazard tape and put up warning signs. This made it clear to other persons in the laboratory that the equipment was dangerous and to be given a wide berth.

The precautions that were to be followed by the operator were largely taken from the Colorado State University's High Voltage Safety Manual [53], a summarised list of which is included below.

1. Do not work alone.
2. Allow time for capacitors to discharge.
3. Do not probe circuits using two hands. Use only one.
4. Never assume anything. Check it yourself.
5. Do not work with high voltage equipment when tired.
6. Wear rubber-soled shoes.
7. Remove wrist-watch and all jewellery.
8. Call for an ambulance on 10177 in an emergency.

8.4.2.2 Test Equipment

- ROV 400 VDC PSU
- Power Pod 15 VDC & 5 VDC power supply PCB
- Power Pod 48 VDC & 12 VDC power supply PCB
- Variable resistor to provide 1.9-20 Ω with a minimum current rating of 25 A
- Variable resistor to provide 1-10 Ω with a minimum current rating of 5 A
- FLIR® Thermovision A320 thermal camera, tripod and laptop with FLIR® software
- F.W. Bell® CG100D clamp-on current meter
- Agilent® U1242B Multimeter

A schematic showing how the equipment was wired up is shown in Figure 120.

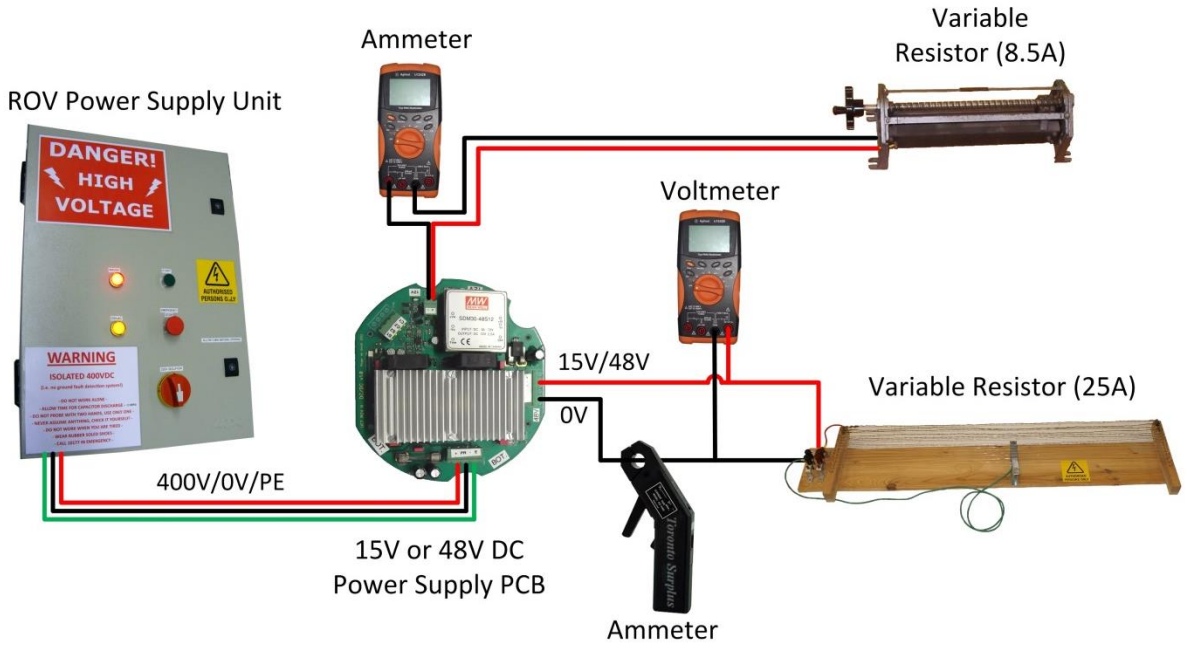

Figure 120: Wiring Schematic for Power Pod DC-DC converter circuit thermal tests

8.4.2.3 Preparation of Equipment

8.4.2.3.1 Thermal Camera

The FLIR Thermovision camera was set up on its tripod to look down on each of the circuit boards as seen in Figure 121 below. The temperature range was fixed from 15 °C to 100 °C in the IR Monitor® software and an Isotherm warning, which was set at 95 °C, would automatically identify any areas above this temperature.

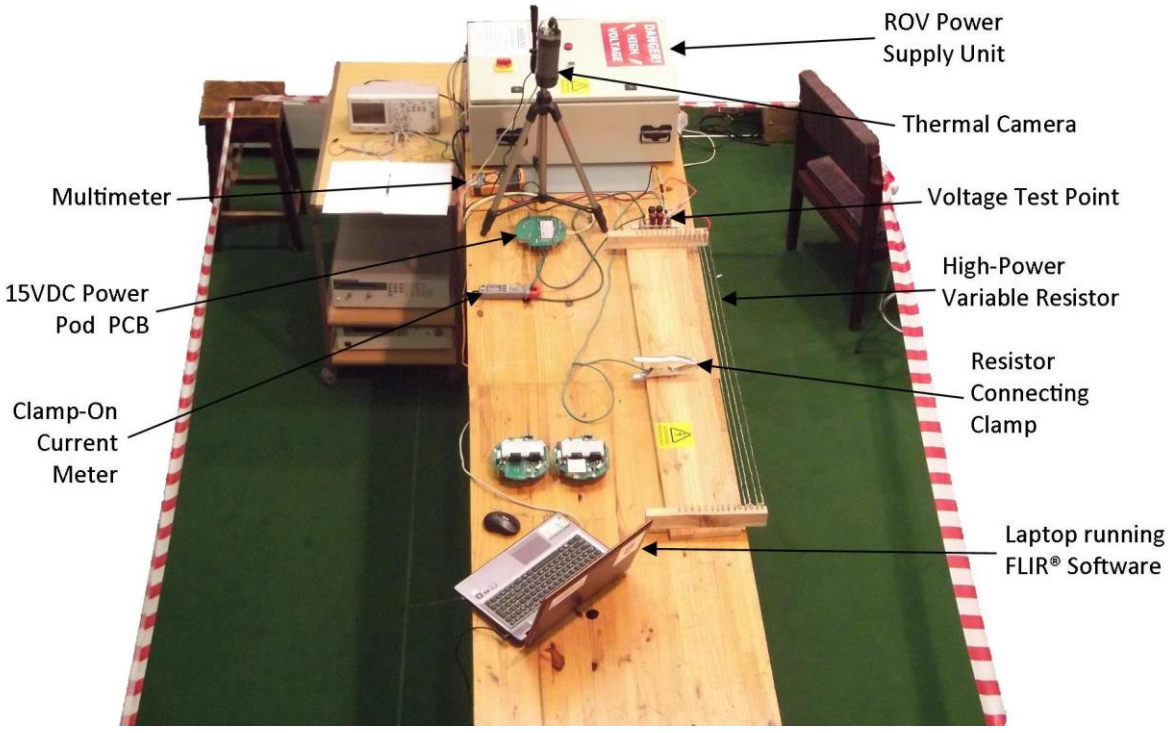

Figure 121: Photo of thermal test setup for Power Pod PCBs

8.4.2.3.2 Connection to Load Resistors

Due to the heavy currents being conducted, all wire terminations were thoroughly fastened and ensured to have good contact. The maximum current to be drawn was 25A. Working on a conservative rule of 10A per 1 mm^2 of copper conductor [31], connections to the variable resistor were made with wire no less than 2.5 mm^2 in cross-sectional area.

8.4.2.4 Test Procedure

Each of the three DC-DC converter PCBs was identical, but each one was populated with slightly different components to provide the different voltage levels required by the ROV. To test the thermal performance of the Power Pod circuits there were three critical components, or parts thereof, that required thermal analysis. These are described below, each under its own heading.

8.4.2.4.1 Temperature Rise in 15 V Supply Circuit

The first critical measurements were those of the copper track temperatures on the 15 V power supply output. This circuit was designed to deliver the heaviest current out of all the DC-DC converter circuits in the Power Pod. The capacity of these 7 mm wide copper tracks was tested at 25A, which was close to the maximum output current rating for the 375/15 V DC-DC converter. The temperature of the actual converter itself was monitored at the same time to determine its operating temperature relative to the other converters in the Power Pod.

The 15 V power supply PCB was connected to the 400 V PSU and the 15 V output was connected to the load resistor as shown in Figure 120. The 5 V output was left unconnected for this test.

Because the capacity of the 7 mm tracks was unknown, the 15 V output was loaded incrementally in four stages, starting with a relatively light load of 10A. At each setting, the load was maintained until the maximum temperature on the PCB had ceased to rise more than 0.2 °C/min, and a record of the temperature was captured every minute using the thermal imaging software. The variable resistor values and corresponding current drawn at each increment are presented in Table 32 below.

Table 32: Variable resistor settings for testing 15 V power supply PCB

15 V Supply	Current [A]			
Test	**1**	**2**	**3**	**4**
Resistance [Ω]	1.5	1.0	0.75	0.60
Current [A]	10	15	20	25

The power supply was turned off between each adjustment of the variable resistor and the Agilent® multimeter was used to measure the voltage across the variable resistor as a safety check before handling the connecting clamp.

8.4.2.4.2 Temperature Rise in 375/48 V DC-DC Converter

The second critical component was the 375 VDC/48 VDC converter which could deliver the greatest power and, due to inherent inefficiencies, would dissipate the most heat of the five DC/DC

converters. At 600W and an efficiency of 88.5% the converter would need to dissipate 78W of heat [54].

As shown in Figure 120, the 48 V power supply PCB that also had the 48/12 V DC-DC converter mounted on it was connected to the PSU. This PCB was expected to operate at a slightly higher temperature than the other 48 V PCB without the smaller DC-DC converter. The cooling fans on this board were powered by the on-board 12 V supply which also made it preferable to the other 48 V circuit board which required an external power supply for its fans. The 48 V output was connected to the larger load resistor, and the 12 V output was left unconnected.

Similar to the 15 V test, the 48 V output was loaded incrementally in three stages. At each setting, the load was maintained until the maximum temperature on the PCB had ceased to rise more than 0.2 °C/min, and a record of the temperature was captured every minute using the thermal imaging software. The variable resistor values and corresponding current drawn in each increment are presented in Table 33 below.

Table 33: Variable resistor settings for testing 48 V power supply PCB

48 V Supply	Current [A]		
Test	**1**	**2**	**3**
Resistance [Ω]	9.6	4.8	3.8
Current [A]	5.0	10.0	12.5

The power supply was turned off between each adjustment of the variable resistor and the Agilent® multimeter was used to measure the voltage across the variable resistor as a safety check before handling the connecting clamp.

8.4.2.4.3 Temperature Rise in 5 V Supply Circuit

The final critical circuit to be analysed in these preliminary tests was the 5 V supply. The 15/5 V DC-DC converter was rated for the greater current and greater heat dissipation out of the two smaller DC-DC converters. The temperature rise of the converter and of the copper tracks serving the 5 V output connector were analysed with thermal imagery.

The 15 V circuit board was reconnected to the 400 V PSU, but this time the 5 V output was connected to the smaller variable resistor and the 15 V output was left unconnected.

The resistor was set to 1 Ω which resulted in a 5 A load on the supply circuit. The load was maintained until the maximum temperature on the PCB, visible via the thermal camera, had ceased to rise more than 0.2 °C/min, and a record of the temperature was captured every minute using the thermal imaging software.

8.4.2.5 Test Results and Analysis

8.4.2.5.1 Temperature Rise in 15 V Supply Circuit

The 15 V power supply was loaded incrementally as described above without any components or tracks overheating. When loaded with the heaviest current of 25 A, the temperature finally stabilised after 24 minutes at a maximum just above 88 °C as seen in Figure 122 below. This temperature was measured on the surface of the converter that was flush with the underside of the PCB and was not mated with a heat sink. The heat sink of the Maxi converter was force-cooled in an ambient air temperature of 20 °C. The cooling was provided by two cooling fans that were integrated into the circuit board.

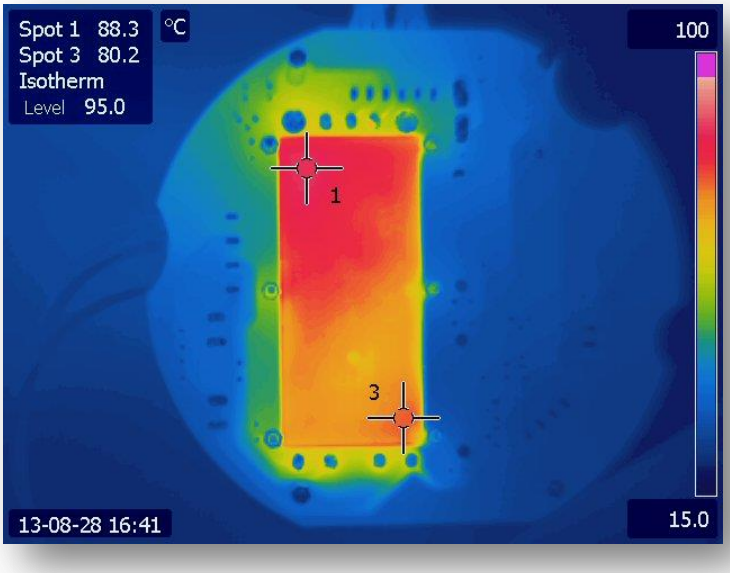

Figure 122: Thermal image of the underside of the 15 V power supply circuit after 24 minutes at 25A

The heat sink of the converter was much cooler than the underside. Figure 123 shows the relatively cool heat sink on the top of the PCB shortly after power was removed. What is also evident in the circled area in Figure 123 is that there was very little heat build-up in the 7 mm wide copper tracks between the converter output, the current sensor and the output connector pins. There is a small region of heat on the one leg of the current sensor, but this appeared to be a highly localised spot and was attributed to a flaw in the solder joint at that point or a reflection of heat from the adjacent converter. Otherwise temperatures in these tracks did not appear to rise more than 30 °C above ambient.

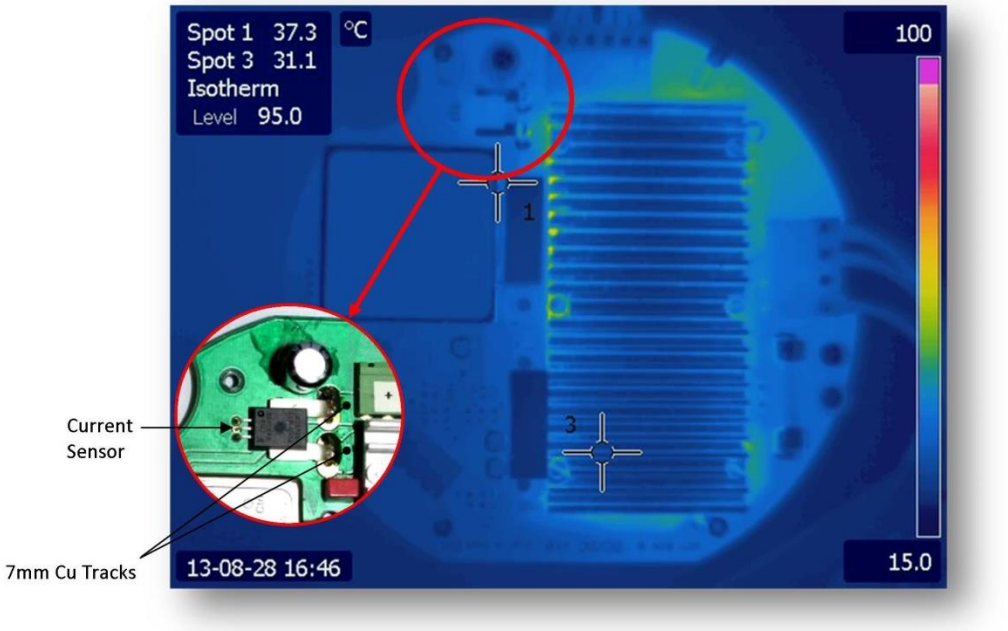

Figure 123: Thermal image of the topside of the 15 V power supply circuit with photo insert showing critical copper tracks

8.4.2.5.2 Temperature Rise in 375/48 V DC-DC Converter

At its full load, the 375/48 V DC-DC converter reached its maximum operating temperature of 100 °C after 19 minutes, as shown in Figure 124 below. This result was obtained on the labelled surface of the converter which was not fitted with a heat sink. This surface was also in its worst-case orientation – face-down – where natural convective cooling would have been least effective. The other side of the converter with the heat sink was cooled with its two fans in an ambient temperature of just below 20 °C.

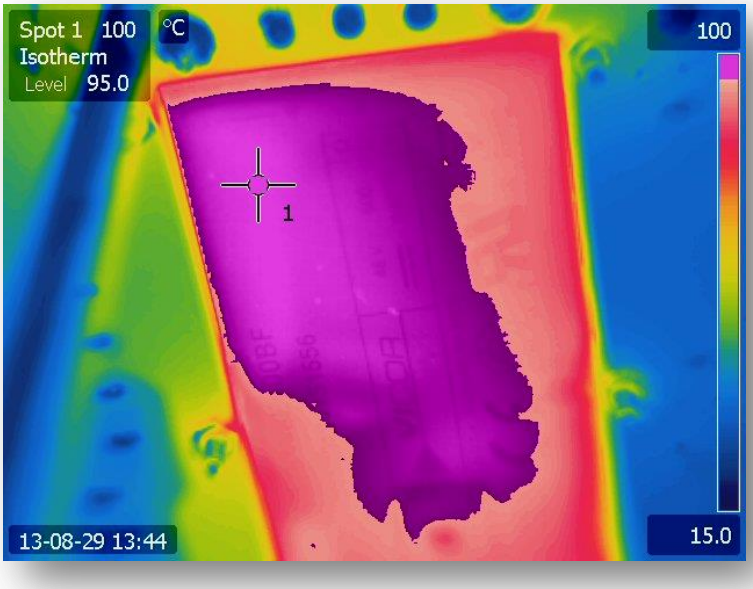

Figure 124: Thermal image of the downward-facing 375/48 V DC-DC converter, from below, after 19 minutes at 12.5 A

When the same converter was tested at full load in the same conditions, but with its labelled surface facing upwards, the temperature stabilised after 30 minutes just above 97 °C as shown in Figure 125 below.

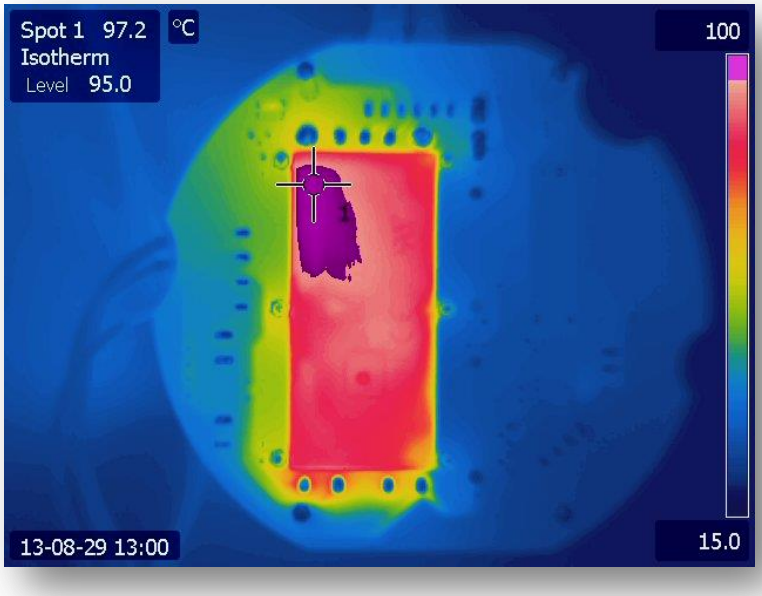

Figure 125: Thermal image from above the upward facing 48 V power supply board after 30 minutes at 12.5A

Figure 126 below shows that the maximum temperature on the top side of the converter was about 35 °C cooler than that on the underside, at the end of testing the converter, with the labelled surface facing upward.

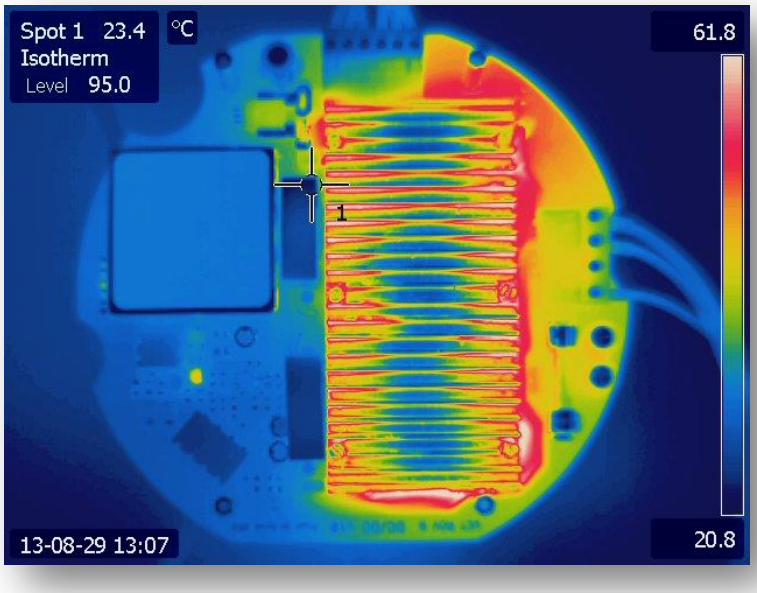

Figure 126: Thermal image of the topside of the 48 V power supply board, from above, just after it was flipped over (temperature colour automatically scaled to suit measured range)

8.4.2.5.3 Temperature Rise in 5 V Supply Circuit

The thermal imagery revealed an unexpected heat build-up in the copper track between the 5 V output current sensor and the output connector on the PCB, as seen measured by Spots 2 and 4 in Figure 127 below. This track was discovered to be 0.5 mm in width, rather than the 2 mm width which was used between the 15/5 V DC-DC converter output and the current sensor. The 2 mm width was supposed to be the standard track width for a 5 A load in the design of the PCB.

The 5 V power supply was run for 32 minutes before its maximum surface temperature stabilised just above 63 °C as seen in Figure 127 below. This temperature was reached with an ambient temperature just below 20 °C and cooling helped slightly by the air drawn through the larger DC-DC converter's cooling fans.

No other heat build-ups were discovered in this circuit.

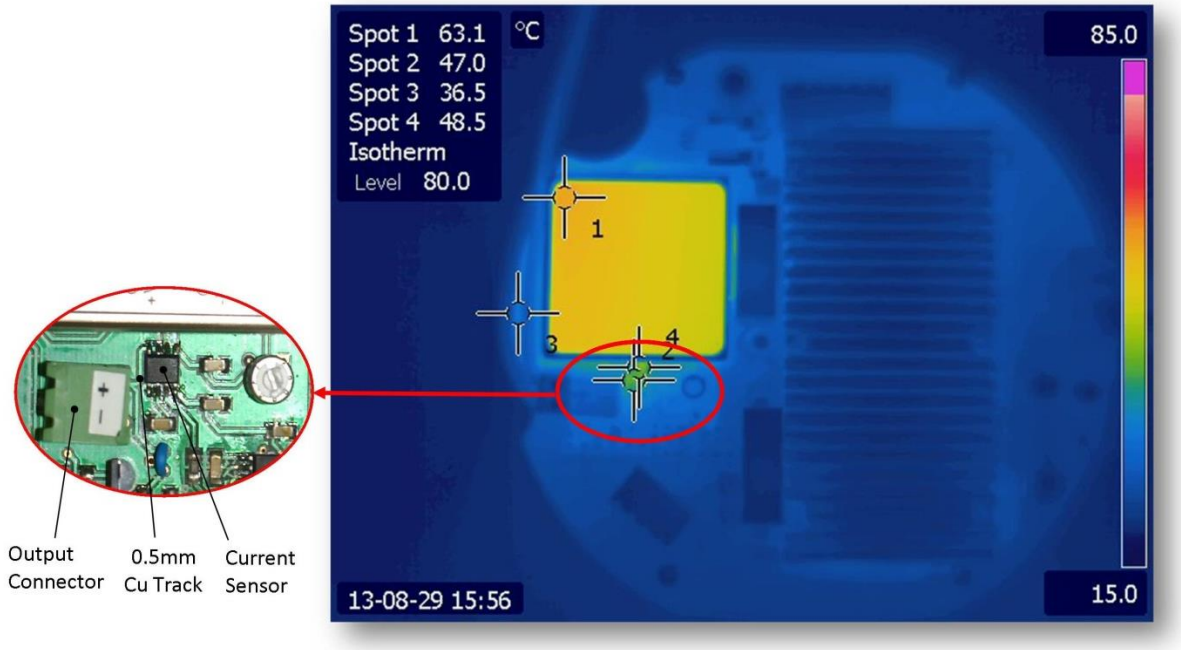

Figure 127: Thermal image of the 5 V power supply circuit after 32min at 5 A with photo insert showing region surrounding Spots 2 and 4

8.5 FINAL THERMAL TESTS

8.5.1 Dry and Wet Thermal Tests on Complete Power Pod and E-Pod Assemblies

8.5.1.1 Purpose and Scope of the Test

After the preliminary thermal tests and calibration of the temperature and current sensors, the E-Pod and Power Pod needed to be put through a set of thermal tests to determine their operational limits.

The individual PCBs of each pod had been tested successfully, but the combined heating effect of the components inside the sealed pods needed to be characterised in order to establish whether there were any operational limits for the ROV power supply system. Because the ROV would be operated underwater and also often tested out of the water, both wet and dry thermal tests were performed.

8.5.1.2 Test Equipment

- Completely assembled and sealed E-Pod
- Completely assembled and sealed Power Pod connected to E-Pod
- ROV 400 VDC PSU connected to Power Pod
- Fibre optic patch cord to connect E-Pod to PSU
- Variable resistor to provide 1.9-20 Ω with a minimum current rating of 25 A
- Variable resistor to provide 1.5-10 Ω with a minimum current rating of 8.5 A
- Terminal strip to connect E-Pod connectors to the variable resistors, complete with diodes wired in line with each connection as established in the preliminary tests
- F.W. Bell® CG100D clamp-on current meter
- Agilent® U1242B Multimeter
- Laptop running the ROV user interface with temperature and current indicators' digital displays enabled
- 50 Litre basin, filled with water

A photograph of the equipment setup for the operational tests is shown in Figure 128. Figure 101 in section 7.3 shows a screen shot of the Labview® UI used for the testing, complete with digital displays enabled for all temperature and current indicators.

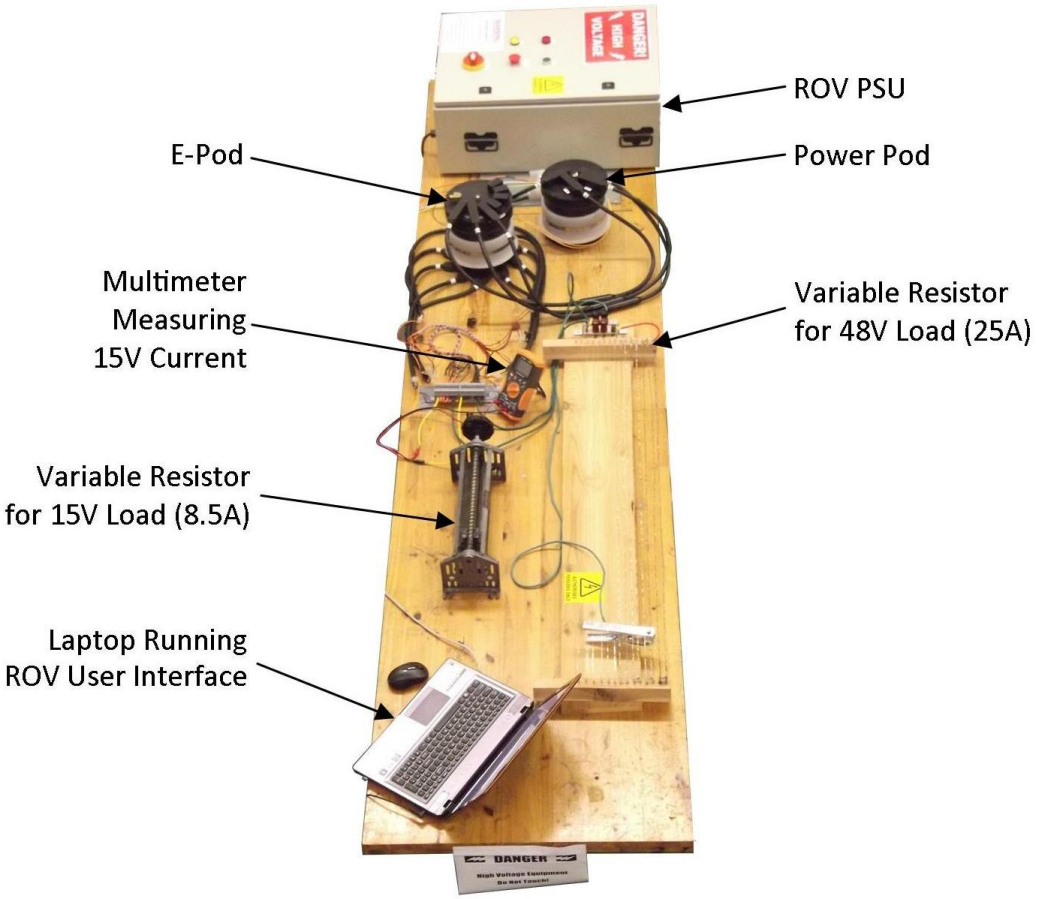

Figure 128: Photograph of equipment setup for dry thermal test of completely assembled Power Pod and E-Pod

8.5.1.3 Preparation of Equipment

8.5.1.3.1 Sealing of Pods

Before the E-Pod and Power Pod were powered up underwater, both were cleaned thoroughly and sealed using the procedures described in a set of instructions that can be found on the accompanying DVD. The pods were then completely submerged in a tub of water for not less than one hour. The pods were then removed, thoroughly dried off using paper towels and compressed air. They were opened and inspected for signs of water ingress.

If successfully free from water ingress, the pods were then resealed and made ready for the operational thermal tests.

8.5.1.4 Test Procedure

The major power consuming subsystems on the ROV when completed would be the thrusters and lights. The output channels of the E-Pod were therefore loaded to simulate these loads. A total of 22.5 A would be drawn from the 48 V lines of the five thruster channels and a total of 8.5 A would be drawn from the 15 V lines on the four light channels and one aft camera channel.

To load each of these outputs as described above, the 48 V lines were connected through OR-ing diodes to the larger variable resistor, and the 15 V lines were also connected through OR-ing diodes

on each line, but to the smaller 8.5 A variable resistor. Both of these resistors were monitored with an ammeter to confirm that the correct current was being drawn. The clamp-on meter was used to measure the 48 V load and the Agilent® multimeter was connected in series with the 15 V load.

To start the testing, the power was turned on and the system was run at one quarter of its rated load on the 48 V lines (5.6 A) with both pods out of the water. This would determine how long basic tests could be performed at an ambient temperature of 20 °C. The test was run until the pods overheated or until the temperature settled and rose no more than 2 °C in 3 minutes on any of the sensors.

The pods were then allowed to cool off and return to room temperature. The power was then switched back on and the full load was drawn to determine how long the system would take to overheat at full load and out of the water when the ambient environment was at room temperature.

After these dry tests were completed, the pods were submerged in the tub of water as shown below in Figure 129. The subsea connectors were used to connect the pods in the water and great care was taken to keep all other temporary electrical connections dry. Electrical cables were tied back to ensure that their connectors could not slip into the water.

Figure 129: Photo of Power Pod and E-Pod submerged in water in a plastic tub

For the wet tests, the power was switched on and the outputs were loaded incrementally to determine at what point the pods would overheat. After each increment in load the pods were monitored and the load was not incremented again until the “Stable Temperature” Boolean indicators in the UI had turned on for all four temperature readings. The test would be considered successful if the full load of 22.5 A on the 48 V lines and 8.5 A on the 15 V lines could be maintained for 1 hour without either pod overheating.

Throughout each of the tests described above, records of the four temperature measurements inside the pods were captured regularly. Temperature limits for each sensor were programmed into the UI so that, if overheating, the power on all E-Pod output channels would be turned off. The value of each of these temperature limits is provided in Table 34 below.

Table 34: Temperature limits programmed into Labview® UI

Power Pod		E-Pod	
Ambient	48 V DC-DC	Bottom	Top
60 °C Max	80 °C Max	55 °C Max	55 °C Max

8.5.1.5 Test Results and Analysis

8.5.1.5.1 Dry Tests

The E-Pod was loaded with a total of 5.8 A on the five 48 V lines and a total of 8.6 A on the 15 V lines. The environment ambient temperature was 19 °C. As shown below in Figure 130, the ambient temperature rise inside the Power Pod was the limiting property, overheating after 15 minutes. It can be seen that the Top E-Pod PCB temperature was also getting close to its limit of 55 °C.

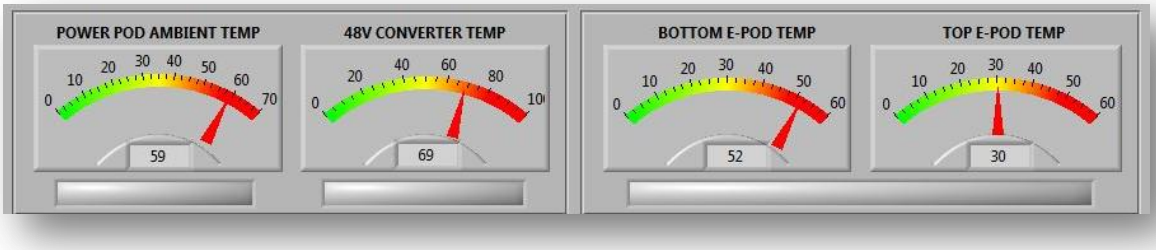

Figure 130: Dry test Power Pod and E-Pod temperature readings at one-quarter load just before the ambient temperature in the Power Pod reached its limit after 15 minutes

After the pods had cooled off, they were loaded with a total of 22.6 A on the five 48 V lines and a total of 8.6 A on the 15 V lines. The environment ambient temperature was still 19 °C. Figure 131 below shows that the 48 V DC-DC converter and the ambient temperature in the Power Pod reached their upper limits almost together after 15 minutes.

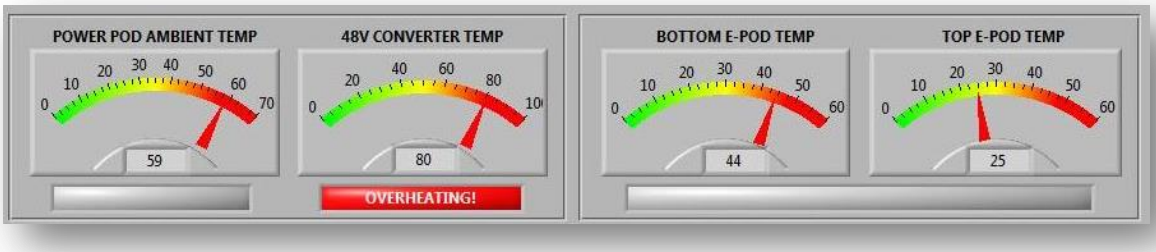

Figure 131: Dry test Power Pod and E-Pod temperature readings just as the 48 V DC-DC converter overheated at 13m42s

8.5.1.5.2 Wet Tests

Both pods were submerged in the tub of water and the power switched on and run with no load to start with. As the temperature stabilised, an initial load of 2.3 A combined on the 15 V lines and 4.3 A combined on the 48 V lines was connected. The set of results from the ensuing load increments is presented in Table 35.

Table 35: Test results from initial attempt at wet full-load thermal test

Time [min]	Water Temp [°C]	15 V Current [A]	48 V Current [A]	P-Pod Ambient [°C]	P-Pod DC-DC [°C]	Bottom E-Pod [°C]	Top E-Pod [°C]
0	18.5	0	0	-	-	-	-
5	18.7	2.3	4.3	-	-	-	-
13	18.9	4.5	11.3	-	-	-	-
29	19.1	6.6	13.4	40	49	40	25
40	19.3	8.5	15.5	44	55	44	26
59	19.7	8.5	17.3	50	64	48	-
73	20.0	8.5	19.3	53	69	50	27
91	20.4	8.5	20.0	58	77	52	28
101	21.0	8.5	20.0	59	**80**	48	26

As seen in Table 40 above, the 48 V DC-DC converter reached its limit with a load of 20.0 A on the 48 V lines and 8.5 A on the 15 V lines. The ambient temperature in the Power Pod had also nearly reached its 60 °C limit at this point. The water temperature rose slightly during the test, but was not considered enough of a rise to significantly impact the heat transfer rate from the pods.

The pods were left to cool off for a while after this initial wet test. It was decided that the pods be tested again at half-load on the 48 V lines for an hour. The water temperature at the start of the test was 21.0 °C. After one hour with an 8.5 A load on the 15 V lines and 11.4 A on the 48 V lines, the temperatures measured in the two pods were still below their limits as seen in Figure 132 below.

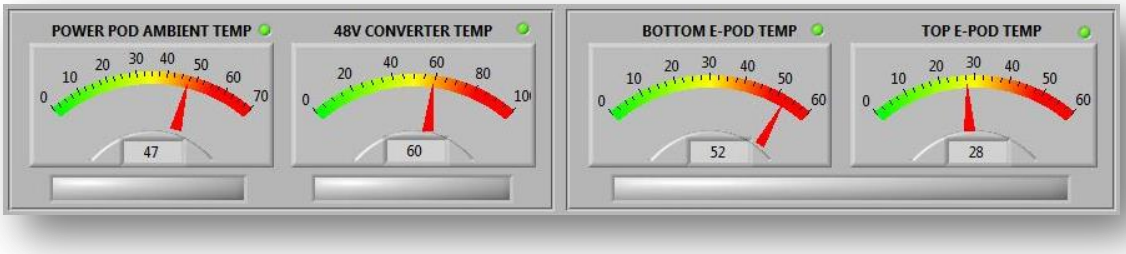

Figure 132: Wet test Power Pod and E-Pod temperature readings at steady state, half load after 60 minutes

In this test, with the reduced loads, it was found that the bottom E-Pod circuit board, through which all the load was being drawn, was the component closest to its maximum allowable temperature of 55 °C.

Based on the measured current drawn from each of the DC-DC converters in the Power Pod and their respective known inefficiencies [6][7], it was possible to calculate the rate at which the Power Pod was dissipating heat into the water by summing the estimated power losses in each converter. These values are shown in Table 36, and the total indicates that the Power Pod is capable of dissipating heat at a rate of at least 85 W when submerged in water 21 °C or colder.

Table 36: Values of system load currents and DC-DC converter power losses

DC-DC Converter	Voltage [V]	Load [A]	Efficiency [%]	Power Dissipated as Heat [W]
375/48 V (1)	48	5.7	88.5	31.5
375/48 V (2)	48	5.7	88.5	31.5
375/15 V	15	9.5	85.3	20.9
48/12 V	12	0.2	84.0	0.4
15/5 V	5	0.7	77.0	0.8
			Total	**85.1**

8.6 Power Supply Unit Tests

8.6.1 Input and output voltages over full load range

8.6.1.1 Purpose and Scope of the Test

The Power Supply Unit (PSU) provides electrical power at 400 VDC and communications over optical fibre to the ROV via the hybrid tether. The PSU needed to be tested to ensure that the rated load demanded by the ROV could be delivered to the ROV's Power Pod within the specified voltage range of 250-425 VDC.

The input and output voltages of the PSU were also measured so that the operating ranges for both could be specified for both 220 V and 230 V input connection options on the PSU's transformer. This would be important information for the operator because the mains supply to the PSU was likely to be provided by a generator on a small boat during operations and voltage levels were expected to vary from generator to generator.

8.6.1.2 Test Equipment

- ROV 400 V PSU connected to mains power supply
- Junction box
- 120m Hybrid tether
- Power Pod connected to PCU via junction box and tether
- E-Pod connected to Power Pod
- Fibre optic patch cord to connect E-Pod to PSU
- Variable resistor to provide 1.9-20 Ω with a minimum current rating of 25 A
- Variable resistor to provide 1.5-10 Ω with a minimum current rating of 8.5 A
- Terminal strip to connect E-Pod connectors to the variable resistors, complete with diodes wired in line with each connection as established in the preliminary thermal tests of Section 8.4.1
- F.W. Bell® CG100D clamp-on current meter
- Agilent® U1242B Multimeter
- Laptop connected via a network cable to the PSU and running the ROV user interface

- Agilent® DSO1004 60MHz Oscilloscope, complete with 3 probes
- Tektronix® P5200 High Voltage Differential Probe connected to the oscilloscope

8.6.1.3 Preparation or Calibration of Equipment

The Agilent oscilloscope would be used to measure the high voltage output of the PSU and because the output was ungrounded, it was necessary to use a high voltage differential probe in place of the usual scope probe used for ground-referenced signals. The probe also isolated the oscilloscope from the high voltage signals which provided essential protection of the equipment.

The differential probe was set to produce a ratio of 50 V per division on the oscilloscope's screen when the oscilloscope was set to 1 V per division. In other words, a 400 V potential difference between the probes would result in an 8.0 V reading on the oscilloscope.

8.6.1.4 Test Procedure

The same setup as that used for the Final Thermal test of Section 8.5 was used for these tests of the PSU.

The variable resistors were adjusted so that a current of 22.5 A was drawn on the 48 V lines from the E-pod and 8.5 A on the 15 V lines. These loads simulated the rated load to be drawn by the ROV thrusters and lights.

To characterise the performance of the PSU, measurements of the input and output voltages and currents were required, both at no load and at full load. Measurements of the output power were required at both ends of the tether so that the voltage drop across it could be calculated.

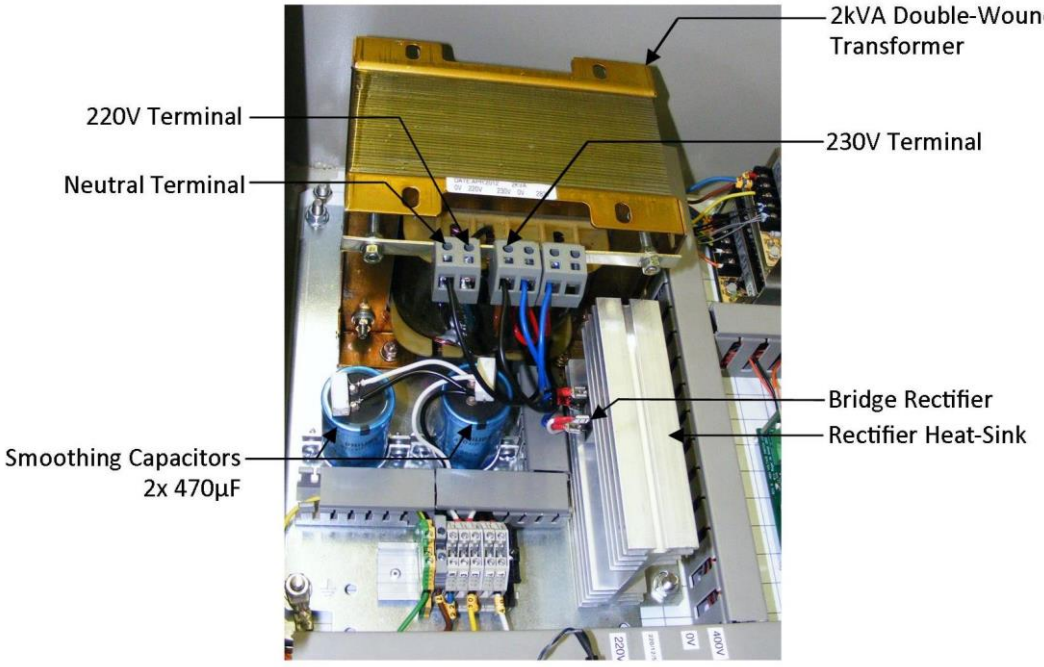

Figure 133: Photo of PSU 2kVA transformer

Because the input and output voltages of the power supply were directly proportional at zero load, the test results were easily extrapolated over the allowable input range for the Vicor Maxi DC-DC converters in the Power Pod. This set of calculations was tabulated to provide the operator with the allowable input range for the PSU for both input terminal options (see Figure 133).

8.6.1.5 Test Results and Analysis

The PSU voltages and currents were measured with no load on the system and at full-load, for both transformer input options. A screen capture of the oscilloscope reading of the input voltage to the Power Pod at full-load can be seen below in Figure 134 and the rest of the measurements are presented in Table 37 below.

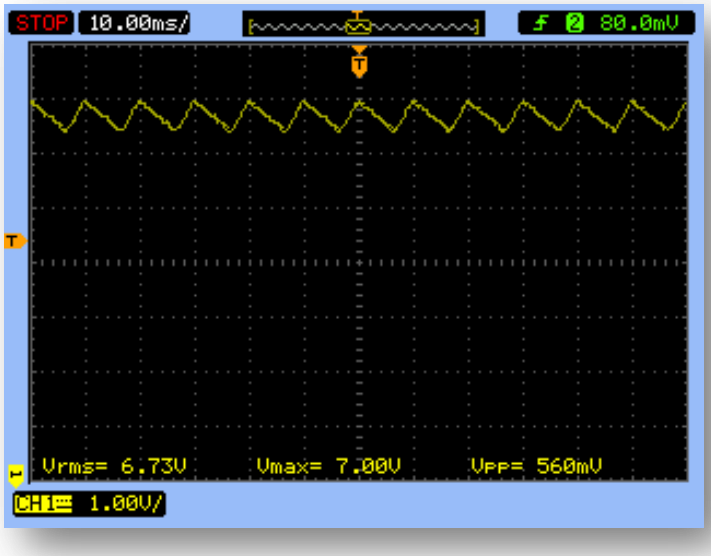

Figure 134: Oscilloscope measurement of the Power Pod input voltage using a 50:1 differential probe

Table 37: Input and output voltage readings of PSU and tether

Mains			PSU Output		ROV Input		Tether	
V_{Mains} [VAC]	I_{Mains} [A]	Xfmr	V_{rms} [V]	V_{ripple} [V]	V_{rms} [V]	V_{ripple} [V]	I_{Tether} [A]	ΔV_{Tether} [V]
221.5	0.6	220/N	386.0	0	383.5	4.0	0.3	2.5
219.2	6.2	220/N	358.5	26	348.5	26.0	4.1	10.0
221.2	0.5	230/N	367.5	0	366.5	4.0	0.3	1.0
218.1	6.2	230/N	340.5	26	331.5	28.0	4.2	9.0

Once the measurements in Table 37 had been obtained it was possible to calculate the limits of mains input voltage based on the allowable range of input DC voltage to the Power Pod DC-DC converters and a maximum rated current of 5 A in the tether.

Using Eq. 1 below [11] and it can be seen that the ripple voltage, V_{ripple}, is directly proportional to the current, I.

Eq. 1…

$$V_{ripple} \approx \frac{I.T}{C}$$

where I = current, T = ripple period, C = capacitance

The capacitance of the supply to the ROV, including the smoothing capacitors of the 400 VDC supply, the tether and the bypass capacitors on the ROV, was measured at 1040 µF. At a load of 4.1 A and a ripple frequency of 100 Hz, this would result in a ripple voltage of approximately 39 V using the equation above. The measured value of 26 V for the ripple voltage at 4.1 A attributed to additional internal capacitance of the DC to DC converters on board the ROV that came into effect when powered up.

The measured ripple voltage of 26 V was extrapolated to **31 V** at the rated current of **5.0 A**.

Eq. 2 below describes the relationship between the input voltage to the PSU and its peak output voltage.

Eq. 2…

$$V_{out_{peak}} = \sqrt{2}.V_{in_{rms}}.\frac{n_{secondary}}{n_{primary}} - 2(0.7)$$

where V_{out} = output voltage, V_{in} = input voltage, n = no. turns of transformer

Because the relationship is again linear, the measurements in Table 37 could be extrapolated to determine the maximum and minimum input voltages for the PSU, as presented in Table 38 below.

Table 38: Input voltage limits for PSU

	PSU Output [VDC]	Tether Current [A]	Ripple Voltage [V]	Power Pod Input [VDC]	V_{in} 220 V Terminal [VAC_{rms}]	V_{in} 230 V Terminal [VAC_{rms}]
Min. Voltage	281	5.0	31	250	**152**	**158**
Max.Voltage	425	0.0	0	425	**230**	**239**

8.7 JUNCTION BOX TESTS

8.7.1 Relative Oil Pressure

8.7.1.1 Purpose and Scope of the Test

The tether junction box on the ROV was designed to be filled with oil and pressurised in such a way that the internal pressure would always be greater than the ambient external pressure. This would ensure that, should it start to leak during service, the oil would leak out rather than water leak in. The relative internal pressure was to fall within a range of 0.7-1.0 bar, as per specifications laid out in Section 0.

The oil-compensated junction box was designed to operate with 4 springs that were 135 mm long, but these original-length springs were already slightly compressed before the oil was even added to the junction box. This made assembly more awkward and the springs were therefore shortened to 110 mm.

This set of tests was performed to determine whether the shortened springs would provide the required oil-pressure, and if not, how many more springs would need to be added.

8.7.1.2 Test Equipment

- Junction box
- Sasko Africa SI122 Scale, 2-300 kg
- Empty old ROV light module
- 23 mm thick wooden block
- Vernier calliper

8.7.1.3 Test Procedure

The junction box was opened and the end cap containing all cable glands was removed. The base board insert on which the terminal block was mounted was removed and re-inserted back-to-front. This would provide a solid surface to press up against from the open end of the junction box tube, as seen in Figure 135. The old ROV light pod was used only because it was a convenient size and shape, but any similar sized object could have been used. The light pod was stood on one end in the centre of the scale bed and then the junction box stood vertically on top of it as shown in Figure 135.

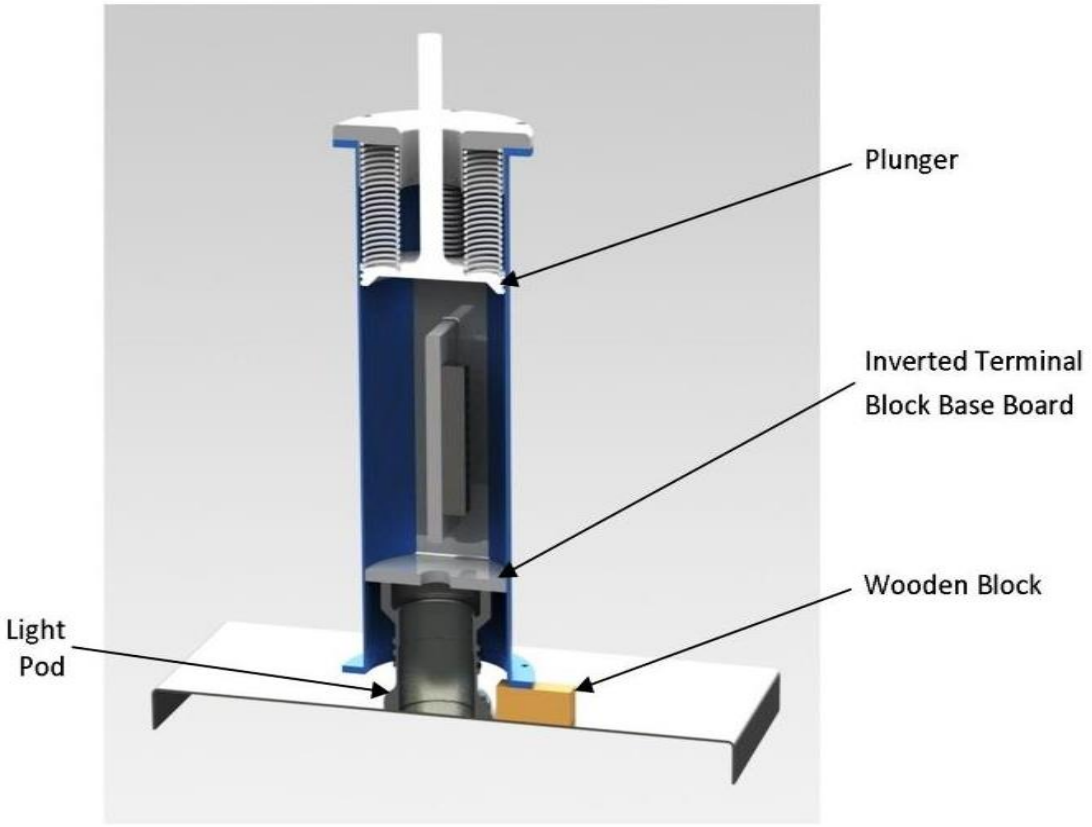

Figure 135: Rendered cross-section of part of the ROV Junction Box assembly showing the test setup for measuring its springs' properties

For the first set of tests, the junction box would be pushed down the 66 mm until it touched the scale. As it touched the scale, but before it loaded the scale directly, the scale mass measurement was recorded. The test was started with 6 springs in the junction box and repeated after removing 1 spring after each measurement until only 2 springs remained.

The second set of tests followed the same process as the first, except the displacement of the junction box was reduced. A 23 mm thick block was placed on the scale below the flange of the junction box tube, as seen in the figure above, and the mass measurement recorded just as the junction box touched the block.

The required oil pressure inside the junction box could be calculated using the surface area of its plunger and the combined compressive force of the springs behind it. Equation Eq. 3 and Eq. 4 below describe the relationship between the spring force $\boldsymbol{F}$, the plunger cross-sectional area A, and the resultant oil pressure $\boldsymbol{P}$.

Eq. 3… $$\boldsymbol{P = F.A}$$

Eq. 4… $$\boldsymbol{P = m.g.\pi.r^2}$$

where P = pressure, F = force, A = area, m = mass,
g = gravitational constant (9.81 m.s^{-2}) and r = radius

8.7.1.4 Test Results and Analysis

The five spring configurations were tested at both displacements. The graph in Figure 136 below shows the calculated oil pressure for the given plunger displacements with 2, 3, 4, 5 and 6 springs behind the plunger. 60 mm was the ideal displacement for the plunger because the springs were almost at their solid height at 66 mm displacement and had already started to buckle by this point too.

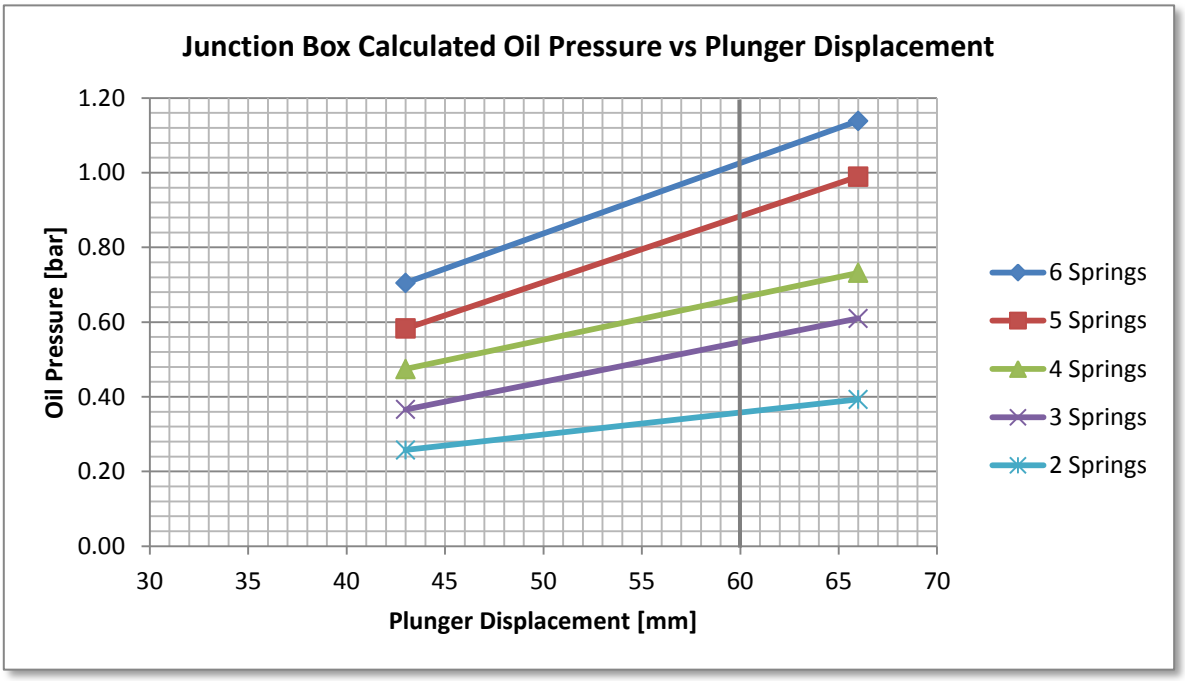

Figure 136: Graph of the calculated Junction Box relative oil pressure against plunger displacement for different quantities of springs used

8.8 SUMMARY

Each of ROV systems that were developed within the scope of this project were thoroughly tested to determine whether the design of each system met its specifications. Detailed results have been presented in this section with particular focus on the power and communications distribution system performance.

The following chapter takes the results of this chapter further by drawing conclusions on the design of the various ROV systems and providing recommendations for future additions and modifications.

9 CONCLUSIONS AND RECOMMENDATIONS

9.1 PRESSURE VESSELS

It was found that the three types of seals on each pod – the lid seals, the bulkhead electrical connector seals and the vent plug seals – all performed as intended and were effective at 150% of their rated pressures. The structural design of the vessels and lids also proved to be adequate at this depth.

The lack of water ingress into the chambers confirmed the assumption that the gradual decreases in pressure during the test were due to system leakages, most likely through the piston seals of the hydraulic pump.

Marine Solutions staff recommended that, for future tests, each module be weighed on a high-precision scale before and after pressure testing. By calculating the difference of the two values, it would be easier to determine whether water had leaked into the chamber than it would be to remove the lid. This method would be necessary when doing final pressure tests on modules that were fitted with all their respective electronics and hardware because the modules should not be re-opened before operating underwater. However, during these early tests there is nothing quite like seeing with one's own eyes to put one's mind at ease.

9.2 COMMUNICATIONS

9.2.1 Fibre Optics

The bandwidth of the temporary fibre link for the ROV was measured at 11.6 Megabytes per second or 93.0 Megabits per second. This rate was well in excess of the 30 Mbps specified in Section 3.1.

It was expected that the 350 m long optical fibres that would be used in the tether for the final would not decrease the bandwidth much further than the bandwidth measured through the 2 m patch cord, but it is recommended that further tests be performed on the full-length tether once it complete and installed to determine the final bandwidth available through the fibre link.

9.2.2 Serial Network

The measurements taken of the serial communication signals showed that the period of one cycle of communication with all 16 modules on the ROV would take approximately 320 ms. This was well within the specified 0.5 s response time (see Table 8 in Section 3.1).

The controller on the bottom PCB of the E-Pod was the only controller that received its commands split over two packets of data. This meant that the minimum response time for all functions of this controller would be 640 ms, twice that of the rest of the network. Because the E-Pod's control

functions were only to switch power to each module and would not affect the manoeuvring, video feedback or lighting control response of the ROV, it was deemed acceptable to have a marginal delay that was only 140 ms longer than the desired specification.

The introduction of an XOR checksum into the packets of data would improve the reliability of the transmitted data and then the bit error rate could also be determined as a measure of performance. The implementation of a checksum in the data packets is recommended for future implementation.

The simplified version of the Labview® UI was found to halve the communication cycle period. While the simpler user interface would not be useful for controlling the whole ROV, it did show that there may well be further optimisations possible in the standard ROV UI that would result in faster communication cycles.

The user interface was connected to the RS-485 network via a virtual serial port (VSP) that limited the baud rate to a maximum of 115 200. The VSP was also suspected as a source of some of the delays between sending and receiving packets of data. It is therefore recommended that the Tibbo® 1102 Ethernet-to-serial convert for the RS-485 network be programmed to convert directly from Ethernet to RS-485 so that the baud rate can be increased and suspected delays on the VSP avoided.

9.3 THERMAL TESTS

9.3.1 Preliminary E-Pod Thermal Tests

The most important results of these preliminary thermal tests of the E-Pod control circuit boards were that the copper tracks of each channel on the PCB had capacity to carry the specified currents without overheating. This meant that the 2 mm wide copper tracks in 55 µm thick copper were sufficient for the maximum current of 4.5A that could be drawn by each thruster.

The switching components of each channel, namely the MOSFETs, heated up to temperatures not much below 60 degrees at 4.5 A. During these tests the ambient conditions were a lot cooler and the natural convective cooling more effective than that which was expected inside the sealed E-Pod.

It was determined to be safe to calibrate the current sensors on the E-Pod Control PCBs without any danger of overheating components, provided currents were kept within their specified values. However, there was concern that the combined heating effect of all the power MOSFETs, when all channels were being used at their maximum capacity, would cause the PCB temperatures to rise above 60 °C – the maximum ratings of the lowest rated components on the board.

It was decided to incorporate some small fans in the E-Pod to help cool these PCBs before load-testing the E-Pod as a sealed unit.

9.3.2 Preliminary Power Pod Thermal Tests

9.3.2.1 Temperature Rise in 15 V Supply Circuit

The tests on the 15 V power supply showed that a load of 25 A could be drawn through the 7 mm wide copper tracks serving the 15 V output pins of the PCB without rising more than 30 °C above ambient. This meant that both 48 V power supply circuit boards, which use the identical PCB to this 15 V circuit, could operate comfortably at their rated loads of 12.5 A.

Although the ROV control and lighting system was not designed to have drawn more 40% of the converter's available power at the time this report was written, it had been determined in these tests that a further 15 A capacity was available from the 375/15 V DC-DC converter.

The 375/15 V DC-DC converter operated at full load without exceeding its maximum operating temperature of 100 °C. This result was establish in open air at an ambient temperature just below 20°C, which was cool compared to that expected inside the sealed Power Pod during operation of the ROV. Further testing of the 375/15 V DC-DC converter in the sealed and fully operational Power Pod, where it would be subjected to increased ambient temperatures, would have been required to establish a full set of operational limits for the circuit.

9.3.2.2 Temperature Rise in 375/48 V DC-DC Converter

It was seen in Figure 124 that when the temperature limit of 100 °C was reached on the labelled surface of the 375/48 V DC-DC converter, the temperature at its edges did not appear to rise above 85 °C. This was estimated using the temperature scale in the image and would provide a useful limit for a temperature sensor placed in a convenient position against the edge of the converter.

The 375/48 V DC-DC converters were identified as being the limiting components in the Power Pod in terms of thermal performance. In this set of preliminary tests, the converter was found to overheat when cooling of its labelled surface was poor, despite having been tested in an environment with a relatively low ambient temperature.

When assembled and sealed inside the Power Pod, the 375/48 V DC-DC converters would have had their labelled surfaces facing upward and heat sinks facing downward, as seen in Figure 137. This would allow better cooling of the converter and it would have the cooling fans of the circuit board above to force some air over it, further improving its cooling rate. However, the ambient temperature inside the Power Pod when sealed and the radiated heat from the adjacent DC-DC converters were expected to have more of an effect on the performance of the converter than the cooling fans.

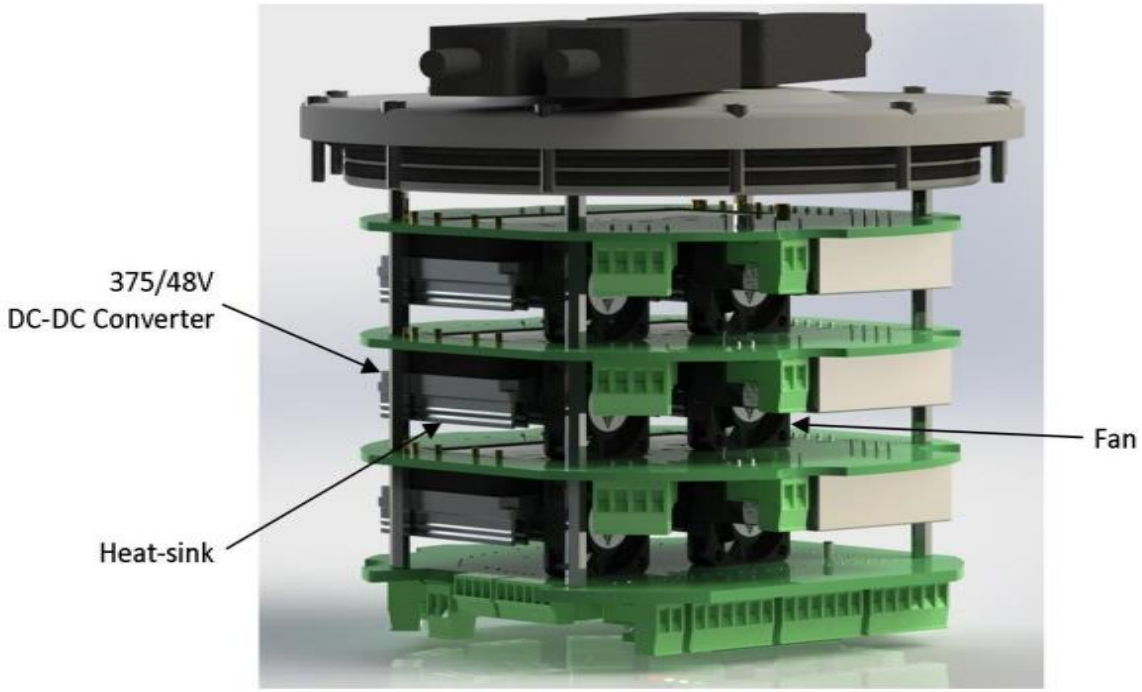

Figure 137: Rendering of the stack of power supply PCBs inside the Power Pod

The thermal characteristics of the 375/48 V DC-DC converter that were needed to identify where to place a temperature sensor, and what its limiting reading should be, had been captured. Further tests were now needed to establish the operational limits of the converter when assembled and sealed in the Power Pod.

9.3.2.3 Temperature Rise in 5 V Supply Circuit

The full load test on the 15/5 V DC-DC converter caused the copper track between its current sensor and the 5 V output connector to heat up. The copper track was found to be under-designed. The correct track width of 2 mm had been stopped short at the current sensor input and not carried through to the output connector. Figure 138 shows the existing problem on the left and the corrected design on the right for future manufacture. A wire bridge was inserted in parallel with the narrow track to solve the issue on the existing PCB.

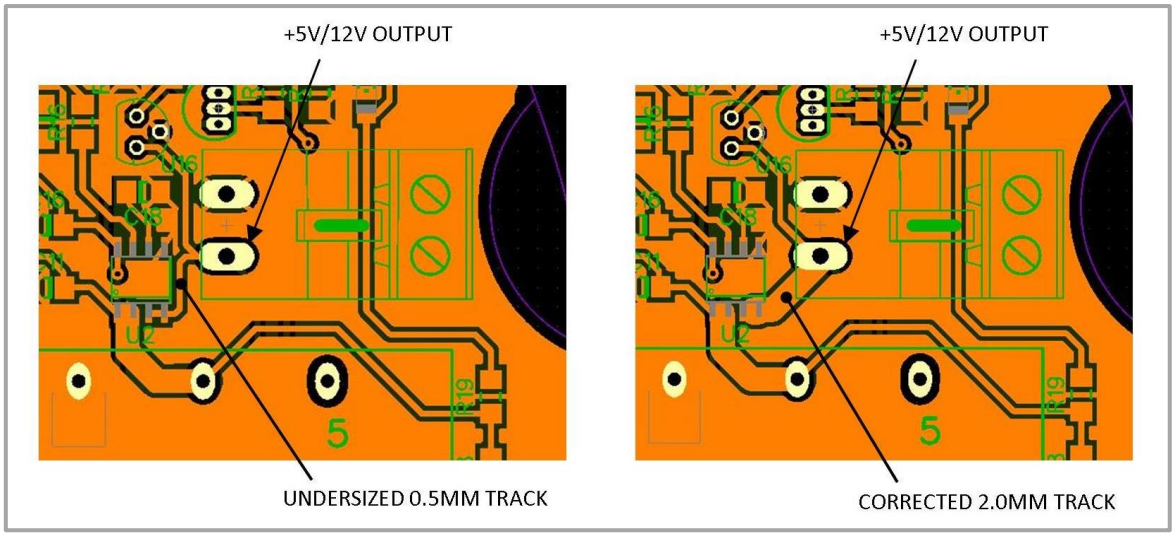

Figure 138: Diagram of recommended correction to power supply PCB 5 V/12 V output

While this track did warm up, the temperature rise was still less than 30 °C above ambient after 32 minutes at full load and was considered fit for use until the PCB could be upgraded and replaced.

9.3.3 Final Thermal Tests

The thermal tests performed on the sealed Power Pod and E-Pod showed that the ROV would be capable of general tasks that would not require full-throttle operation of the thrusters for prolonged periods. The rate at which the pods could dissipate heat would limit the performance of the ROV unless some modifications were made to the system.

The time taken to overheat when the pods were out of the water was very similar whether fully loaded on the 48 V lines or only loaded at one quarter of the rated current. It seemed that this period of 13-15 minutes was the time it took for the pods to absorb the heat from the internal components, but due to poor heat transfer in still air, the heat could not be dissipated. However, the ROV thrusters, which would be the primary electrical load on the Power Pod, would only be spun in air at no load so current draw on from the Power Pod was not expected to be great out of the water anyway.

Under water the pods dissipated significantly more heat, as expected. It was estimated that the Power Pod could dissipate heat at a rate of 85W into the still, 21 °C water. The E-Pod calculation would have been a great deal more complex, but because the pods were so similar in design, it was assumed that the E-Pod would dissipate heat at a rate within 10% of the Power Pod's result.

The ability of the pods to sink heat into the water was, however, not sufficient to run the system at full load continuously. In the final wet test, it was determined that if the 48 V lines were reduced to half their rated load, while the 15 V lines remained at 8.5 A (simulating full-power lighting), the pods would not overheat in the 21 °C water.

During actual operation, the water temperatures around Cape Town, South Africa, where the ROV would most likely be deployed, would generally provide greater cooling because water temperatures range from 14 °C to 19 °C. The ROV would be moving through the water which would also increase the heat transfer rate from the pods, compared to the stationary tests. These environmental factors, even if they were ideal, were still not expected to provide the full rate of heat dissipation required for the Power Pod. Using a similar set of values to those found in Table 36, but instead calculating for a full load of 11.25 A on each of the 375/48 V converters, it can be calculated that an approximate heat transfer rate of 170W would be required from the Power Pod. This would require a modification to the existing system.

Once all of the ROV modules are fully operational, further testing should be performed on the temperature control system to quantify the overshoot and correct for it.

Two concepts were provided for future modification of the Power Pod. The first concept was to add insulating transformer oil to the Power Pod before sealing it. The thermal conductivity of air at 60 °C and atmospheric pressure is approximately 0.03 $W.m^{-1}.K^{-1}$ compared to 0.11 $W.m^{-1}.K^{-1}$ for transformer oil [57][58]. This would be expected to increase the rate of heat conduction, between the DC-DC converters and the inner walls of the pod, quite significantly. However, the use of oil would be extremely messy and inconvenient to work with so it was left as an option for future use only if really necessary. The second concept involved deepening the Power Pod by 30 mm to make room for a large heat sink to be incorporated inside the pod. The heat sink would be fixed to the bottom of the pod with an extra four fans fitted to force air through its fins. The redesigned housing had been put into production at the time of writing, and a rendering of this concept can be seen in Figure 139.

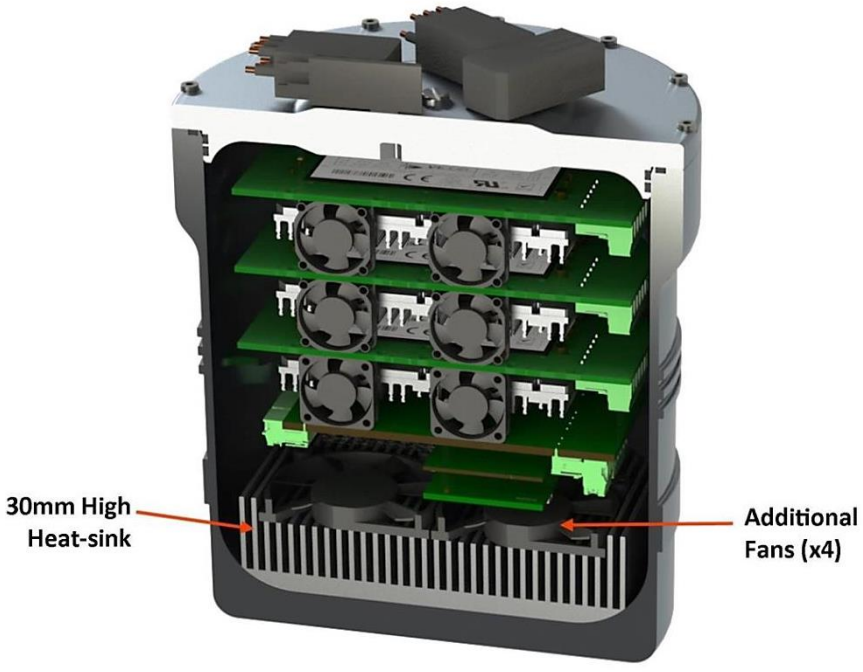

Figure 139: Rendered cross-section of a concept to integrate a heat sink into the Power Pod

9.4 SURFACE POWER SUPPLY

The PSU input and output voltages and currents were tested and found to provide adequate power to the ROV's Power Pod. The PSU provided power at the upper end of the allowable input range for the Power Pod DC-DC converters so there was plenty of scope to lengthen the tether, thereby increasing the voltage drop across it.

The input voltage limits were calculated for the PSU and found to provide a large range below the nominal 230 VAC, but operators would need to be careful not to exceed the 239 VAC input upper limit.

The development of the complete surface control station was in itself worthy of its own separate project and the PSU designed for this project was merely to provide the basics to enable full testing of the ROV. A console that integrated the UI and PSU that was also water-resistant could become the scope of a future undergraduate project.

9.5 SUBSEA JUNCTION BOX

According to the calculations and data represented in Figure 136, 6 springs would provide the ideal pressure with 1.0 bar at 60 mm displacement and 0.7 bar at about 53 mm displacement.

The junction box provided the correct pressure and sealing for the insulating oil, but was found to be cumbersome on the ROV. The process to remove the junction box from the ROV and open or to re-seal it and mount it on the ROV was a timeous affair. As a result of these two factors, the following recommendations have been put forward for future modifications:

- Shorten the junction box chamber so that it does not take up so much space where it is mounted on the ROV
- Redesign the junction box brackets so that they operate as a hinged pair and can be released by unscrewing a wing-nut.
- Manufacture the end cap for the junction box that incorporates the gland holes and the terminal block base board from one piece of material, rather than two. This will reduce the number of parts in the assembly and keep the position of the cables fixed relative to their terminal connections when removed from the chamber.
- Use thicker flanges for the ends of the chamber and tap the screw holes so that the screws can be fastened directly into the chamber. This will reduce the time taken to open and close the junction box and will also reduce the number of tools required.

REFERENCES

[1] P. Henson, "Development of a Gripper/Sample Retrieval System for a Remote Underwater Inspection Robot," 2009.

[2] T. E. Knight, "ROBIN: A Remotely Operated Underwater Inspection Vehicle," 2010.

[3] VideoRay, "Pro 4 Standard BASE." [Online]. Available: http://www.videoray.com/homepage/professional-rovs/videoray-pro-4/standard-base/wfmenucpanel.html#6102-P4PACKAGING_web. [Accessed: 30-Oct-2013].

[4] FMC Technologies, "UHD™ ROV." [Online]. Available: http://www.fmctechnologies.com/en/SchillingRobotics/Technologies/Schilling-UHD-ROV.aspx. [Accessed: 30-Oct-2013].

[5] R. D. Christ and R. L. Wernli Sr, "The ROV Manual: A User Guide for Observation-Class Remotely Operated Vehicles," Oxford: Elsevier, 2008.

[6] JW Fishers, "JW Fishers Sea Lion-2 / Sea Otter-2." [Online]. Available: http://www.jwfishers.com/rov.htm. [Accessed: 30-Oct-2013].

[7] Seabotix, "SeaBotix Inc. - LBV150-4." [Online]. Available: http://www.seabotix.com/products/lbv150-4.htm. [Accessed: 30-Oct-2013].

[8] Teledyne Benthos, "Powerful, Rugged, Reliable," *Price List*, 2009.

[9] Outland Technology, "Outland Technology: Products - ROV Model 100." [Online]. Available: http://www.outlandtech.com/rov100.php. [Accessed: 30-Oct-2013].

[10] SAAB, "Seaeye - Falcon & Falcon DR." [Online]. Available: http://www.seaeye.com/falcon.html. [Accessed: 30-Oct-2013].

[11] Seatronics, "Predator ROV." [Online]. Available: http://www.predator-rov.com/system/. [Accessed: 30-Oct-2013].

[12] Seaview Systems, "Saab Seaeye Falcon DR | Seaview Systems Inc." [Online]. Available: http://www.seaviewsystems.com/toolbox/saab-seaeye-falcon-dr/.

[13] "Outland Technology: Products - Cables." [Online]. Available: http://www.outlandtech.com/cables.php.

[14] "UT2 The magazine of the Society for Underwater Technology," no. January, p. 18, 2007.

[15] VideoRay, "VideoRay University Research Kit." [Online]. Available: http://www.videoray.com/homepage/university-research-kit.html.

[16] "ROVInfo.com • View topic - 500m/2000ft pipe inspection help :)." [Online]. Available: http://www.rovinfo.com/viewtopic.php?p=836.

[17] "The RS-232 Standard." [Online]. Available: http://www.camiresearch.com/Data_Com_Basics/RS-232_standard.html.

[18] F. Durda, "Serial and UART Tutorial." [Online]. Available: http://www.freebsd.org/doc/en/articles/serial-uart/. [Accessed: 04-Nov-2013].

[19] Maxim, "Selecting and Using RS-232 , RS-422 , and RS-485 Serial Data Standards," *Appl. Note 723*, 2000.

[20] "Dataproducts Plus, Inc." [Online]. Available: http://www.dataproductsplus.com/RS-232-FAQ.asp.

[21] "Serial Communication Using RS-232." [Online]. Available: http://www.z80.info/1656.htm.

[22] Tibbo Technology, "DS1206N Evaluation Board," 2011.

[23] "RS-485 (EIA/TIA-485) Differential Data Transmission System Basics - Tutorial - Maxim." [Online]. Available: http://www.maximintegrated.com/app-notes/index.mvp/id/736.

[24] B&B Electronics, "RS-422 and RS-485 Application Note," no. June, 2006.

[25] B. Perrin, "The Art and Science of RS-485," *Circuit Cellar® Online*, vol. July, no. July, 1999.

[26] H. Marais, "RS-485/RS-422 Circuit Implementation Guide," *AN-960 Appl. Note*.

[27] R. I. Davis, A. Burns, R. J. Bril, and J. J. Lukkien, "Controller Area Network (CAN) schedulability analysis: Refuted, revisited and revised," *Real-Time Syst.*, vol. 35, no. 3, pp. 239–272, Jan. 2007.

[28] "IXXAT [Article Controller Area Network (CAN) Introduction]." [Online]. Available: http://www.ixxat.com/can-controller-area-network-introduction_en.html.

[29] Modbus.org, "MODBUS APPLICATION PROTOCOL SPECIFICATION V1.1b," 2006.

[30] T. Nakamura, "Using MODBUS for Process Control and Automation - White Paper," 2008.

[31] SABS, *SANS 10142-1 : 2009 SOUTH AFRICAN NATIONAL STANDARD The wiring of premises Part 1 : Low-voltage installations*. 2009, p. 55,99.

[32] Parker Hannifin O-ring Division, "Parker O-ring Handbook," 2003.

[33] ERIKS - Sealing Elements, "ERIKS - Sealing Elements - Technical Handbook O-rings -," pp. 7–8, 2010.

[34] Webtec, "Port & Pipe Connections in Hydraulic Circuits – Webtec Products Ltd." [Online]. Available: http://www.webtec.co.uk/tech/connections. [Accessed: 30-Oct-2013].

[35] "EPM Inc.," "The Seal Man ' s O-Ring Handbook ™," 2004.

[36] R. de Smidt, "ROV Training Site Visit," Cape Town, 2011.

[37] Douglas Westwood, “The World ROV Market Forecast 2011-2015.” [Online]. Available: http://www.douglas-westwood.com/shop/shop-infopage.php?longref=821~6#.UnDYF3oaKP8.

[38] G. Gereffi, L. C. Brun, J. Lee, M. Turnipseed, C. Cggc, M. Hensen, K. Fernandez-stark, S. Frederick, and J. Xu, “NOVA SCOTIA ’ S OCEAN TECHNOLOGIES,” pp. 61–87, 2012.

[39] “SERS GROUP Subsea Engineering & ROV Services.” [Online]. Available: http://www.sersgroup.net/#. [Accessed: 31-Oct-2013].

[40] “Marine Solutions.” [Online]. Available: http://marinesolutions.co.za/overview.shtml. [Accessed: 31-Oct-2013].

[41] “INFORMATION ON FISHERIES MANAGEMENT IN THE REPUBLIC OF SOUTH AFRICA.” [Online]. Available: http://www.fao.org/fi/oldsite/FCP/en/zaf/body.htm.

[42] T. E. Knight, “Development of the Thruster, Camera and Lighting Systems for an Underwater Remotely Operated Vehicle,” 2012.

[43] E. Mellinger, A. Pearce, and M. Chaffey, “Distributed Multiplexers for an ROV Control and Data System.” [Online]. Available: http://www.mbari.org/staff/meed/dcpaper/dcpaper.htm. [Accessed: 05-Nov-2013].

[44] Shanghai Nanya Copper Clad Laminate Co. Ltd, “Nouya NY2150,” 2010.

[45] “PCB Specs.” [Online]. Available: http://www.pcb-specification.com/uk.

[46] Vicor, “Design Guide & Applications Manual For Maxi, Mini, Micro Family DC-DC Converter and Accessory Modules,” 2013.

[47] “Vicor Module and Power Supply Design & Selection Tools.” [Online]. Available: http://asp.vicorpower.com/calculators/calculators.asp?calc=2. [Accessed: 03-Dec-2013].

[48] The Institute for Interconnecting and Packaging Electronic Circuits, “IPC-2221 Generic Standard on Printed Board Design,” no. September 1991, 1998.

[49] R. C. Juvinall and K. M. Marshek, *Fundamentals of Machine Component Design*, 3rd ed. John Wiley & Sons, Inc., 2000.

[50] D-Link, “DMC-300SC 100BASE-TX to 100BASE-FX Multimode SC Media Converter,” p. 92708, 2010.

[51] J. S. Ingleton, “Stride Unmanaged Industrial Ethernet Switches,” vol. 14, 2012.

[52] N. Codreanu, R. Bunea, and P. Svasta, “New Methods of Testing PCB Traces Capacity and Fusing,” Bucharest, 2011.

[53] Colorado State University, “High Voltage Safety Manual,” pp. 5–6, 2006.

[54] Vicor, “375 V Input Maxi Family DC-DC Converter Module Data Sheet,” 2011.

[55] Meanwell, “SDM30 Series Datasheet,” 2013.

[56] P. Horowitz and W. Hill, “The Art of Electronics,” 2nd ed., Cape Town: Cambridge University Press, 1989, p. 47.

[57] “Thermal Conductivity Common Liquids.” [Online]. Available: http://www.engineeringtoolbox.com/thermal-conductivity-liquids-d_1260.html.

[58] “Air Properties.” [Online]. Available: http://www.engineeringtoolbox.com/air-properties-d_156.html.

APPENDIX A: MECHANICAL DRAWINGS

CONTENTS

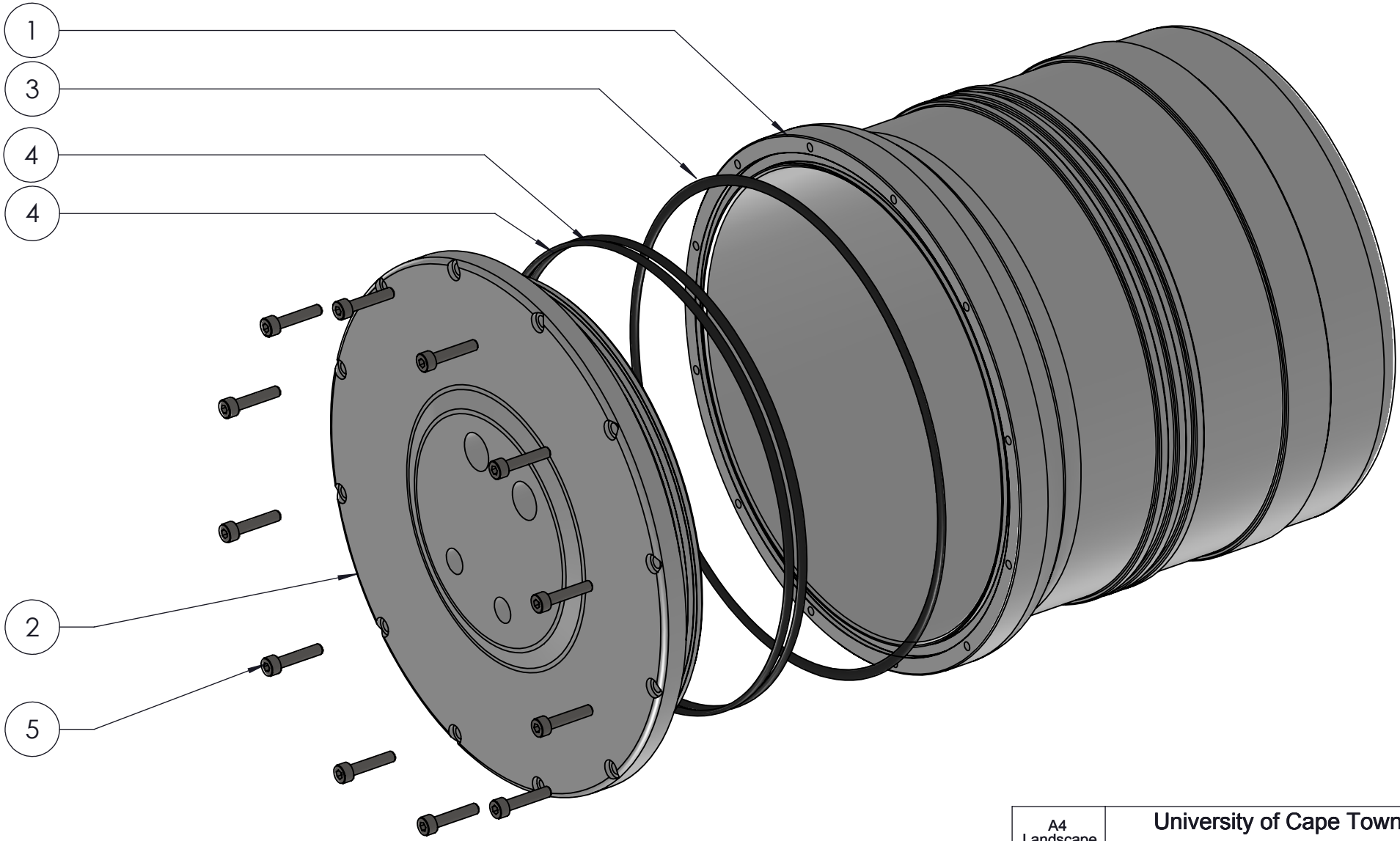

ITEM NO.	PART NUMBER	Power Pod/QTY.
1	IMU Housing	1
2	PPOD-09-End Plate	1
3	182x3 Neoprene O-Ring, Durometer 70	1
4	175x3 Neoprene O-Ring, Durometer 70	2
5	Hexagon socket head cap screw ISO 4762 - M4 x 20	12

A4 Landscape	University of Cape Town Department of Mechanical Engineering			
	Title: PPOD-10-Pod			
Assembly Drawing	Scale: 1:2	Date: 2011/11/04	Sheet1	of 3
	Drawn By: Roger de Smidt DSMROG001		Drawing Number PPOD-01-01-01	

POWER POD HOUSING

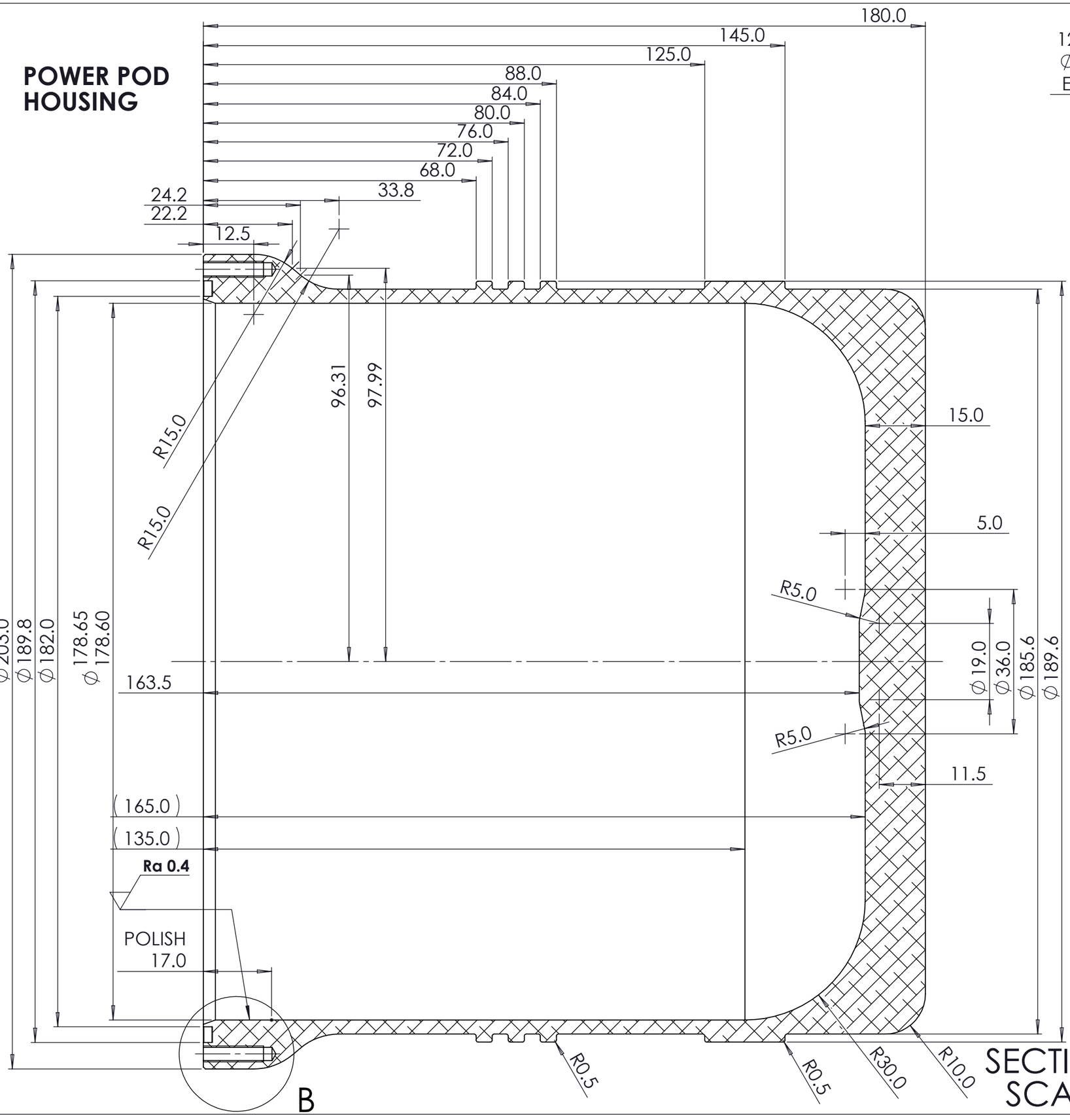

SECTION A-A
SCALE 1 : 1

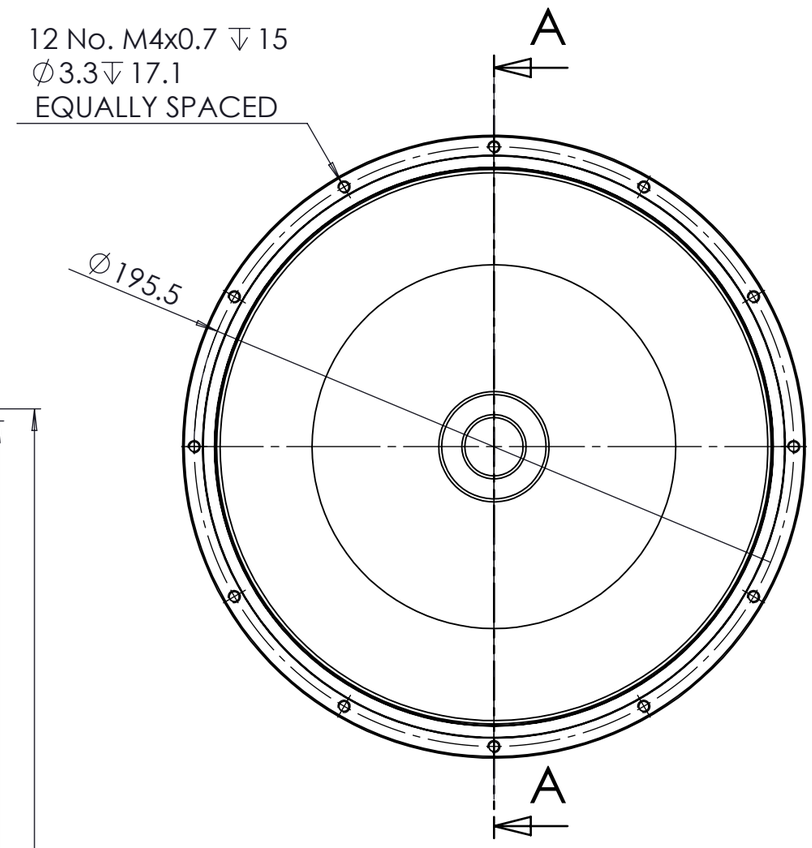

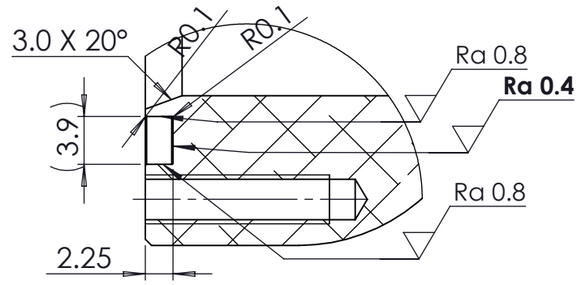

DETAIL B
SCALE 2 : 1

NOTES:
Ra 0.4: 320 GRIT/ P500 WATER PAPER
Ra 0.8: 180 GRIT/ P220 WATER PAPER

A3 Landscape	University of Cape Town Department of Mechanical Engineering				
	Title: PPOD-P01-Chamber				
Quantity: 1	Part Finish	Date: 2012/03/07	Scale: 1:2	Sheet1	of 1
Material: AL 6351 T6	Drawn By: Roger de Smidt DSMROG001			Drawing Number PPOD-00-01-02	

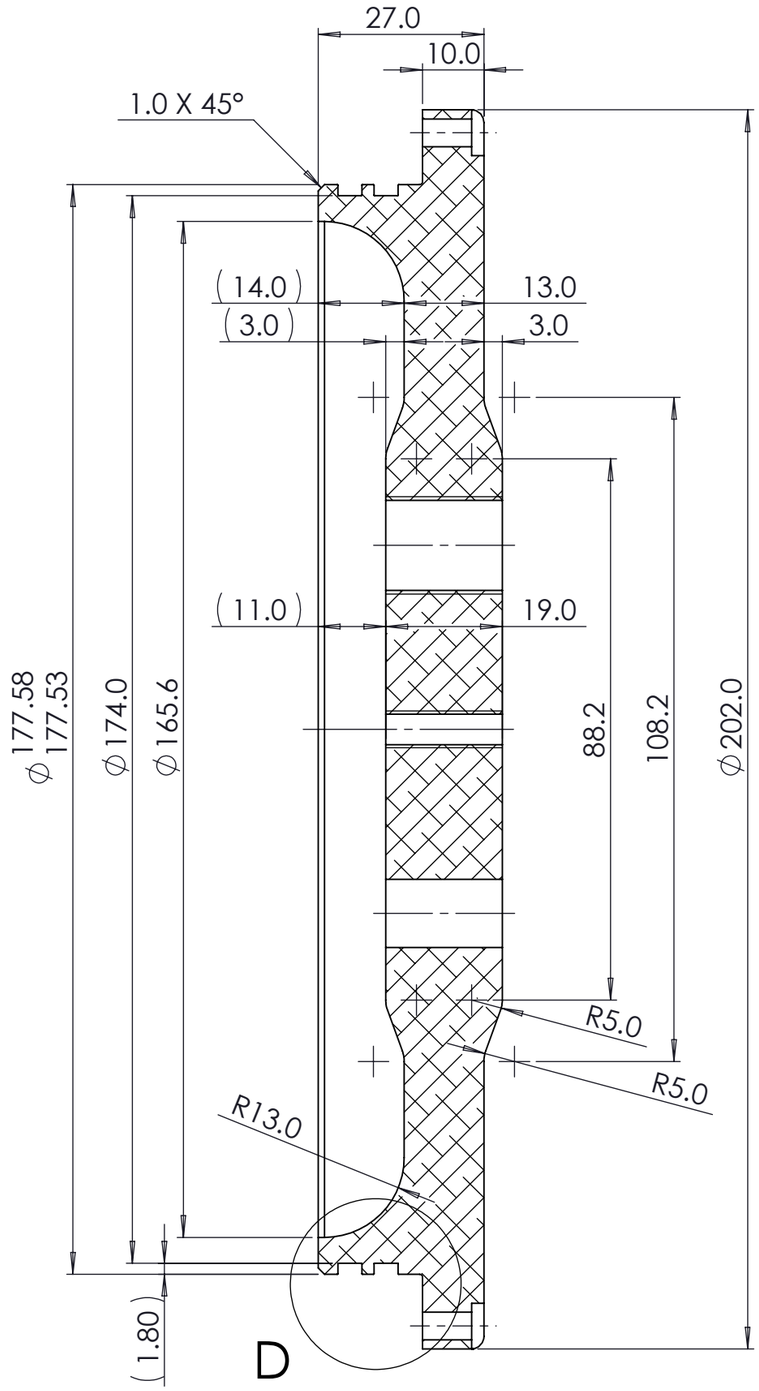

SECTION C-C
SCALE 1 : 1

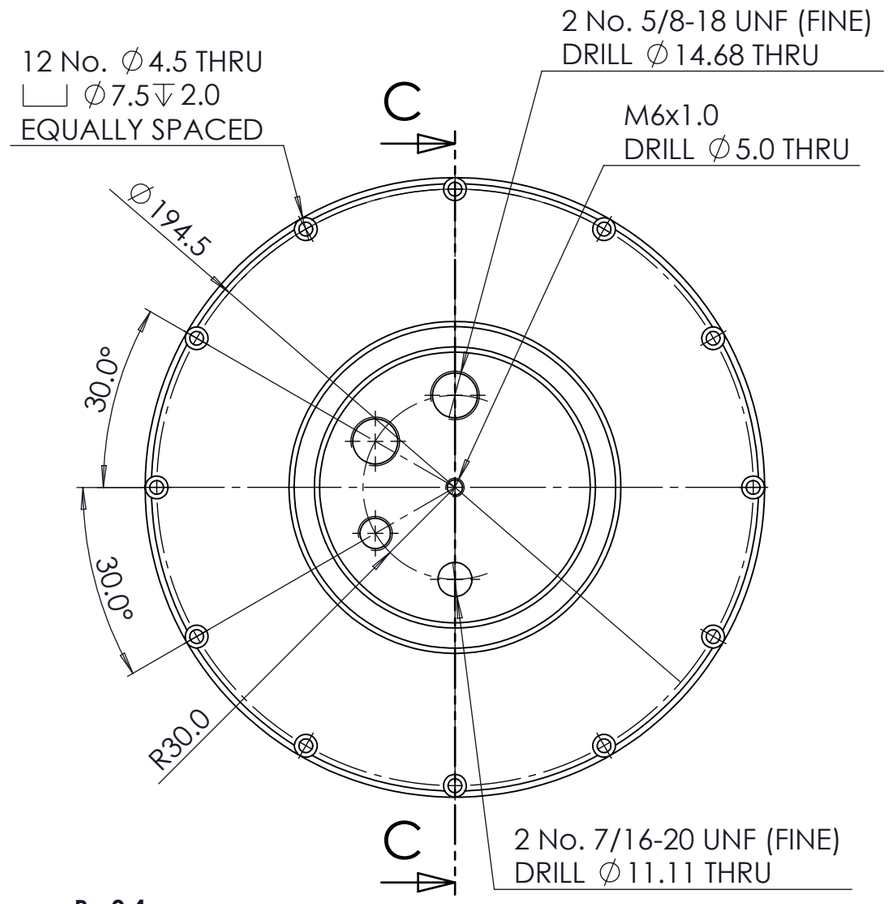

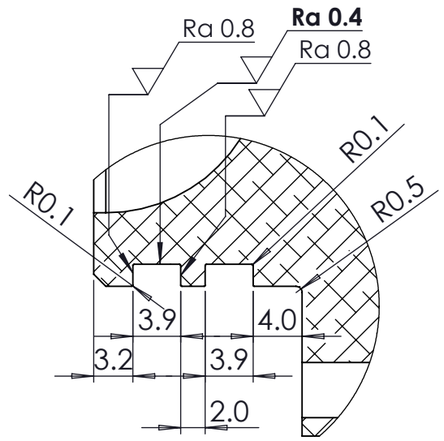

NOTE:
USE SAME SURFACE FINISH FOR
BOTH O-RING GROOVES

DETAIL D
SCALE 2 : 1

NOTES:
Ra 0.4: 320 GRIT/ P500 WATER PAPER
Ra 0.8: 180 GRIT/ P220 WATER PAPER

A3 Landscape	University of Cape Town Department of Mechanical Engineering				
	Title: PPOD-09-End Plate				
Quantity: 1	Part Finish	Date: 2011/10/27	Scale: 1:2	Sheet3	of 3
Material: AL 6082 T6	Drawn By: Roger de Smidt DSMROG001			Drawing Number PPOD-01-03-00	

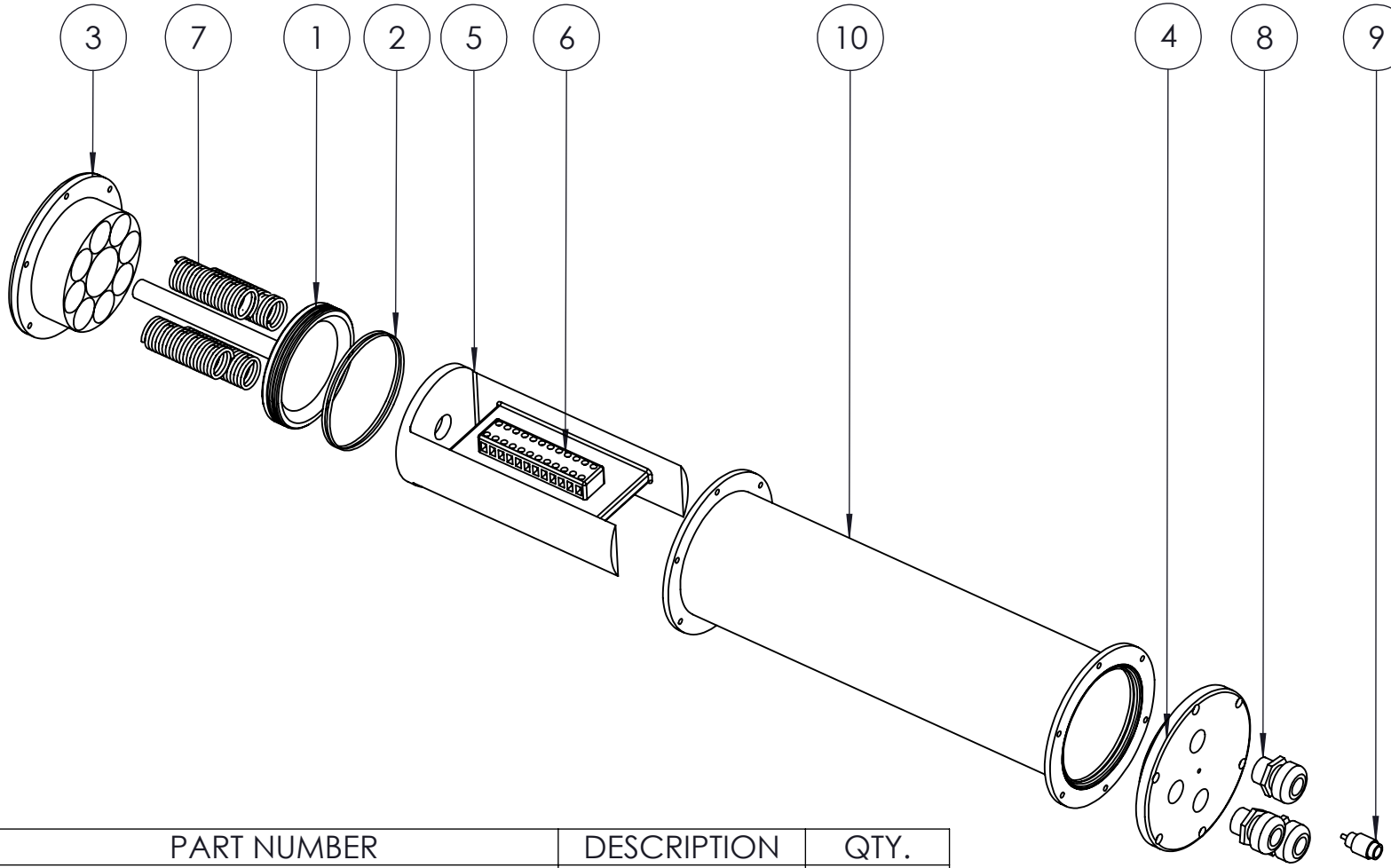

ITEM NO.	PART NUMBER	DESCRIPTION	QTY.
1	JBX-P02-Plunger		1
2	91x2 Viton		4
3	JBX-P03-Spring End Plate		1
4	JBX-P04-Housing End Plate		1
5	JBX-P06-Chocolate Block Board		1
6	JBX-P05-Chocolate Block		1
7	JBX-P07-Spring		4
8	GLND-P01-CCG M20		3
9	QCON-P01- 1-8th Quick Disconnect		1
10	JBX-A01-Housing Weldment		1

A4 Landscape	**University of Cape Town** Department of Mechanical Engineering			
	Title: JBX-A00-Oil Filled Junction Box			
Assembly Drawing	Scale: 1:5	Date: 2011/12/02	Sheet1	of 1
	Drawn By: Roger de Smidt DSMROG001		Drawing Number JBX-00-00-00	

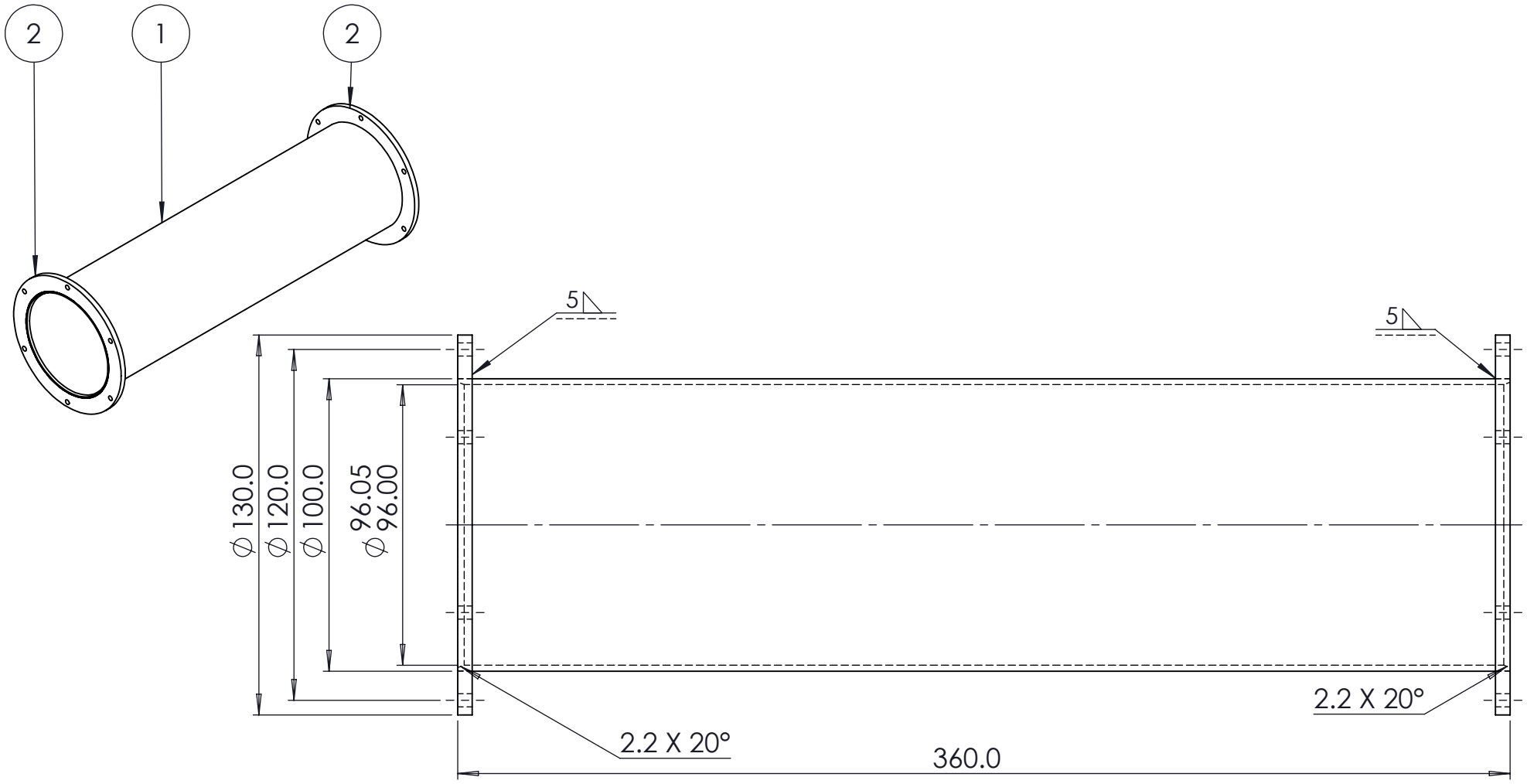

NOTE:
Aluminium Housing to be 5mm wall thickness before welding. Bore out Housing Assembly after welding.

ITEM NO.	PART NUMBER	DESCRIPTION	QTY.
1	JBX-P01-Housing		1
2	JBX-P08-Flange		2

A4 Landscape	University of Cape Town Department of Mechanical Engineering			
	Title: JBX-A01-Housing Weldment			
Assembly Drawing	Scale: 1:2	Date: 2012/03/07	Sheet1	of 1
	Drawn By: Roger de Smidt DSMROG001		Drawing Number JBX-01-00-01	

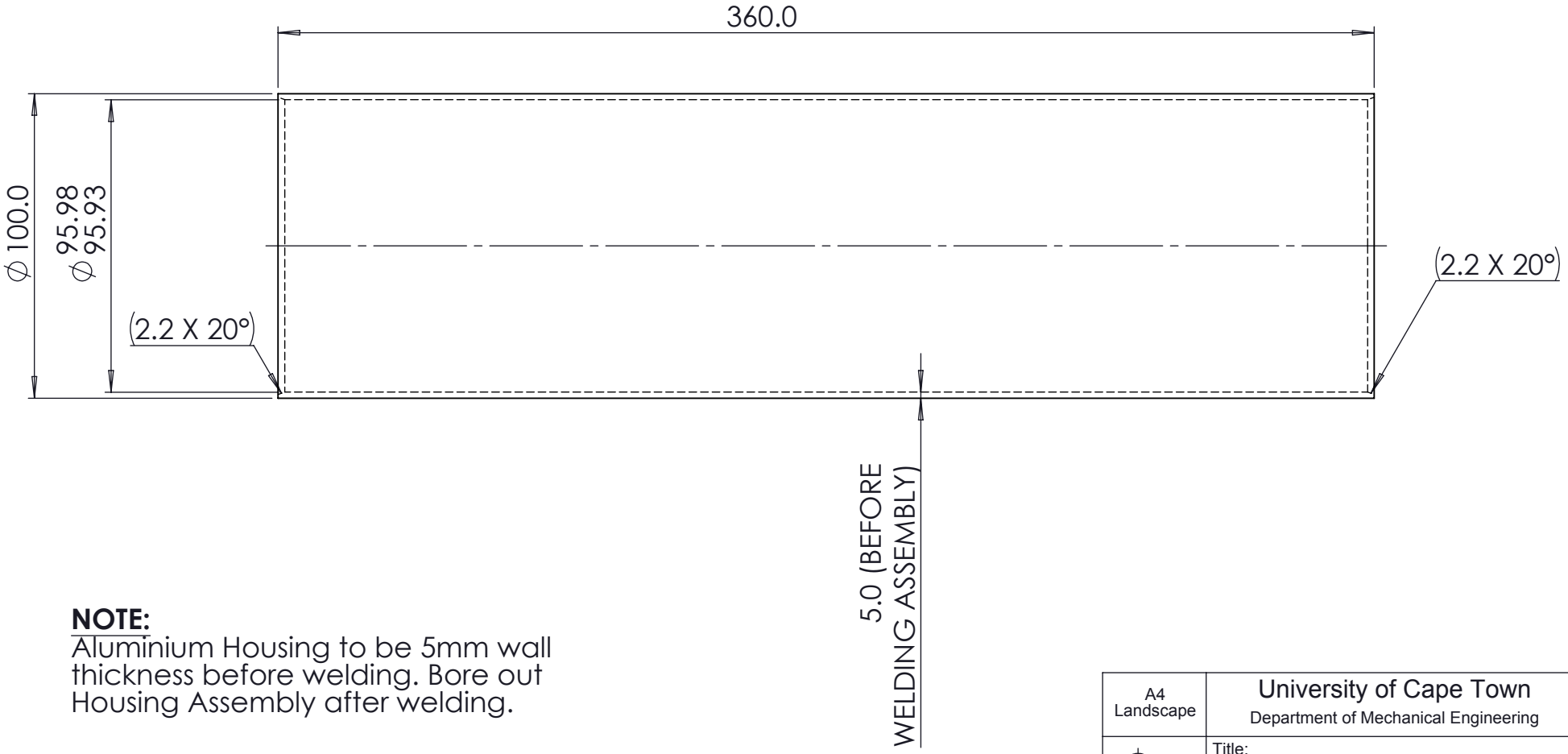

NOTE:
Aluminium Housing to be 5mm wall thickness before welding. Bore out Housing Assembly after welding.

SolidWorks Student Edition.
For Academic Use Only.

A4 Landscape	University of Cape Town Department of Mechanical Engineering				
	Title: JBX-P01-Housing				
Quantity: 1	Part Finish	Date: 2012/03/07	Scale: 1:2	Sheet1	of 1
Material: AL 6082 T6	Drawn By: Roger de Smidt DSMROG001			Drawing Number JBX-01-01-01	

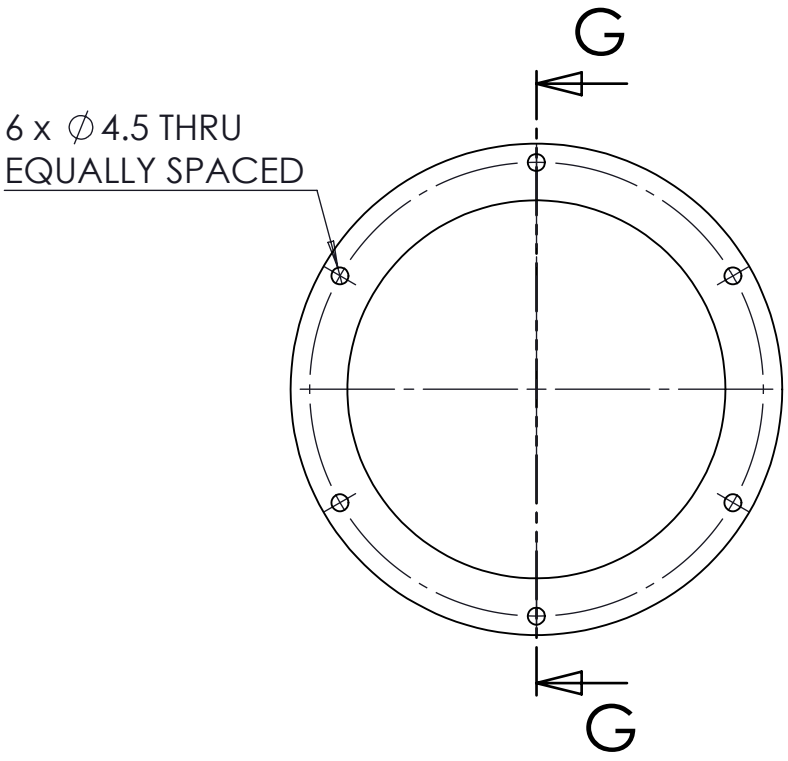

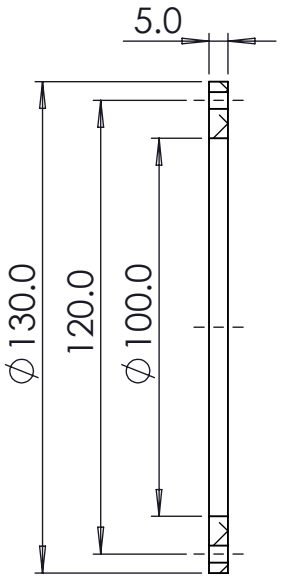

SECTION G-G

A4 Landscape	University of Cape Town Department of Mechanical Engineering				
	Title: JBX-P08-Flange				
Quantity: 2	Part Finish	Date: 2011/12/01	Scale: 1:2	Sheet1	of 1
Material: AL 6082 T6	Drawn By: Roger de Smidt DSMROG001			Drawing Number JBX-01-08-00	

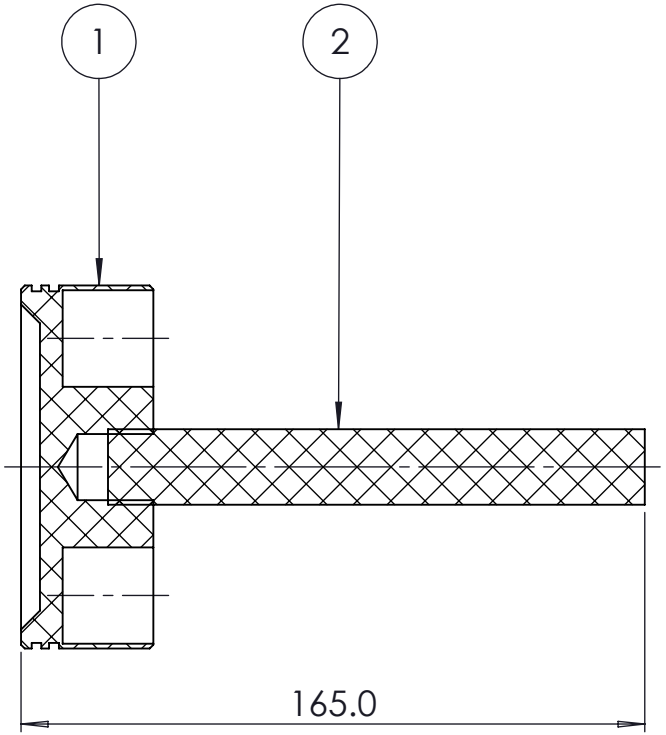

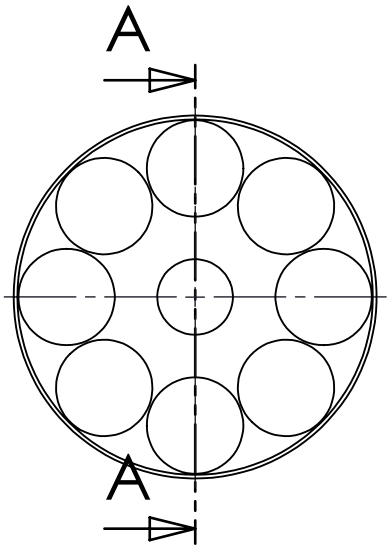

SECTION A-A
SCALE 1 : 2

ITEM NO.	PART NUMBER	DESCRIPTION	QTY.
1	JBX-P02-Plunger	Acetal (Black or White)	1
2	JBX-P10-Plunger Rod	Acetal (WHITE)	1

A4 Landscape	University of Cape Town Department of Mechanical Engineering			
	Title: JBX-A02-Plunger			
Assembly Drawing	Scale: 1:5	Date: 2012/03/14	Sheet1	of 1
	Drawn By: Roger de Smidt DSMROG001		Drawing Number JBX-02-00-00	

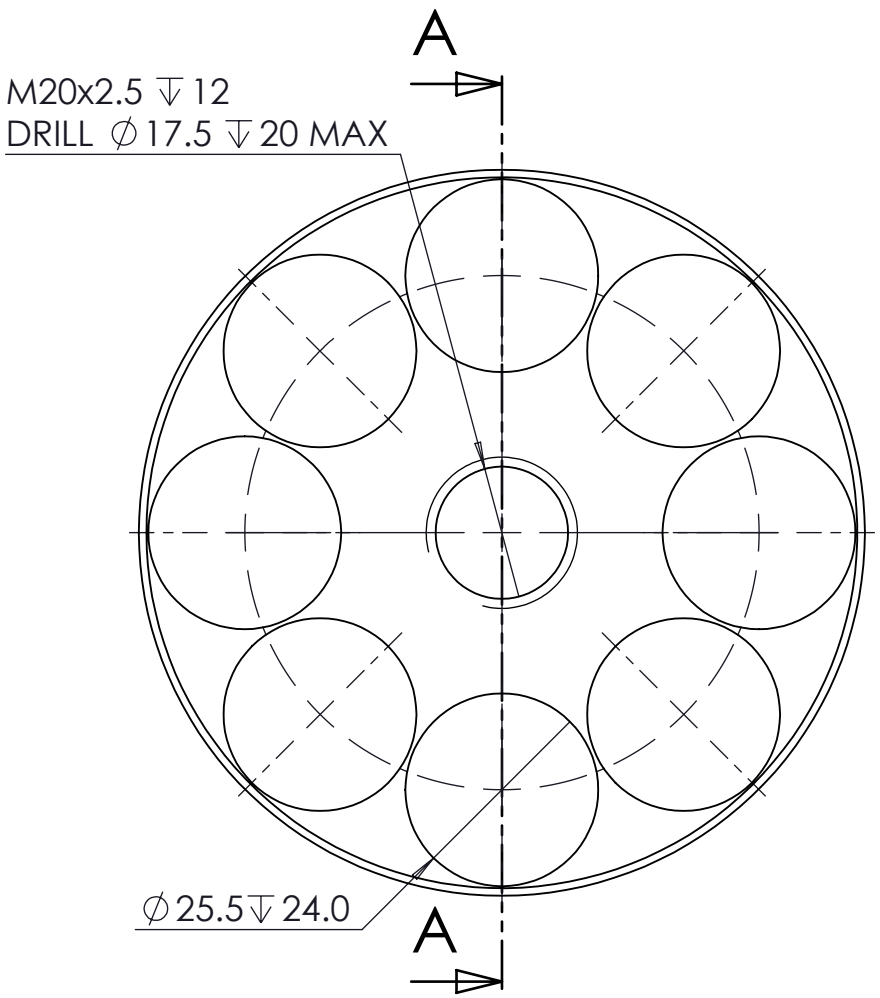

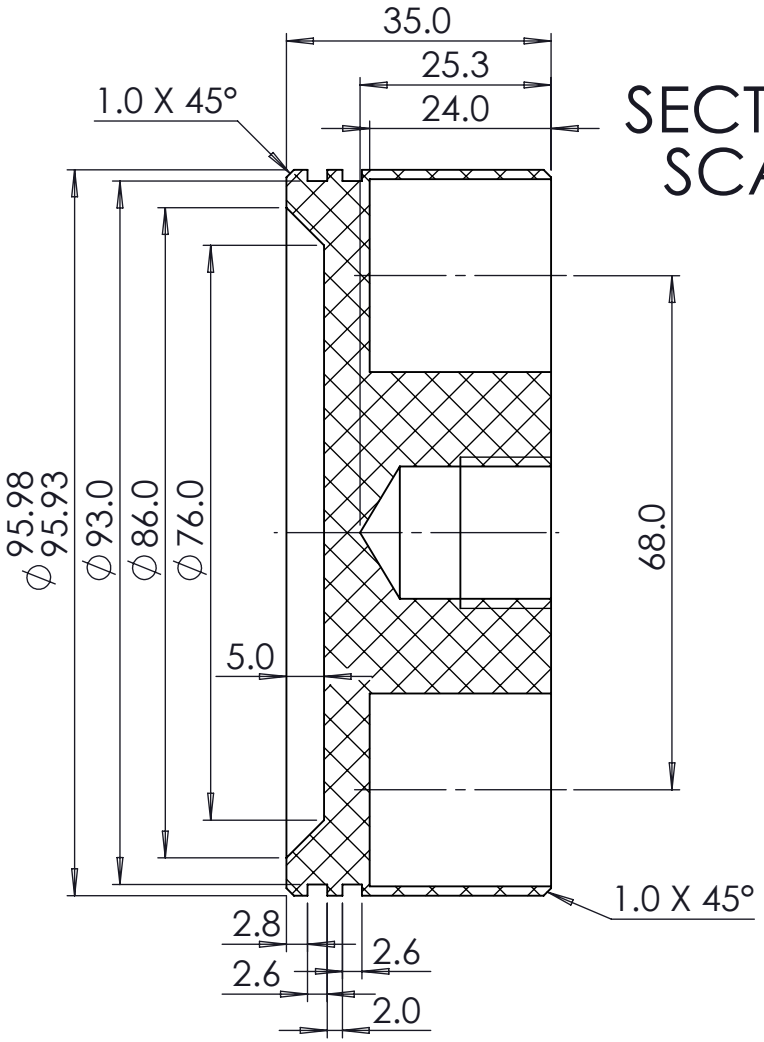

SECTION A-A
SCALE 1 : 1

SolidWorks Student Edition.
For Academic Use Only.

A4 Landscape	University of Cape Town Department of Mechanical Engineering				
	Title: JBX-P02-Plunger				
Quantity: 1	Part Finish	Date: 2012/03/14	Scale: 1:1	Sheet1	of 1
Material: POM Acetal Copolymer	Drawn By: Roger de Smidt RSMROG001			Drawing Number JBX-00-02-02	

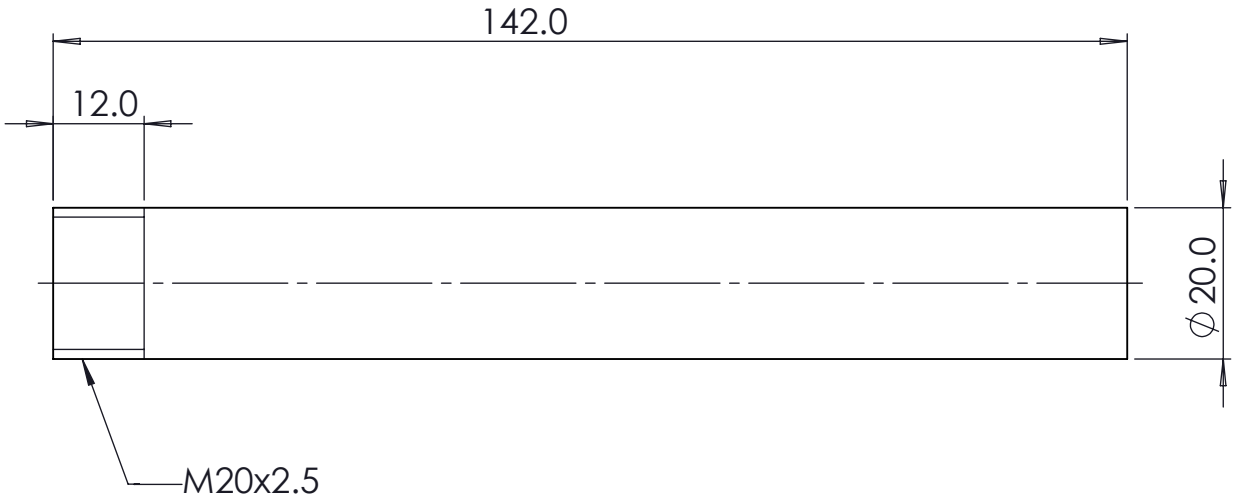

SolidWorks Student Edition.
For Academic Use Only.

A4 Landscape	University of Cape Town Department of Mechanical Engineering				
	Title: JBX-P10-Plunger Rod				
Quantity: 1	Part Finish	Date: 2012/03/14	Scale: 1:1	Sheet1	of 1
Material: POM Acetal Copolymer	Drawn By: Roger de Smidt DSMROG001			Drawing Number JBX-00-10-00	

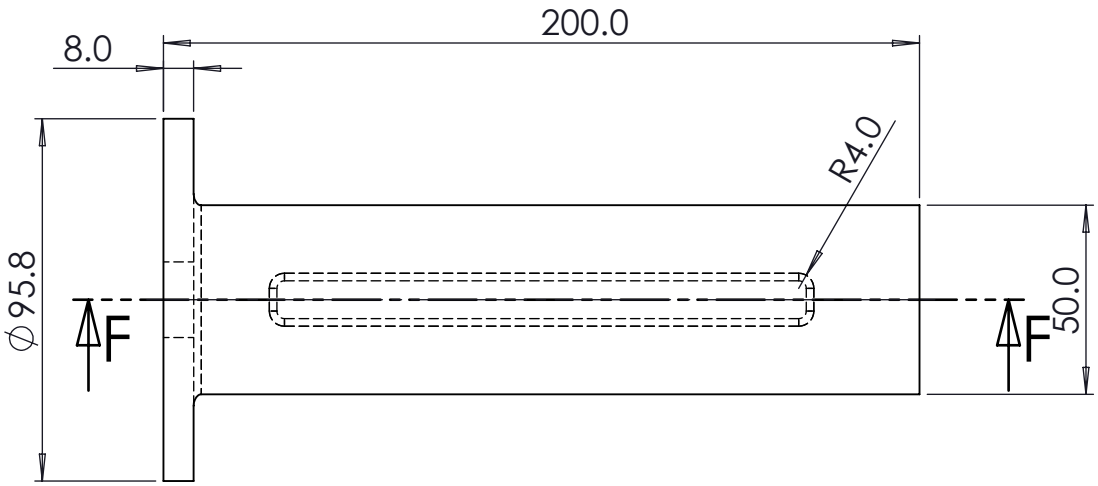

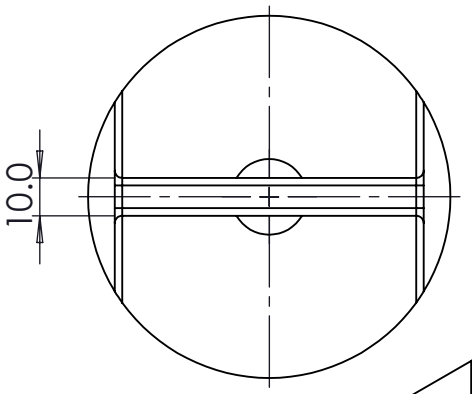

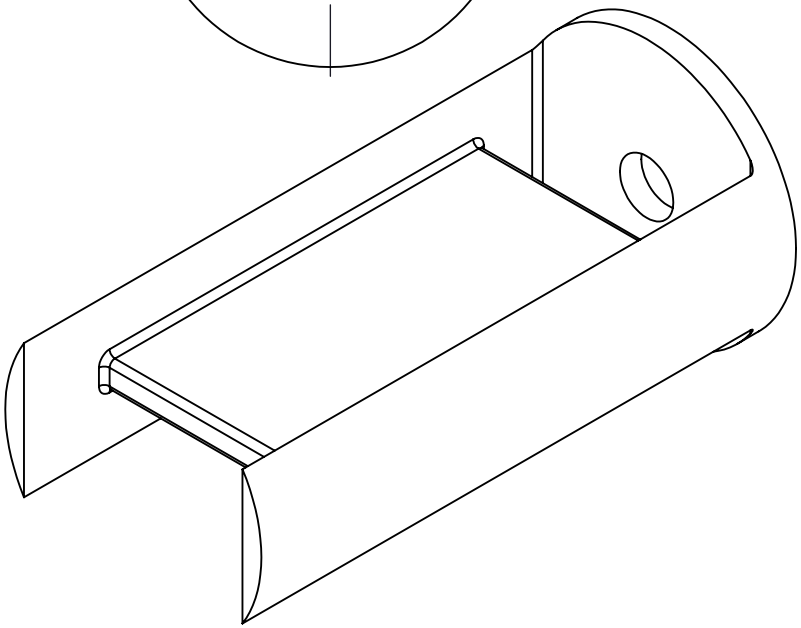

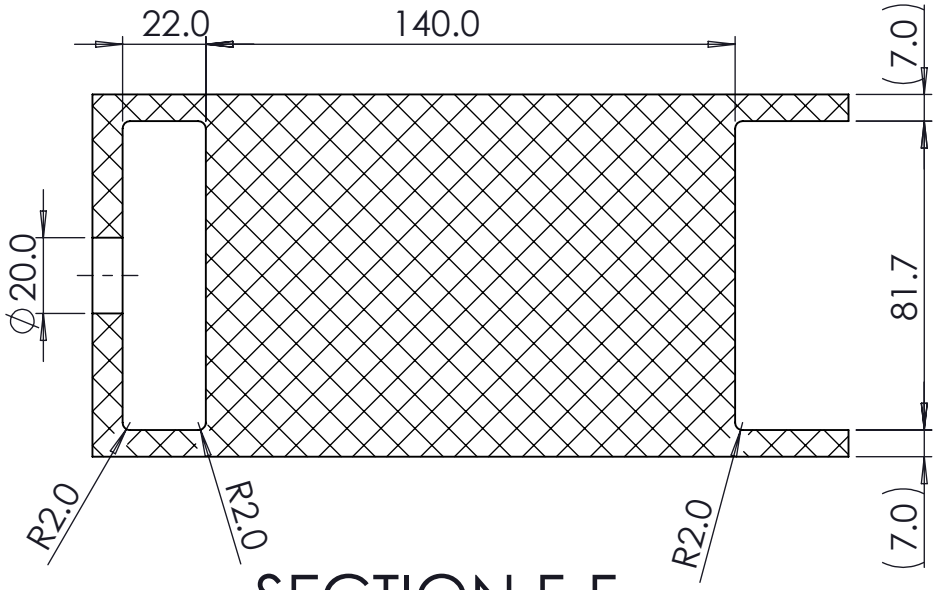

SECTION F-F

SolidWorks Student Edition.
For Academic Use Only.

A4 Landscape	University of Cape Town Department of Mechanical Engineering				
	Title: JBX-P06-Chocolate Block Board				
Quantity: 1	Part Finish	Date: 2012/01/12	Scale: 1:2	Sheet1	of 1
Material: PP Copolymer (White)	Drawn By: Roger de Smidt DSMROG001			Drawing Number JBX-00-06-00	

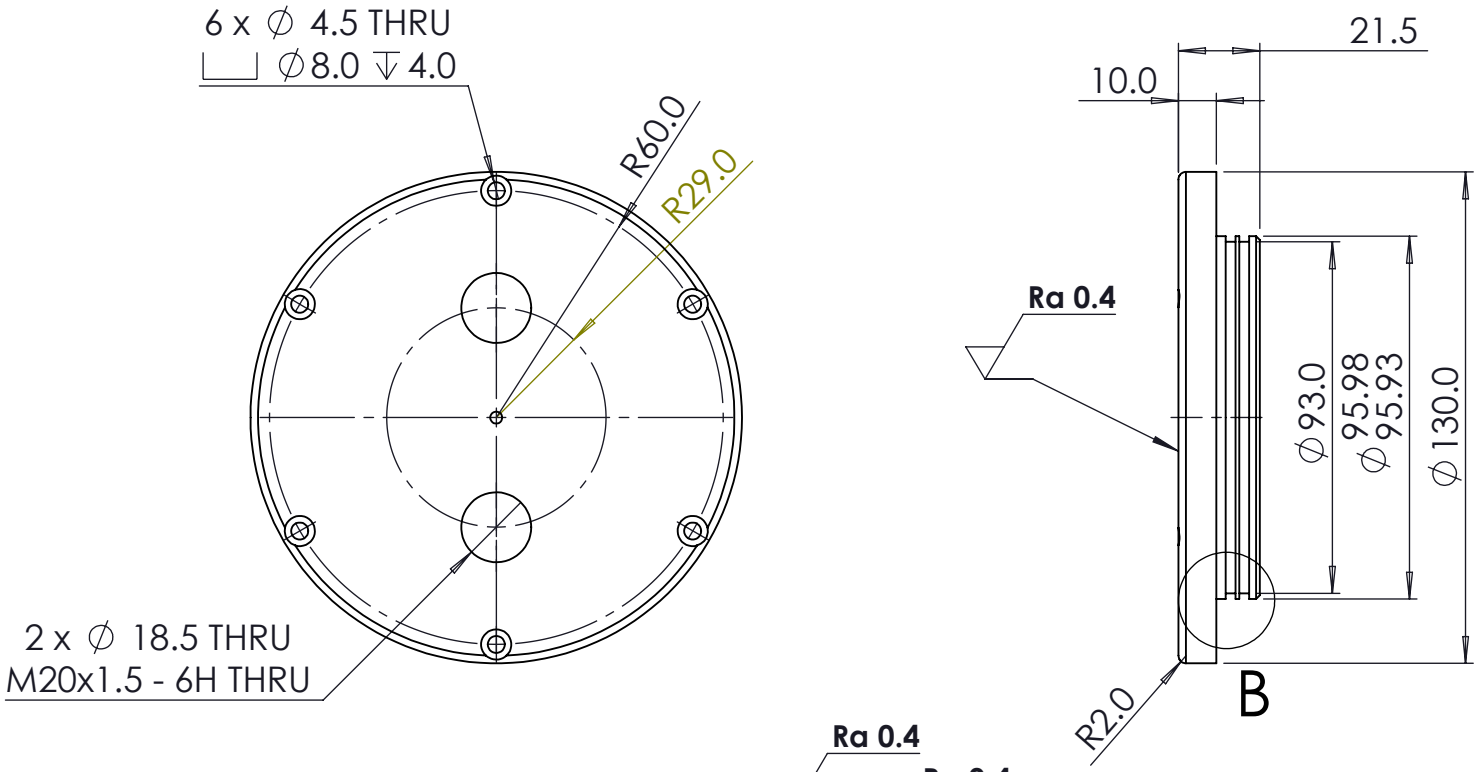

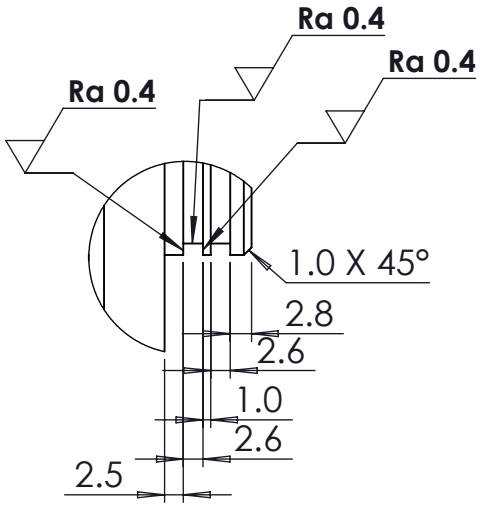

DETAIL B
SCALE 1 : 1

SolidWorks Student Edition.
For Academic Use Only.

A4 Landscape	University of Cape Town Department of Mechanical Engineering				
	Title: JBX-P04-Housing End Plate				
Quantity: 1	Part Finish	Date: 2012/03/12	Scale: 1:2	Sheet1	of 1
Material: POM Acetal Copolymer	Drawn By: Roger de Smidt DSMROG001			Drawing Number JBX-00-04-01	

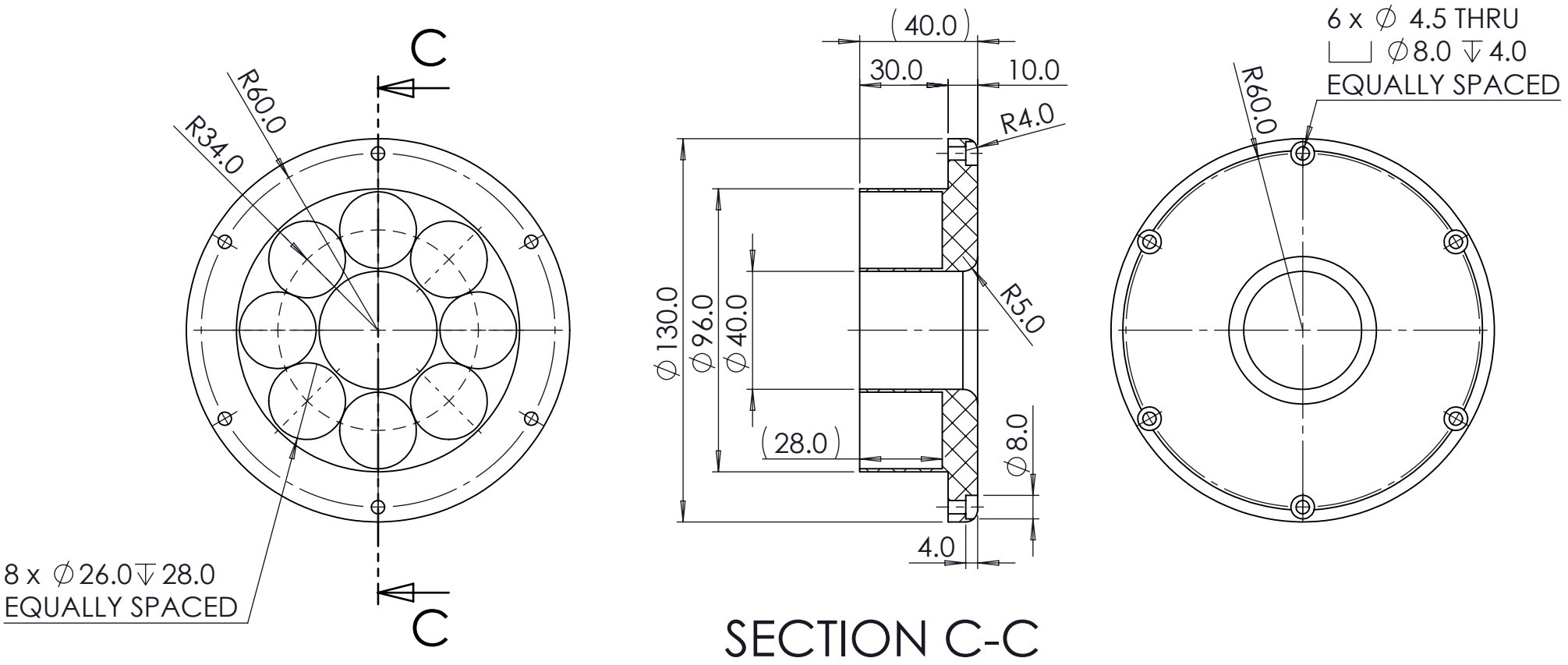

SECTION C-C

SolidWorks Student Edition.
For Academic Use Only.

A4 Landscape	University of Cape Town Department of Mechanical Engineering				
	Title: JBX-P03-Spring End Plate				
Quantity: 1	Part Finish	Date: 2012/01/12	Scale: 1:2	Sheet1	of 1
Material: POM Acetal Copolymer	Drawn By: Roger de Smidt DSMROG001			Drawing Number JBX-00-03-00	

APPENDIX B: ELECTRICAL SCHEMATICS

CONTENTS

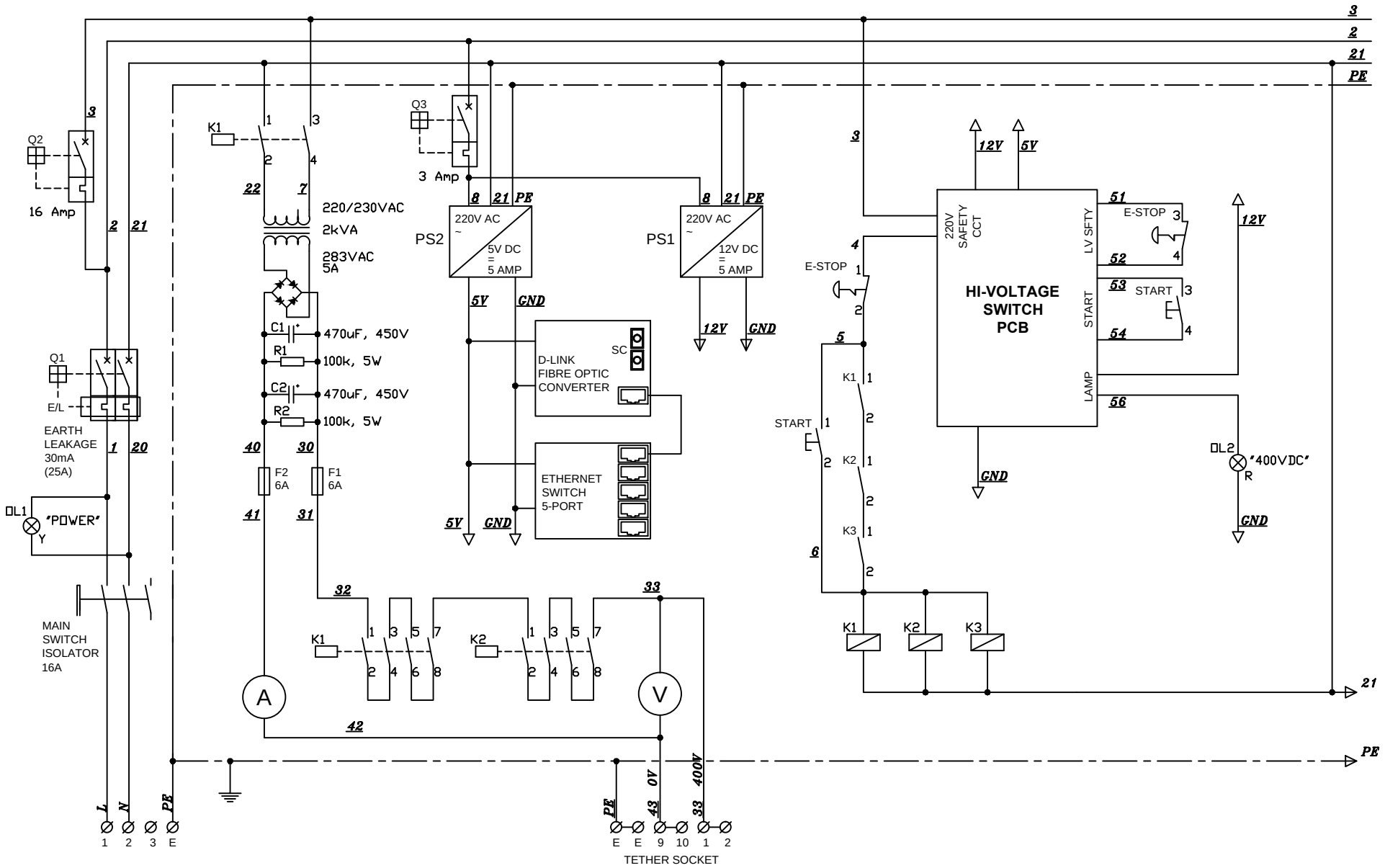

Designed by	Checked by	Project	Date	Drawing Number	Revision
RDS	-	ROV_III	2013/09/16	SURF-01-00	00

UNIVERSITY OF CAPE TOWN

SURFACE_PSU_WIRING

Department	Sheet Size	This Sheet	Next Sheet
MECHANICAL ENGINEERING	A4	1	1

ROV WIRING SCHEMATIC

AFT PORT THRUSTER

FWD PORT THRUSTER

Motor Controller

ARM µ P

I_{tot}: 4.5A I_{max}: 4.5A P: 120W LPBH6M

Tether

GLAND 1 F.O. & Cu

EARTH

400VDC

0VDC

Fiber Optic

CHOCOLATE BLOCK

GLAND 2

OIL-FILLED JUNCTION BOX

GLAND 3 F.O.

POWER POD

CON 1 6P, 7A LPBH6M

TEMP

LEAK DETECTOR

GT16 µP

12 V DC-DC 30W

5 V DC-DC 30W

15 V DC-DC 400W

48 V DC-DC 600W

48 V DC-DC 600W

I_{tot}: A I_{max}: A P: W LPBH6F

I_{tot}: 16.7A I_{max}: 13.8A P: 225W LPBH6F

I_{tot}: 20.8A I_{max}: 10.5A P: 1000W LPBH6F

Sonar Unit

I_{tot}: 0.24A I_{max}: 0.06A P: 6.48W

IMU

I_{tot}: 0.68A I_{max}: 0.5A P: 6.82W MCBH6M

Light Drive

GT16A

I_{tot}: 1.35A I_{max}:1.05A P:18.36W MCBH6M

Front Lights (Port)

I_{tot}: 0.98A I_{max}: 0.8A P: 21.1W MCBH6M

Sensor Pack

GRIPPER (Provisional)

Servo Drive

Tilt Motor (Provisional)

PEN 3 F.O.

ELECTRONICS POD

CON 2 6P, 7A LPBH6M

CON 3 6P, 7A LPBH6M

CON 4 6P, 7A LPBH6M

CON 7 6P, 7A LPBH6F

CON 22 6P, 7A LPBH6F

CON 21 6P, 7A LPBH6F

CON 5 6P, 7A LPBH6F

CON 20 6P, 7A LPBH6F

CON 10 6P, 7A LPBH6F

CON 15 6P, 7A LPBH6F

CON 16 6P, 7A LPBH6F

CON 23 6P, 7A LPBH6F

CON 12 6P, 7A LPBH6F

CON 11 6P, 7A LPBH6F

CON 14 6P, 7A LPBH6F

CON 13 6P, 7A LPBH6F

CON 8 6P, 7A LPBH6F

CON 6 6P, 7A LPBH6F

CON 9 6P, 7A LPBH6F

STRIDE FO/ Ethernet

F.O.

Eth (4L)

Tibbo RS232

ARM

GT16

Bosch Box

RCA

RS485-A(1)

RS485-B(1)

RS485-A(2)

RS485-B(2)

I_{tot}: 0.94A I_{max}: 0.6A P: 9.52W LPBH6M

12V,0.2A

0V,0.2A

RCA

SCI (Tx, Rx, GND)

Foward Camera

Light Drive

GT16A

Camera Lights

Aft Cam

I_{tot}: 0.6A I_{max}: 0.5A P: 4.2W MCBH6M

Aft Light

Motor Controller

ARM µ P

AFT STBD THRUSTER

FWD STBD THRUSTER

VERTICAL THRUSTER

Front Lights (Starboard)

DIAGRAM NO.: RW-01-00

POWER POD WIRING SCHEMATIC

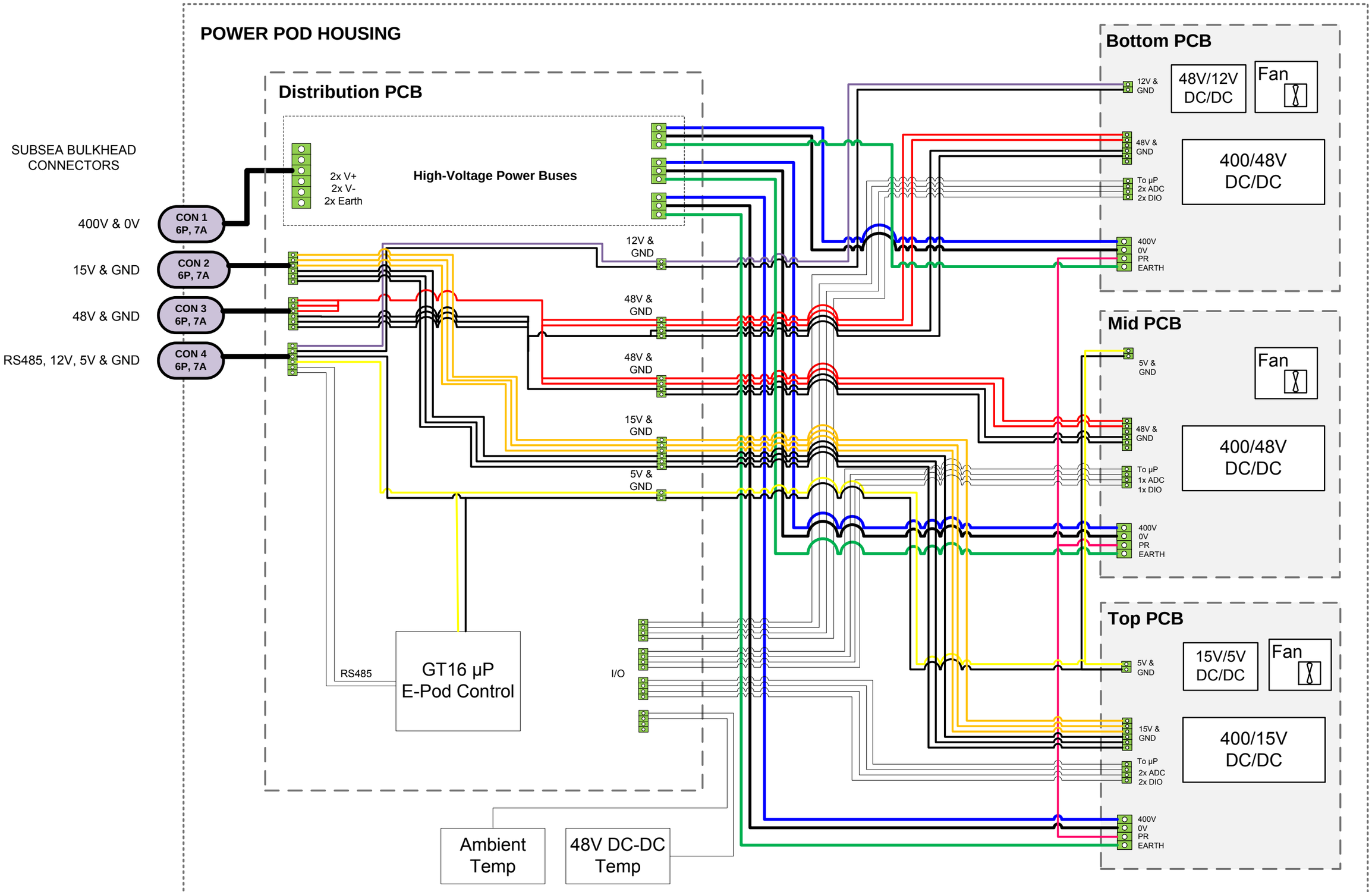

DIAGRAM NO.: RW-02-00

ELECTRONICS POD WIRING SCHEMATIC

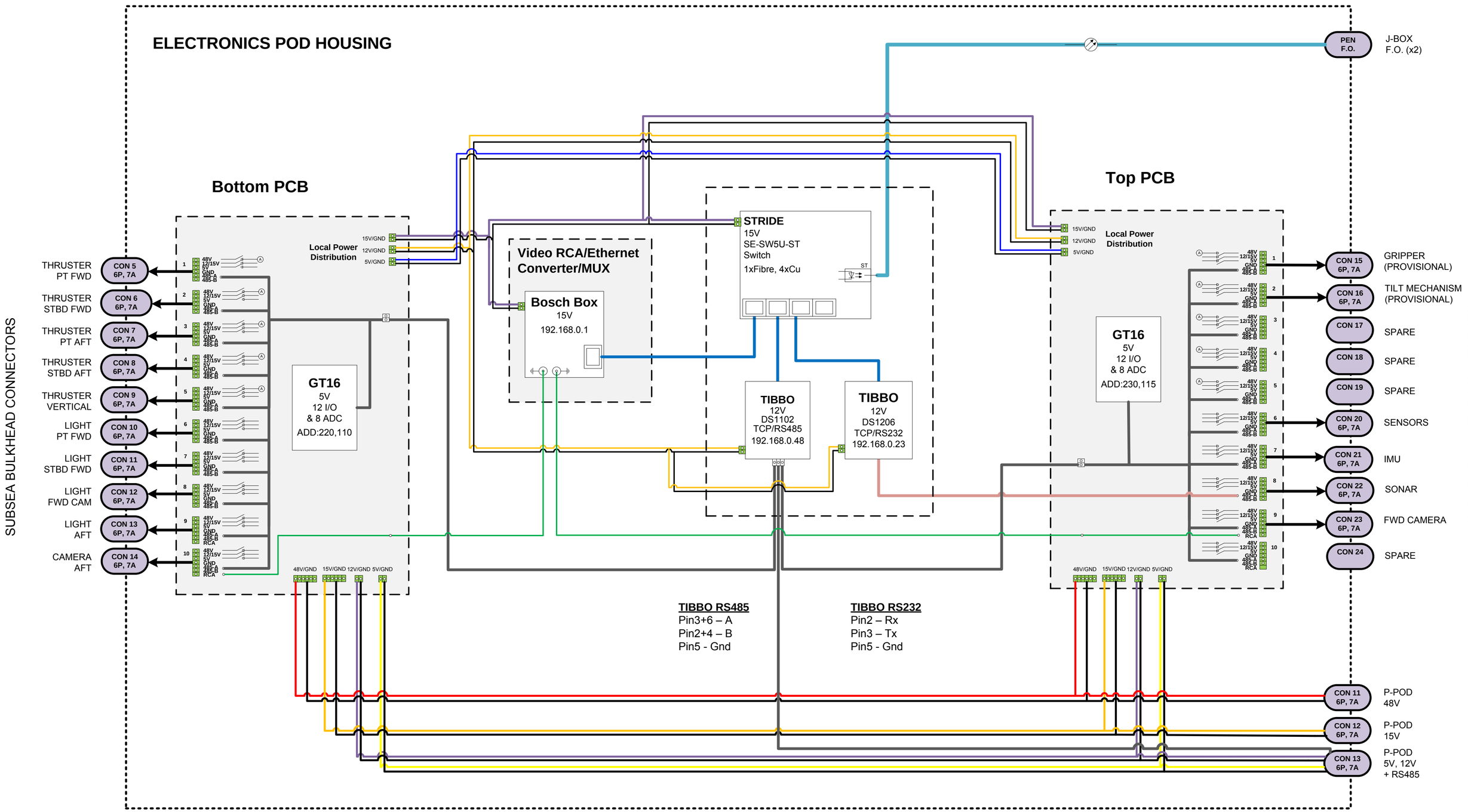

DIAGRAM NO.: RW-03-00

OPTICAL FIBRE CABLES AND CONNECTIONS

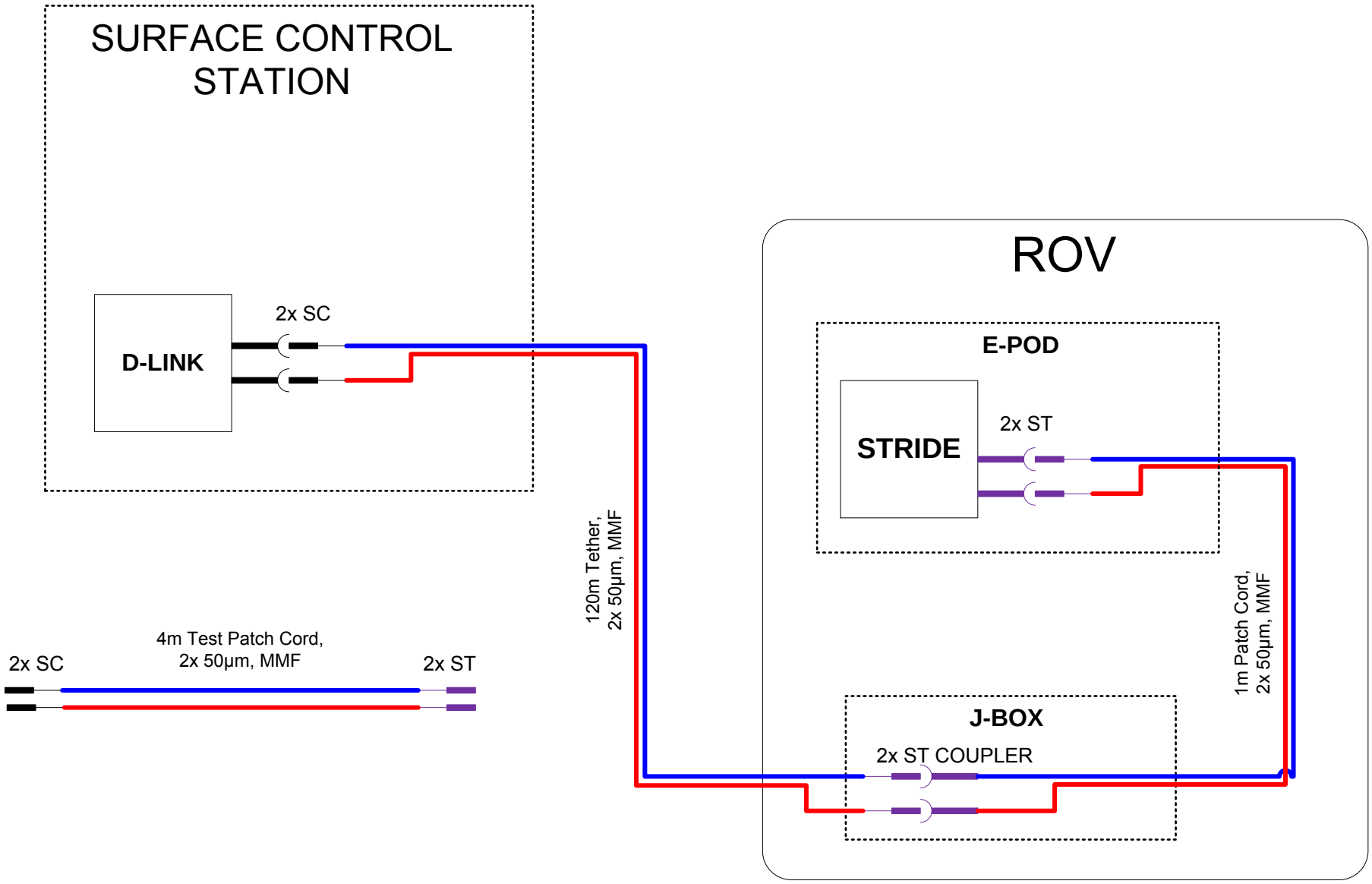

DIAGRAM NO.: RW-04-00

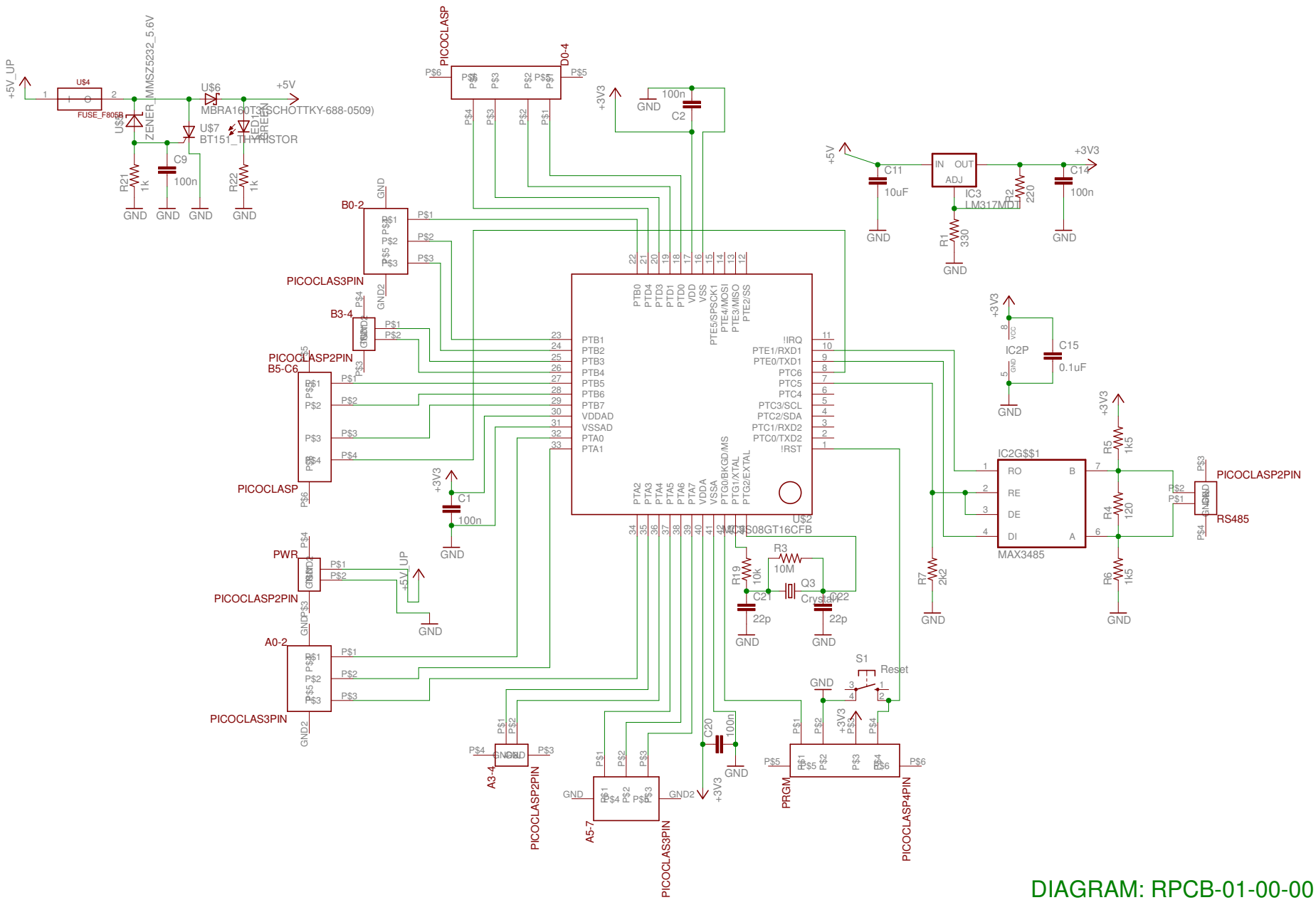
+5V_UP
U$4
FUSE_F805B
ZENER_MMSZ5232_5.6V
U$6
MBRA160T3(SCHOTTKY-688-0509)
+5V
U$7
BT151_THYRISTOR
LED1
GREEN
R21
1k
C9
100n
R22
1k
GND
PICOCLASP
D0-4
+3V3
C2
100n
B0-2
PICOCLAS3PIN
B3-4
PICOCLASP2PIN
B5-C6
PICOCLASP
C1
100n
PWR
PICOCLASP2PIN
A0-2
PICOCLAS3PIN
A3-4
PICOCLASP2PIN
A5-7
PICOCLAS3PIN
C20
100n
PRGM
PICOCLASP4PIN
S1
Reset
R19
10k
R3
10M
Q3
Crystal
C21
22p
C22
22p
R7
2k2
C11
10uF
IC3
LM317MDT
R2
220
R1
330
C14
100n
IC2P
C15
0.1uF
IC2G$$1
MAX3485
R5
1K5
R4
120
R6
1K5
PICOCLASP2PIN
RS485
PTB0
PTD4
PTD3
PTD1
PTD0
VDD
VSS
PTE5/SPSCK1
PTE4/MOSI
PTE3/MISO
PTE2/SS
PTB1
PTB2
PTB3
PTB4
PTB5
PTB6
PTB7
VDDAD
VSSAD
PTA0
PTA1
!IRQ
PTE1/RXD1
PTE0/TXD1
PTC6
PTC5
PTC4
PTC3/SCL
PTC2/SDA
PTC1/RXD2
PTC0/TXD2
!RST
PTA2
PTA3
PTA4
PTA5
PTA6
PTA7
VDDA
VSSA
PTG0/BKGD/MS
PTG1/XTAL
PTG2/EXTAL
U$2
S08GT16CFB
DIAGRAM: RPCB-01-00-00
GT16A MICROCONTROLLER PCB SCHEMATIC

APPENDIX C: PRESSURE VESSEL DESIGN

CONTENTS

LIST OF FIGURES

LIST OF TABLES

C1 PRESSURE VESSEL DESIGN

In order to protect the ROV electronics from water ingress and from being crushed by the water pressure at the ROV's working depth, each module needed its own pressure tolerant housing. The housings would need to retain their shape with negligible deformation at the working depth and incorporate adequate sealing for its openings and penetrations.

Although the dimensions differ between each module's housing, the same design principles and similar geometry were applied throughout the ROV's pressure vessels. However, this section focuses on the design of the Power Pod and E-Pod housings only. A list of specifications is presented in the section below and is followed by the details of the structural design and O-ring seal design for these housings.

Figure C1: Rendering of a cross-section of the Power Pod housing

C1.1 Specifications

Table C1: Power Pod specifications

Number	Description of Requirement	Target Values
Functional Specifications		
C1.1.1	Internal air pressure	Same as surface
C1.1.2	Re-usable seals	Yes
Mechanical Specifications		
C1.1.3	Minimum internal diameter	178mm
Material Specifications		
C1.1.4	Galvanic protection	Yes

C1.2 Internal Air Pressure

The electronics to be housed in the Power Pod and E-Pod were to operate at atmospheric pressure so that standard electronics components could be used throughout the design of the ROV. If any of the electronics housings were to be oil-filled, certain electronic components, such as electrolytic capacitors for example, would need to be exchanged for pressure tolerant components. The housing was to provide negligible compression of the internal cavity when operating at its rated depth.

C1.3 Re-Usable Seals

Maintenance and repairs were expected to be performed regularly on the ROV modules. Each housing was therefore to be designed with seals that could be opened and resealed without having to replace components.

C1.4 Internal Diameter

In order to house the electronic components that would be fitted inside the Electronics Pod and Power Pod, a minimum internal diameter of 178mm was required.

C1.5 Galvanic Protection

Dissimilar metals, such as aluminium and stainless steel, often have sufficient difference between their electrode potentials to create localised galvanic cell when immersed in an ion rich solution such as sea water. The result is that the anode in the reaction (aluminium in the case mentioned above) is oxidised rapidly and if not protected, fasteners and mating parts can seize. Galvanic protection is therefore required where dissimilar metals are used on the ROV.

C1.6 STRUCTURAL DESIGN

Round cylinders and spheres are the two most common shapes used in the design of pressure vessels because the stresses induced in the walls of these vessels are almost entirely compressive in the case of externally applied pressures or tensile in the case of internal pressures. Compared to the flat walls of a rectangular cylinder, the walls of a round cylinder or sphere experience negligible bending or shear stresses.

The diagram in Figure C2 below shows how hoop and longitudinal stresses are setup in the walls of an internally pressurised round cylinder. The symbols used are described in Table C2 that follows.

Table C2: Symbols used in pressure vessel design calculations

Symbol	Description
P	Pressure
d	Internal diameter
t	Wall thickness
σ_H	Hoop stress
σ_L	Longitudinal stress
$P_{collapse}$	Collapse pressure
L	Cylinder length
E	Modulus of elasticity
μ	Poisson's Ration
δ_{max}	Maximum deflection
I	Second moment of area
σ_{max}	Maximum stress

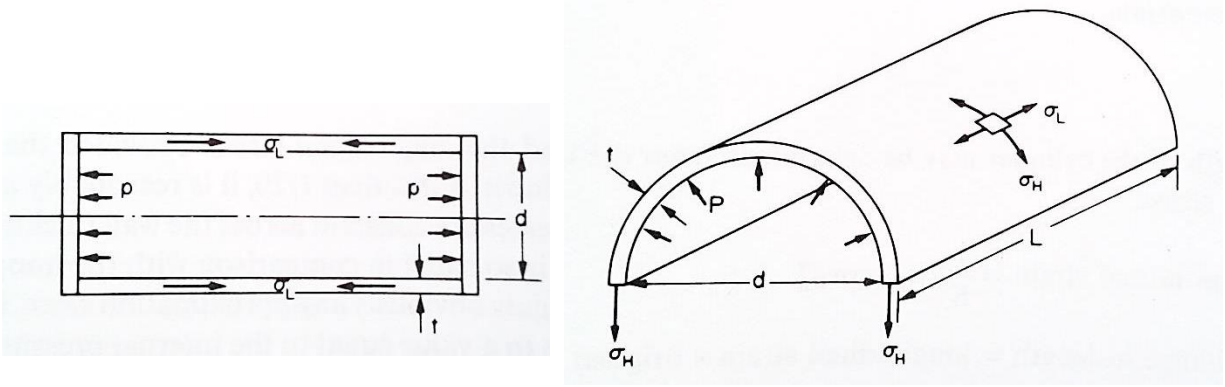

Figure C2: Stresses induced in a thin-walled internally pressurised round cylinder

In thin-walled cylinders where the wall thickness is less than 1/20th of the internal diameter, it can be safely assumed that the stresses are evenly distributed over the cross-section of the wall. However, when designing vessels to withstand external pressures, the possibility of the cylinder collapsing in a buckling type of failure needed to be factored in to the calculations. The equation below was derived by the United States Experimental Model Basin for the collapse pressure of an externally pressurised vessel [1].

Eq. C1…

$$P_{collapse} = \frac{2.42E}{(1-\mu^2)^{\frac{3}{4}}} \cdot \frac{\left(\frac{t}{d}\right)^{\frac{5}{2}}}{\frac{L}{d} - 0.45\left(\frac{t}{d}\right)^{\frac{1}{2}}}$$

$P_{collapse}$ was treated as the factored load that the system would experience. $P_{collapse}$ therefore was equivalent to the system safety factor multiplied by the working pressure, P. Due to the lack of experience with ROV operating at such depths and the uncertainty of how the housing penetrations would concentrate the stresses, a value of 2.5 was set for the safety factor.

Spherical end plates would be thinner walled than flat or elliptical endplates, but due to space requirements on the ROV it was decided to use flat end plates, even though they would be thicker and heavier [2]. Penetrations in the housing end plates were also required for the electrical connectors on each vessel and they would be considerably easier to drill into a flat plate than an elliptical or spherical plate.

The equations below describe the maximum deflection and maximum stress at the centre and circumference of the plate respectively, as depicted in Figure C3, where $a = \frac{d}{2}$ [3].

Eq. C2…

$$\delta_{max} = \frac{P\left(\frac{d}{2}\right)^4}{64E\left(\frac{td^3}{12}\right)}$$

Eq. C3…

$$\sigma_{max} = \frac{3P\left(\frac{d}{2}\right)^2}{4h^2}$$

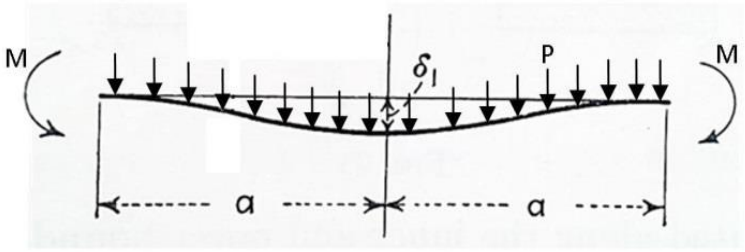

Figure C3: Bending moment diagram for pressure vessel end plate

The E-Pod and Power Pod housings were design so that the one end plate would be integral to the housing cylinder and the other end was designed as a lid that would be bolted to the cylinder complete the housing. To reduce material costs, condemned aluminium dive cylinders were sourced for the E-Pod and Power Pod housings. The 6351-T6 grade aluminium used in the 12.2 litre dive tanks was a high-strength alloy and its dimensions were well suited to house electronic equipment required for the ROV.

The dive tanks also incorporated a large radius to reduce stress concentration between the cylinder wall and base, as seen in Figure C1 above. Siemon recommends that the minimum value for this radius be three times the thickness of the cylinder wall [1].

The design principles and formulae described above were used to create a spread sheet calculator in Excel®. The inputs and outputs of this calculator are listed below in Table C3 and the final dimensions and design used for both the Power Pod and E-Pod housings complete with end plate, is shown below in Figure C4.

Table C3: Input and output values for housing stress and deflection calculations

Input Values		Output Values	
Working depth	300m	Max. principal stress in cylinder	200 MPa
Safety factor	2.5	Max. stress in cylinder base	265 MPa
Cylinder internal diameter, d	178.6 mm	Max. deflection in cylinder base	0.52 mm
Cylinder wall thickness, t_c	3.5 mm	Max. stress in lid	268 MPa
Cylinder depth	165 mm	Max. deflection in lid	0.53 mm
End plate thickness, t_{EP}	13.0 mm		
Lid plate thickness, t_L	13.0 mm		
Cylinder Material	Aluminium 6351 T6		
Yield Stress 6351, S_y	283 MPa		
Lid Material	Aluminium 6082 T6		
Yield Stress 6082, S_y	250 MPa		
Elastic Modulus, E	68.9 GPa		
Poisson's Ratio, v	0.33		

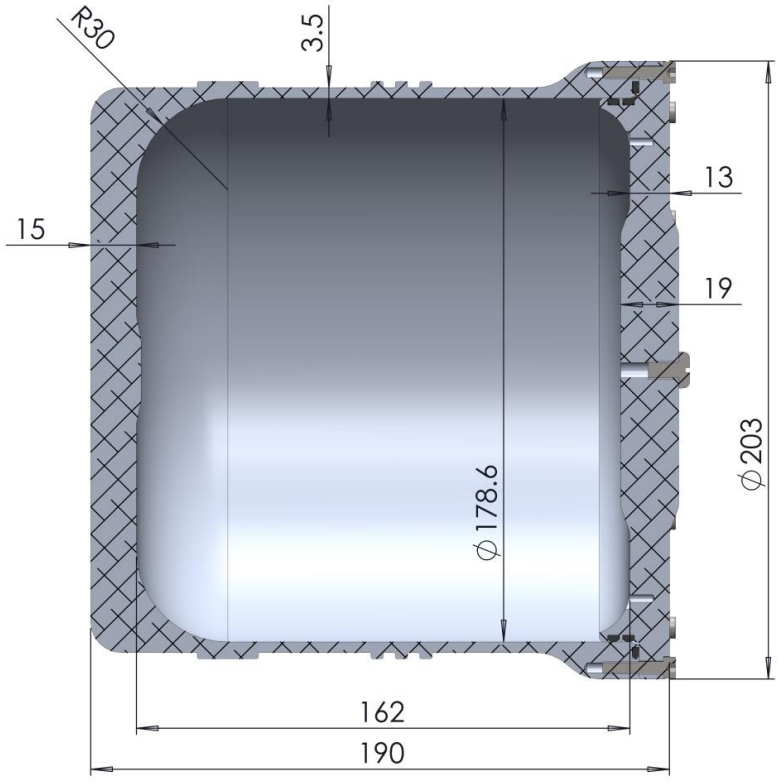

Figure C4: Dimensions of the pressure vessel housing for the Power Pod and E-Pod

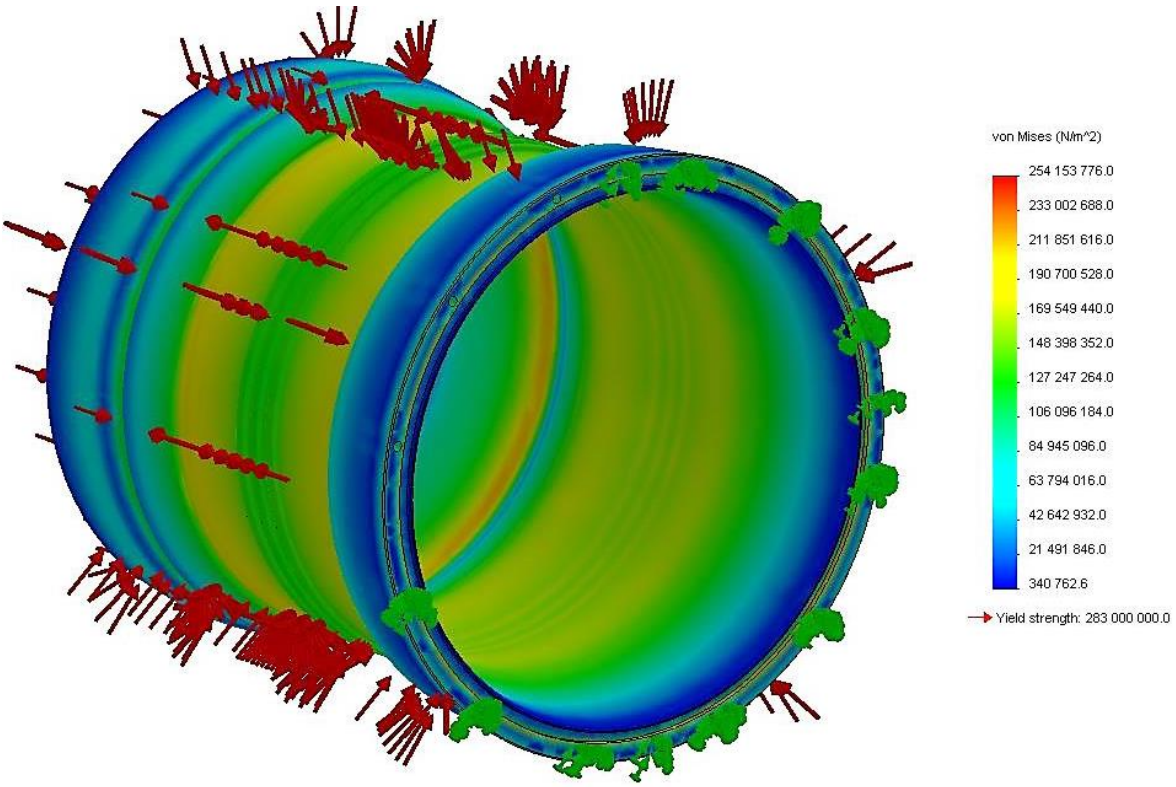

Figure C5: FEA results for stresses induced in the Power Pod cylinder

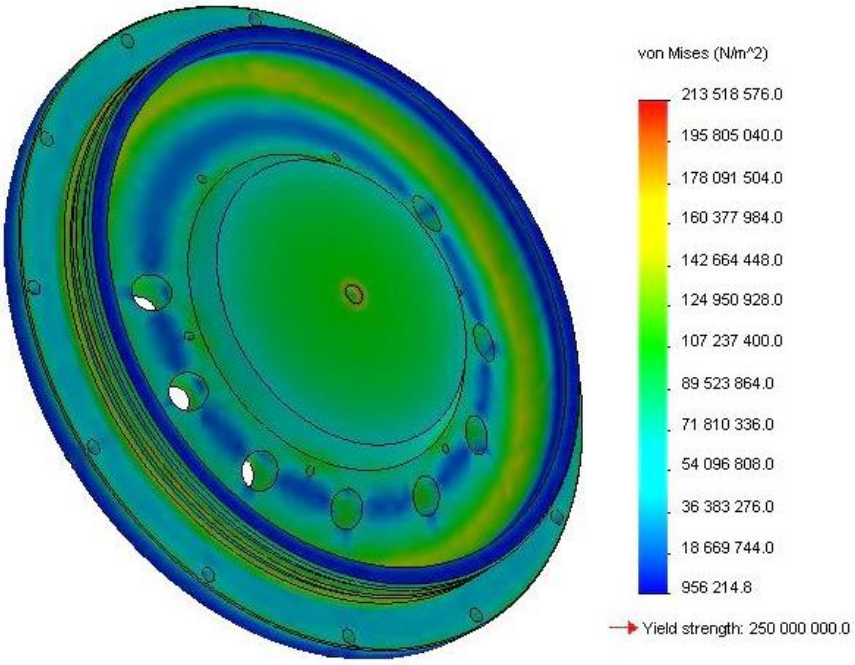

Figure C6: FEA results for stresses induced in the E-Pod lid

Solid Works® Computer Aided Design (CAD) software was used to run a Finite Element Analysis (FEA) of the stresses and deflections in both the housing cylinder and lid. This study was run as a tool to verify that the dimensions calculated for the housing above were adequate. Each component was

constrained on their mating surfaces to correlate as closely as possible with the manner in which they would be constrained in reality. A uniform pressure equivalent to a depth in water of 750m was applied to the external surfaces of the cylinder and lid. The results of the FEA study are presented above in Figure C5 and Figure C6.

As seen in the FEA results, both the cylinder and the lid were predicted not to exceed their yield stress values of 283MPa and 250Mpa respectively, which correlated with the manual calculation results presented in Table C3. The maximum induced stresses are represented by the highest number on the legend on the right of each FEA image.

The maximum deflection for the cylinder and lid determined in the FEA study was 0.54mm and 0.34mm respectively. Rerunning the FEA study for a working pressure equivalent to 300m depth, maximum deflections for the cylinder and lid were predicted to be 0.02mm and 0.01mm respectively. These deflections were negligible compared to the internal diameter and depth of the pod and would have no significant effect on its internal pressure.

C1.7 PRESSURE SEALS

In order to provide the necessary sealing on each of the pressure vessels O-ring glands were incorporated in the design of each pod. O-rings were to be used to provide the seal between each lid and its mating cylinder, and between each electrical connector and the housing end plates that it penetrated.

Two radial O-rings were considered the primary seals for each of the ROV module housing lids or end caps. The ROV would be maintained and run on a tight budget and the expense in time and finances to replace damaged circuitry inside a module was to be minimised. An additional face seal was therefore incorporated in each housing lid to further reduce the risk of electronics being flooded. A cross section of the O-rings and their glands in which they are seated can be seen in Figure C7 below.

Nitrile O-rings with a Shore A hardness of 70 were specified for use on the ROV. A Shore 70 hardness would be sufficient for the pressures expected at 300m depth below the water's surface and would also remain sufficiently ductile in the cooler waters expected off the South African coast. Nitrile was not as durable as Viton® O-ring material, but was significantly more cost effective and would meet the sealing requirements for prototype testing of the ROV.

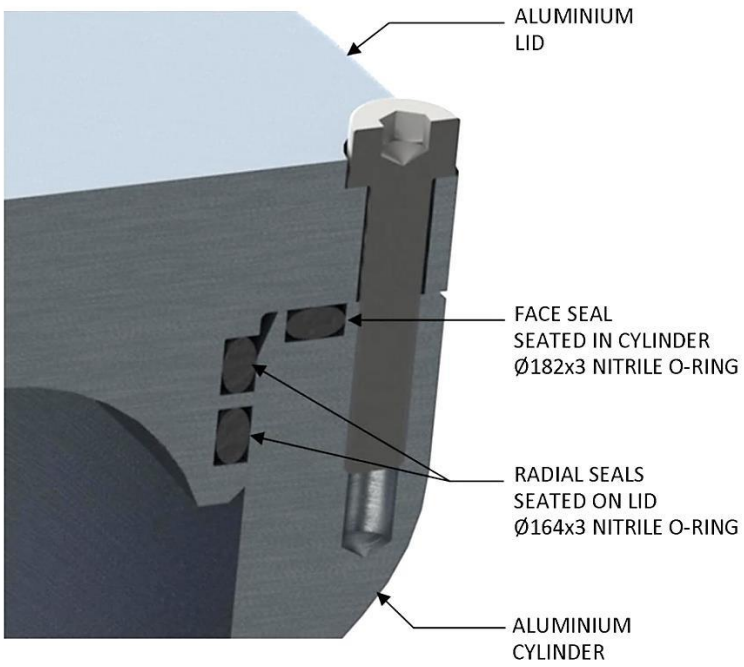

Figure C7: Rendered cross-section showing O-ring glands in Power Pod

As described in Section 2.4.3.2 the size of the gland machined to contain the O-ring was critical to how it would perform. The gland dimensions on this ROV were based on those recommended by industry specialists and by O-ring manufacturer Parker® [4]. The gland cross-sectional dimensions used for this ROV are listed in Figure C8 below.

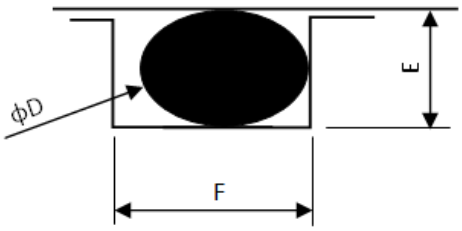

[mm]	Face Seal		Radial Seal	
D	F	E	F	E
2.0	2.6	1.5	2.6	1.2
3.0	3.9	2.0	3.9	1.8

Figure C8: O-Ring gland dimensions

C1.8 GALVANIC PROTECTION

The E-Pod and Power Pod housings were manufactured from aluminium and would be assembled using aluminium fasteners. In flowing seawater he electrode potential of aluminium is -0.79V and the electrode potential of 304 stainless steel -0.08V, resulting in a 0.71V difference [5].

The first step taken to protect the aluminium housings was to have them anodised. A "hard-anodising" process was used to provide a 40µm coating of aluminium oxide over the components, which was thicker and would be more durable than the standard 25µm thick anodised layer. The anodising would protect the natural aluminium surface from oxidising in the presence of salty sea air, and would be the first line of defence against oxidisation potential in a galvanic cell reaction.

The second step was to install sacrificial anodes close to where the dissimilar metals would interact. Zinc anodes that had an electrode potential of -1.03V would oxidise instead of the aluminium because of the greater potential difference between the anodes and the stainless steel fasteners.

The sacrificial zinc anodes were designed to screw onto customised stainless steel screws that would replace one of the lid screws on each Aluminium pod. A photo of one of these anodes secured to the top of the Power Pod is shown below in Figure C9. Zinc is a softer material than stainless steel and the anodes were designed so that they could still be removed and the customised stainless screw unfastened even if the anode was severely corroded.

Figure C9: Zinc anode fitted to the Power Pod

In order to provide some protection between each of the fasteners and the threads into which it was screwed, Aquashield® lubricant was applied to the threads each time the screws were re-inserted. Aquashield® was recommended by the Marine Solutions ROV technicians and had proved to be highly effective.

C1.9 SUMMARY

The pressure vessels for each of the ROV modules were designed to operate at the ROV's working depth and to meet each of the specifications as laid out at the beginning of this appendix. The pressure vessels were designed for manufacture from aluminium and condemned dive tanks were used as the material for the Power Pod and E-Pod cylinders. Nitrile O-rings were used in face and radial seal configurations to provide the sealing required on each of the pressure vessels. Galvanic protection was also provided on each housing by anodising the aluminium components of the housing, installing sacrificial anodes and using corrosion inhibiting lubricant on the fasteners.

Testing of the E-Pod and Power Pod seals was performed at the Marine Solutions workshop, the details of which are presented in Section 9.2.

C1.10 REFERENCES

[1] K. Siemon, “Manual for the Design of Frrous and Non-Ferrous Pressure Vessels and Tanks,” 3rd ed., Ann Arbor, Michigan: Edwards Brothers, Inc., 1948, p. 94.

[2] E. J. Hearn, *Mechanics of Materials 1*, 3rd ed. Oxford: Butterworth Heineman, 2001, pp. 198–206.

[3] S. Timoshenko and S. Woinowsky-Krieger, “Theory of Plates and Shells,” New York: McGraw-Hill Book Company, Inc., 1959.

[4] Parker Hannifin O-ring Division, “Parker O-ring Handbook,” 2003.

[5] About.com, “Galvanic Corosion,” 2013.

APPENDIX D: SENSOR CALIBRATIONS

CONTENTS

LIST OF FIGURES

LIST OF TABLES

D1 CALIBRATION OF TEMPERATURE SENSORS

The two temperature sensors in each of the E-Pod and Power Pod needed to be calibrated to ensure accurate feedback to the UI on the surface. The temperature readings were displayed as information for the ROV pilot and were also used by the UI to activate power-limiting functions within the software when temperature limits were exceeded.

A thermal camera which provided accurate surface temperature measurements was used to calibrate the temperature sensor while a hot air gun was used to increase the sensor temperatures. A formula was derived for each sensor output that would convert its analogue-to-digital conversion (ADC) value to a temperature in degrees Celsius.

D1.1 TEST EQUIPMENT

- E-Pod assembly of circuitry on E-Pod lid (without E-Pod chamber)
- Power Pod assembly of circuitry on Power Pod lid (without Power Pod chamber)
- ROV 400VDC Power Supply Unit (PSU)
- PC running a the ROV user interface with temperature indicator digital displays enabled (for Power Pod tests)
- PC running a simplified version of the ROV user interface (for E-Pod tests)
- FLIR Thermovision A320 thermal camera, tripod and laptop with FLIR® IR Monitor software
- Bosch heat gun

The setup of the equipment to calibrate the E-Pod temperature sensors was the same as that shown in Section 9.4.1. The E-Pod had to be disassembled for the thermal camera to obtain an image of the Top PCB's temperature transducer, while still maintaining connections between the PCBs and other E-Pod devices.

The setup of equipment for the Power Pod temperature sensor calibration is shown below in Figure D1. Silicone sheets left over from the assembly of each pod was used to protect the Power Pod PCBs and wiring from the hot air that would be used to heat up the temperature transducers.

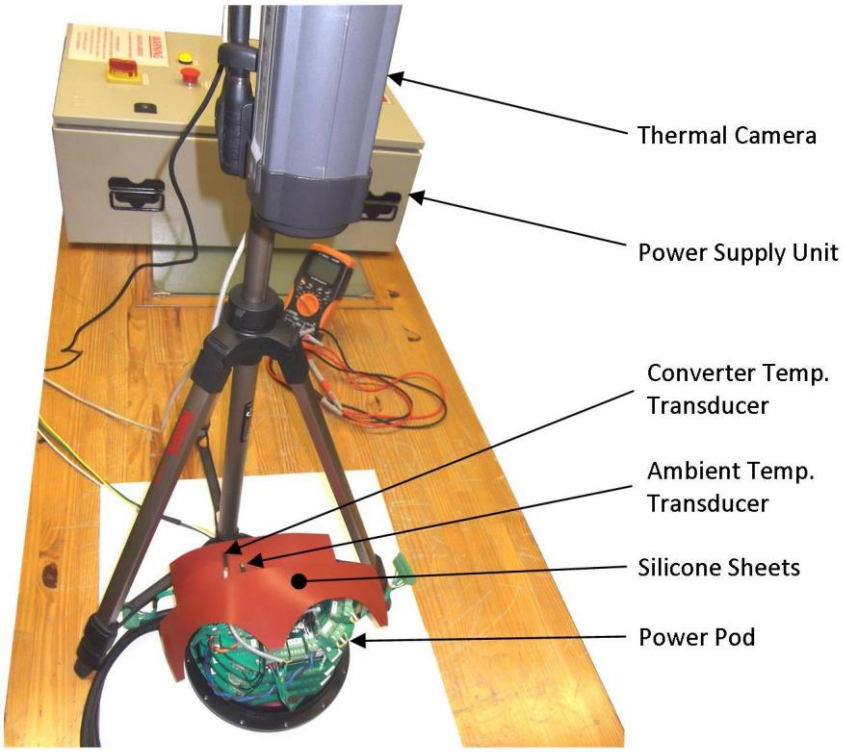

Figure D1: Photo of Power Pod temperature sensor calibration setup

D1.2 Preparation of Equipment

The FLIR Thermovision camera was setup on its tripod to look down on each of the circuit boards with spot markers setup in the IR Monitor® software directly over the temperature transducers on the circuit boards (see Figure 110 for position of temperature sensor on E-Pod PCBs).

D1.3 Test Procedure

The procedure for calibrating each sensor was very similar. Before heating the sensors, a screen-capture was saved of the UI readout of the sensor ADC value and the thermal image showing the actual surface temperature of the transducer. The heat gun was then used to slowly heat the temperature transducer up to about 100°C and then was slowly withdrawn so that the temperature would drop at a very slow and stable rate. It was found that the temperature was easier to control as the transducer cooled compared to when it was being heated up. This was important because the ADC reading lagged the actual reading by a couple of seconds. The lag was also the reason that the screen-capture method was used rather than hand-written records.

As the temperature of the transducer slowly dropped, further screen-captures of the ADC values and temperatures were saved until the transducers had cooled to about 30°C. Care was taken not to overheat components surrounding the transducer while using the heat gun.

Once all the ADC and temperature values had been captured for each sensor, the values were tabulated in a spread sheet and plotted to determine the relationship between the ADC values and the actual temperature for each sensor.

The Microchip® TC1047 temperature transducer on each of the E-Pod PCBs was specified to convert temperature to an output voltage at a rate of 10mV/°C, with an offset of 520mV at 0°C.

The Texas Instruments® LM35 temperature transducers connected to the Power Pod microcontroller were also specified to convert temperature to an output voltage at a rate of 10mV/°C, with a zero offset at 0°C.

The ADC on each on the microcontrollers was set to a resolution of 10 bits, which provided a precision of 0.3°C at the average reference voltage of 3.1V.

D1.4 TEST RESULTS AND ANALYSIS

D1.4.1 E-Pod Temperature Calibration Results

Figure D2 below shows a screen capture of the ADC value and temperature of the temperature sensor on the bottom E-Pod PCB.

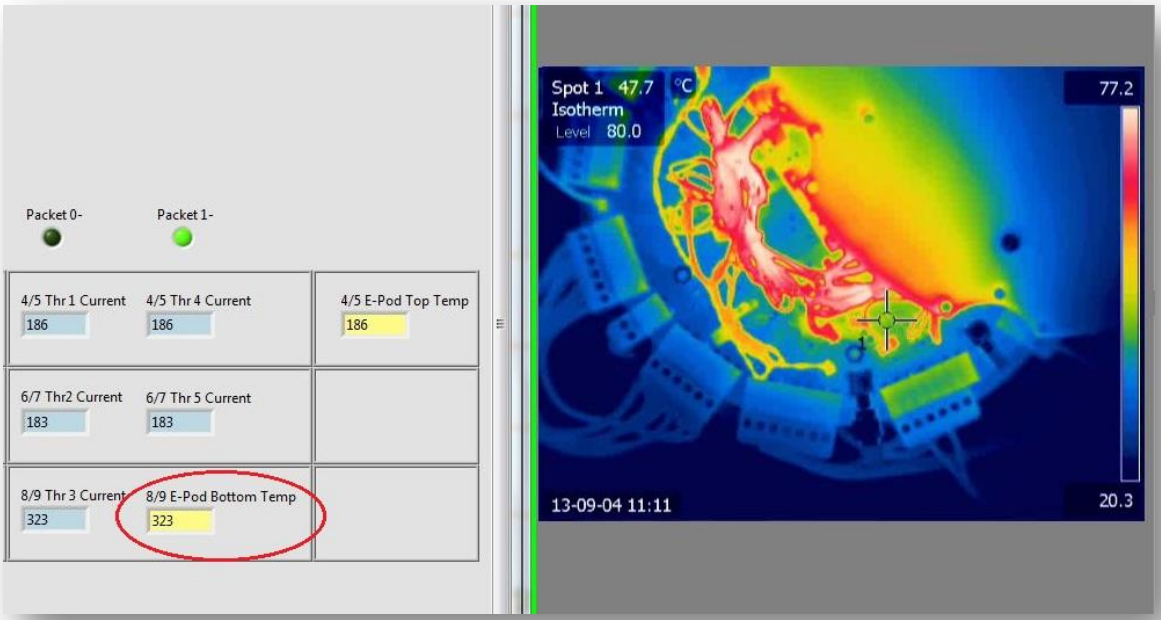

Figure D2: Screen capture of ADC readout in a Labview® User Interface and thermal reading of bottom E-Pod PCB temperature sensor in FLIR® IR Monitor software

The 10-bit ADC values and thermal readings of each sensor were tabulated and graphed using Microsoft® Excel®. The relationship was expected to be, and was found to be, linear. Eq. D1 below was used to describe the plot, where m is the slope of the curve and c is its y-intercept value.

Eq. D1… $$y = mx + c$$

The values for m and c were calculated using the formulae below, where n is the number of readings for each sensor.

Eq. D2… $$m_{avg} = \frac{\sum_{i=0}^{n-1} \frac{y_{i+1} - y_i}{x_{i+1} - x_i}}{n-1}$$

Eq. D3… $$c_{theoretical} = y_n - m_{avg} x_n$$

Table D1: Calculated values for E-Pod temperature sensor curves

E-Pod Temp. Sensor	m_{avg} [°C^{-1}]	$c_{theoretical}$ [word]	Max Error [°C]
Top PCB	3.36	160	1.1
Bottom PCB	3.34	165	0.8

The calculated values are tabulated above in Table D1 and were added to the plot of each graph to show how close the actual readings were to the calculated curve. These values would be used for programming the UI. The graph for the top E-Pod temperature sensor readings are shown below in Figure D3. The errors between the theoretical temperatures and the actual temperature readings were calculated and are also reflected in the table above.

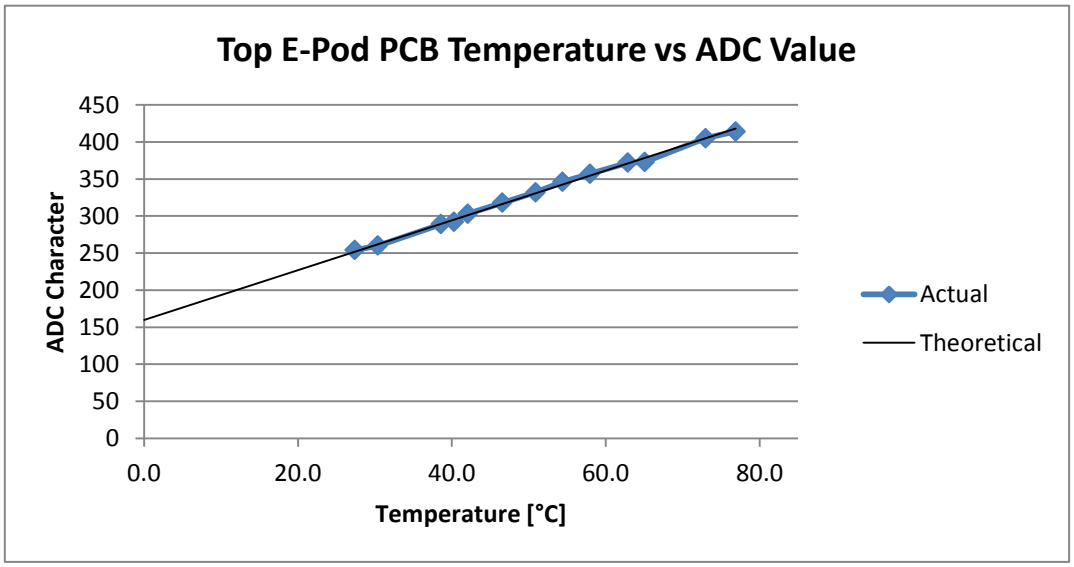

Figure D3: Graph of Top E-Pod PCB temperature sensor ADC values against actual temperature

The blue data series with the diamond-shaped markers on each graph above show the actual readings and the straight black lines indicate the theoretical relationship as described by the calculated values for m and c.

D1.4.2 Power Pod Temperature Calibration Results

During testing of the Power Pod temperature sensors the ADC value was found to be very unstable, particularly at lower temperatures. After some investigation it was determined that the noise on the ground line of the DC power supplies was the cause of the fluctuating ADC readings. The LM35 sensors had a zero offset output voltage so it was not surprising that the ground plane noise was affecting the readings while temperatures were low. The noise on the ground line of the 15V power supply fluctuated between 200mV and 400mV peak-to-peak.

The temperature sensors were replaced with Texas Instruments® LM60s, which were specified for an offset voltage of 424mV at 0°C. This offset would raise the readings above most of the noise in the ground line.

A rolling pass filter was also implemented in the microcontroller embedded software to average out the ADC readings and thereby reduce the amount of fluctuation in the readings.

After the sensors had been replaced and the microcontroller software edited, far more stable readings were obtained through the UI. A screen capture of the readings of the Power Pod temperature sensors can be seen below in Figure D4.

Figure D4: Screen capture of ADC readout in Labview® and thermal reading of Power Pod LM60 temperature transducers in FLIR® IR Monitor (Spot 1: Ambient sensor; Spot 2: 48VDC converter sensor)

As with the E-Pod temperature calibrations, the temperature and ADC values were captured, and then tabulated and graphed. Using Equations D1, D2 and D3 above the theoretical ADC values for 0°C readings, $c_{theoretical}$, on each sensor as well as the average rate, m_{avg}, were calculated. The error between the theoretical temperature and the actual temperature readings was then also calculated.

Table D2: Calculated values for Power Pod temperature sensor curves

Power Pod Temp. Sensor	m_{avg} [°C^{-1}]	$c_{theoretical}$ [word]	Max Error [°C]
Ambient Temperature	2.08	139	0.6
48V DC-DC Converter	2.10	137	1.9

The calculated values for each of the Power Pod sensors are tabulated in Table D2 above, and would be used to program the Labview® UI temperature indicators for the Power Pod.

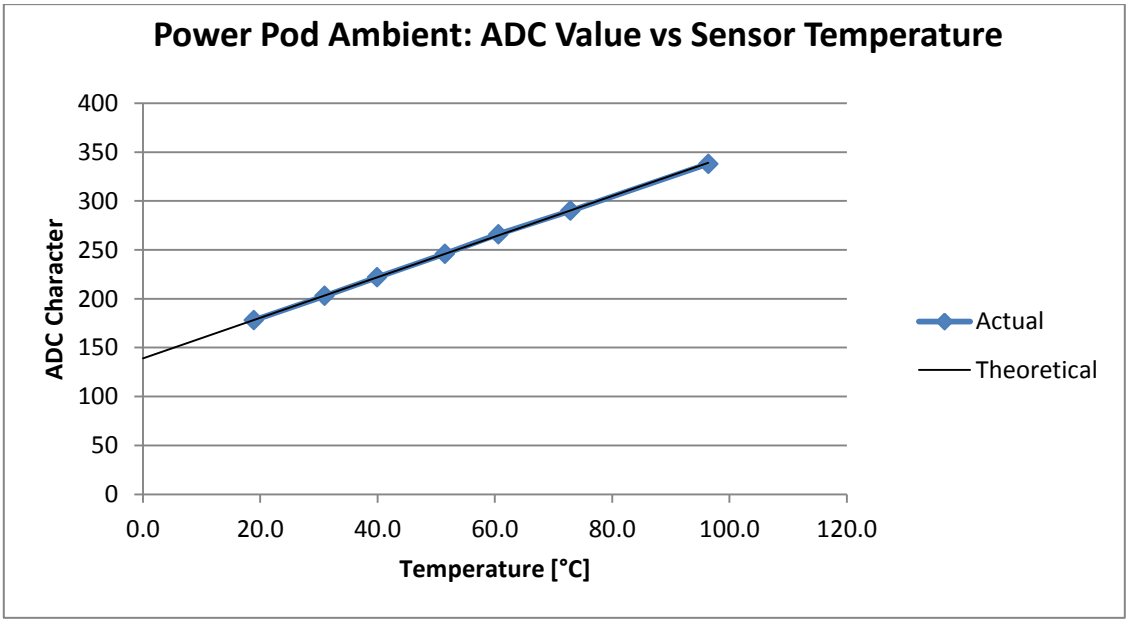

Figure D5: Graph of Power Pod Ambient temperature sensor ADC values against actual temperature

The ADC and temperature readings were plotted against each other and the curves for the ambient temperature sensor can be seen above in Figure D5. The best-fit curve was plotted alongside the actual readings.

D1.5 SUMMARY

The measurements of the temperature sensors for both the E-Pod and Power Pod were found to be very linear. This allowed for accurate programming of the Labview® UI. The maximum error of 1.9°C between the programmed value and the actual reading on the Power Pod's 48V DC-DC converter temperature sensor was still within the 3°C accuracy required for the ROV temperature sensors (see Section 4.1.11).

The rolling pass filter implemented on the microcontrollers to smooth out the ADC outputs worked very well, although a lag in the actual reading was experienced. This would not be an issue during operation because temperature feedback only needed to be updated every 5 seconds. The lag in sensor readings would have affected the accuracy of the ADC calibrations to some degree. If the

control of the transducers' temperatures was more tightly controlled, the 1.9°C error could probably be reduced quite significantly.

D2 CALIBRATION OF CURRENT SENSORS

Each of the two control distribution circuit boards inside the Electronics Pod had its own integrated current sensors on the 48V power lines of the first five output channels. These were included in the E-Pod because of space constraints in each of the thruster housings. The Power Pod was also designed with integrated current sensors, which were used to monitor the output of each DC-DC converter. In total, 10 current sensors needed to be calibrated before proceeding with the final thermal tests so that the current levels could be monitored and recorded via the UI. The top PCB in the electronics housing did not need to have its current sensors calibrated because no thrusters were to be connected to it.

Similar setups to the preliminary thermal tests on the E-Pod and Power Pod were used. The E-Pod and Power Pod were connected to load resistors in two separate sets of tests and commercial ammeters used to calibrate the current sensors over their designed operational range. A formula was derived for each sensor output and programmed into the control software to convert the ADC reading from sensors into a meaningful current value.

The accuracy of the current sensors was specified in Section 4.1 and Section 5.1 to be within 10% of the actual value, which would provide sufficient accuracy for the purposes of controlling the ROV.

D2.1 TEST EQUIPMENT

- Top and bottom Electronics Pod control distribution circuit boards, completely assembled and wired up in E-Pod and connected to host controller interface on a PC
- Power Pod completely assembled and connected to E-Pod comms
- ROV 400VDC PSU
- Manson® HCS-3302 Power supply set at 5V
- Topward 6303D Power supply set at 12V and 15V
- Topward 6303D Power supply set at 48V
- Variable resistor network to provide 1-24Ω at 4.5A minimum
- Variable resistor to provide 1.9-20Ω with a minimum current rating of 25A
- F.W. Bell® CG100D clamp-on current meter
- Agilent® U1242B Multimeter

The setup for the E-Pod current sensor calibration tests was the same as for the preliminary thermal tests and a schematic of the wiring connections can be seen in Figure 111 of Section 9.4.1.3. Likewise, the setup for the Power Pod sensor calibrations can be seen in Figure 118 of Section

9.4.2.2. The only difference from the preliminary tests for the E-Pod was that the 15V lines on channels 6 to 10 did not need to be connected.

The high voltage equipment was again handled with great caution and the same safety measures describe in Section 9.4.2.1.1 were followed.

D2.2 TEST PROCEDURE

The output serviced by each current sensor was loaded using the relevant variable resistor and controlling the power ON/OFF status via the UI on the laptop.

Each current sensor's ADC output on the UI was recorded alongside the measurement of the current passing through it. The current in each sensor was started at zero current and then increased in roughly 10% increments through its full operating range. The upper current limit of each circuit monitored with a current sensor was the most important point of each sensor's range to calibrate correctly. The upper limits were potentially to be used to create protective features in the UI software so as not to burn out lights or thrusters on the ROV and therefore needed to be reasonably accurate.

Once all of the current sensor values had been recorded, they were tabulated in a spread sheet and plotted on graphs. Equations were then developed to best describe the curves that were generated by the plotted current sensor data. These equations would in turn be used to convert the ADC words received by the UI into meaningful current readings for the operator.

D2.3 TEST RESULTS AND ANALYSIS

D2.3.1 E-Pod Current Sensors

The E-Pod current sensor outputs and current measurements were tabulated and graphed in Microsoft® Excel®. It was found that the ADC readings were linearly related to the current measurements over the 0-4.5A range. The graph in Figure D6 below shows the plot of sensor measurements for the first thruster channel of the E-Pod, which was representative of all five sets of results.

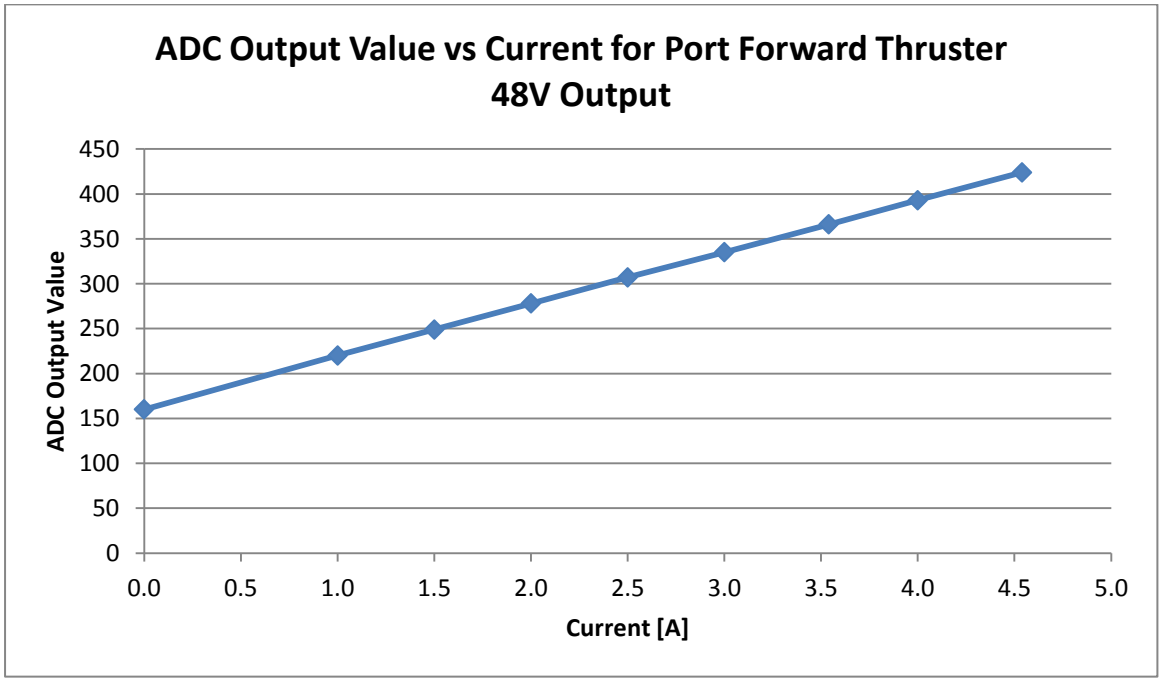

Figure D6: Graph showing measured and theoretical ADC values plotted against current for the Current sensor on channel 1 of Bottom E-Pod PCB

Using Equations D1-D3 from Section D1.4, the tabulated data for each sensor was used to calculate the rate and zero offset for each sensor. The percentage error between the actual readings and the theoretical values was also calculated, and a list of all the theoretical coefficients and maximum errors for the E-Pod sensor calibrations can be seen in Table D3 below.

Table D3: E-Pod current sensor function values

Current Sensor	Slope m_{avg} [mA^{-1}]	Offset c_{actual} [word]	Max Error [mA]	Allowable Error [mA]
E-Pod Bottom Ch. 1 (Port Fwd Thruster)	57.94	160	18	100
E-Pod Bottom Ch. 2 (Stbd Fwd Thruster)	59.19	167	21	
E-Pod Bottom Ch. 3 (Port Aft Thruster)	59.46	163	21	
E-Pod Bottom Ch. 4 (Stbd Aft Thruster)	59.85	163	30	
E-Pod Bottom Ch. 5 (Vertical Thruster)	59.24	162	42	

D2.3.2 Power Pod Current Sensors

The Power Pod current sensors provided linear outputs as expected and could be well approximated by Equation 1 from Section D1.4 over the full current range of each sensor. The readings of the sensors were tabulated and the coefficients for Equations D1-D3 calculated using Microsoft® Excel®. Because the theoretical and measured current readings needed to converge reliably at zero, the measured ADC value for 0A was used together with the calculated slope to produce the equation that would approximate each sensors output. The measured values and the calculated coefficients, m and c, are tabulated below in Table D4 and Table D5.

Table D4: Power Pod current sensor readings

48V(1) Supply Current		48V(2) Supply Current		15V Supply Current		12V Supply Current		5V Supply Current	
I	ADC	I	ADC	I	ADC	I	ADC	I	ADC
0	433	0	426	0	305	0.21	575	0.51	311
2.2	528	2.2	522	3.4	403	0.91	699	0.96	348
3	564	3.1	558	4.2	428	1.00	717	1.27	376
4.6	637	4.1	605	5.9	475	1.25	758	1.50	397
7.6	764	4.7	630	8	533	1.51	805	1.78	423
8.6	808	7.6	758	9.8	582	1.76	849	2.01	443
9.7	852	8.6	801	13	666	2.01	892	2.53	493
11	908	9.8	845	15.4	730	2.25	936	2.65	508
12.7	983	11.1	903	17.7	794	2.54	986	3.06	550
		12.7	970	19.1	833			3.52	596
		14	1017	21.8	895			3.77	621
				24.2	967			4.04	650
				25.5	1003			4.53	705
								5.09	770

The maximum error between the measured values and the theoretical approximation for each sensor is also shown in Table D5 below.

Table D5: Power Pod current sensor function values

Current Sensor	Slope m_{avg} [mA^{-1}]	Offset c_{actual} [word]	Max Error [mA]	Allowable Error [mA]
Power Pod 48V Current (1)	43.4	433	100	500
Power Pod 48V Current (2)	41.9	434	360	
Power Pod 15V Current	27.7	305	460	
Power Pod 12V Current	177	537	10	100
Power Pod 5V Current	103	247	80	

The graph in Figure D7 below has been included to show the neatly linear plot of current sensor reading for the first 48V output of the Power Pod.

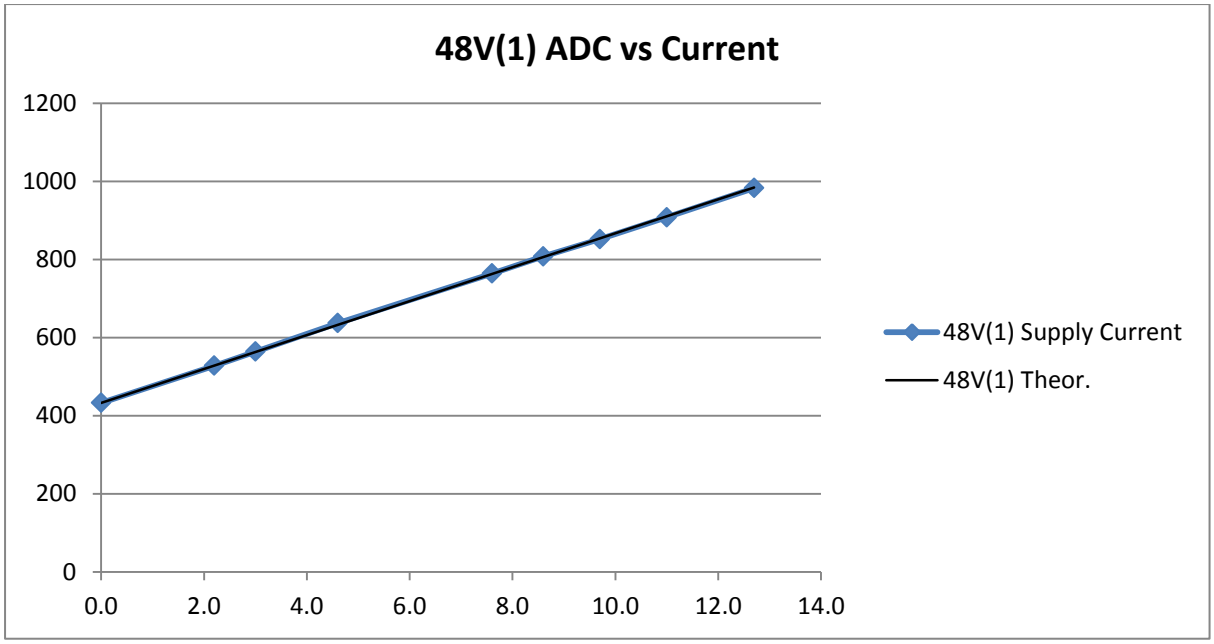

Figure D7: Graph showing measured and theoretical ADC values plotted against current for the current sensor on the first 48V output of the Power Pod

D2.4 SUMMARY

Both the E-Pod and Power Pod current sensors were calibrated successfully and all reading errors were found to be within their allowable limits.

APPENDIX E: RS-485 PACKET DATA ALLOCATION

E1. Data Allocation in RS-485 Packets for the E-Pod Microcontrollers

Table E1: E-Pod top microcontroller serial communications data assignment

	Addr. 1	Addr. 2	Data 1	Data 2	Data 3	Data 4	Data 5	Data 6	Data 7	Data 8
RECEIVE	1st Address	2nd Address	Packet ID	Sensor Pod Pwr	IMU Pod Pwr	Sonar Pwr	Fwd Camera Pwr	-	-	-
	230	115	1	0/255	0/255	0/255	0/255	0	0	0
SEND	Addr. 1	Addr. 2	Data 1	Data 2	Data 3	Data 4	Data 5	Data 6	Data 7	Data 8
	1st Address	2nd Address	Packet ID	Temp (hi byte)	Temp (lo byte)	-	-	-	-	-
	230	115	1	0-3	0-255	0	0	0	0	0

Table E2: E-Pod bottom microcontroller serial communications data assignment

	Addr. 1	Addr. 2	Data 1	Data 2	Data 3	Data 4	Data 5	Data 6	Data 7	Data 8
RECEIVE	1st Address	2nd Address	Packet ID	Port Fwd Thruster Pwr	Stbd Fwd Thruster Pwr	Port Aft Thruster Pwr	Stbd Aft Thruster Pwr	Vertical Thruster Pwr	Port Fwd Light Pwr	Stbd Fwd Light Pwr
	220	110	**1**	0/255	0/255	0/255	0/255	0/255	0/255	0/255
	Addr. 1	Addr. 2	Data 1	Data 2	Data 3	Data 4	Data 5	Data 6	Data 7	Data 8
	1st Address	2nd Address	Packet ID	Centre Light Pwr	Aft Light Pwr	Aft Camera Pwr	-	-	-	-
	220	110	**2**	0/255	0/255	0/255	0	0	0	0
SEND	Addr. 1	Addr. 2	Data 1	Data 2	Data 3	Data 4	Data 5	Data 6	Data 7	Data 8
	1st Address	2nd Address	Packet ID	Port Fwd Thruster I_{sense} (hi)	Port Fwd Thruster I_{sense} (lo)	Stbd Fwd Thruster I_{sense} (hi)	Stbd Aft Thruster I_{sense} (lo)	Port Aft Thruster I_{sense} (hi)	Port Aft Thruster I_{sense} (lo)	-
	220	110	**1**	0-3	0-255	0-3	0-255	0-3	0-255	0
	Addr. 1	Addr. 2	Data 1	Data 2	Data 3	Data 4	Data 5	Data 6	Data 7	Data 8
	1st Address	2nd Address	Packet ID	Stbd Aft Thruster I_{sense} (hi)	Stbd Aft Thruster I_{sense} (lo)	Vertical Thruster I_{sense} (hi)	Vertical Thruster I_{sense} (lo)	Temp (hi byte)	Temp (lo byte)	-
	220	110	**2**	0-3	0-255	0-3	0-255	0-3	0-255	0

APPENDIX F: EXPENSES REPORT

TABLE OF CONTENTS

LIST OF TABLES

F1.1 BREAKDOWN OF EXPENSES

This appendix provides a brief analysis of the finances allocated to the manufacturing of the ROV components. Due to a large degree of overlap in expenses between the project scope of the author and Thomas Knight, the expenses have not been separated between the two projects. Incorporating both project scopes into the budget will, in any case, provide a better idea of the development cost of the ROV to this point.

F1.1.1 Materials

A breakdown of the expenses incurred during the project has been compiled in Table F1 below. Most of the actual expense values were used, but for some components only estimates were available, particularly for items not within the scope of the author's project.

Table F1: Breakdown of estimated material costs

Material Description	Price (Excl. VAT)	Price (Incl. VAT)
Electrics Estimate	R 49 000	R 55 860
Mechanical Components Estimate	R 44 300	R 48 222
Tether (actual)	R 24 950	R 28 443
Subsea connectors (actual)	R 70 925	R 80 855
Sonar (actual)	R 66 000	R 75 240
Machined Material Estimate	R 16 100	R 18 354
General expenses & Sundries	R 20 000	R 22 800
Total Estimated Material Cost	**R 291 275**	**R 332 054**

F1.1.2 Labour

The direct labour costs were estimated for the project by totalling machining hours assigned to each component and adding them to an estimate of the hours spent by the author and Thomas Knight designing the ROV. A summary of these figures is presented in Table F2. The estimated 6000 hours of design spent on the ROV was based on an estimated 17 months, five days a week, and 8 hours per day worked by the two engineers.

Table F2: Estimated labour hours for the ROV

ROV Component	Qty	Machining Hours			
		Turning	Milling	Hand Work	Sub Total
E-Pod	1	8	-	2	10
P-Pod	1	8	-	2	10
P-Pod Bracket	2	3	-	-	6
Light Pod	4	6.5	-	1.25	31
Main Camera Pod	1	6.5	-	1.25	8.25
Aft Camera	1	5	-	-	5
Thruster	5	13	29.5	-	212.5
ROV Brackets	1	-	40	-	40
Frames	4	-	5	-	20
Brass Nuts for Bulkhead Connectors	30	-	0.1	-	3
Anodes & Screws	20	0.2	0.1		6
Pipe-Nuts	20	-	-	0.15	3
Total Estimated Machining Hours					**355**
Estimated Artisan Cost/Hour (Excl. VAT)					R 100
Sub Total Artisan Cost Estimate (Excl. VAT)					**R 35 500**
Estimated Design Hours					6 000
Estimated Engineer Cost/Hour (Excl. VAT)					R 200
Sub Total Design Cost Estimate (Excl. VAT)					**R 120 000**
Total Estimated Labour Costs (Excl. VAT)					**R 155 500**

F1.1.3 Summary

At the point of departure with these projects for both the author and Thomas Knight, the ROV had been designed and built at an approximate cost of R 446 775 as shown in Table F3 below.

Table F3: Summary of costs

Description	Cost
ROV Material Cost	R 291 275
ROV Labour Cost	R 155 500
Sub Total Direct Cost	R 446 775

The overheads associated with this project have not been considered because, given that the ROV was produced in the laboratory of a university, it would have been a complicated task to estimate such costs. The overheads have not been estimated for this project, but will need to be estimated as part of a feasibility study should this ROV ever be considered for manufacture.